MECHANICAL REGULATION OF BREAST TUMOR CELL DEATH IN BLOOD CIRCULATION AND BRAIN METASTASIS UNDER NATURAL KILLER CELL SURVEILLANCE

HU BING

PHD

The Hong Kong Polytechnic University

2025

The Hong Kong Polytechnic University

Department of Biomedical Engineering

Mechanical Regulation Of Breast Tumor Cell Death In Blood Circulation And Brain Metastasis Under Natural Killer Cell Surveillance

Hu Bing

A thesis submitted in partial fulfillment of the requirements for the degree of Doctor of Philosophy

December 2024

CERTIFICATE OF ORIGINALITY

I hereby declare that this thesis is my own work and that, to the best of my knowledge and belief, it reproduces no material previously published or written, nor material that has been accepted for the award of any other degree or diploma, except where due acknowledgment has been made in the text.

_____ (Signed)

_____Hu Bing_____ (Name of student)

Publication list

Bing Hu, Ying Xin, Guanshuo Hu, Keming Li, and Youhua Tan. "Fluid shear stress enhances natural killer cell's cytotoxicity toward circulating tumor cells through NKG2D-mediated mechanosensing." APL bioengineering 7, no. 3 (2023).

Xin Ying, **Bing Hu**, Keming Li, Guanshuo Hu, Cunyu Zhang, Xi Chen, Kai Tang, Pengyu Du, and Youhua Tan. "Circulating tumor cells with metastasis-initiating competence survive fluid shear stress during hematogenous dissemination through CXCR4-PI3K/AKT signaling." Cancer Letters 590 (2024): 216870.

Du, Pengyu, Kai Tang, Xi Chen, Ying Xin, **Bin Hu**, Jianfeng Meng, Guanshuo Hu, Cunyu Zhang, Keming Li, and Youhua Tan. "Intercellular contractile force attenuates chemosensitivity through Notch-MVP-mediated nuclear drug export." Proceedings of the National Academy of Sciences 122, no. 19 (2025): e2417626122.

Tang K, Zheng Y, Hu G, Xin Y, Li K, Zhang C, Chen X, Zhang B, Li X, **Hu B**, Jia Q. Local soft niches in mechanically heterogeneous primary tumors promote brain metastasis via mechanotransduction-mediated HDAC3 activity. Science advances. 2025 Feb 26;11(9):eadq2881.

Abstract

Metastasis is the primary cause of death among cancer patients. Malignant tumor cells preferentially metastasize to specific organs, termed organotropism. Compared with other organs, brain metastasis shows higher lethality with limited clinical strategies for treatment. The molecular mechanisms underlying brain metastasis, however, remain largely elusive. Tumor metastasis is tightly regulated by both intrinsic and extrinsic factors, such as the immune system, the surrounding mechanical microenvironment, and the mechanics of tumor cells. In particular, at the primary tumor site, infiltrated immune cells, like natural killer (NK) cells, selectively kill some tumor cells but spare others. Whether the mechanical properties of tumor cells play any role in this immunosurveillance process is yet to be addressed. Whether the remaining immune-resistant tumor cells contribute to organotropism remains unknown. Upon entry into blood circulation, circulating tumor cells (CTCs) experience fluid shear stress (FSS) and robust immune surveillance from NK cells. However, whether NK cells and FSS affect CTCs' viability synergistically or independently during hematogenous dissemination is still poorly understood.

To solve these fundamental questions, we first investigated the co-localization between different types of infiltrated immune cells and the organotropism pattern by analyzing spatial transcriptomics data from patients, followed by a series of in vitro and in vivo assays. Our results showed that NK cells, rather than other immune cells, correlated with brain metastasis in breast cancer. Importantly, co-culture with NK cells selected a subpopulation of breast cancer cells with enhanced brain metastatic ability. Mechanistically, NK cells secreted and injected granzyme B into tumor cells that directly cleave ezrin, leading to the reduction of cell membrane tension. The low membrane tension activated PI3K-Akt signaling in NK-selected cells to upregulate GLUT3 via CREB signaling, which potentiated glucose uptake and metabolism to promote brain colonization. The intervention of ezrin-PI3K/Akt-GLUT3 signaling

inhibited brain metastatic potential of NK-selected cells. Single-cell transcriptomics analysis of patient-derived tumor biopsies revealed a clinical correlation between ezrin-PI3K/Akt-GLUT3 signaling and brain metastasis-associated genes. Further, lower membrane tension rendered tumor cells more resistant to NK-mediated cytotoxicity. These findings demonstrate that except the well-known cytotoxic effect, NK cells can promote breast cancer brain metastasis via the reduction of cell membrane tension, providing compelling evidence to unveil the pro-organotropism effect of NK cells.

To investigate the effect of FSS on NK-mediated cytotoxicity against CTCs, we applied physiologically relevant magnitudes of FSS on CTCs with or without NK cells. FSS enhanced NK cell cytotoxicity by delivering more granzyme B into CTCs with negligible changes in the secretion of cytokines or the expression of Trail. Knocking down a mechano-sensitive receptor, NKG2D, erased the FSS-enhanced cytotoxicity. NKG2D mechano-sensing was further validated by FSS-dependent CD107a expression induced by direct NKG2D-ligand interaction. These results indicate that the cytotoxicity of NK cells is augmented by FSS for the effective elimination of metastatic CTCs during hematogenous dissemination.

To summarize, these studies provide evidence to unveil that 1) NK cells' roles in cancer are not only anti-metastatic (killing malignant tumor cells) but also pro-metastatic (promoting brain metastasis); 2) tumor cell membrane tension is a mechanical checkpoint for NK cell surveillance and dictates both immune evasion and brain metastatic potential. FSS strengthens NK cell cytotoxicity through NKG2D-mediated mechano-sensing. Thus, targeting the membrane tension of breast tumor cells and the NKG2D-ligand axis could be new mechanotargeting strategies for the treatment of metastasis.

Acknowledgments

I'd like to thank my supervisor, Dr. Tan, for his direction during my five-year academic career as both a research assistant and PhD candidate. The research was profound and complicated. Only the smartest person could develop talented ideas to figure out questions and pave the way for scientific advances. These were my thoughts about research and science. My three-year experience in mechanobiology as a postgraduate provided me with some background knowledge about research and methods to conduct it before coming to PolyU. But I knew that I was not enough. Initially, I was muddleheaded and tried anything that might be right. Dr. Tan's critical thinking about FSS, immune cells, and CTCs directed me to real research. I am not the smartest, not talented, nor the most experienced, but I can do research only if I find an interesting and important question that has not been solved. After some time in Y503 (our lab), I knew that experiments needed limited intelligence. Following mature instructions and summarizing experience was almost enough. Thanks a lot to Xin Ying, Ke Ming, Chen Xi, Peng Yu, Jian Feng, Tang Kai, Yu Fan, Cun Yu, Guan Shuo, Dr. Ren Wei, Zhang Bai, Xue Yi, Li Silu, Fan Xiangli, Fang Tingting, Han Xiaomei, Wu Hu, and Liu Zejin for your kind help in my research and life. You created a good atmosphere that benefited me very much both physically and mentally.

Research is interesting but experiments sometimes are the opposite. Those who conduct WB or single-cell clone or animal experiments must understand me. Those time-consuming and spirit-draining experiences were not that boring with all your (mentioned above) sharing about research. I thank Xin Yi for her affection, accompaniment, and support. She is adorable, and so is life and research. I thank my father, mother, and brother for their selfless support and care during the past years. Thanks to Prof. Yang Mo, Dr. Wen, all BME staff in GO, Rachel, Ryan, and Michael (ULS), and all CAF staff for your generous help in my research. And finally, thanks to my Nei Nei and Xi Xi for their accompaniment and endless fairs.

Table of contents

List of figures

List of tables

List of abbreviations

ADCC	**antibody-dependent cellular cytotoxicity**
ADCP	**antibody-dependent cellular phagocytosis**
APC	**antigen-presenting cell**
AR	**aspect ratio**
BBB	**blood-brain-barrier**
BFP	**biomembrane force probe**
Bleb	**Blebbistatin**
BoM	**bone metastasis**
BrM	**brain metastasis**
BRMFS	**brain-metastasis-free survival**
BSA	**Bovine serum albumin**
CAF	**cancer-associated fibroblast**
CAPN1	**Calpain 1**
CA-ROCK	**constructively active ROCK**
CDK5	**Cyclin-dependent kinase 5**
C-ERMAD	**C-terminal ERM-association domain**
CM	**conditioned medium**
c-Myc	**BHLH transcription factor**
Cox2	**cyclooxygenase 2**
CRS	**cytokine release syndrome**
CTC	**circulating tumor cell**
Cyto D	**Cytochalasin D**
DC	**Dendritic cell**
DCIS	**ductal carcinoma in situ**
DMEM	**Dulbecco's Modified Eagle Medium**
DNA-PK	**DNA-dependent protein kinase**
DR4	**TRAIL receptor I**

DR5	**TRAIL receptor II**
DTC	**disseminated tumor cell**
E-Cad	**E-cadherin**
ECAR	**extracellular acid ratio**
ECM	**extracellular matrix**
EGFR	**epidermal growth factor receptor**
EGFR1	**epidermal growth factor receptor type**
EMT	**epithelial–mesenchymal transition**
ER	**estrogen receptor**
ERM	**ezrin-radaxin-moesin**
FADD	**FAS-associated death domain protein**
FasL	**Fas ligand**
FRET	**Fluorescence Resonance Energy Transfer**
FSS	**fluid shear stress**
GAPDH	**human glyceraldehyde 3-phosphate dehydrogenase**
GLUT1	**glucose transporter 1**
GLUT3	**glucose transporter 3**
GPCR	**G protein-coupled receptor**
HA	**hyaluronic acid**
HCMEC	**human cerebral microvascular endothelial cell line**
HRAS	**harvey rat sarcoma viral oncogene homolog**
HRP	**Horseradish peroxidase**
HSC	**hematopoietic stem cell**
HUVEC	**human umbilical vein endothelial cell**
ICAM1	**intercellular adhesion molecule 1**
IFN-γ	**interferon gamma**
IL2	**interleukin II**
ISG	**interferon-stimulated gene**
JAS	**Jasplakinolide**

LCDS	**lobular carcinoma in situ**
MAp3K14	**NF-κβ-inducing kinase**
MD	**molecular dynamics**
MEMα	**Minimum Essential Medium α**
MFSD2A	**Major facilitator superfamily domain-containing protein 2a**
MICA	**MHC class I polypeptide–related sequence A**
MMP	**Matrix Metalloproteinase**
MTOC	**microtubule organization center**
NC	**Negative control**
NHERF2	**Na+/H+ exchange regulatory factor 2**
NK	**natural killer**
OCR	**oxygen consumption ratio**
OS	**overall survival**
PBS	**phosphate-buffered saline**
PD-1	**Programmed cell death protein 1**
PDGFR	**platelet-derived growth factor receptor**
PDK1	**Phosphoinositide-dependent kinase 1**
PDL	**poly-D-lysin**
PD-L1	**Programmed death-ligand 1**
PFA	**paraformaldehyde**
PI(3,4)P2	**phosphatidylinositol-(3,4)-bisphosphate**
PI(3,5)P2	**phosphatidylinositol-(3,5)-bisphosphat**
PI3K	**phosphoinositide 3-kinase**
PI3P	**phosphatidylinositol-3-phosphate**
PI4P	**phosphatidylinositol 4-phosphate**
PI5P	**phosphatidylinositol-5-phosphate**
PIK3CA	**phosphatidylinositol-4,5-bisphosphate 3-kinase, catalytic subunit alpha**
PIP2	**Phosphatidylinositol-4,5-bisphosphate**

PIP3	**Phosphatidylinositol (3,4,5)-trisphosphate**
PKCα	**protein kinase Cα**
PPI	**inositol phospholipid**
PPP1R12A	**protein phosphatase 1 regulatory subunit 12A**
PR	**progesterone receptor**
PTEN	**phosphatase and tensin homolog**
PTP4A1	**protein tyrosine phosphatase type IV A 1**
RhoA	**Ras homolog family member A**
ROCK	**Rho-associated protein kinase**
RTK	**receptor tyrosine kinase**
SK1	**sphingosine kinase 1**
STK10	**lymphocyte-oriented kinase**
TAM	**tumor-associated macrophage**
TGF-β	**tumor growth factor β**
TME	**Tumor microenvironment**
TNBC	**triple-negative breast cancer**
TNF-α	**tumor necrosis factor alpha**
TRAIL	**TNF-related apoptosis-inducing ligand**
WSS	**wall shear stress**
Y-27	**Y-27632**
YAP	**Yes-associated protein**

Chapter 1: Introduction

1.1 Mechanics and NK cell surveillance in metastasis

It has been believed for a long time that intrinsic genetic alterations of healthy tissue cells are responsible for both cancer initiation and metastasis. Typical mutations include the mutation of tumor suppressor genes (e.g., TP53, phosphatase and tensin homolog or PTEN, etc), and the gain-of-function mutation of oncogenes (e.g., phosphatidylinositol-(4,5)-bisphosphate-3-kinase catalytic subunit alpha or PIK3CA, BHLH transcription factor or c-Myc, harvey rat sarcoma viral oncogene homolog or HRAS, etc). However, advances over the last two decades in the mechano-biology of cancer have indicated the important roles of mechanical cues (e.g., FSS FSS and cellular mechanical properties) in metastasis. NK cells, as a major part of the human innate immune system, take part in every step of cancer progression and metastasis and may reshape tumor cell mechanics to regulate metastatic potential and organotropism.

1.1.1 Cell membrane tension in metastasis

Disseminated tumor cells (DTCs) experience multiple biochemical and mechanical challenges during the long journey of metastasis, which eliminate the majority of them and eventually contribute to low efficiency of metastasis. It is reasonable to hypothesize that those of DTCs that successfully survive the whole metastatic process should possess unique mechanical properties to withstand these challenges. Cell membrane tension is composed of the in-plane lipid membrane tension and membrane-to-cortex attachment[1]. Multiple cell functions are directly controlled by membrane tension, such as migration, endocytosis/exocytosis, division, and differentiation[2-5]. Evidence has been provided that low membrane tension is a mechanical marker of invasive tumor cells [6]. Lower cell membrane tension renders tumor cells with higher motility by liberating actin filaments for polymerization among protrusions. This property of tumor cells may promote trans-blood-brain-barrier (BBB) migration and,

as a result, brain metastasis.

1.1.2 NK cells in metastasis

As a member of the innate immune system, NK cells show robust anti-tumor cytotoxicity without the priming of tumor antigens. NK cells sense and transduce the biological stimuli of target tumor cells through specific receptors. Tumor cells with high/low levels of activating/inhibitory ligands of NK cells can induce different cytotoxic responses, and a subgroup of immune-resistant tumor cells can eventually survive the immune cell attack. Currently, the two major immune checkpoints, PD-1 and CTLA-4, inhibit anti-tumor killing and promote tumor cell immune evasion. Recent advances show that killer cells can sense the mechanical properties of the environment and the target cells and rely on external or endogenous forces for tumor cell recognition, immunity activation, and completion of killing. Tumor cells with specific mechanical properties render themselves more vulnerable or resistant to immune cytotoxicity, leading to the concept that the mechanical properties of tumor cells can serve as new checkpoints of immune cells [7]. However, whether NK cells select and/or induce a subgroup of tumor cells that have high metastatic potential and unique organotropism remains largely unknown.

1.1.3 FSS and NK cell surveillance in blood circulation

The whole metastatic process includes multiple major steps, and failure at any one of these steps prevents the final formation of secondary tumors. The overall efficiency of the metastasis process is rather low (e.g., less than 0.02%) due to several rate-limiting factors such as immunological barriers, challenges in circulation, extravasation limitations, and microenvironmental compatibility [8,9]. Once entering the bloodstream, CTCs face various environmental stresses, including loss of attachment, FSS, and immune attack [10,11]. Only a small subset of CTCs can withstand those challenges to initiate metastasis. The presence of CTCs in the bloodstream is linked to cancer patients' prognosis and survival[12,13].

Immune cells are involved in every step of tumor metastasis[14]. Given that CTCs have a relatively short lifespan in the bloodstream (approximately 30 minutes)[11,15-17], effective elimination by immune responses necessitates rapid recognition and cytotoxic action. NK cells play a crucial role in the immune system, serving as the primary defender against CTCs. Based on germline-encoded receptors like NKG2D, NK cells can quickly identify and eliminate malignant cells[18,19]. The quantity and activation status of NK cells are closely linked to cancer patients' survival[20-23]. Most blood NK cells are the $CD56^{dim}$, which exhibits strong cytotoxicity but has a relatively lower capacity for cytokine secretion when compared to the $CD56^{bright}$ subtype[24-26]. Revealing how these critical factors work together to influence the survival of CTCs during bloodborne dissemination is essential for developing new therapeutic strategies against CTCs and metastasis.

1.2 Current challenges and limitations

Tumor cells are highly heterogeneous among different cancer types, cancer patients, and even within the same tumor tissue. Gene mutations, DNA instability, cell competition among tumor cells, and the selection pressure of the immune system promote diversity. The intrinsic genetic/phenotypic differences dictate tumor cells' metastatic potential. Chemotherapy and radiotherapy target this fast-growing characteristic of tumor cells and can effectively kill most tumor cells. However, many cancer patients experience recurrence after treatment. One of the main reasons is tumor cell heterogeneity.

Tumor cells are also mechanically heterogeneous. The stiffness of tumor cells within a single tumor can be largely different[27]. Cell mechanics have been found to regulate tumor cell chemoresistance potential by influencing key drug-resistant-associated genes[28]. Further, tumor cell rigidity has been proposed to influence metastasis organotropism[29].

The immune system is tasked with monitoring and eliminating tumor cells. The

infiltration of killer cells is positively correlated with patients' survival. Immunotherapy is currently the most promising therapy for cancer treatment. However, immune cells can also be pro-metastatic. Data from mouse models indicate that the recruitment of suppressive immune cells to tumors shields metastatic cancer cells from detection by killer cells. This protection diminishes the effectiveness of immunotherapy, facilitating the establishment of metastasis. For killer cells themselves, NK cells are commonly considered to positively target and kill tumor cells. Tumor cells evading T/NK cell killing have a higher likelihood of forming metastasis. However, whether these immune-resistant tumor cells have unique mechanical properties and show metastasis organotropism remains largely unknown.

After entering blood circulation, CTCs encounter two major challenges: FSS and NK cell surveillance. Current research only investigates the killing of NK cells against tumor cells in a static condition or examines how FSS solely regulates tumor cells' survival and metastasis. There is a high possibility that FSS and NK cells synergistically contribute to the eradication of CTCs.

1.3 Scientific questions, objectives, and scopes

Based on the above research gaps, challenges, and limitations, my current project aims to answer two key questions:

① Whether NK cells select/induce a subset of tumor cells with unique mechanical properties that promote tumor cells to metastasize to specific organs (organotropism)?

② Within the blood system, whether FSS can influence NK cell-mediated killing of CTCs?

To answer the first question, we proposed the following objectives:

1. Identify the correlation between the co-culture of NK cells with tumor cells and a unique organotropism pattern from a patient-derived database.
2. Confirm the influence of NK cells on tumor cell organotropism both in vitro and

in vivo.

3. Identify the changes in mechanical properties among co-cultured tumor cells.
4. Investigate the influence of the changes in tumor cell mechanical properties on NK cell resistance.
5. Investigate the influence of the changes in tumor cell mechanical properties on organotropism.
6. Detect the downstream signaling pathway that is responsible for the changes in organotropism.

To answer the second question, we proposed four more objectives:

1. Based on an in vitro microfluidic system, the effect of FSS on NK cells' killing will be investigated.
2. Unveil the mechanisms underlying the FSS magnitude-dependent NK cells' killing.
3. Further, identify the key mediator that regulates the FSS-induced NK activation, and the mediated CTCs death.
4. Finally, detect the mechano-sensitivity and associated mechano-signaling pathway of NKG2D under the stimulation of FSS.

1.4 Significance and values

First, this study proves the important role of mechanical cues from both tumor cells and the environment in influencing immune cells and metastasis. We provide evidence for the first time that NK cells show different killing abilities against tumor cells with high/low membrane tension. Surviving tumor cells with low membrane tension, unfortunately, gain a high brain metastatic potential. Based on this, increasing tumor cell membrane tension can enhance NK cell killing efficiency and at the same time inhibit the brain metastatic potential of NK cell-selected tumor cells. Thus, our findings on the one hand provide a new strategy to target tumor cell membrane tension to improve current cancer immunotherapy. On the other hand, new methods that specifically increase tumor cell membrane tension can be designed to inhibit cancer

brain metastasis.

Second, our results indicate that blood circulation not only passively functions as a tool for the transport of NK cells but also positively influences their function. FSS strengthens NK cell cytotoxicity when it encounters a CTC(s) by a mechano-sensitive receptor NKG2D. This synergistic effect of NK cells and FSS provides a new explanation for the extremely low efficiency of metastasis and a new strategy for inhibiting metastasis through the blood system, both for treatment and as a precaution for patients.

1.5 Thesis outline

The current study focuses on the mechanical regulation of breast cancer metastasis, organotropism, and NK cell cytotoxicity. Chapter 2 introduces the related background information and current research progress in this area. Chapter 3 provides detailed experimental designs, methods, and related materials. Results regarding the role of membrane tension on NK cell killing and brain metastasis are introduced in Chapter 4. The FSS-regulated NK cell killing of CTCs is discussed in Chapter 5. We summarize this study and propose our limitations and future perspectives in Chapter 6.

Chapter 2: Literature review

2.1 Overview of breast cancer

Breast cancer is the most prevalent cancer among women both in Hong Kong (28.5%) and globally (31%), and its metastasis is the principal cause of women's cancer-associated death[30-32]. According to the molecular signature, including three hormone receptors: progesterone receptor (PR), estrogen receptor (ER), and human epidermal growth factor receptor (HER2), four major subtypes have been revealed: ER positive, PR positive, HER2 positive, and TNBC which does not express any of the above receptors[33]. ER is the most common marker among patients, taking up to 70–75%[34]. More than 50% of ER-positive breast cancer patients carry PR; therefore, both ER and PR are regarded as diagnostic and prognostic signature molecules of breast cancer[35]. HER2 overexpression contributes to nearly 15–25% of breast cancer patients[36]. Unlike PR, which is positively associated with patients' survival, HER2 expression level has a negative correlation with disease-free period[37]. It carries the P53 mutation, which is one of the most well-known cancer suppressor genes. The HER2-positive subtype is more invasive and proliferative. TNBC is an ER^-, PR^-, and $HER2^-$ subtype, constituting about 15% of breast cancer patients. The lack of expression of these hormone markers on TNBC has remarkable disadvantages in its diagnosis and therapy choice because common effective therapeutic drugs target PR, ER, and/or HER2. This makes TNBC the most aggressive, highly metastatic, and with low overall survival rates. It carries gene mutations of both P53 and BRCA1 (another tumor suppressor gene). It is most prevalent in African American women under 40. It is highly proliferating, has alternative DNA repair genes, and increases chromatin instability. Immunohistochemically, TNBC can be further subdivided into basal-like and non-basal-like subsets. Basal-like TNBC carries human epidermal growth factor receptor type 1 (EGFR1) and cytokeratin 5/6, while the non-basal-like TNBC does not express cytokeratin 5/6. One of the most cultured human-derived basal-like TNBC cell lines is

MDA-MB-231.

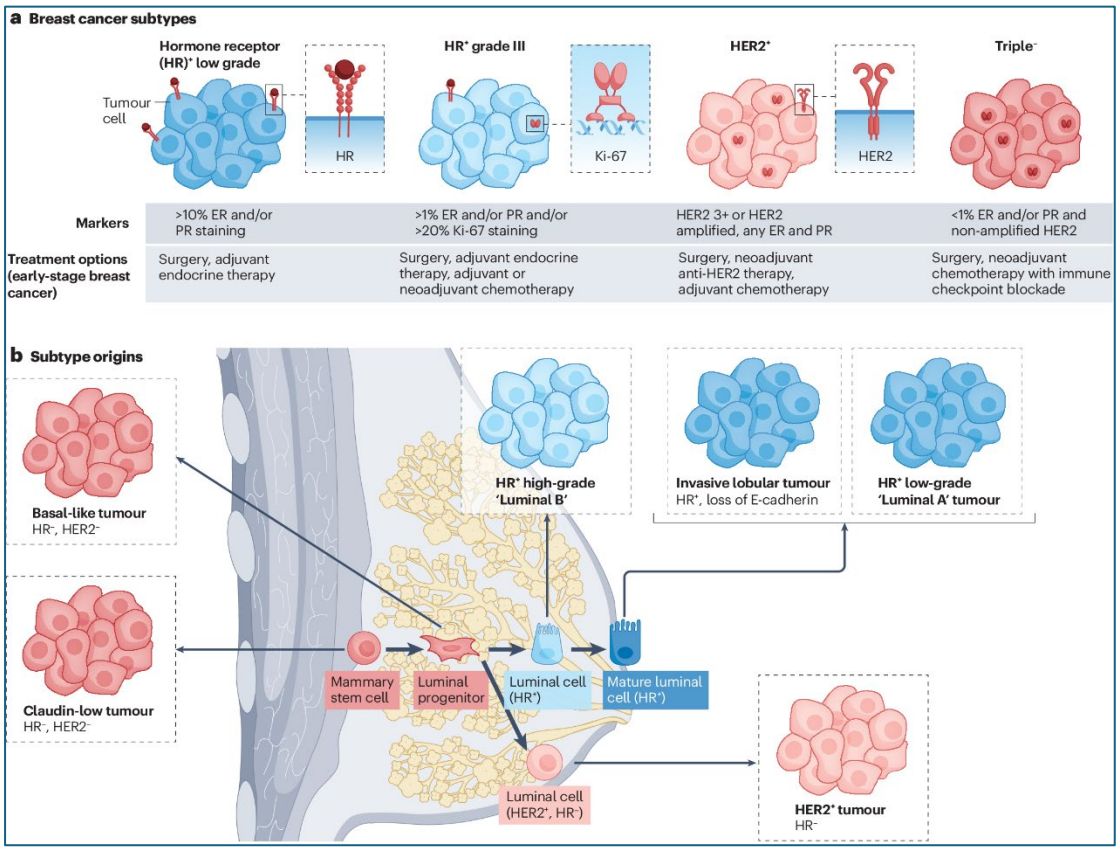

Figure 2-1 Subtypes and origins of breast cancer[38].

2.2 Cancer metastasis

Metastasis accounts for ~ 90% of cancer-associated deaths[10,39,40]. About 20 ~ 30% of breast cancer patients (early-stage) will develop distant metastases[41]. Distant metastasis is a complex multistep process (Figure 2-2). Basically, it involves the following steps: malignant tumor cells first locally break out the thin but stiff basement membrane that surrounds the primary tumor; then they invade the surrounding tissue, search for microvasculature of the blood and lymph systems, and enter the circulation system (intravasation), survive and translocate through the circulation system to micro-vessels of other organs, evade from the blood/lymph vasculature (extravasation), finally survive and adapt to the foreign microenvironment of distant organs with enhanced cell proliferation and form a secondary tumor (colonization)[10,42,43].

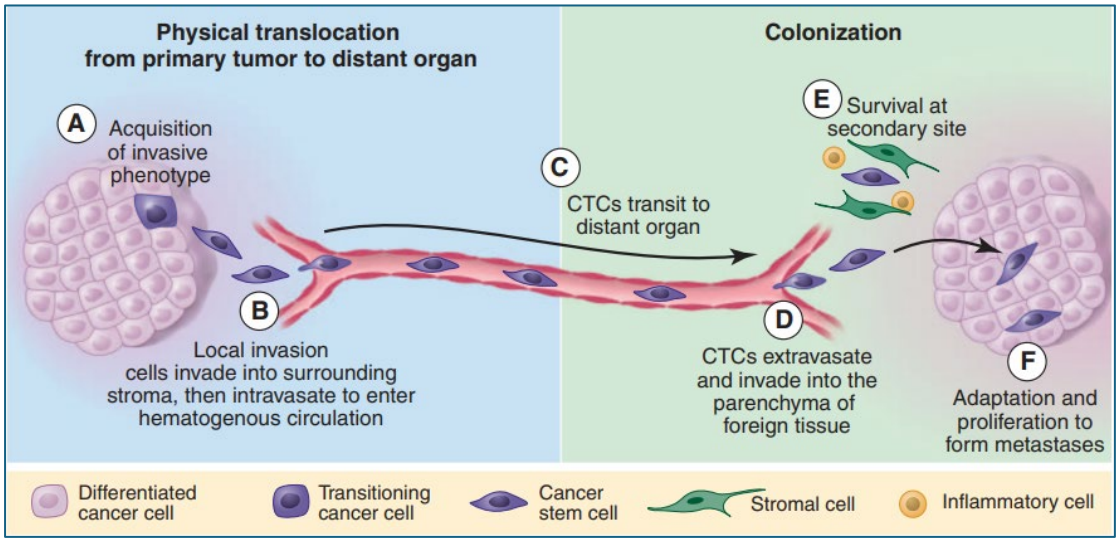

Figure 2-2 The metastatic cascade[10].

2.3 Metastatic inefficiency

Tumor cell metastasis is a low-efficiency process due to several intrinsic and extrinsic challenges that cancer cells face[44]. It is found that no more than 0.02% of DTCs can form secondary tumors[8,9,44,45]. Most cells die within 1-2 days once detached from primary tumor sites[46]. Here are the key reasons contributing to the inefficiency of metastasis.

2.3.1 A complex multistep process

The process of metastasis is a death parade. As mentioned above, metastasis is a complex, multistep process. To successfully seed a secondary tumor, one tumor cell must overcome all the challenges from physical barriers, surveillance of the immune system, variable mechanical cues-induced damages, anoikis, and different microenvironments from the primary site. Each of these steps not only selects the most adapted subpopulations but also influences and regulates relevant transcription and phenotypes. Under this huge selective pressure, most tumor cells undergo apoptosis/necrosis. Those who successfully arrive at a distant organ usually transfer to a dormant status to temporarily avoid death[44].

2.3.2 Detachment and invasion difficulties

Eighty-five percent of breast cancer patients have ductal carcinoma, while ten percent have lobular carcinoma[47]. These tumor cells originate from normal epithelial cells. Epithelial cells always keep tight cell-cell junctions and cell-ECM connections to maintain tissue integrity[48]. Transformed cells with these connections will be limited to the primary sites and only form carcinoma in situ with low malignancy. Typical examples include ductal carcinoma in situ (DCIS) and lobular carcinoma in situ (LCIS). One of the key cell adhesion molecules is the E-cadherin (E-Cad). E-Cad preferentially interacts with itself in a homophilic manner. Tumor cells like MCF-7 with high E-Cad expression are usually epithelial-like and form a monolayer of cell clusters on a cell culture dish. MCF-7 moves more slowly than malignant cell lines [49]. Besides, cells are unable to effectively invade due to the lack of specific proteolytic enzymes. ECM is a relatively dense three-dimensional network crosslinked by ECM proteins like collagens, elastin, fibronectins, laminins, and some other proteins. These confined network fibers crosslink with each other, generating pores that range from 100 nm to several micrometers (up to about 10 μm), depending on the specific ECM components and tissue architecture. The limited invasion is observed when tumor cells try to invade through the ECM with sub-nuclear pore size[50].

2.3.3 Immunological barriers

The immune system poses significant obstacles to metastatic cells. Tumor microenvironment (TME) is well-recognized as an immune-suppressive scenario[51-53]. Lack of nutrients and oxygen, enrichment of lactic acid, and immune-suppressive cytokines in TME reshape infiltrated immune cell metabolism, phenotype, and function[54-57]. Immune checkpoint therapies targeting PD-1 or CTLA4 have also shown less effect on solid tumors than leukemia[58]. However, once tumor cells leave the primary tumor sites, they are exposed to functional host immune surveillance, especially in circulation systems where tumor cells are surrounded by a large number of NK cells[59,60].

2.3.4 Challenges in circulation

For the importance of the timely exchange of oxygen, nutrients, and metabolic products, the heart beats robustly all the time to drive the bloodstream and generates considerable FSS. Professional blood cells and endothelial cells have evolved over billions of years to adapt to that physical strike. However, breast tumor cells can not inherit that ability from their normal epithelial ancestors. Cells that enter the bloodstream will experience FSS and may be physically trapped in capillaries. The majority of tumor cells undergo apoptosis/necrosis for the FSS-induced damage and loss of adhesion-induced anoikis if staying in the blood for too long[61-64]. Tumor cells are usually larger than all blood cells and blood capillaries in diameter. They are also stiffer than blood cells, making it hard to go through capillaries, which leads to higher blood compression force on them and induces cell deformation[65]. Given these, as they navigate the circulatory system, there are reduced numbers of tumor cells that can reach distant sites.

2.3.5 Extravasation limitations

Even if tumor cells survive the bloodstream, extravasation is a challenging step. FSS can limit the adhesion of CTCs to blood vessels. Besides, in vivo and ex vivo observations have indicated that CTCs are usually packaged by blood cells like platelets and neutrophils, forming clusters to evade FSS-induced damage and killer cell recognition[66]. This isolation strategy also decreases CTC adhesion to endothelial cells. In some cases, CTCs succeed in attaching to interblood vessels to squeeze through the narrow space between endothelial cells, which is very hard. Blood is the origin of plasma and contains higher concentrations of nutrients, oxygen, and growth factors. In vitro migration and invasion models mostly adopt fetal bovine plasma to generate a nutrient concentration gradient, which utilizes the chemotaxis of tumor cells. Thus, tumor cells may prefer intravasating rather than extravasating.

2.3.6 Microenvironmental compatibility

The specific microenvironment of the target tissue (e.g., specific growth factors, ECM

components, and stromal cells) may influence the capacity of metastatic cells to survive, proliferate, and form secondary tumors. Most disseminated tumor cells (DTCs) can not successfully establish secondary tumors[44,67]. Extravasated DTCs prefer seeding at perivascular niches, where nutrients are sufficient[67,68]. Thrombospondin-1 secreted by endothelial cells induces DTC quiescence[67].

Due to these various hurdles, it is estimated that only tiny subgroups of tumor cells complete all these steps, leading to the overall low efficiency of metastasis.

2.4 Metastatic organotropism of breast cancer

Organotropism of metastasis is defined as a non-random phenomenon with a preference for secondary organs. Commonly diagnosed metastatic organs for breast cancer are bone (70%)[69], lung (60%)[70], liver (30%)[71], brain (10-30%)[72], and spleen (3%)[73]. A seed-soil theory proposed by Stephen Paget in 1889 is still generally accepted as a metastasis mechanism[74]. Basically, to successfully form a secondary tumor, the DTCs (seed) must adapt to the respective microenvironment of the organs (soil). DNA sequence and transcriptome analysis of the primary tumor cells indicated that tumor cells are both genetically and epigenetically different[75]. This huge heterogeneity provides a solid foundation for organotropism based on this theory. Recent advances in exosomes provide a new theory. Tumor cells among the primary sites secrete organ-specific exosomes. For example, α6β4 and α6β1-containing exosomes specifically target the lung tissue and form a premetastatic niche that is friendly to DTCs[76,77]. Besides, as a supplement to the seed-soil theory, the mechanical memory of DTCs has recently been raised[78]. Human organs are biophysically different. For example, tissue stiffness varies from ~1 KPa for brain, lung, and breast, ~5 KPa for liver and kidney, ~100 KPa for Skeletal muscle, to 10 GPa for bone[79,80]. Tissue stiffness influences tumor cell proliferation, morphology, migration ability, cytokine or hormone secretion, cell-cell communication, and some other functions. More importantly, the influences may be memorized by DTCs epigenetically and promote DTC colonization at a mechanically similar organ. For example, our recent

works showed that breast tumor cells seeded on soft hydrogels or growing among soft niches of breast tissue have a higher potential to metastasize to soft tissue like the brain.

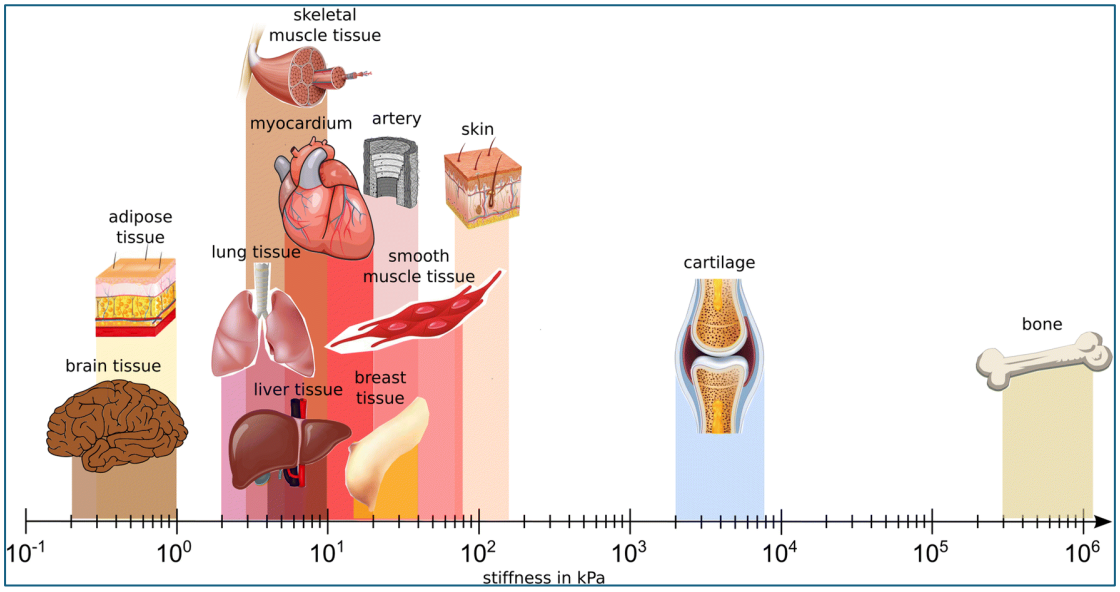

Figure 2-3 Mechanical properties of different human tissues[81]

2.4.1 Breast cancer brain metastasis

Nearly 10% of cancer patients develop brain metastases[82], and breast cancer patients exhibit a higher overall probability with 20%-40% brain metastasis occurrence, making it the second most common among all cancer types[83,84]. 45.3% of HR^+ cancer patients, 35%-50% of $Her2^+$ patients, and 46% of triple-negative patients are diagnosed with brain metastasis[83]. Compared with other organs, brain metastasis is more lethal, with only a median 10.8-month brain-metastasis-free survival (BRMFS) and, more seriously, an average 7.8-month overall survival (OS) after diagnosis[83]. It is worth noting that the OS of brain metastasis patients is also subtype dependent, with ~19 months for $HER2^+/HR^+$ patients, ~13 months for $HER2^+/HR^-$ patients, ~7 months for $HER2^-/HR^+$ patients, and only ~4.4 months for TNBC patients[83]. Current therapies for brain metastasis include surgical resection, whole-brain or stereotactic radiation, chemotherapy, and a combination of the above therapies. However, chemical agents can hardly penetrate the BBB, rendering the brain a sanctuary for colonized breast

tumor cells. Immune checkpoint therapy has also been actively investigated, but its effectiveness is still limited currently[85-87]. The underlying molecular mechanisms of brain metastasis, though, remain unclear. Therefore, an insightful understanding of the mechanisms will greatly benefit brain metastasis patients.

The brain-specific microenvironment presents the challenges and advantages for breast cancer cells to metastasize to the brain. These include the limitation of BBB, softness of brain stroma, and the immune suppression microenvironment.

Limitations of the BBB. Most CTCs scarcely extravasate into the brain because of the BBB. Even small-molecule drugs cannot efficiently penetrate the BBB because the tight junction between brain endothelial cells is so strong that the normal BBB pores are only 1.4 to 1.8 nanometers in diameter[88,89]. Considering the 20 μm or even longer breast CTCs, the CTCs size is 4 orders larger than BBB pores. This nature of the BBB is a result of evolution to protect the central nervous system from harmful drugs, pathogens, and excessive immune cell infiltration. BBB is mainly composed of tightly sealed brain endothelial cells, pericytes that surround brain endothelial cells, and astrocytic perivascular end feet[90]. The various tight junction proteins impede the paracellular diffusion of most molecules. Major facilitator superfamily domain-containing protein 2a (MFSD2A) on brain endothelial cells endows the BBB with low transcellular transcytosis[91].

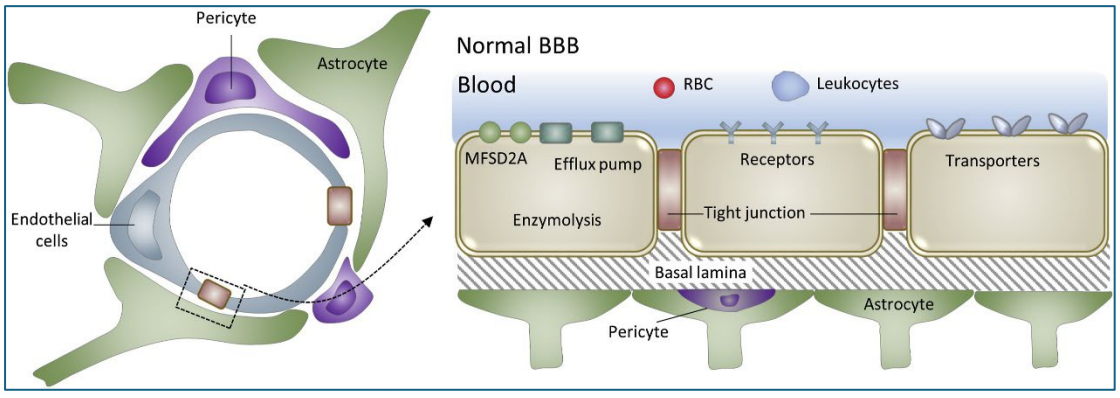

Figure 2-4 Structure of the blood-brain-barrier (BBB)[92]

Softness of brain stroma. The brain is the softest tissue of the human body for its relatively low composition of fibrous ECM, and the typical Young's modulus of brain tissue is only 100 Pa ~ 1 Kpa [81,93]. Fat makes up about 60% of the adult human brain, with water, protein, carbohydrates, and salts for another 40%. ECM proteins account for only a small portion of the extracellular space of the brain. The main components of brain ECM are hyaluronic acid (HA)[94,95]. For patients, this soft structure is also a self-protecting design to inhibit metastatic tumor cell growth. As mentioned above, breast tumor cells seeded on a soft surface and among soft hydrogel showed decreased proliferation.

Immunosuppressive microenvironment. The brain is one of the immune-privileged regions in the human body. It is believed to be an evolutionary adaptation that safeguards vital structures from damage caused by inflammatory responses to pathogens. Common features of these tissues include a lack of lymphatic flow, relatively low MHC molecule expression, increased expression of surface molecules, like CD59, that inhibit complement activation, enrichment of immunosuppressive cytokines such as TGF-β, appearance of neuropeptides, and constitutive expression of death receptor ligand-Fas ligand (FasL). Other immune-privileged sites include the eyes and testes. Brain immune homeostasis is mainly guarded by brain-specific macrophages, microglia, but with a relatively low number of cytotoxic cells like NK cells and effector T cells[96]. Microglia has a low potential to kill metastatic breast cancer cells due to both the lack of antigen recognition proteins like TCR and functional effector proteins like perforin and granzyme B[97]. In this immunodeficient environment, metastatic breast cancer cells are more privileged to generate secondary brain tumors.

Several strategies are adopted by breast cancer cells to break down the BBB. A subtype of breast cancer cells prefers adhering to brain endothelial cells[98]. Breast cancer cells can overexpress cyclooxygenase 2 (Cox2) to generate and secrete PEG and then MMP1 to augment brain metastasis[99]. Transcriptome analysis of brain metastatic breast

cancer cells shows that they specifically upregulate some genes like PTGS2, EREG, NDRG1, LTBP1, PTEN, ST6GALNAC5, HBEGF, SERPINB2, IL6, and some other genes[100,101]. These genes were also used as brain metastasis-associated genes in this thesis.

2.4.2 PI3K signaling in brain metastasis.

Genes mutation of PI3K signaling pathways like PIK3CA and PTEN is a common feature of breast cancer and breast cancer brain metastasis[102,103]. Active mutation of PI3K or signals-induced activated PI3K from tumor cell membrane proteins like hormones, receptors of growth factors, and integrins can phosphorylate PIP2 of the plasma membrane and produce PIP3. As a specific docking site, PIP3 recruits cytoplasmic Akt through its PH domain to the cell membrane. Engagement with PIP3 leads to the conformational change of Akt and makes it prone to be phosphorylated. Several kinases (PDK1, PDK2, ILK, mTORC2, and DNA-PK) can phosphorylate and activate Akt. It is worth noting that these kinases, like PDK1, are also recruited to the plasma membrane through PIP3[104]. The tumor suppressor PTEN, on the contrary, dephosphorylates PIP3 and inhibits plasma membrane docking of both Akt and its kinases. With active mutation of PI3KCA, or loss-of-function of PTEN, or input of extracellular signaling, Akt will be activated and translocate to cytoplasm and nucleus where it phosphorylates multiple proteins involved in metabolism[105], proliferation[106], apoptosis[107], angiogenesis[108], and EMT[109] promoting survival and proliferation of tumor cells. Direct monitoring of tumor cells during metastasis to the brain reveals that tumor cells gradually upregulate their PI3K-Akt signaling activity from circulating in the blood, adhering to brain endothelial cells, extravasating the BBB, to seeding in the brain tissue[110]. Targeting PI3K-Akt signaling has been proposed and proved effective for the treatment of brain metastasis in mice[110,111].

2.5 Immune surveillance of breast cancer

In agreement with all the other cancer types, breast cancer originates from genetic

mutations[112,113]. Common mutation events occur through the way of activation of oncogenes or the inhibition of tumor suppressor genes. BRCA1, BRCA2, PTEN, PIK3CA, CDH1, STK11, and TP53 are popular mutated targets[112,114-119]. These mutations provide huge advantages for tumor cell growth, drug resistance, and migration/invasion, which are vital for tumor initiation and progression[119-122]. For example, PI3K is downstream of some RTKs, like insulin receptors, and is responsible for cell proliferation. PIK3CA is the gene of P85, the regulatory domain of PI3K. A statistical analysis showed that 40% of patients with early-stage breast cancer held a PIK3CA mutation, which induced a gain-of-function of PI3K[123]. PTEN and TP53 are both tumor suppressors that are involved in apoptosis. Nearly 45% of PTEN and 30% of TP53 in all breast cancer patients have these mutations[124,125]. Cells with mutations happening in critical proteins that influence normal cell function will undergo apoptosis or exhibit eat-me signals to phagocytes like macrophages[126]. After being digested by phagocytes as antigen-presenting cells (APC), mutated protein peptides will be presented to helper T cells for the initiation of the adaptive immune response. Effector T cells recognize mutated protein peptides presented by MHC-I on tumor cells and generate cytotoxicity. Mutations that happen on other sites cause cell apoptosis and can be extruded actively or passively by surrounding healthy cells[127]. The mutation-induced genetic pressure, lack of nutrients induced growth pressure, outgrowth-induced gene instability, and tumor microenvironmental biological/chemical/mechanical cues induced survival pressure provide dangerous signals, that is, stress-induced proteins on the cell membrane, for NK cells. NK cells directly recognize tumor cells by binding to these stress-induced ligands without MHC-antigen-TCR recognition and generate cytotoxicity against tumor cells. This brings NK cells to the first line against cancer with great advantages. Tumor cell endogenous dangerous signals, rather than mutation-generated antigens, help NK cells bypass the processes of antigen processing, APC lymph node homing, antigen-presenting, and T cell clone expanding, enabling NK cells to be the first primary killer against tumor cells. Other immune cells like neutrophils and Dendritic cells (DCs) have negligible tumor cell-killing ability[128,129]. Tissue-

resident macrophages eliminate tumor cells relying on CD16-mediated antibody-dependent cellular cytotoxicity (ADCC) and phagocytosis (ADCP), which are much less effective for the lack of infiltrated tumor antigen-specific antibodies in solid tumors[130-132]. In many cases, especially for malignant cancer patients, tumor cells

downregulate MHC-I molecules on the cell membrane, which significantly inhibits their recognition by T cells and tumor-associated macrophages (TAM)[133-136]. Again, this immune evasion strategy does not work for antigen-independent NK cell killing and provides the second advantage for developing NK cell-based immunotherapy. Thirdly, NK cells also express CD16 and have ADCC-mediated target cell killing[132,137]. According to these, NK cells are robust and comprehensive tumor cell killers.

2.5.1 NK cell-mediated killing

NK cells are innate lymphocytes derived from bone marrow multipotent hematopoietic stem cells (HSCs) with an average 2 weeks of renewal cycle[138,139]. NK cells make up ~10% of peripheral lymphocytes[140-142]. The two major subtypes of are $CD56^{bright}$ $CD16^{-}$ NK cells and $CD56^{dim}CD16^{+}$ cells. $CD56^{bright}$ NK cells are mainly located in lymphoid tissue, like bone marrow, secondary, liver, and skin, with robust cytokine-releasing ability[143]. On the contrary, $CD56^{dim}$ NK cells are primarily circulated in the bloodstream and are therefore the major circulating subsets, representing at least 90% of all blood NK cells[144]. $CD56^{dim}$ NK cells store a large number of effector proteins, granzyme B, and perforin, and have strong target cell killing ability[145]. $CD56^{bright}$ NK cells are thought to differentiate into $CD56^{dim}$ cells[146,147]. Mounting research showed that NK cell number and function status are highly associated with cancer patients' survival[148]. NK cells have been developed as potential immunotherapy targets for cancer patients[149,150]. One important role of NK cells is to target virus-infected cells or transformed cells through a mechanism different from T cells. $CD8^{+}$ T cells can only utilize TCR to bind to the antigen presented on the tumor MHC-I. Instead, NK cells have a series of germline-encoded activating/inhibitory receptors[142,151,152](Figure 2-

6). NK cells' inhibition/activation upon engaging with transformed cells relies on a signal strength from multiple inhibitory/activating receptors[152,153]. Transformed cells usually express several stress-induced ligands in the cell membrane, like MICA/B and ULBPs[154,155]. These can all bind with the NK cell activating receptor NKG2D. Besides, NK cells have many other activating receptors (Figure 2-5) which can also activate NK cells alone or together. Besides, NK cells can bind with inhibitory ligands (e.g., HLAs)[142]. Another type is non-MHC molecules like PD-L1 [156]. If signals transferred from activating receptors are higher than inhibitory ones, NK cells will turn to be activated to release cytokines like TNF-α, IFN-γ, and effector proteins granzyme B and perforin. On the contrary, if signals transferred from activating receptors are lower than inhibitory ones, NK cells will turn out to be inhibited and disassociated from the target cell[25] (Figure 2-6). NK cells adopt three ways to induce tumor cell apoptosis: ①secretion of cytokines, ②degranulate, and ③death receptor.

TNF-α belongs to the TNF family. By binding to the TNF receptor, it initiates the NFκB signaling pathway and exerts direct anti-tumor activity by inducing apoptosis or necrosis of tumor cells, destruction of vasculature, and severe thrombosis among tumors[157].

IFN-γ is the only member of type II interferon. By binding with IFNGR1 or IFNGR2, IFN-γ initiates the JAK-STAT1 signaling pathway and induces a series of interferon-stimulated genes(ISGs) like OAS proteins, CIITA, B2M, GBPs, MHC-I, MHC-II, IRFs, ICAM-1, VCAM-1, CD44, and NCAM-1, through which IFN-γ induces tumor cells' apoptosis or stressed phenotype, which can make cells easier for immune cell recognition[158,159].

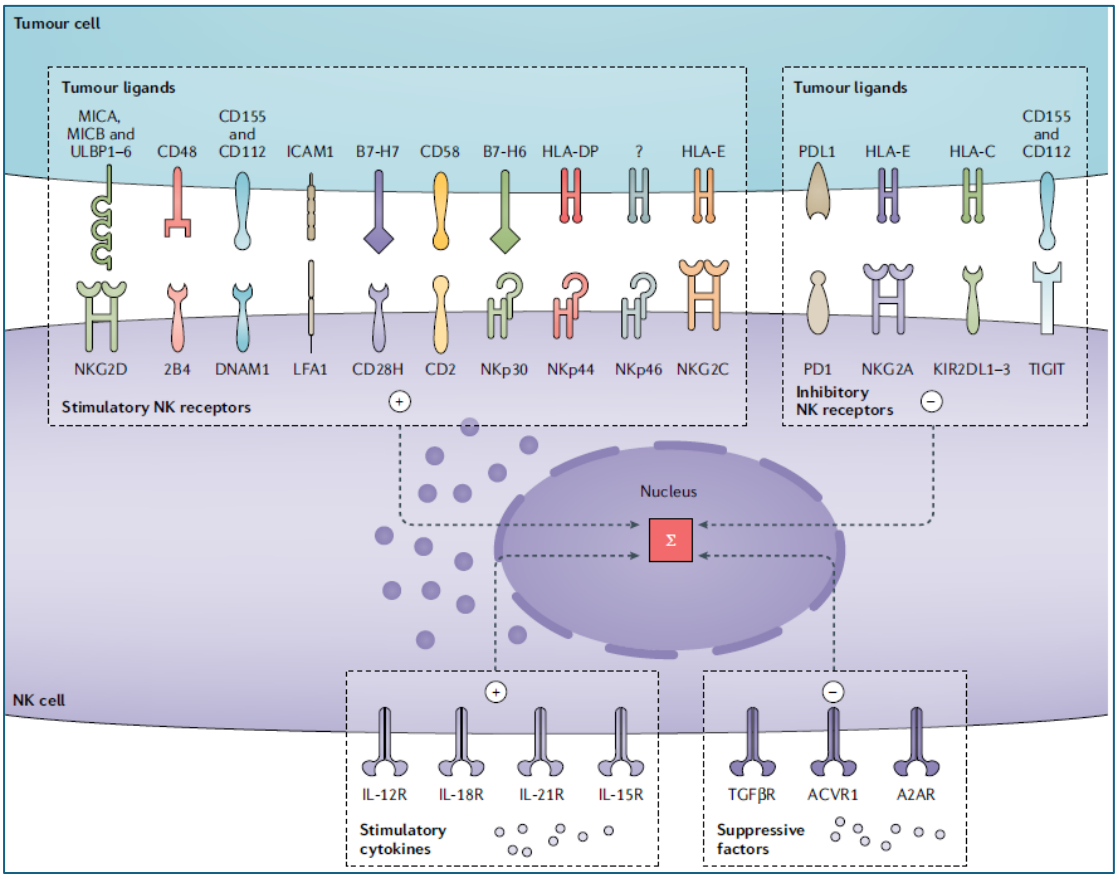

Figure 2-5 NK activating/inhibitory receptors and their ligands[142].

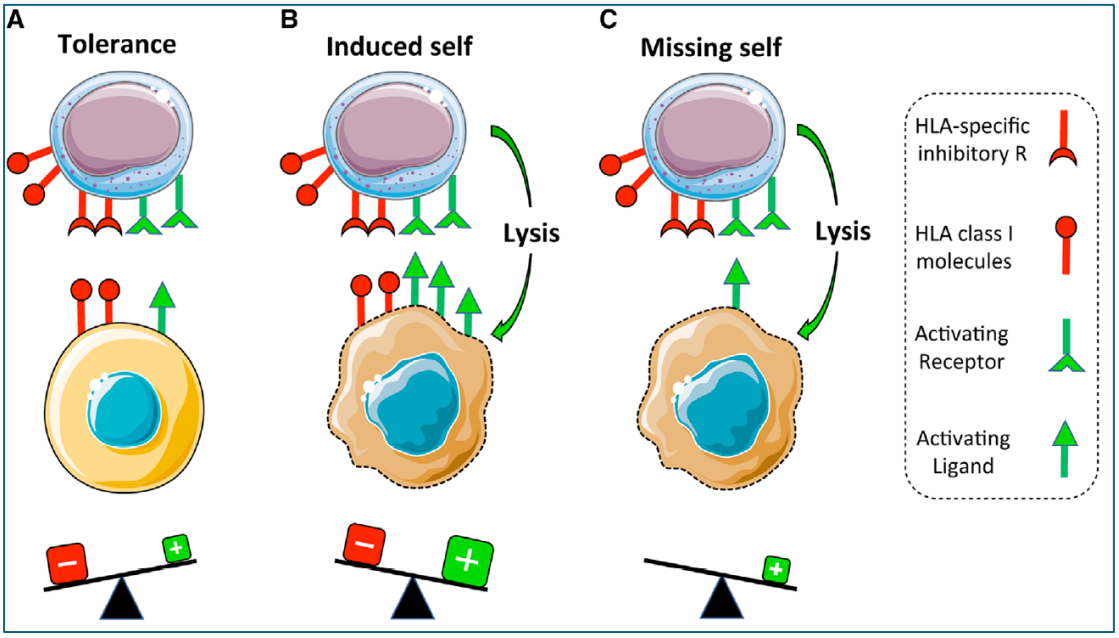

Figure 2-6 Determination of NK cell function by target cell ligands.[25]

NK cells express the TNF-related apoptosis-inducing ligand (TRAIL), which can recognize the TRAIL receptors I and II (DR4 and DR5) on tumor cells. The binding of DR4 or DR5 with TRAIL directly recruits several proteins and forms the death-inducing signaling complex (DISC). Caspase 8 is then activated and induces subsequent caspase 3-mediated apoptosis[160]. Although TRAIL can be cleaved as a soluble as, cytokine membrane-bound TRAIL seems to dominate NK cell-mediated apoptosis[161]. Compared to cytokines and TRAIL, pore formation protein perforin and effector protein granzyme B are believed to be the major executors.

2.6 Mechanical regulation of NK cells

NK cells belong to nonspecific immunity, and function at the initial line of host defense against virus infection and tumor progression[162,163]. To fulfill these goals, NK cells need to continuously scan the whole body from blood/lymph node vessels to different tissues for dangerous signals so that they can arrive at the organs of disease at the earliest time point[163]. During these processes, NK cells have to encounter environmental mechanical stimulations like fluid shear stress, confinement spaces during intravasation/extravasation, extracellular matrix (ECM) stiffness, extracellular fluid viscosity alteration, tissue compression force, stretching force, and tensile force arising from the rhythm of heartbeat and breath[164]. Once arriving at tissues of diseases, NK cells may recognize target cells with different cell mechanical properties[165,166]. How these mechanical cues regulate NK cell recruitment, metabolism, epigenetic phenotype, and functions is still largely unknown.

2.6.1 NK cell mechanics

NK cell cytoskeleton controls its mechanics. VAV-Rac pathway-induced actin polymerization leads to lamellipodium formation and promotes stable conjugation with target cells[167]. Microtubule organizing center (MTOC) polarization upon NK cell activation delivers effector proteins toward the immune synapse[168]. When seeded on MICA-coated nanowires, 10 pN traction force can be actively generated by NK cells,

indicating a contractile force-gated NK cell activation[169]. Matalon *et al*[170] also observed that SHP-1, a key regulator of inhibitory signaling molecules, was regulated by the actin dynamics of NK cells and finally regulated NK cell status. The finish of target cell killing is through mechano-sensing of increased target cell contractile force after granzyme B-induced Rho-associated protein kinase (ROCK) activation[171]. Through targeting actomyosin contractility, mechano-sensitive TAZ but not YAP limits NK cells' cytotoxicity. Utilizing a synthetic double-stranded RNA, Hilton enhances RhoA and myosin light chain activity and triggers TAZ cytoplasm compartmentalization, which limits c-Myc-initiated granzyme B and perforin transcription[172]. Transcription factor Eomes was claimed to be mechanically sensitive to NK cell actomyosin contractility alteration and translocated to the nucleus upon hypertonic and tumor growth factor β (TGF-β) treatment[173]. NK cell stiffness was found to impair its passage through blood vessels and dense tissues, which could be reversed by inhibiting the cytoskeleton[174]. However, reducing cell stiffness also compromised NK cells' cytotoxicity against tumor cells[174]. Similarly, interleukin II (IL2), secreted by activated helper T cells to stimulate effector killer cell proliferation and activation, was found to stiffen NK cells in vitro for up to 96 h after withdrawing IL2[175]. These findings indicate that NK cell-generated contractile force promotes activation, and NK cell stiffness may promote target cell killing but impair extravasation from blood/lymph node vessels and migration among tissues.

2.6.2 Substrate/target cell stiffness

Lital Mordechay et al[176] reported that NK cell activation was substrate stiffness-dependent when NK cells were seeded on an MICA-coated surface. Although CD107a (activation marker) expression is highest when NK cells are seeded on a 150 kPa substrate. It is worth noting that most human tissues are much softer than this. *Friedman et al* [177] observed similar phenomena (higher level of activation markers like cytokine secretion and degranulation) when stimulating NK cells with stiffer substrate or beads. Although tumor tissue is stiffer than adjacent normal tissues, tumor cells are relatively

softer than healthy ones. Malignant tumor cells are even softer[178-180]. Tumor cell softness is utilized to evade T cell surveillance by impairing the membrane pores of perforin[181,182]. Cancer stiffening through depleting membrane cholesterol shows similar enhanced anti-tumor potential[183]. However, whether tumor cell stiffness rather than ECM or bead stiffness can affect NK cell activation and cytotoxicity remains elusive.

2.6.3 Mechano-sensing

Cells sense, transduce, and respond to mechanical inputs, which is defined as mechano-transduction[184]. Although much work has been done about the mechanical response of NK cells to ECM stiffness, little is now known about how NK cells sense ECM elasticity or other mechanical cues. More recently, *Juan Fan* and her colleagues[185] demonstrated that NKG2D, a typical activating receptor of NK cells, could discriminate diverse ligands recognizing the differences between force-induced 3D structure alterations. It is observed that the binding of NKG2D with MICA/MICB but not UPBPs has a force-dependent catch-bond signature, that is, with the increase of loaded stretching force on NKG2D-MICA/B molecules conjugate the bond lifetime/affinity also increases. After rising to a threshold value, however, the bond lifetime/affinity decreases with the increase of the loaded stretching force. This catch-bond signature was confirmed by both BFP and MD. This study suggests NKG2D could be a potential mechanical sensor.

2.7 Metastasis: a force journey of cancer cells

Cancer progression and metastasis have long been considered a process of biological transformation driven by intrinsic genomic changes. However, over the past 2 decades, researchers have begun to appreciate that mechanical changes in cells and tissues are involved in this process. More and more research has found that metastasis can be inhibited by targeting the mechanical properties of tumor cells or ECM, termed as mechanical checkpoints of cancer progression and metastasis. From a mechanical perspective, metastasis is a force journey in each step. Targeting force sensors like integrins and Yes-associated protein (YAP) has been proven effective for inhibiting metastasis[186,187].

2.7.1 Mechanical cues within solid tumors

Due to the outgrowth of tumor cells, imbalance of entry and exit of fluids into the interstitial space[188], and continuous deposition of ECM over its degradation[189], tumor cells undergo a significant increase in compression. ECM deposition and expression of ECM crosslinker protein LOX induce stiffening of tumor tissue[190]. It has been found that most solid tumors are stiffer than the surrounding tissues and the counterpart healthy tissues, like breast tumors, liver cancer, pancreatic ductal adenocarcinoma, and colorectal carcinoma[191]. ECM deposition is mainly derived from cancer-associated fibroblasts (CAF). Besides, CAF also positively exerts a considerable actomyosin-generated contractile force on ECM through adhesion molecules, mediating an additional strain-induced stiffening[192]. Stiffened ECM activates tumor cell mechano-sensors like Yap, which is a transcription regulator, and promotes proliferation-associated gene expression. Furthermore, stiff ECM induces epithelial-mesenchymal transition (EMT) characterized by increased expression of twist, snai1, N-cadherin, vimentin, and decreased E-Cad expression[193,194].

2.7.2 Confinement during migration and invasion

To migrate and invade through tissues, tumor cells must break down the dense basement

membrane and squeeze among the fibrillar ECM. The pore size varies between tissues but is typically much smaller than the tumor cell and nucleus size. Tumor cells secrete matrix metalloproteinases (MMPs) at invasive protrusions to mediate the degradation of ECM proteins. Compression forces and confinement reshape tumor cells and nucleus morphology. Multiple mechanisms have been proposed to resist these force challenges. Confinement lower than the most nuclear diameter of tumor cells (~3μm) significantly reduces the nuclear envelope excess of the perimeter, increasing the nuclear envelope and associated endoplasmic reticulum tension. As a result, calcium is released from the endoplasmic reticulum, and actomyosin is relocated and activated to protect the nucleus[195]. Both microtubules and actin filaments are redistributed and reinforced to position the nucleus and protect it from rupture[196,197].

2.7.3 Fluid shear stress and CTCs

FSS regulates the survival and metastatic potential of CTCs. The magnitude of FSS in physiological conditions varies according to location (capillaries, veins, or arteries). Typical range is between 1 ~ 30 dyn/cm^2[198]. FSS was shown to directly kill more CTCs under large magnitudes or with more time[28,63], which could be attributed to direct physical damage[199] or apoptosis[200]. Sensitivity to cytokine-induced apoptosis can also be enhanced[201]. While malignant tumors seem to be more resistant to FSS-induced damage. Actomyosin was pointed out to protect CTCs from damage in circulation[28,199]. Our previous work also found that upregulated histone acetylation in FSS-treated CTCs mediated nuclear expansion and promoted CTC survival[202]. Besides, FSS was shown to induce EMT[63,203], promote stemness[204], and enhance drug resistance[205].

2.8 Cell mechanics in cancer

Apart from outgrowth, alteration of cell mechanics is another feature of transformed tumor cells[206]. Cell mechanics mainly includes cellular mechanical properties, mechano-transduction (force transmission from the extracellular space to the cytoplasm

and nucleus), and cell-generated forces. The cell membrane, cytoskeleton, and nucleus are the main components of cell mechanics[207,208]. Among these, the plasma membrane is too soft and mainly contributes to the mechanical regulation of membrane proteins like mechano-sensitive ion channels PIEZO1/2, TRPVs, and TRPMs through membrane tension[209-211]. The nucleus is the stiffest structure in a cell, but its relatively small size limits its role to a confined microenvironment during migration/invasion. The cytoskeleton is an interlinking filament network mainly present at the cortical layer and the cytoplasm. Its main function includes maintaining cell shape, withstanding and transducing mechanical forces, carrying intracellular cargo, mediating cell movement, and so on.

2.8.1 Cytoskeleton

Microtubule, intermediate filament, actin filament, and their associated proteins contribute to the cytoskeleton[207]. The expression level, filament structure, posttranslational modification, and crosslinking between themselves and each other are the sources of cell mechanical variability. **Actin filaments** (F-actin) make up 1 to 10 percent of total proteins in most cells, and muscle cells have even higher concentrations[212,213]. Three types of actin isoforms are expressed in vertebrates: α, β, and γ-actin. Non-muscle cells mainly express β and γ-actin. Monomers of globular actin (G-actin) form linear polymers by binding to each other in a head-to-tail way. At the barbed (plus) end, ATP-G-actin has a higher affinity, leading to a fast-growing. ADP-G-actin dissociates at the pointed (minus) end. The overall effect of continuous polymerization and depolymerization at the opposite ends maintains a relatively steady state of F-actin, and this dynamic status is defined as actin filament treadmilling[214]. Many actin-associated proteins are involved in the dynamics of F-actin. Polymerization is initiated by Arp2/3-mediated nucleation. Arp2/3 also functions as an initiator for the branching of F-actin, especially for filopodia formation[215,216]. Formins and profilin promote elongation[217,218]. The dynamics of F-actin are the key to its function, like migration. Polymerization of actin generates forward pushing forces at the leading edge.

Depolymerization and myosin activity generate retracting forces at the trailing edge. Malignant breast cancer cells usually exhibit high motility, which relies on the quick dynamics of F-actin. Actin filament is the main contributor to cell stiffness, among others[219]. Basically, both tumor tissues and tumor cells are highly heterogeneous in stiffness[27]. However, recent investigations have suggested a negative correlation between tumor cell stiffness and malignancy. Breast tumor cells have 40-66% fewer actin filaments and are softer than healthy breast cells detected by immunofluorescence and atomic force microscope (AFM)[220]. Invasive breast tumor cells are usually mesenchymal-like and even softer compared with more epithelial-like non-invasive breast tumor cells[221]. Soft breast tumor cells have been found to have higher stemness, which can form a tumor with 100 cells in immunologically competent mice. These soft cells upregulate Wnt signaling protein BCL9L and gain enhanced stemness and tumorigenicity[222]. Softness renders a cell with advantages in both migration, invasion, and stemness[222].

Actin filament dynamics can be regulated by selective drugs. Cytochalasin D (Cyto D), originating from a fungus, specifically binds with the barbed end of F-actin and inhibits both assembly and disassembly of G-actin. Latrunculin A and B, derived from sponges and nudibranchs, bind with G-actin and block actin polymerization[223]. Besides, they also bind with F-actin with relatively lower affinity but sever and depolymerize actin filaments[224]. On the contrary, Jasplakinolide (JAS) directly binds with F-actin and promotes polymerization[225,226].

2.8.2 Cell tension

Cell tension is the combination of cell membrane tension and cortical tension. Membrane tension is defined as the force needed for the deformation of a unit length of the cell membrane lipid bilayer. Cortical tension is the force for the deformation of cortical actin filaments. Membrane tension is driven by the disturbance of the

equilibrium distance between phospholipid molecules, mainly including phosphatidylcholine, phosphatidylethanolamine, phosphatidylserine, sphingomyelin, and inositol phospholipids (PPIs)[227]. Among them, PPIs exhibit less abundance but have primary roles in signaling transduction and cell tension control. By phosphorylating the inositol ring at positions 3, 4, and 5 PPIs have three PIP subtypes: phosphatidylinositol-5-phosphate (PI5P), PI4P, PI3P; three PIP2 subtypes: phosphatidylinositol-(3, 4)-bisphosphate (PI(3,4)P2), PI(3,5)P2, PI(4, 5)P2; and a PIP3: phosphatidylinositol (3,4,5)-trisphosphate (PI(3,4,5)P3). PI(4, 5)P2 (commonly called PIP2) is primarily located in the cell membrane and contributes to less than 1% of all PPIs[228]. PIP2 is the only PPIs that bind ERM proteins through which the ccell membrane is anchored to the underlying cortical actin filaments and contributes to cell tension[229]. ERM proteins have a plasma membrane-associated FERM that binds with PIP2, a long α helical propensity, and a C-terminal domain that binds with F-actin (active status) or with itself at the FERM domain (inactive closed status). The head-to-tail binding of FERM with the C-ERMAD domain will generate a closed conformation with an inactive status, masking the binding site with F-actin[230,231]. A two-step activation model for ERM proteins has been introduced: first, ERM proteins are recruited to PIP2-enriched plasma membrane regions, which renders relatively high accessibility of ERM kinase to the phosphorylation site of ezrin at Thr576, or Moesin at Thr558, or Radixin at Thr564. Together, ERM proteins will shift from a self-inhibited conformation to an active conformation, exposing the binding sites for F-actin at the C-ERMAD domain[232,233]. In vertebrate cells, Ras homolog family member A (RhoA), Rho kinases (ROCK1, ROCK2), protein kinase Cα (PKCα), PKCθ, NF-κβ-inducing kinase (MAp3K14/NIK), lymphocyte-oriented kinase (STK10), STE20-like serine/threonine-protein kinase, Cyclin-dependent kinase 5 (CDK5), sphingosine kinases (SK1, SK2), and Serine/threonine-protein kinase MRCK α can phosphorylate respective Thr sites of ERM proteins at the C-ERMAD domain[234-238]. ERM proteins can also indirectly connect with the plasma membrane through adaptor proteins like ezrin-Radixin-Moesin-binding Phosphoprotein 50 (EBP50) and Na+/H+ exchange

regulatory factor 2 (NHERF2) or through binding with receptor tyrosine kinases (RTKs), epidermal growth factor receptor (EGFR), platelet-derived growth factor receptor (PDGFR), hepatocyte growth factor receptor (HGFR), adherent proteins like CD44, CD43, intercellular adhesion molecule 1 (ICAM1) and ICAM2[239-242]. On the contrary, dephosphorylation of ERM proteins at the same Thr sites by protein tyrosine phosphatase type IV A1 (PTP4A1) and protein phosphatase 1 regulatory subunit 12A (PPP1R12A) [243,244]. Calpain 1 (CAPN1) can directly target the α helical domain of ERM proteins and release the tethering of the plasma membrane from the cortical actin filaments[245]. Since cortical tension and membrane tension are hard to decouple, we use membrane tension from here to represent both.

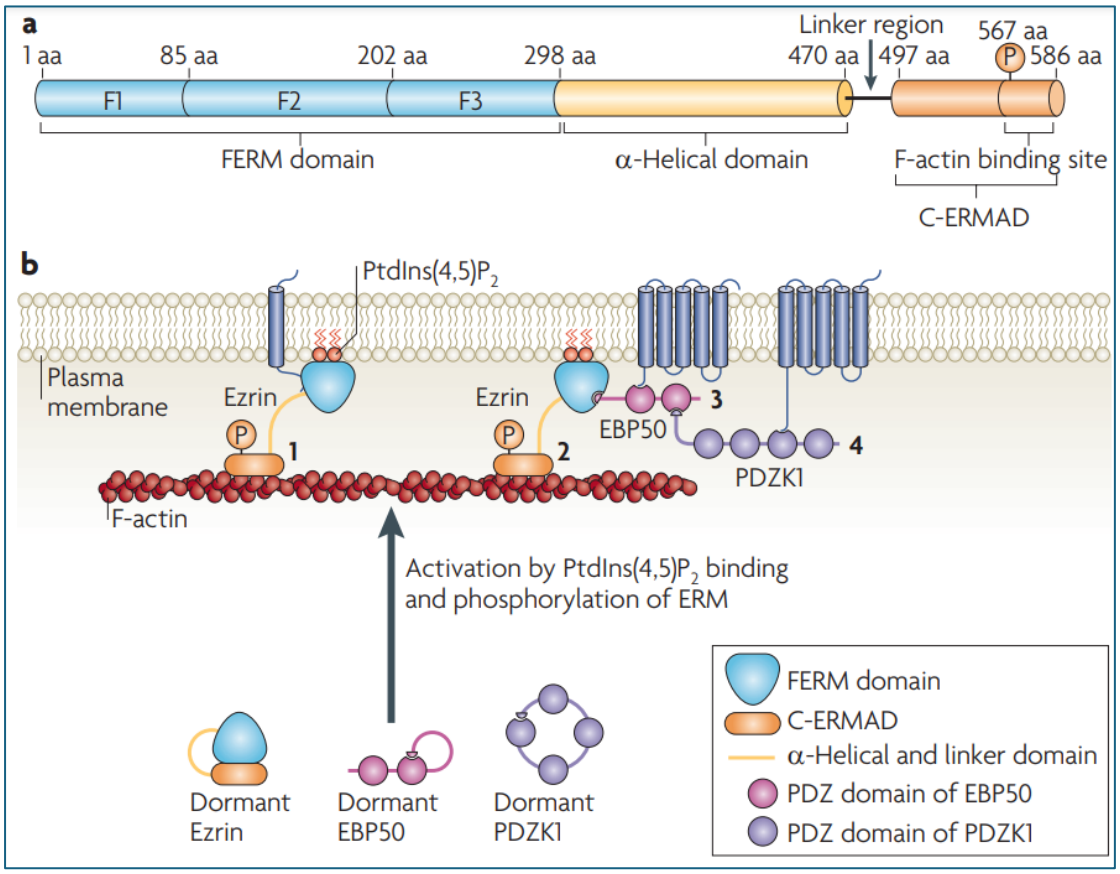

Figure 2-7 Structure and binding of ezrin with PIP2[230]

Chapter 3: Materials and Methods

3.1 Animals

Female, 4–6-week-old, BALB/c nude mice were purchased from Centralized Animal Facilities of The Hong Kong Polytechnic University. The serve immunocompromised female NOD/SCID mice, 4-6 weeks of age, were purchased from the Laboratory Animal Services Centre of the Chinese University of Hong Kong. All the animals were raised in pathogen-free centers at The Hong Kong Polytechnic University. All experiments were approved by the Animal Subjects Ethics Subcommittee of The Hong Kong Polytechnic University.

3.2 Cell lines

The NK92 cell line was generously provided by Prof. Sun Lei (The Hong Kong Polytechnic University). MDA-MB-231 and MDA-MB-231-derived brain/bone metastasis breast cancer cell line TGL-BrM/TGL-BoM were purchased from Memorial Sloan Kettering Cancer Center. MDA-MB-468 breast cancer cell line and A549 lung cancer cell line were purchased from ATCC. The human brain endothelial cell line, HCMEC, was purchased from FuHeng Biology. The human umbilical vein endothelial cell line, HUVEC, and human astrocytes isolated from the human brain were kind gifts from Prof. Mo YANG (The Hong Kong Polytechnic University). The HEK-293T cell line was generously provided by Dr. RUAN Yechun (The Hong Kong Polytechnic University). NK92 cell line was maintained in MEM-α (Gibco), which was added with fetal and horse bovine serum (12.5% FBS + 12.5% HBS) (Gibco), 200 μM inositol (Sigma), 100 μM β-mercaptoethanol (Sigma), 20 μM folic acid (Sigma), 100 U/ml recombinant human IL-2 (Peprotech), and 1% penicillin/streptomycin (P/S, Gibco). The HCMECs were maintained in human endothelial medium (Gibco) supplemented with 5% FBS, 200 ng/mL human basic fibroblast growth factor (bFGF; PeproTech), and 1% P/S. The HUVECs were maintained in human endothelial medium (Gibco). The astrocytes were maintained in DMEM (Gibco).

For other cancer cell lines, cells were cultured in Dulbecco's Modified Eagle Medium (DMEM, Gibco), containing FBS (10%) and P/S (1%). All cells were cultured in 5% CO_2 at 37°C.

3.3 Co-culture assay

For simple co-culture of MDA-MB-231/MDA-MB-468/A549 cells with NK cells, tumor cells in a complete DMEM culture medium were seeded on collagen I-coated cell culture dishes. After total spreading (0.5-3 h), the same volume of NK92 cell culture medium containing 4-fold numbers of NK92 cells was added to the tumor cell-seeded culture dishes for 24 h. After co-culture NK92 cells in the culture medium were washed out with PBS, and fresh full DMEM was added to the culture dishes. For the lack of human IL-2, the remaining NK92 cells in the dishes would undergo apoptosis within 24-48 h. Surviving tumor cells without NK92 cells would be collected for experiments.

For co-culture of mixed tumor cells with NK cells, tumor cells with low and high membrane tension were first stained with a Green/Deep Red cell tracker (Gibco) for distinguishment and then mixed at the ratio of 1:1. The mixed tumor cells then were seeded on collagen I-coated cell culture dish followed by addition of NK92 cells as mentioned above.

3.4 Transfection

The plasmids used in this study are listed in Table 1. The virus was generated through co-transfecting targeting plasmids with packaging and envelope plasmids into HEK-293T cells. The collected virus-containing suspension was further concentrated with a virus concentrating solution (20% w/v PEG8000 + 3.5% w/v NaCl in water) at a ratio of 1:4 (virus concentrating solution: virus suspension). Shake the solution mixture every 15 minutes for 4 times, and maintain it at 4°C overnight. After centrifugation at 3000 g × 40 min, the virus could be obtained. For NK cells, 2×10^5 cells in a 24-well plate were pre-treated with 6 μM BX795 (InvivoGen) was started 30 min before transduction and continued during the transfection process. 100-200 μL virus solution

was added to the wells. A centrifugation at 1000 g×1 h was conducted to promote transfection efficiency. After incubation at 37°C, 5% CO_2 for 5 h, the supernatant was replaced with fresh full medium. For other cells, 2×10^5 cells in a 24-well plate were transfected with 20-100 μL virus solution together with 6 μg/ml polybrene. 5 h later, the supernatant was replaced by fresh full medium. Successfully transfected cells were validated by RT-qPCR and enriched by selective drug treatment.

For KLRK1 gene knocking down, 6×10^5 cells in 400 μL Opti-MEM medium (Gibco), which contains 10 nM KLRK1-targeting siRNA (Invitrogen), were added to the chamber of the Gene Pulser Xcell Electroporation Systems (Bio-Rad). 3 pulses of electroporation with 150 μF plus 300 V were conducted. 48 h later, the RT-qPCR was adopted to confirm the knockdown efficiency.

In some experiments, ROCK1-targeting siRNA was introduced into MDA-MB-231 cells with lip3000 (Invitrogen). Briefly, MDA-MB-231 cells were first seeded on a collagen I-coated 6-well plate. A final concentration of 75 pM siRNA within 250 μL Opti-MEM medium plus 7.5 μL lip3000 was added to each well. Fresh growth medium was added to replace the supernatant after 6 h. The knockdown efficiency of target genes was measured using qRT-PCR and immunofluorescence.

Table 1 List of plasmids and siRNAs

Plasmids	**Source**	**Cat. No.**
Lifeact-tdTomato	Addgene	64048
mTurquoise2-Paxillin	Addgene	176107
Ezrin	oobio	H37899
PH-PLC-delta-EGFP	Addgene	136998
PH-Akt-Cerulean	Addgene	50837
CA-ROCK	Addgene	84649
granzyme B FRET sensor	Addgene	59587
FOXO1 reporter	Addgene	67759
Lck FRET sensor	Addgene	131584

NDRG1 reporter		
psPAX2	Addgene	12260
pMD2.G	Addgene	12259
si-RNAs		
si-ROCK1	Silence	142844
KLRK1 siRNA	Silence	108247
Negative Control siRNA	Silence	AM4641

3.5 Shear Stress Treatment

The blood flow-mimicking in vitro circulation system (Figure 5-1-1 **A**) was set up as mentioned before[63]. Briefly, it is mainly composed of a peristaltic pump (Harvard Instruments) as a force generator, a silicone microtube (0.255 mm radius) to mimic the blood vessel, and a syringe as a pool of the cell suspension. The system could simulate blood FSS by producing a continuous pulsating flow. According to Poiseuille's law, the wall shear stress (WSS) in the microtube can be calculated by $\tau = \frac{4\mu Q}{\pi R^3}$. Here, μ represents the viscosity of the cell suspension (0.001 Pa), Q represents the flow rate of the cell suspension, and R represents the radius of the microtube. The whole circulation system was pre-treated with 1% BSA (Sigma) to prevent non-specific attachment of CTCs. The FSS treatment under 0-20 dyn/cm^2 was conducted at 37°C and 5% CO_2 for 4 h.

For WSS treatment, the above circulation system was connected to a fluid chip. The chip was pre-coated with recombinant human MICA or ICAM-1, or the chip was coated with poly-D-lysine followed by tumor cell seeding. NK cells in suspension spontaneously attach to the chip surface with WSS treatment.

3.6 Cytotoxicity assay

For measuring NK92 anti-tumor cell cytotoxicity in suspension, these two cells were

pre-stained with deep red and green dyes (Invitrogen), respectively, followed by mixing NK92 cells and tumor cells at a ratio of 4:1 for 4 h under a series of FSS treatments. Propidium iodide (PI, Beyotime) was used to indicate apoptotic tumor cells after finishing treatment. Tumor cell lysis ratio (Lr) was detected by flow cytometry (BD FACSymphony A3 Cell Analyzer, BD Biosciences) and calculated according to the following formula:

$$Lr = (1 - survived\ target\ cell\ number/total\ target\ cell\ number) * 100\% \quad ①$$

The increment was calculated by:

$$Increment = (Lr_{NK\_5\ dyn/cm^2} - Lr_{Spontaneons}) - (Lr_{NK\_0\ dyn/cm^2} - Lr_{Spontaneons}) - (Lr_{5\ dyn/cm^2} - Lr_{Spontaneons}) \quad ②$$

The relative increment was calculated by:

$$Relative\ Increment = {Increment}/{(Lr_{NK\_0\ dyn/cm^2} - Lr_{Spontaneons})} \quad ③$$

In some experiments, caspase 3 activation was used as a marker to indicate tumor cells' apoptosis. Briefly, Caspase-3 Substrate (Beyotime) at a final concentration of 5 μM was added to the cell suspension after co-culture. Following incubation at 37°C, 5% CO_2 for 20 minutes, the caspase 3^+ tumor cells were imaged by fluorescent microscope (Nikon Ti2). The incremental calculation of the caspase 3^+ ratio after combined treatment of NK cells and FSS was similar to formula ②.

In another experiment, target cell death was detected using fluorescent imaging, indicated by propidium iodide under WSS treatment. The increment of the propidium iodide positive ratio calculation was similar to formula ②.

In some experiments, TNF-α (Abcam) or IFN-γ (Abcam) were used to treat tumor cells under static conditions or FSS to detect their contributions to MDA-MB-231 cell death.

In some experiments, NK92 cells were treated with anti-Trail antibody before and during the co-culturing process to detect the death receptor's contribution to MDA-MB-231 cell death.

3.7 ELISA assay

The secretion level of cytokines in the cell suspension after co-culture and FSS treatment was detected by ELISA (Abcam). The supernatants were collected after centrifugation and directly quantified by the Thermo Scientific Varioskan LUX Multimode Microplate Reader without further dilution.

3.8 qRT-PCR

For analysis of mRNA expression, tumor/NK cells were collected, and then total RNA was isolated with the NucleoSpin RNA Plus Kit (TAKARA). We assessed the RNA purity and concentration by using the NanoDrop™ (Thermo). We generated the complementary DNA by using the PrimeScript RT Master Mix (TAKARA). RT-qPCR was conducted with Forget-Me-Not EvaGreen qPCR Master Mix with Rox (Biotium) using the ABI QuantStudio 7 Flex Real-time PCR System (Thermo). The primers were designed and purchased from Thermo and are listed below. For gene expression quantification, the ΔΔcycle threshold method is used with GAPDH as an internal reference for normalization.

Table 2 List of primers

Gene	Forward (5'-3')	Reverse (5'-3')
IL-6	CCTTCTCCACAAACATGTAACAAGA	TCACCAGGCAAGTCTCCTCA
CXCL8	AGAAACCACCGGAAGGAACC	AATCAGGAAGGCTGCCAAGA
EREG	CTGCCTGGGTTTCCATCTTCT	GCCATTCATGTCAGAGCTACACT
EZR	ACCGTGGGATGCTCAAAGATA	CAAGGGCATCAACTCCAAGC
GAPDH	AGCCGTTAGGAAAGCCTGC	GCCCAATACGACCAAATCAGAG
HBEGF	GGACCCATGTCTTCGGAAAT	CCCATGACACCTCTCTCCAT

HLA-ABC	CCACTCACAGACTGACCGAG	TGGATGGTGTGAGAACCGTC
HLA-E	AGGAAGAAGAGCTCAGGTGGAA	CAAGGCAGCTGTGCATCTC
ITGB3	CCGTGACGAGATTGAGTCA	AGGATGGACTTTCCACTAGAA
KLRK1	AATTCTAGATCAGGAACTGAGGACA	TGCACAAAGGATTCCTGCTCA
LTBP1	CTTCCCCTGCCCGGTCT	CTGCATCTTTATAGTTCTCACCACCA
MICA/B	ACCAGAAAGGAGGCTTGCAT	GGGCACTGTCGATTCTTGAGT
MSN	CCATGCCCAAAACGATCAGTG	ACCAAACTTCCCTCAAGCCA
PD-L1	TGGCATTTGCTGAACGCATTT	AGTGCAGCCAGGTCTAATTGT
PIEZO2	GACGGACACAACTTTGAGCCTG	CTGGCTTTGTTGGGCACTCATTG
PTGS2	TTCAACACACTCTATCACTGGC	AGAAGCGTTTGCGGTACTCAT
RDX	TGAGTTTGAAGCAATGTGGGG	CCATAAGTCAGTAGCCAGGGG
SERPINB2	GTTCATGCAGCAGATCCAGA	CGCAGACTTCTCACCAAACA
SERPINI1	TAAAAGAGTCCGCGTTGGGT	GGAGCCATCACTAAATTCCCCATAA
ULBP1/3	AGTTGTTTAGAGTGACAGGTGGAAA	GCACAGTGGTGAGTAGACAGG

3.9 Cell adhesion assay under FSS

To detect tumor cell adhesion to endothelial cells under FSS, a similar in vitro FSS system was used as mentioned above. First, HCMECs and HUVECs were stained with Green and Deep Red cell trackers, respectively, for distinguishment. Then, 0.1 million HCMECs/HUVECs were seeded into the microfluid chip (ibidi, Cat. No: 80166). After the formation of the endothelial monolayer (overnight growth in the microfluid chip), 1×10^5 control/co-cultured tumor cells were injected into the chip under 2 dyn/cm^2 FSS using the above system. Tumor cells spontaneously adhered to the HCMECs/HUVECs monolayer, which was continuously captured by a fluorescent microscope (Nikon Ti2). Adhesion events within 5 min were used for statistical analysis.

3.10 Trans-BBB migration assay

Transwell inserts with 3 μm pore size (Corning, cat. no. 3415) were first coated with collagen I on both sides for 1 h. The inserts were then washed and put upside down in a 30 cm sterile dish, followed by adding 1×10^5 primary human astrocytes onto the insert. The dish was placed into the incubator (Thermo) for 5 h to allow attachment of astrocytes. Then the inserts with adhered astrocytes were placed back into a 24-well plate with 500 μL complete DMEM in each well. 5×10^4 HCMEC/HUVEC endothelial cells within 150 μL DMEM (containing 1% FBS) were added into the inserts. The plate was then placed back into the incubator for 3 days without perturbation. 1×10^5 Control/co-cultured/other treated tumor cells were first labeled with a Deep Red cell tracker and then collected. 1×10^5 tumor cells were added to each insert. After 24 h, the inserts were then washed with PBS three times, followed by fixation with 4% paraformaldehyde (PFA). Cells on the inside bottom of the inserts, including the HCMEC/HUVEC endothelial cells and left tumor cells, were wiped out with swabs. The cells on the other side of the inserts, including trans-BBB/HUVEC migrated tumor cells (red) and astrocytes (green), were then stained with DAPI solution for 10 min, followed by washing with PBS. Blue (DAPI) and red double-positive tumor cells were captured and counted as trans-BBB/HUVEC migrated tumor cells using a fluorescent

microscope (Nikon Ti2).

3.11 Wound healing assay

Sterilized 500 μm gap inserts (ibidi) were placed on a collagen I-coated 6 cm cell culture dish. 70 μL of cell suspension (3×10^5 cells/mL of tumor cells) was added into both wells of the gap insert. The dish was then placed into an incubator for tumor cell attachment for 24 h. Avoid media evaporation and perturbation during the incubation. After 24h, confirm the formation of a 100% confluence of tumor cells with a microscope and detach the gap insert with sterile tweezers. Gently washed the cells to eliminate any non-attached cells. and carefully filled the cell culture dish with a pre-warmed culture medium. The gaps were captured at 6-12-24 h using the bright field of the microscope. The gap closure was analyzed using Image J.

3.12 Single-cell trajectory assay

The single-cell trajectory was conducted according to the manufacturer's instructions. Briefly, the μ-Slide Chemotaxis (ibidi, Cat. No: 80326) was placed into a sterile Petri dish with wet cotton around the slide to avoid evaporation. Use a 20 μL pipette (Eppendorf) to add 6 μL tumor cell suspension (3×10^6 cells/mL) into the adhering area of the slide. After full attachment of tumor cells, wash out the cells with pre-warmed PBS and refill it with worm culture medium. To create a chemotactic CXCL12 gradient, the normal culture medium and the CXCL12-containing medium were gently and respectively added into the left and right reservoir (Figure 3-1). Then placed the slide into the stage-top incubator of our inverted microscope (Nikon Ti2). After a ~20 min temperature equilibration, the single-cell trajectory was captured every 15 min overnight. The trajectory of single cells was measured using the Manual Tracking plug-in in Image J.

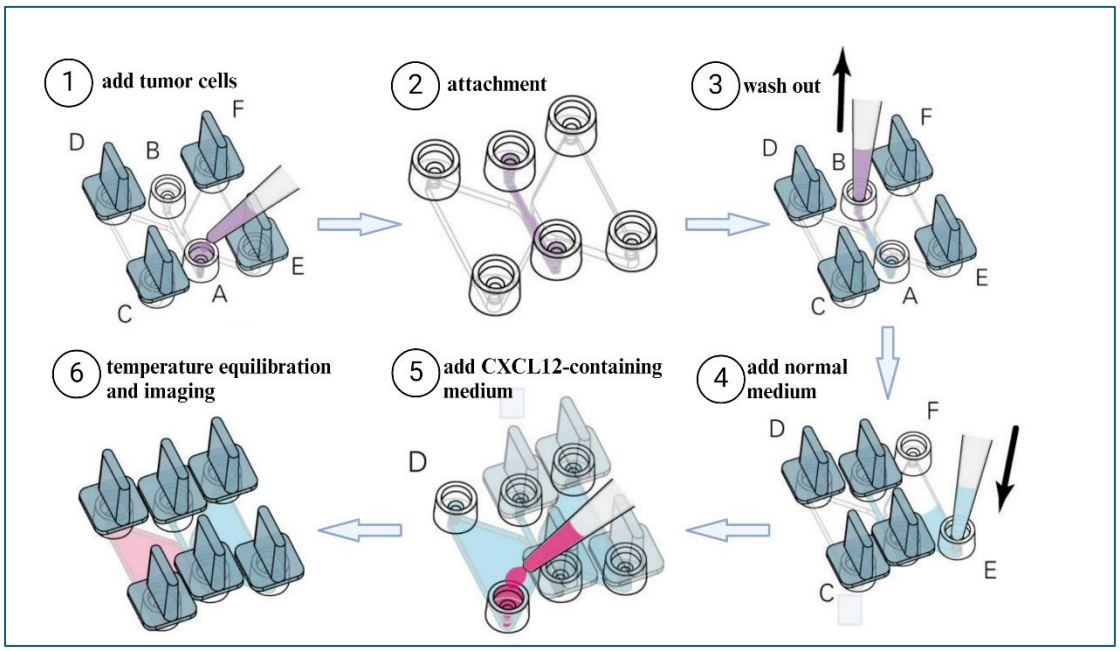

Figure 3-1 Diagram of single-cell trajectory assay

3.13 RNA-seq and bioinformatics analysis

For RNA-seq of MDA-MB-231 cells, 3 biological repeats of control and cultured tumor cells were collected. Tumor cells were lysed with TRIzol (Invitrogen) for transcriptome sequencing (oobio).

For spatial transcriptome analysis of patient-derived breast tumor tissue slides, the raw data (V1_Breast_Cancer_Block_A_Section_2) were downloaded from 10×genomics and analyzed with Loupe Browser 7.0.1. For the annotation of cell types, bar codes, which were NCAM1$^+$, IL2R$^+$, NCR3$^+$, KLRK1$^+$, KLRD1$^+$, GZMB$^+$, and CD3$^-$, were considered NK cell positive. CD3$^+$ plus CD8$^+$ or CD4$^+$ bar codes were considered as CD8 T cells and CD4 T cells positive. CD80$^+$, CD86$^+$, CCR5$^+$, TLR2$^+$, and TLR4$^+$ bar codes were considered as macrophage-positive. CD19$^+$, CD34$^+$, and PAX5$^+$ bar codes were considered as B-cell positive. CD33$^+$ and CEACAM8$^+$ bar codes were considered neutrophil-positive. IL6, PTGS2, Serpinb2, EREG, ITGB3, and CXCL9 were used to annotate brain metastasis-associated genes positive bar codes. IL11, IL1B, PTHLH, F2RL1, ADAMTS1, and FST were used to annotate bone metastasis-associated genes positive bar codes. F5, ABCC2, GIMAP2, DOCK5, FTCD, ADAMTS8, RNF138,

ACTL10, ABHD5, and DDR2 were used to annotate liver metastasis-associated genes positive bar codes. MFAP1, ROR1, ID1, ISG20, KYNU, JAG1, NR2F1, MAFN2, EPHX1, ROBO1, and EFEMP1 were used to annotate lung metastasis-associated genes positive bar codes. Gene scores were calculated as the sum of respective genes.

For single-cell RNA-seq analysis of primary tumor tissues, the online website Single Cell PORTAL was used. The data set, A single-cell and spatially resolved atlas of human breast cancer containing ER^+ (9 patients), $HER2^+$ (3 patients), and TNBC (8 patients), was used to analyze the correlation between EZR expression and brain/bone/lung/liver-associated gene expression.

For analysis of infiltrated NK cells, the online tool Timer 2.0 was used. The infiltrated NK cell numbers of primary tumors of breast cancer patients with and without brain metastasis were predicted from data sets GSE173661 and GSE248836. The correlation between the amount of infiltrated NK cells and the expression of EZR and brain-metastasis-associated genes was analyzed using the Immune Association module.

3.14 Membrane tension measurement

To detect tumor cell membrane tension, control or co-cultured tumor cells were seeded on collagen I-coated confocal dishes (Corning) at a confluence of about 30%. After fully attached (overnight), a final concentration of 1μM Flipper probe (Cytoskeleton, Inc., Cat. No. CY-SC020) was added to the tumor cells. After 15 minutes of incubation, the cells in the dish were ready for membrane tension measurements. The probe was maintained in the cell-containing medium during the whole imaging process, as it was fluorescent only when it bonded with the cell membrane. The Abberior Facility STED Super-resolution/Confocal Microscope was used to capture the lifetime of the probe. A pulsed laser with a 485 nm wavelength and a 600/50 nm bandpass filter was chosen for excitation and photon collection. For the time-lapse imaging of cell membrane tension and FOXO1 nucleus/cytoplasm translocation of the same cells, the FOXO1-clover-expressed MDA-MB-231 cells were seeded on collagen I-coated confocal dishes and

stained with the Flipper probe. Since the lifetime of fluorescent protein Clover is only 3.2 ns, which is much lower than the typical lifetimes of the cell membrane binding Flipper probe (>4 ns), a lifetime threshold setting of>4 ns was adopted for membrane tension analysis, which would not be influenced by excited photons from the Clover. After NK cell addition, both signals of the clover channel (FOXO1) and Flipper channel (membrane tension) were collected at respective time points. The lifetime of the probe was analyzed using Image J.

3.15 Cell morphology assay

Tumor cells with or without co-culture with NK cells were seeded on collagen I-coated 6-well plates. After 24 h, the cell morphological parameters, including spreading area and aspect ratio, were captured with the bright field of the Nikon Ti2 microscope and were analyzed with Image J.

3.16 Western blot

The total protein of control/co-cultured tumor cells or cells with other treatments was extracted with RIPA Lysis and Extraction Buffer (Thermo Scientific™, Cat. No. 89901) plus Protease and Phosphatase Inhibitor Cocktail (100X) (Thermo Scientific™, Cat. No. 78440). The extracted protein concentration was detected using the BSA assay (Solarbio, Cat. No. PC0001) as per the manufacturer's instructions. 20-50 μg total protein loaded with loading buffer (Bio-rad, Cat. No. 1610747) was used for electrophoresis, followed by transferring to methyl alcohol pretreated PVDF membrane (Millipore). The PVDF membrane was then blocked with blocking buffer (Beyotime, cat. no. P0252) for 15 min, followed by a quick washing with TBST buffer within 5 min. Respective primary antibodies were added to the membrane, which was kept at 4°C overnight. After washing the membrane with TBST for 15 min × 3 times, the secondary antibodies conjugated with HRP diluted in 5% BSA (1:2000) were then added onto the membrane, followed by incubation and TBST washing (3 times). The protein-containing PVDF membrane was developed with Clarity Western ECL

Substrate (Bio-Rad) and captured with the blot imaging system (Bio-Rad). The respective protein level was quantified with Image J and normalized to GAPDH. All the used antibodies were listed in **Table 2.**

Table 3 List of antibodies

Antibody	Source	Cat. No.
Akt polyclone antibody, human	Cell Signaling Technology (CST)	9272
Anti-Human CD107a-APC	Biolegend	328620
Anti-Human CD54 (ICAM-1)-PE	eBioscience	12-0549-41
Anti-Human Cox2	Abcam	ab188183
Anti-Human Ezrin	CST	3145
Anti-Human FOXO1	CST	2880
Anti-Human granzyme B	Abcam	ab134933
Anti-Human PhosPho-Akt	CST	9271
Anti-Human PhosPho-ERM	CST	3141
Anti-Human PI3K-P85	Abcam	ab191606
Anti-Human Serpin B2	Abcam	ab267463
Anti-Human γ-tubulin	Abclonal	A9657
Anti-Human ERM	CST	3142
APC anti-human CD355(NKp46) monoclone 9E2	Biolegend	831918
Asialo GM1 polyclonal antibody, functional grade	eBioscienc	16-6507-39
Donkey anti-Chicken IgY (H+L) secondary antibody, FITC	Invitrogen	SA172000
GFP polyclonal antibody	Invitrogen	A10262
Goat anti-mouse IgG-HRP conjugate	Bio-rad	1706516
488-conjugated mouse IgG antibody, goat	Abcam	ab150113
594-conjugated mouse IgG antibody, goat	Abcam	ab150116

647-conjugated mouse IgG antibody, goat	Abcam	ab150115
Goat Anti-Rabbit IgG-HRP conjugate	Bio-rad	1662408EDU
488-conjugated rabbit IgG antibody, goat	Abcam	ab150077
594-conjugated rabbit IgG antibody, goat	Abcam	ab150080
647-conjugated rabbit IgG antibody, goat	Abcam	ab150079
TRITC-conjugated Rat IgG antibody, goat	eBioscience	26-4826-82
Granzyme B-PE	eBioscience	12-8896-42
mCherry monoclonal antibody (16D7)	Invitrogen	M11217
MICA/B monoclonal antibody (6D4)	eBioscienc	14-5788-82
Anti-human Trail (CD253) monoclonal antibody	eBioscience	16-9927-82
CD314 monoclonal antibody, human	eBioscience	14-5878-82
Phospho-Gab2	CST	3882
Anti-phospho-PI3K p85 polyclonal antibody	Invitrogen	PA5118549
Phosphorylated human VAV1 polyclonal antibody	R&D	MAB37861
Human GAPDH polyclonal antibody, rabbit	Abcam	ab8245
Phosphorylated human PI3K monoclonal antibody, rabbit	Abcam	4257
VAV1 polyclonal antibody	Invitrogen	A305-671A-T

3. 17 Immune fluorescence staining

Cell fixation was conducted with 4 % PFA (Beyotime) for 15 min. After 3 times of washing, cells were permeabilized with 0.2% Triton X-100 (SAFC) in PBS for 10 min and were then blocked with rapid protein-free blocking buffer (YamayBio LLC) for 30 min at RT. After 3 times of washing, respective antibodies were added and maintained at RT for 1-2 h, followed by 3 times of washing. The secondary antibodies were then

added for incubation at RT for another 1h. Cells were finally washed 3 times and stained with a DAPI-containing mounting solution (Thermo). At least 30 cells of each group were captured by a Confocal Microscope (Leica TCS SPE). The mean/total fluorescent intensity, nucleus/cytoplasm ratio, synapse/ total ratio, and MTOC polarization were analyzed by Image J (NIH).

For immunofluorescence staining of tissue slides, tumor tissue was fixed with 4% PFA for more than 24 h, followed by a series of dehydration with ethanol and xylene. The dehydrated tumor tissues were then embedded in paraffin as a common procedure. Sections of 5-8 μm were cut by the microtome (Leica) and collected on slides. After a series of dewaxing steps with xylene and ethanol, the slides were unmasked with fresh and boiled antigen retrieval solution (Beyotime) for 10 min, followed by PBS washing. Then, 0.1~0.5% Triton X-100 was used to permeabilize the sections for 15 min, followed by blocking with 5% BSA solution. The primary antibodies targeting NKp46 or Cox2 were added to the slides at a ratio of 1:200. The slides were then placed at 4°C. After an overnight incubation, the slides were washed with PBS, and respective secondary antibodies were added at a ratio of 1:1000. Finally, the slides were washed with PBS and mounted with DAPI-containing solution (Thermo). The slides were imaged with a Leica TCS SPE Confocal Microscope and analyzed with Image J.

3.18 Fluorescence Resonance Energy Transfer (FRET)

To detect granzyme B injection into tumor cells during co-culture with NK cells, a granzyme B FRET sensor, which was based on a specific peptide (VGPDFGR) that linked with CFP and YFP at its C and N ends, was introduced into the MDA-MB-231 cells that were transfected with. Successfully injected granzyme B could cut off the VGPDFGR peptide and reduce FRET efficiency, causing a negative correlation between the injected granzyme B amount and the FRET ratio/efficiency. Similarly, Lck is a downstream kinase of some activating receptors of NK cells, including NKG2D. Lck FRET sensor was composed of ECFP-SH2-linker-LCK substrate-YPet. Under static conditions, the sensor formed a closed conformation with a narrow space between

ECFP and YPet, allowing a high FRET efficiency. Activated Lck phosphorylates the substrate domain of the sensor and induces its conformation change, resulting in the elongated distance between the two fluorescent proteins and a low FRET efficiency. Tumor cells were seeded on collagen I-coated confocal dishes. NK92 cells transfected with the Lck FRET sensor were co-cultured with tumor cells with low or high plasma membrane tension in confocal dishes. A 420 ± 20 nm laser was used to stimulate CFP; signals from the 472 ± 30 nm filter and 542 ± 27 nm filter were considered as emission from CFP and YFP, respectively. The FRET signals (CFP/YFP) were considered to represent the Lck activation level and a relative granzyme B amount among tumor cells. An inverted fluorescent microscope (Nikon H550L) with a 60×/1.40 oil objective (Nikon) was used for capturing and quantification with NIS4.1.2 software.

3.19 Flow cytometry

In some experiments, the granzyme B entering MDA-MB-231 cells was quantified with flow cytometry. NK cells and tumor cells were stained with different colors using dyes. Following standard fixation, permeabilization, and antibody staining procedures, after co-culturing as mentioned above in **Chapter 3.16**, the granzyme B level was quantified by flow cytometry (BD FACSymphony A3 Cell Analyzer, BD Biosciences). The green^{+} deep red^{-} cells were gated and considered as MDA-MB-231 cells.

3.20 Glycolysis and mitochondrial respiration assay

Extracellular acidification rate (ECAR) and oxygen consumption rate (OCR) were used to respectively indicate tumor cell glycolysis and mitochondrial respiration level. Before the assays, first, 80000 tumor cells in 500 μL DMEM full medium were seeded in the XF24 plate (Agilent Technologies), followed by incubating the plate at 37°C, 5% CO_2 overnight. Second, turn on the Agilent Seahorse XFe/XF Analyzer, and let it warm up overnight (minimum of five hours). Third, add 1 mL Agilent Seahorse XF Calibrant into each well of the Agilent Seahorse XFe24 Cell Culture Microplate to hydrate the sensor cartridge. Place the plate in a non-CO_2 37°C humidified incubator overnight. At

day 1, first, to prepare the assay medium, pyruvate (Gibco, 2993916), glutamine (Gibco, 3062766), and glucose (Sigma, G8769) with a final concentration of 1 mM, 2 mM, and 1 mM or 3 mM (for OCR assay) or 0 mM (for ECAR assay) were added into the Seahorse XF DMEM. Cells seeded at day 0 were washed with this assay medium (500 μL for each well) 3 times, followed by placing the cells in a non-CO2 37°C humidified incubator for 1 h before the ECRA or OCR assay. For the OCR assay, 56 μL 15 μM Oligomycin (Cayman, 11341), 62 μL 10 μM FCCP (Cayman, 15218), and 69 μL 5 μM antimycin A (Sigma-Aldrich, A8674) + 5 μM rotenone (Cayman, 13995) mixture were injected into port A, port B, and port C of the sensor cartridges, respectively. For ECAR assay, 56 μL 10 mM or 30 mM glucose, 62 μL 15 μM Oligomycin, and 69 μL 500 mM 2-DG (Cayman, 14325) were injected into port A, port B, and port C of the sensor cartridges, respectively. Open the Wave software (Agilent Technologies) and choose the default methods for ECAR or OCR, then click Run. Place the utility plate with the loaded sensor cartridge on the instrument tray for calibration. After the calibration, replace the empty calibration plate with the cell-seeding plate and start the assay. The data were generated automatically through the Wave software after finishing the assay.

3.21 Cell proliferation assay

CCK8 assay and EdU assay were conducted to evaluate proliferation. For the CCK8 assay, 2000 tumor cells/well were seeded in a 96-well plate. 10 μL CCK8 reagent was added to each well at the time of attachment (0 h), 24 h, 48 h, and 72 h. After 2 h incubating at 37°C in darkness, the absorbance value of each well was detected at 450 nm and 650 nm using a FLUOstar microplate reader (Omega). The absolute absorbance value (OD) was calculated as below:

$$absolute\ OD = OD_{450\,nm} - OD_{650\,nm}$$

For the Edu assay, 20000 cells/well were seeded to a collagen I-coated 24-well plate. The plate was then placed in a 5% CO_2 37°C humidified incubator for 3 h. 500 μL 20 μM EdU (BeyoClick™) was added to each well. After 2 h incubation, the plate was

washed with PBS, and 500 μL 4% PFA was added to fix cells for 15 min. Then the cells were washed with PBS 3 times and followed by permeabilizing with 0.1% Triton X-100 for 10 minutes. Remove the permeabilization buffer and wash the cells 3 times. 500 μL Click Reaction Buffer (containing 20 μL $CuSO_4$, 1 μL Azide 555, and 50 μL Click Additive Solution) was added to each well for 30 min incubation at room temperature in the dark. The reaction buffer was then removed, and the cells were washed with PBS 3 times, followed by nucleus staining with Hoechst 33342 (Beyotime) for 10 min. After the final washing, the cells were imaged using a fluorescent microscope (Nikon Ti2) with a 555 nm laser for EdU and a 395 nm laser for Hoechst 33342. The EdU^+ cell proportion was calculated to indicate the cell proliferation ability.

3.22 Glucose uptake assay

2×10^5 cells were seeded in each well of a 6-well plate. After overnight incubation, the culture medium was removed. 1.5 mL DMEM without glucose but containing 100 μM 2-NBDG was added to each well. Cells were incubated at 37°C for 1 h, followed by washing with PBS 3 times. The cells were then imaged by a fluorescent microscope (Nikon Ti2) with a 488 nm laser for 2-NBDG in cells. The mean fluorescent intensity of 2-NBDG in each cell was calculated, which represented glucose uptake capacity.

3.23 Animal experiments

Tumor cells were detached with trypsin & EDTA (Gibco), collected by centrifugation and resuspension with ice-cold PBS, and counted for use. To detect whether NK cells differentially killed tumor cells with low and high membrane tension, 1 million control-mCherry and constructively active ROCK (CA-ROCK) MDA-MB-231 cells mixture (1:1) were first mixed with the same volume of phenol red-free Matrigel solution (Corning, Cat. No. 356237) and then subcutaneously injected into the axilla of female NOD/SCID mice. This was followed by tail vein injection of 10 million NK92 cells once a week for 1 month, starting from day 0. The endogenous mice NK cells were depleted with Asialo GM1 Polyclonal Antibody (eBioscience, Cat. No. 16-6507-39) 4

days before tumor cell injection.

To detect metastasis organotropism of tumor cells, female BALB/c nude mice were first anesthetized by intraperitoneally injecting ketamine (8.7 mg/100g) and xylazine (1.3 mg/100 g). 0.1 million control/co-cultured/conditioned medium-treated/ezrin-overexpressed MDA-MB-231 cells were intracardially injected into the left ventricle. Successful intracardiac injections were confirmed by IVIS (Perkin-Elmer) imaging with a strong accumulation of luciferin signals in the kidneys and the brain but without the lungs. The occurrence of metastasis to brain, bone, lung, liver, and other organs, and brain metastasis-free survival were detected by IVIS imaging once a week. Metastasis events in the brain/lung/liver were determined by respective organ-specific luciferin signals. For bone metastasis, signals at the four legs, the spine, and the tail were considered positive events. Signals showed out of the above organs were considered as events that metastasize to other organs.

3.24 Statistical analysis

All the statistical results were presented by mean ± standard error of the mean (SEM). The two-tailed Student's t-test was used to analyze the statistics between two groups, and the analysis of variance (ANOVA) was used to analyze the statistics among three or more groups. NS, not significant; * $p<0.05$; ** $p<0.01$; *** $p<0.001$; and **** $p<0.0001$.

Chapter 4 NK cells reduce tumor cell membrane tension to promote breast cancer brain metastasis

Abstract

Metastasis is the primary cause of death among cancer patients[10,32,40]. Compared with other organs, brain metastasis shows higher lethality for the crucial role of brain tissue and with limited treatment strategies. During the process of metastasis, tumor cells continuously interact directly or indirectly with different types of immune cells. Although, immune cells like macrophages[246], neutrophils[247], and CD4 T cells[248] have been found to promote metastasis, the role of immune cells in organotropism is largely unknown.

Here, using special transcriptome analysis, we find a positive correlation between NK cells infiltration and brain metastasis potential. A series of in vitro and in vivo assays confirm the promotive role of NK cells for brain metastasis. Mechanistically, NK cells secret and inject granzyme B to degrade ezrin in tumor cells, which induces decreased tumor cell membrane tension. Further, the PI3K-CREB signaling is activated to increase GLUT3 expression, which promotes glucose uptake and proliferation under brain-mimic low glucose microenvironment. These findings demonstrate that NK cells can promote breast cancer brain metastasis through decreasing tumor cell membrane tension, providing compelling evidence to unveil the pro-organotropism effect of NK cells.

4.1 The correlation between NK cell infiltration and brain metastasis

High NK cell tumor infiltration has been proposed to be a positive factor for cancer patients' survival[148]. However, whether NK cells influence metastasis organotropism is largely unknown. To investigate this correlation, we first analyzed online spatial

transcriptome data from two breast cancer patients. A typical gene signature was used for cell type and metastatic potential annotation. For example, barcodes that were $NCAM1^+$, $GZMB^+$, and $NCR3^+$ but $CD3^-$ were considered to contain NK cells. CD8/CD4 T cells, macrophages, neutrophils, and B cells were annotated using the same principle (as detailed in **Chapter 3.1.3**). For typical breast cancer metastasis organ-brain, bone, liver, lung-metastasis gene signature, and bar code annotation, we adopted genes that are enriched in organ-specific metastasis according to published data. For example, in the brain metastasis of breast cancer, PTGS2, which encodes Cox2, is highly enriched. Cox2 promotes BBB breakdown and CCL7 upregulation in astrocytes, which initiates colony formation in the brain through a COX2-prostaglandins-MMP1 pathway[249]. Additionally, brain metastatic cells express Serpin B2 to inhibit plasmin generation and exert metastasis-suppressive effects through releasing FasL from astrocytes and inactivating L1CAM, which is used by metastatic cells to adhere to brain capillaries[250]. Some other genes like IL6[251], piezo2, EREG, CTSL, and HBEGF were also included for the brain metastasis gene signature. Similarly, metastasis to bone, liver, and lung has its gene signature, and the annotation principle can be found in **Chapter 3.13.**

As shown in Figure 4-1 **A**, infiltrated NK cells showed the most similar spatial pattern to brain metastasis tumor cells compared to other commonly observed immune cells in solid breast tumors. In agreement with this, in the NK cell positive (NK^+) region, brain metastasis-associated genes were highly enriched compared to the NK cell negative (NK^-) region (Figure 4-1 B and C), suggesting that tumor cells with high brain metastatic potential congregated in NK cell niches. However, bone/lung/liver-metastasis-associated genes did not have such a difference in NK^+ and NK^- regions (Figure 4-1 D-F), indicating that NK cells specifically upregulated brain metastasis-associated genes in surrounding breast tumor cells. This was confirmed by immunostaining of breast tumor tissues from immunocompromised mice with weekly human NK92 cell injections. As shown in Figure 4-1 **G**, NK cells, represented by NKp46, had a similar pattern of distribution both in the periphery and within tumor

tissue. Furthermore, analysis of bulk RNA-seq data from primary tumor tissue derived from breast cancer patients with or without brain metastasis predicted that a significantly greater number of infiltrated NK cells (>1000 times) were found in brain metastasis patients (Figure 4-1 **I**). Therefore, we proposed that NK cells are the major contributors to the enriched brain metastasis-associated genes in the surrounding tumor cells.

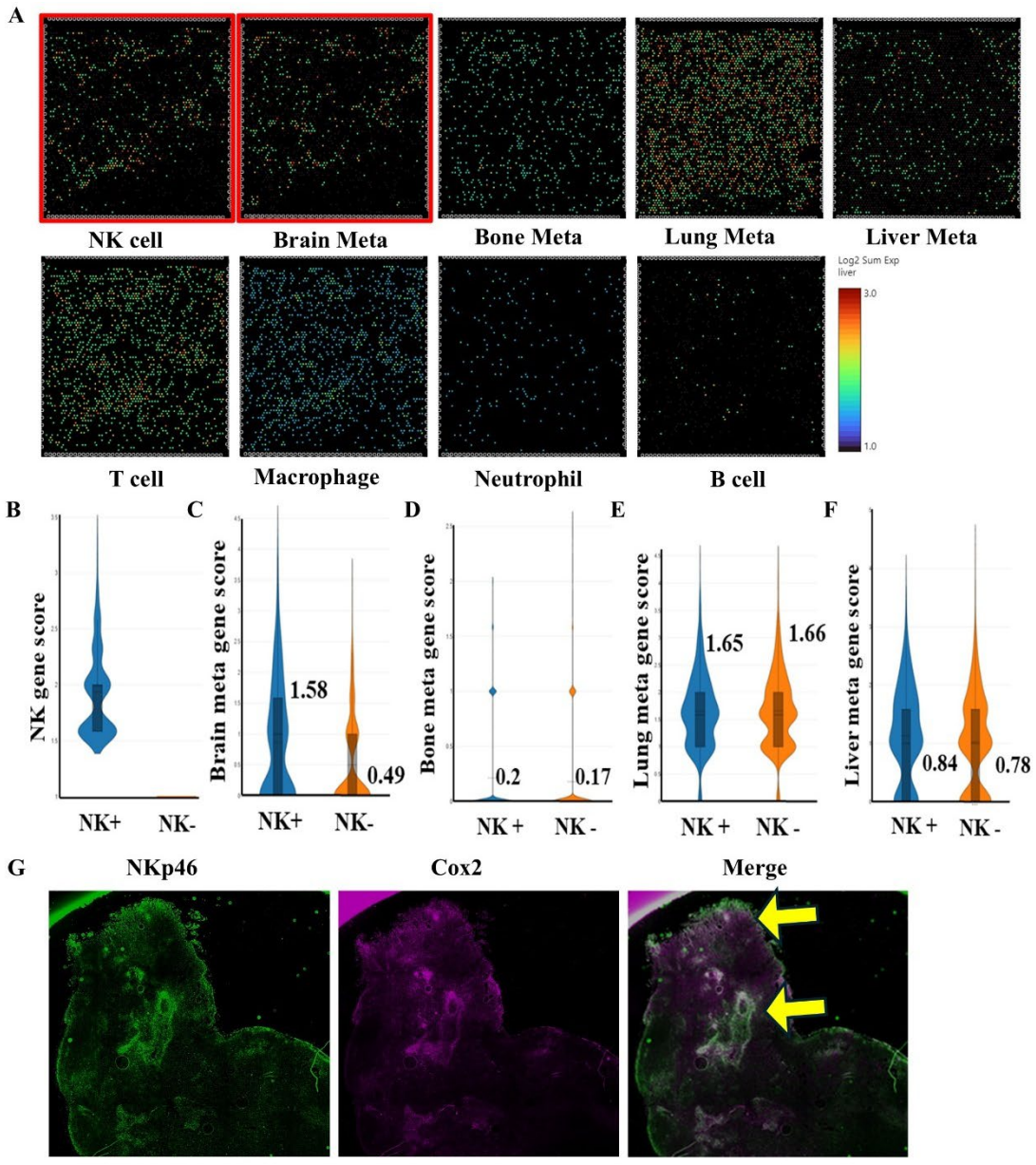

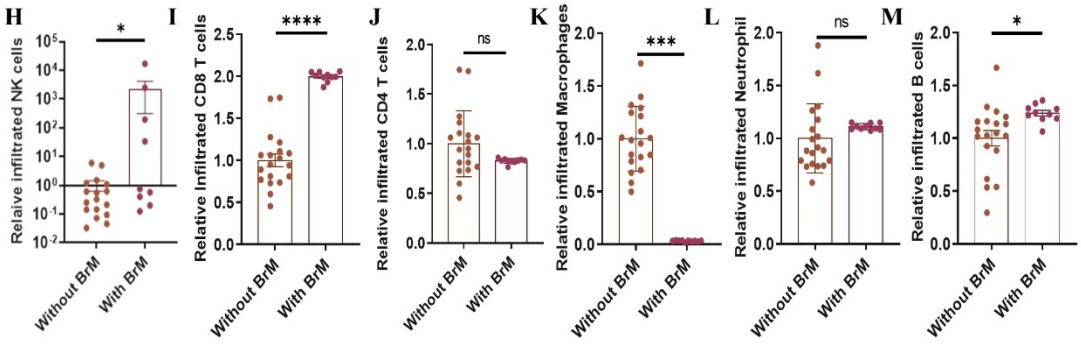

Figure 4-1 The correlation between tumor infiltration of NK cells and brain metastasis

A Spatial distribution of NK cell, T cell, Macrophage, Neutrophil, B cell, and tumor cell with brain, bone, lung, liver metastasis-associated gene markers. **B-F** Gene score of NK positive and negative bar codes for NK genes (**B**), brain-metastasis genes (**C**), bone-metastasis genes (**D**), lung-metastasis genes (**E**), and liver-metastasis genes (**F**). **G** Immunostaining of NKp46 (green) and Cox2 (purple) in breast tumor tissue. Tomor was formed by subcutaneously injecting 1 million MDA-MB-231 cells in nude mice. **H-M** Infiltrated NK cell (**H**), CD8 T cell (**I**), CD4 T cell (**J**), Macrophages (**K**), Neutrophil (**L**), and B cell (**M**) numbers in the primary tumors with and without brain metastasis. The unpaired t-test (**H-M**) was adopted for statistical analysis.

4.2 NK cells promote breast cancer brain metastasis in vitro and in vivo

To verify that NK cells could promote brain metastasis of breast tumor cells, we adopted the human breast cancer cell line MDA-MB-231 and the immortal human NK cell line NK92. After co-culture of NK cells and tumor cells at a 4:1 ratio, the morphology, potential of surviving tumor cells to adhere to brain endothelial cells under FSS, trans-BBB migration in vitro, and metastasis to the brain were detected.

Interestingly, co-cultured MDA-MB-231 cells showed invasive spindle morphology with a high aspect ratio (AR), which was very similar to the morphology of the developed MDA-MB-231-TGL-brain metastasis (TGL-BrM) cells[100] (Figure 4-2-1 **A** & **B**). This phenomenon is not cell line/cell type-dependent because MDA-MB-468 and lung cancer cell line A549 also showed invasive spindle morphology after co-culture with NK cells (Figure 4-2-1 **C** & **D**).

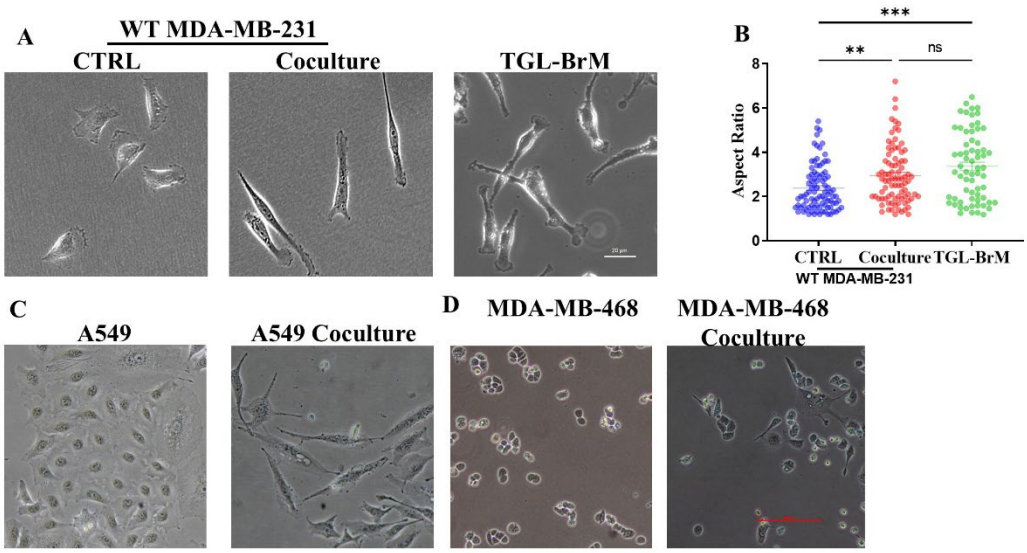

Figure 4-2-1 Tumor cells show brain-metastasis-like morphology after co-culture
A Morphology of control MDA-MB-231 cells, co-cultured MDA-MB-231 cells, and TGL-BrM cells. **B** Statistical analysis of cell aspect ratio in A, n=90, 96, and 66 cells for CTRL, Coculture, and TGL-BrM groups. **C & D** Morphology of control MDA-MB-468 cells and A549 cells with or without co-culture with NK cells. The one-way ANOVA followed by the Kruskal-Wallis test (**B**) was adopted for statistical analysis.

To metastasize to the brain, DTCs need to first adhere to brain endothelial cells under FSS, followed by trans-BBB migration (Figure 4-2-2 **A**). It was found that after co-culture with NK cells, tumor cells significantly adhered more to brain endothelial cells (HCMEC) compared to control cells under 1 dyn/cm^2 FSS using a fluid chip, while they adhered to primary human umbilical vein endothelial cells (HUVEC) with no difference (Figure 4-2-2 **B-D**). This result suggested that NK cells specifically promoted breast tumor cell adhesion to brain endothelial cells.

Further, an in vitro trans-BBB model was used where HCMEC and astrocytes were respectively seeded on the upper and lower side of a 3 μm transwell insert to mimic the BBB, or only HUVEC on the upper side to mimic the umbilical vein (Figure 4-2-2 **A**). The result showed that co-culture with NK cells significantly and specifically enhanced tumor cells' trans-BBB migration ability with no difference in trans-HUVEC migration (Figure 4-2-2 **E-H**).

The above observations of NK cells' effect on brain metastasis were further confirmed in vivo. The two groups of MDA-MB-231 cells, engineered with luciferase, were intracardially injected into female nude mice, followed by luciferin detection every 7 days (Figure 4-2-2 **A**). As expected, mice injected with co-cultured tumor cells showed higher brain metastasis occurrence (83.3%) compared with mice injected with control tumor cells (16.7%) (Figure 4-2-2 **I** and **J**). However, the occurrence of metastasis to bone, lung, and liver did not change (Figure 4-2-2 **K**).

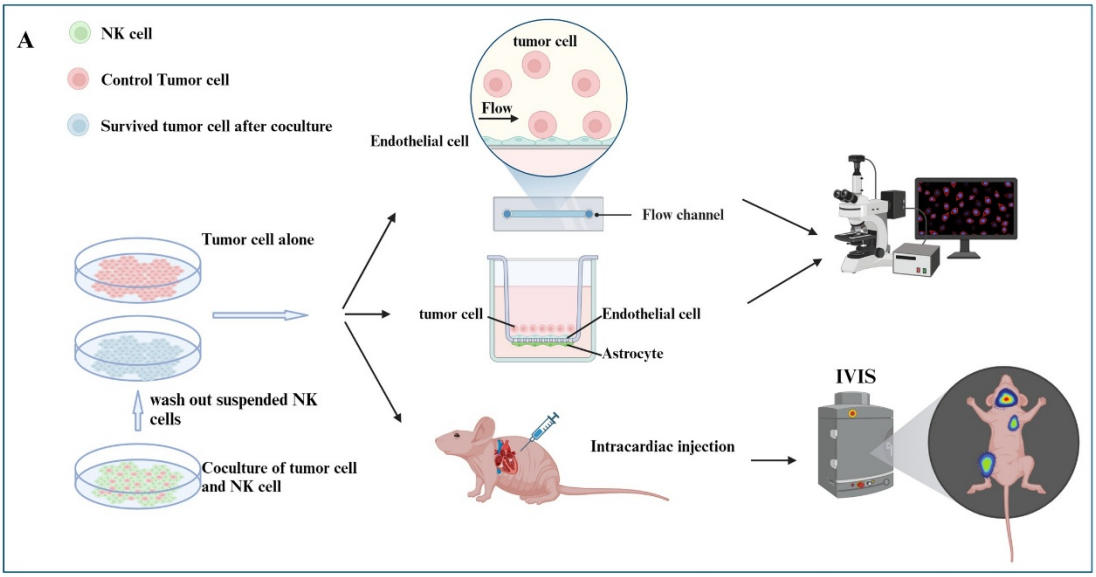
A
NK cell
Control Tumor cell
Survived tumor cell after coculture
tumor cell
Flow
Endothelial cell
Flow channel
Tumor cell alone
tumor cell
Endothelial cell
Astrocyte
wash out suspended NK cells
Coculture of tumor cell and NK cell
Intracardiac injection
IVIS

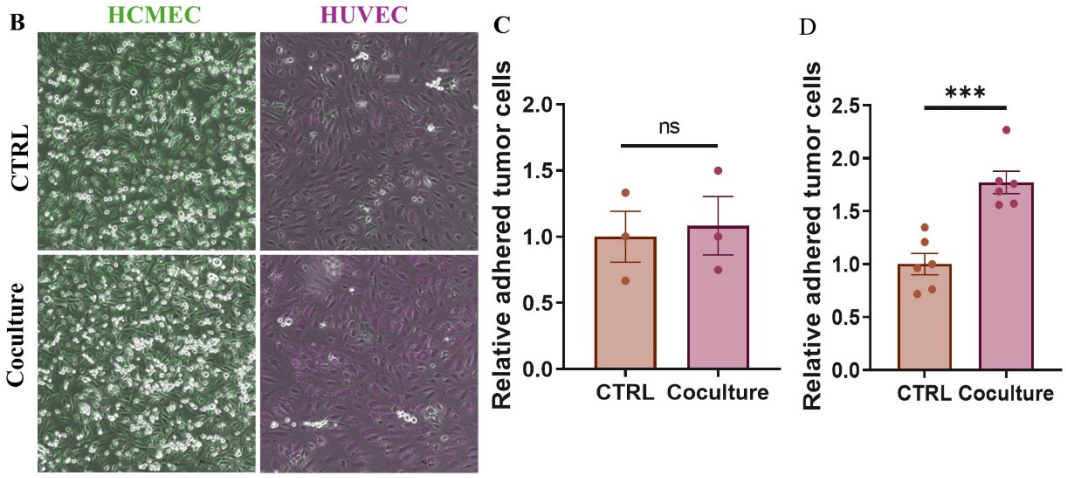
B
HCMEC
HUVEC
CTRL
Coculture
C
Relative adhered tumor cells
ns
CTRL Coculture
D
Relative adhered tumor cells
***
CTRL Coculture

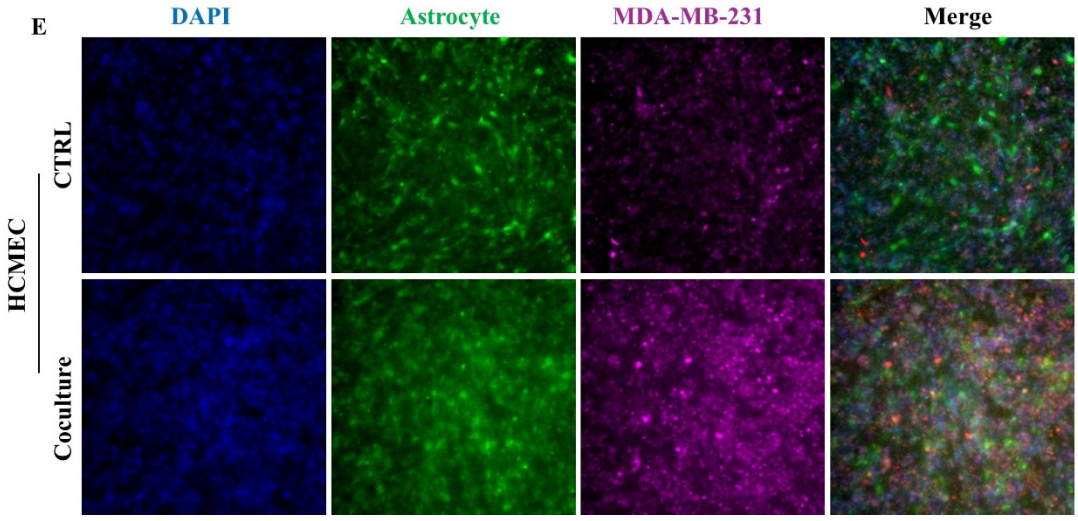
E
DAPI
Astrocyte
MDA-MB-231
Merge
HCMEC
CTRL
Coculture

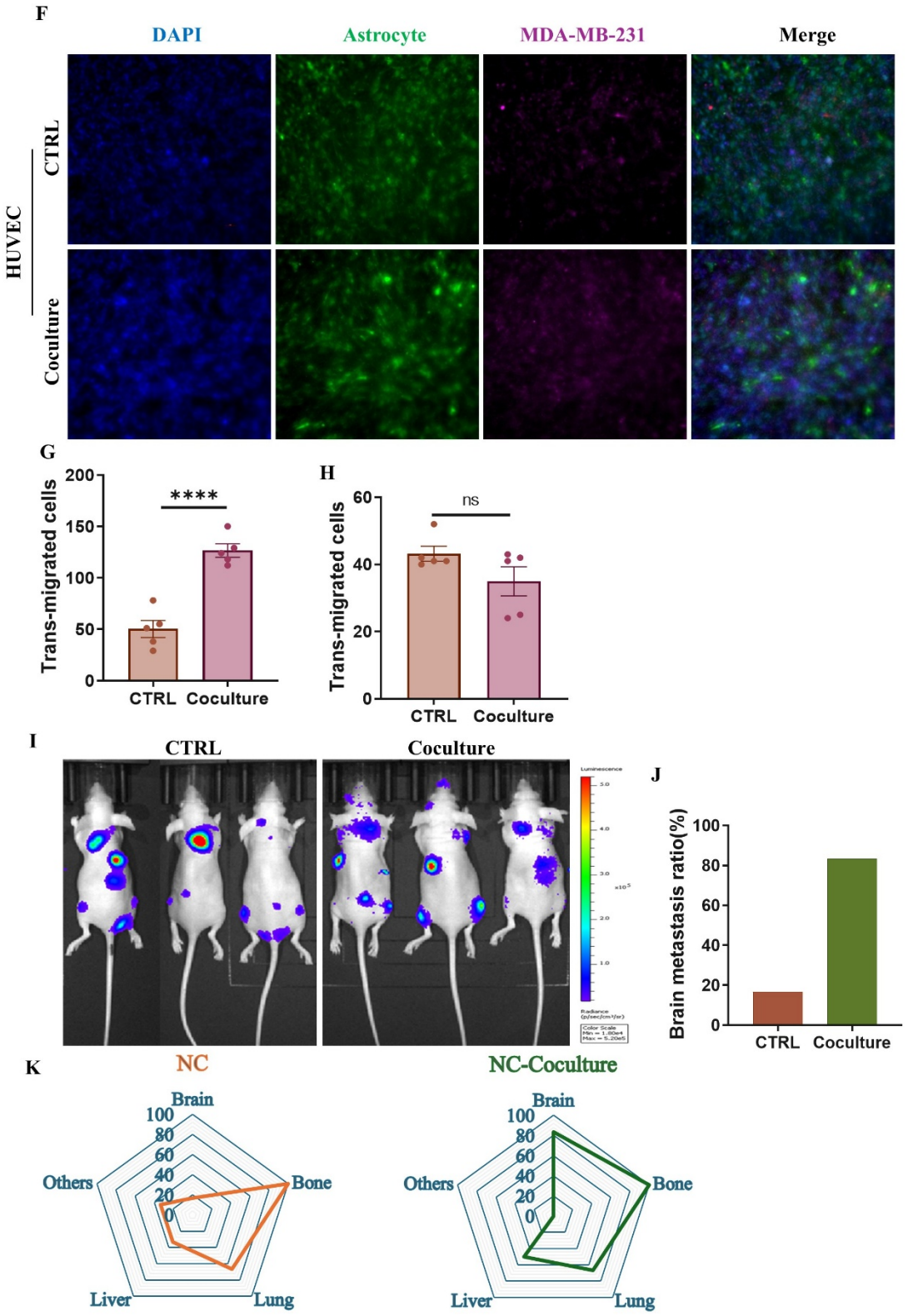

Figure 4-2-2 NK cells promote breast cancer brain metastasis both in vitro and in vivo

A Diagram of experimental design for **B to K**. **B** Representative images of tumor cells adhesion to the HCMEC (green) or HUCEC (purple) monolayer under 1 dyn/cm^2 FSS.

C & D Statistical analysis of cell adhesion in **B**. At least 3 independent experiments. **E** Representative images of tumor cells trans-BBB migration. **F** Representative images of tumor cells trans-HUCEC migration. **G & H** Statistical analysis of trans-BBB migration (**E**) and trans-HUCEC migration (**F**). n=5 independent experiments. **I** Luciferin imaging of nude mice with intracardiac injection of control/co-cultured tumor cells on day 28. n=6 for both groups. **J** BrM occurrence of control/co-cultured tumor cells on day 28. **K** Organ distribution of metastatic events in **I**. The unpaired t-test (**C, D, G, and H**) was adopted for statistical analysis.

According to the above in vitro and in vivo data, NK cells seemed to specifically promote brain metastasis without obvious impact on metastasis to other organs like bone, lung, and liver. To further validate this finding, bulk RNA-seq of control MDA-MB-231 cells with or without co-culture was adopted to analyze brain[100], bone[252], liver[253-255], and lung[256] metastasis-associated genes. As shown in Figure 4-2-3 **A-D**, all brain metastasis-associated genes were upregulated in co-cultured MDA-MB-231 cells. However, co-cultured MDA-MB-231 cells increased the expression of about half of the bone/lung/liver metastasis-associated genes, with the other half decreased. Protein expression (NDRG1, Serpin B2, and Cox2) of typical brain metastasis-associated genes was further detected and showed similar upregulation in co-cultured MDA-MB-231 cells (Figure 4-2-3 **E-G**).

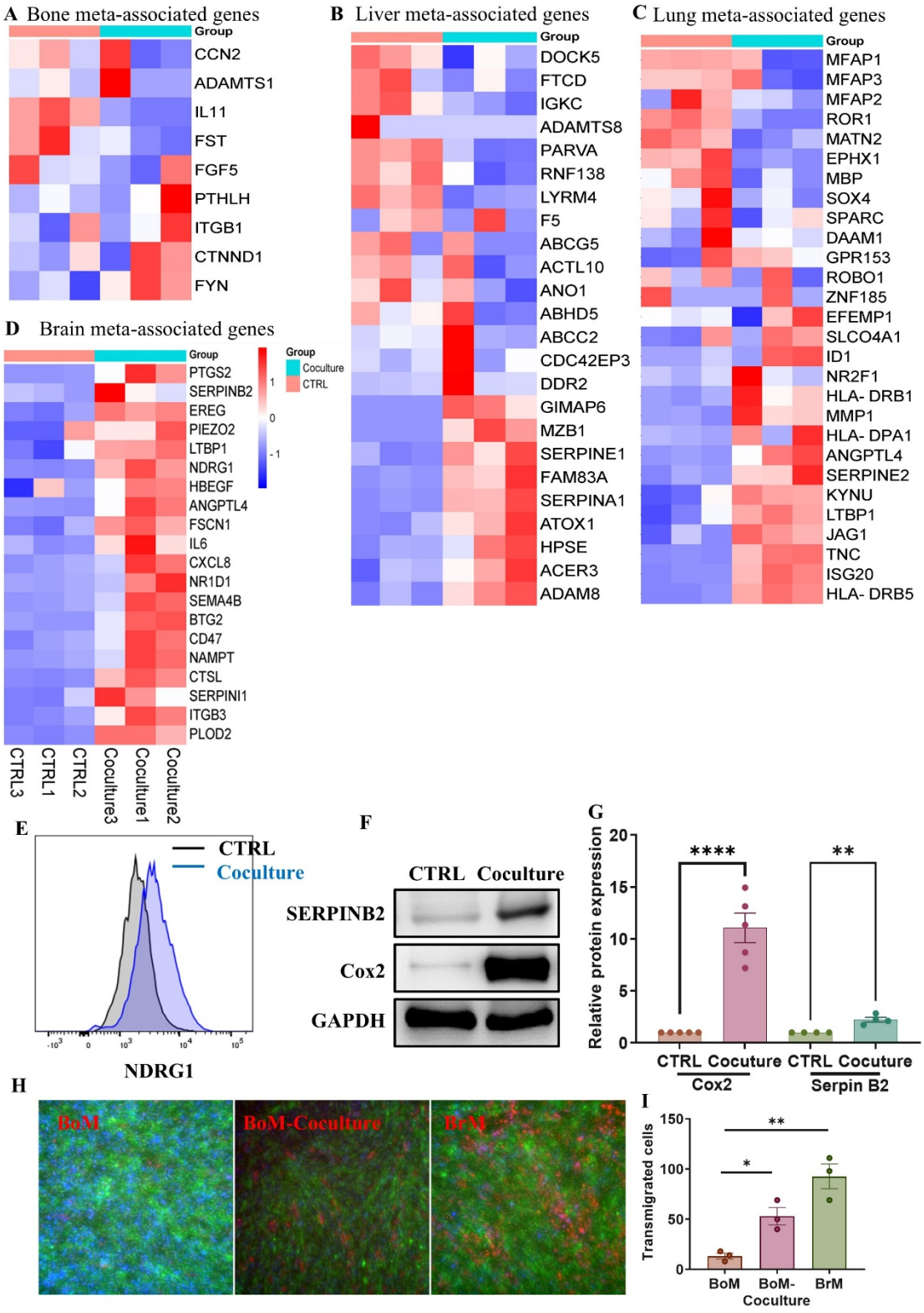

Figure 4-2-3 NK cells upregulate brain metastasis genes of MDA-MB-231 cells

A-D Cluster heatmap of bone (**A**), liver (**B**), lung (**C**), and Brain (**D**) metastasis genes in control and co-cultured MDA-MB-231 cells. **E** Flow cytometry of NDRG1 promoter-driven mCherry expression in control and co-cultured MDA-MB-231 cells.

F Western blot of Serpin B2 and Cox2 expression. **G** Statistical analysis of Serpin B2 and Cox2 expression in **F**. **H** Representative images of TGL-BoM, co-cultured TGL-BoM, and TGL-BrM trans-BBB migration. Blue, nucleus; Green, astrocytes; Red, trans-BBB migrated tumor cells. **I** Statistical analysis of trans-BBB migration in **H**. n=3 independent experiments. The one-way ANOVA followed by Tukey's test (**I**) and unpaired t-test (**G**) were adopted for statistical analysis.

To detect the robustness of NK cells on brain metastasis, a bone metastasis (TGL-BoM) cell line developed from MDA-MB-231 cells was used[100]. Interestingly, TGL-BoM cells had weak basal trans-BBB migration ability, which was significantly enhanced after co-culture with NK cells, although the trans-BBB migration efficiency is still lower than TGL-BrM (Figure 4-2-3 **H** & **I**). These results indicate that NK cells could specifically promote breast tumor cells metastasis to the brain.

4.3 NK cells induce low membrane tension of breast cancer cells

To break down the basement membrane and squeeze through the narrow pore size of the ECM and, more importantly, the BBB, malignant tumor cells need to allow the formation of invadopodia, where the cell membrane detaches from cortical actin filaments, followed by actin polymerization. Strong membrane-to-cortex anchoring (high membrane tension) inhibits protrusion formation and migration[6,257]. Tumor cell malignancy is negatively correlated with membrane tension[6]. The binding of ERM proteins to both membrane PIP2 and cortical actin filaments dominates cell membrane tension[258]. Tumor cells with low cell membrane tension usually have an invasive spindle morphology[6], just like the tumor cells after co-culture with NK cells in Figure 4-2-1 **A** and **B**. Based on these, we proposed that NK cells might induce a decrease in tumor cell membrane tension.

Indeed, bulk RNA-seq data indicated the decreased expression of ezrin and radaxin in

co-cultured tumor cells (Figure 4-3-1 **A** and **C**). More importantly, the expression of a series of enzymes that regulate ERM activity also changed. Among these, the ERM phosphatases PTP4A1, PPP1R12A, and CAPN1, which inhibit ERM activity, were upregulated (Figure 4-3-1 **E**); most ERM kinases like PRKCA, SLK, ROCK1, ROCK2, SPHK1, and SPHK2, which promote ERM activation, were decreased (Figure 4-3-1 **D**) in co-cultured tumor cells. Meanwhile, ERM proteins bind to the plasma membrane through anchoring to PIP2. The amount of PIP2 in the cell membrane determines the availability of its anchoring to the underpinning cortical actin filaments through ERM proteins. A series of enzymes regulate the PIP2 amount in the cell membrane. On the one hand, PLC proteins dephosphorylate PIP2 and generate secondary messengers IP3 and DAG. On the other hand, PI3K phosphorylates PIP2, creating PIP3 to recruit and activate Akt. Both PLC and PI3K genes were upregulated in the co-cultured MDA-MB-231 cells (Figure 4-3-1 **A** and **B**). Moreover, PTEN, a tumor suppressor that dephosphorylates PIP3 and generates PIP2, was downregulated in the co-cultured MDA-MB-231 cells (Figure 4-3-1 **A** and **B**). All these results decreased ERM expression (especially ezrin), activity, and the availability of PIP2 in the cell membrane directed us to the decreased cell membrane tension. Indeed, co-cultured MDA-MB-231 cells showed decreased ezrin expression and phosphorylation (Figure 4-3-1 **F**-H). Interestingly, the western blot data of tumor cells targeting ezrin showed fragmentation strips after co-culture. This result indicates that NK cells may actively cleave ezrin in tumor cells. Granzyme B is the major enzyme that is injected into tumor cells from NK cells. We proposed that NK cells may target tumor cell ezrin through granzyme B. Indeed, by directly incubating recombinant ezrin and granzyme B in vitro, followed by western blot, we observed similar fragmentation strips of ezrin (Figure 4-3-1 I).

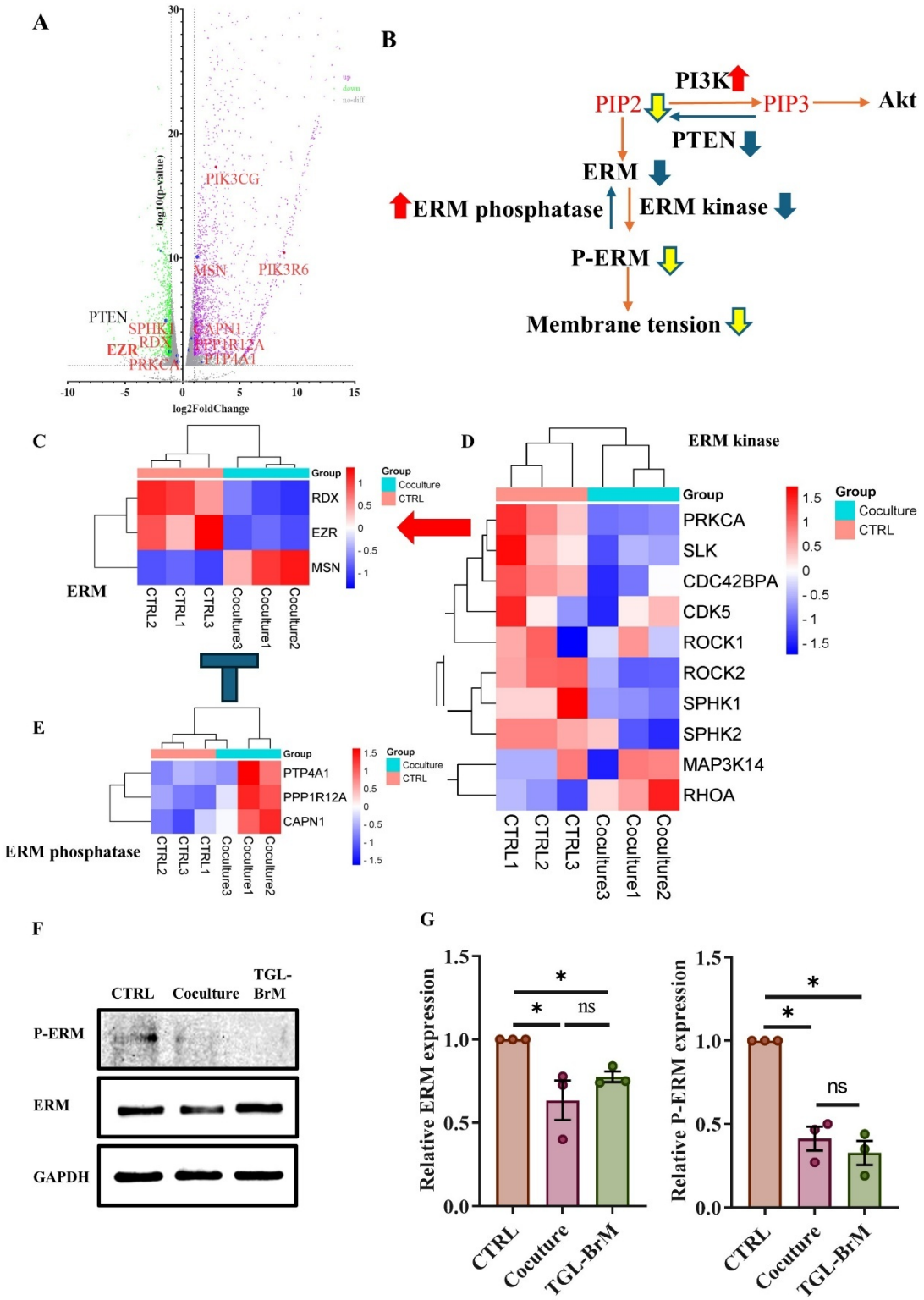
A
B
C
D
E
F
G
PI3K
PIP2
PIP3
Akt
PTEN
ERM
ERM phosphatase
ERM kinase
P-ERM
Membrane tension
PIK3CG
MSN
PIK3R6
PTEN
SPHK1
RDX
EZR
PRKCA
CAPN1
PPP1R12A
PTP4A1
log2FoldChange
-log10(p-value)
ERM
RDX
EZR
MSN
CTRL2
CTRL1
CTRL3
Coculture3
Coculture1
Coculture2
Group
Coculture
CTRL
ERM kinase
PRKCA
SLK
CDC42BPA
CDK5
ROCK1
ROCK2
SPHK1
SPHK2
MAP3K14
RHOA
ERM phosphatase
PTP4A1
PPP1R12A
CAPN1
CTRL
Coculture
TGL-BrM
P-ERM
ERM
GAPDH
Relative ERM expression
Relative P-ERM expression
ns

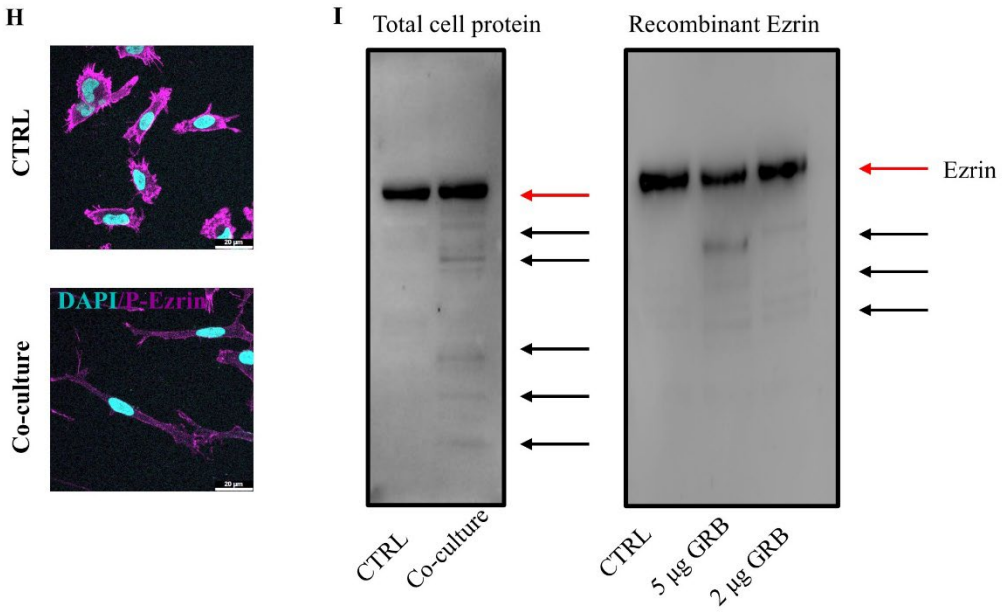

Figure 4-3-1 NK cells downregulate ERM expression and decrease ERM activity in tumor cells

A volcano plot of up- and down-regulated genes of control VS co-cultured MDA-MB-231 cells. **B** Diagram of regulation of PIP2 and ERM phosphorylation and dephosphorylation by respective enzymes that influence plasma membrane tension. **C** – **E** Cluster heatmap of differentially expressed genes of ERM (**C**), ERM kinases (**D**), and ERM phosphatases (**E**). **F** Western blot of ERM and phosphor-ERM of control VS co-cultured tumor cells. **G** Statical analysis of ERM (left) and phosphor-ERM (right) protein expression of control VS co-cultured MDA-MB-231 cells. n=3 independent experiments. **H** Immune fluorescent imaging of phospho-ezrin of control/co-cultured tumor cells. **I** Western blot of ezrin from total cell protein of control VS co-cultured MDA-MB-231 cells or recombinant ezrin with or without incubating with recombinant granzyme B (GRB). Red arrows, ezrin; black arrows, cleaved ezrin fragments. The one-way ANOVA followed by Tukey's test (**G**) was adopted for statistical analysis.

A membrane PIP2 sensor, PH-PLC-delta-EGFP, based on the PIP2 binding domain of PLC, was used to detect live cell membrane PIP2 levels. It was found that co-culture with NK cells significantly decreased membrane PIP2 levels (Figure 4-3-2 **A** & **B**). Also, a membrane PIP3 sensor, PH-Akt-Cerulean, based on the PIP3 binding domain of Akt, was used to detect live cell membrane PIP2 levels. As expected, NK cell co-culture increased PIP3 generation in the plasma membrane (Figure 4-3-2 **C** & **D**). Direct measurement of cell membrane tension was conducted using a Flipper-TR®

probe, which spontaneously inserts into the plasma membrane and senses changes in the organization of lipid bilayer membranes, in particular the tension between lipid layers[259]. High plasma membrane tension induces a conformation change in the probe and extends its emission fluorescence lifetime, which can be detected by Fluorescence Lifetime Imaging Microscopy (FLIM). Indeed, after co-culture with NK cells, the membrane tension of MDA-MB-231 cells significantly decreased from 5.47 ns to 4.8 ns (Figure 4-3-2 **E** & **F**), which could be equal to a 1.0 Osm hyperosmotic shock according to the designer of the probe[259]. It was noted that the isotonic solution for most human cells is only about 0.3 Osm. Since membrane tension is a combination of the cell membrane lipid bilayer tension and the cortical actin filaments tension, cortical tension can significantly influence membrane tension. Here, AFM was used to measure cell cortical tension by limiting the indentation threshold to 300 nm, and it was found that co-cultured tumor cells showed a similar decrease in cortical tension (Figure 4-3-2 **G**). Interestingly, TGL-BoM cells that metastasize to bone showed similar membrane tension with control MDA-MB-231 cells, indicated by a 5.45 ns lifetime of the Flipper probe. TGL-brain metastasis cells shared similar membrane tension with co-cultured tumor cells, indicated by a 4.91 ns lifetime of the Flipper probe (Figure 4-3-2 **E, F, H,** & **I**).

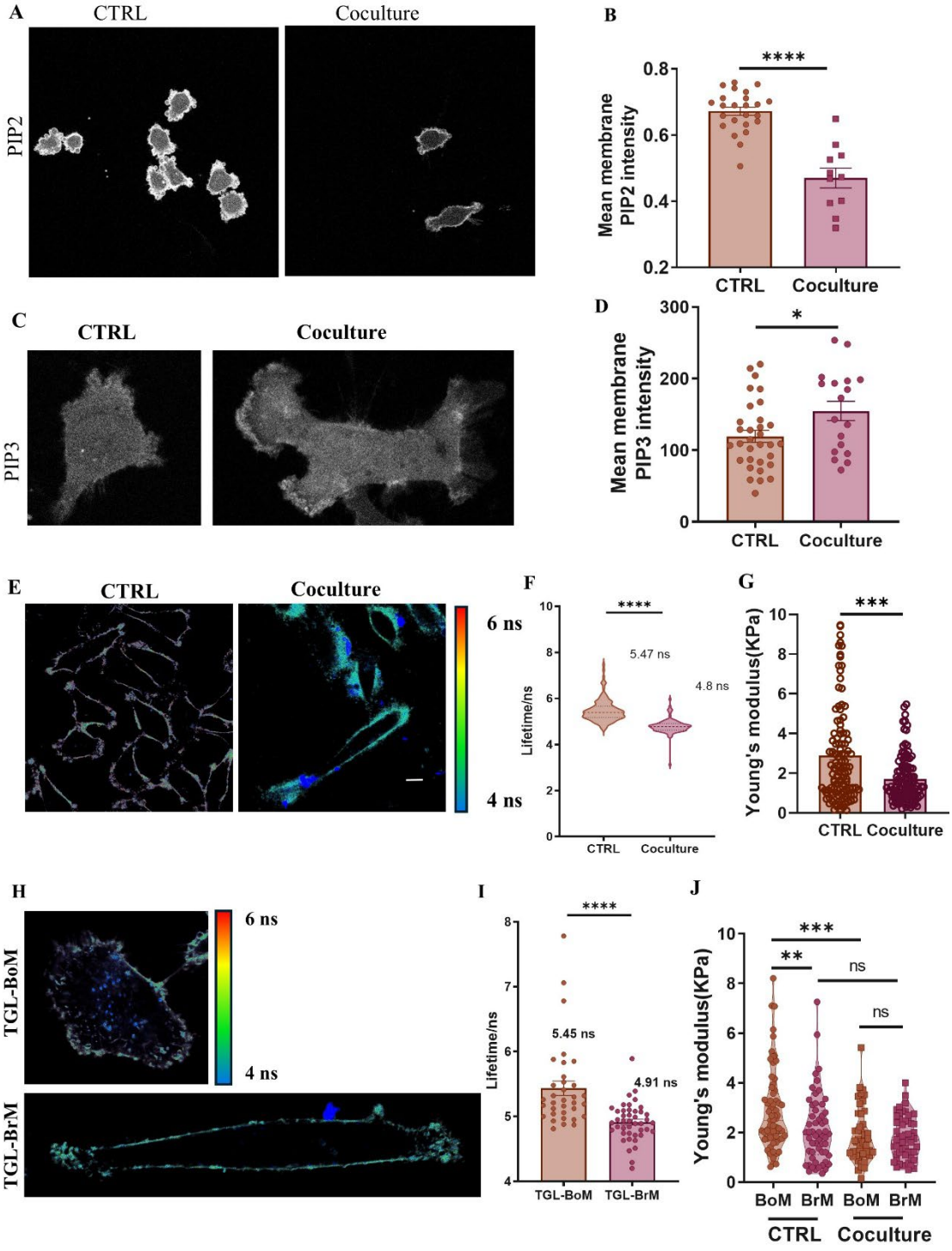

Figure 4-3-2 Tumor cells after co-culture with NK cells show decreased cell membrane tension

A Representative images of PIP2 in live control/co-cultured tumor cells. **B** Statistical analysis of membrane PIP2 intensity of cells in **A**. n>30 cells for each group. **C** Representative images of PIP3 in live control and co-cultured MDA-MB-231 cells. **D** Statistical analysis of membrane PIP3 intensity of cells in **C**. n>30 cells for each group. **E** Representative images of cell membrane tension of control and co-cultured MDA-

MB-231 cells. **F** Statical analysis of membrane tension. n=121 cells for control group, n=90 cells for co-cultured group. **G** Youngs' modulus of control/co-cultured tumor cells. n=109 cells for control group, n=110 cells for co-cultured group. **H** Representative images of cell membrane tension of TGL-bone (BoM) and TGL-brain (BrM) cells. **I** Statistical analysis of membrane tension in **H**. n=34 cells for BoM group, n=43 cells for BrM group. **J** Youngs' modulus of BoM and BrM cells before and after co-culture with NK cells. n=67 cells for BoM group, n=56 cells for BrM group, n=48 cells for co-cultured BoM group, n=54 cells for co-cultured BrM group. The one-way ANOVA followed by Tukey's test (**J**) and unpaired t-test (**B, D, F, J, & I**) were adopted for statistical analysis.

These similarities of membrane tension were further validated by AFM (Figure 4-3-2 **J**). To detect whether decreased cortical tension was correlated with the enhanced trans-BBB migration ability as shown in Figure 4-2-2**,** TGL-BoM and TGL-BrM cells were co-cultured with NK cells, followed by AFM assay. The results indicated that the co-culture of TGL-BoM with NK cells decreased its cortical tension to the level of TGL-BrM cells, while the co-culture of TGL-BrM with NK cells did not significantly change its cortical tension (Figure 4-3-2 **J**).

Tumor cells with low membrane tension exhibited an invasive phenotype[6]. To prove this in our project, wound healing assay and single-cell trajectory were adopted to detect tumor cell migration ability. The results showed that after co-culture with NK cells, the gap closure time was significantly shortened compared to control cells (Figure 4-3-3 **A** & **B**). Moreover, tumor cells showed enhanced migration speed and directness to chemokine CXCL12 (Figure 4-3-3 **C**-**F**).

These results suggested that NK cells selected or induced tumor cells with low membrane tension, which might specifically contribute to tumor cells' brain metastatic potential.

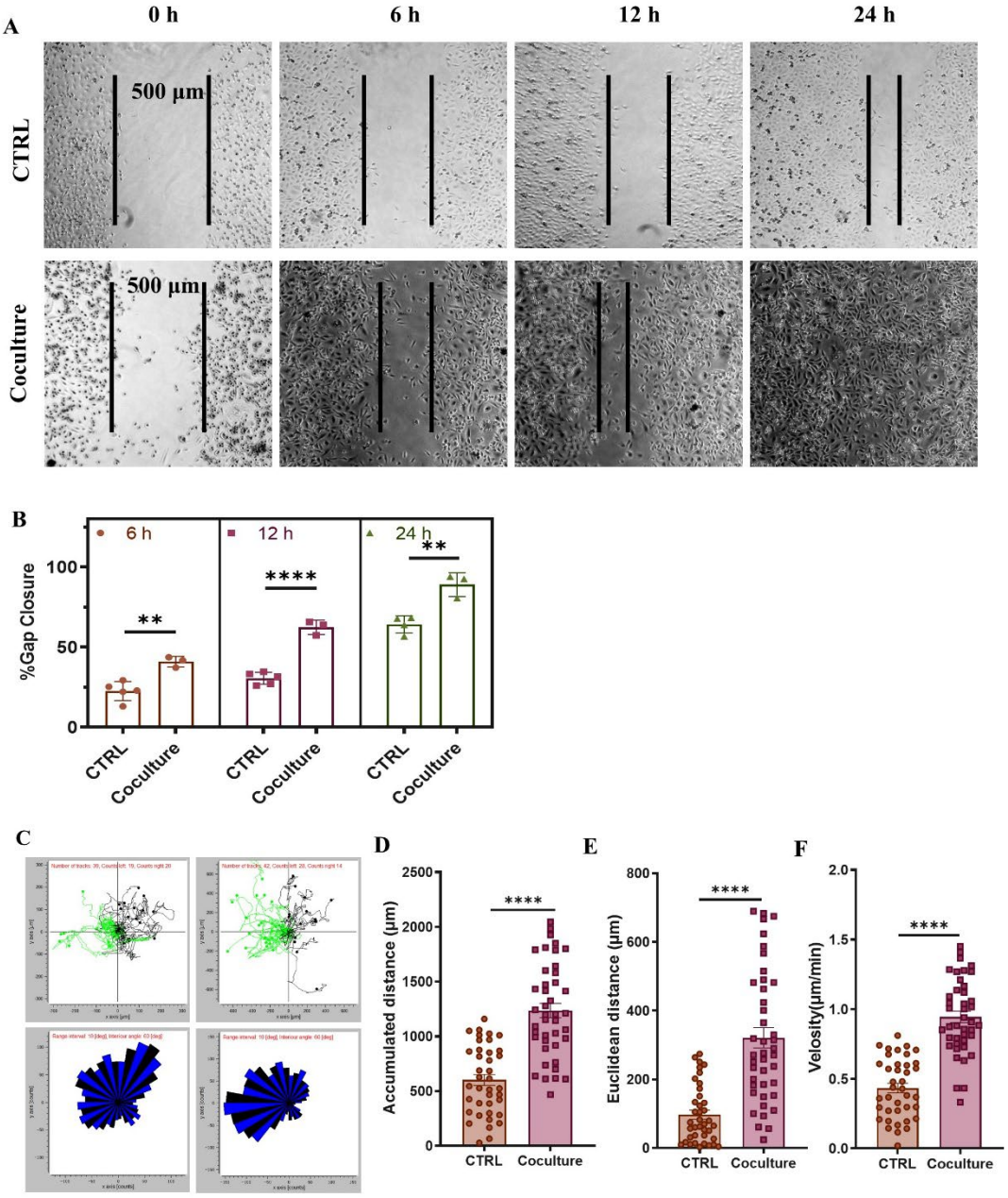

Figure 4-3-3 NK-selected tumor cells exhibit enhanced motility

A Wound healing assay of control and co-cultured tumor cells imaged at 0 h, 6 h, 12 h, and 24 h. **B** Statistical analysis of gap closure of control and co-cultured MDA-MB-231 cells at different time points in **A**. **C** Single cell trajectory of control and co-cultured MDA-MB-231 cells with the administration of 100 µg/mL CXCL12 on one side of the µ-Slide Chemotaxis chip within 12 h. **D-F** Statistical analysis of cell accumulated distance (**D**), euclidean distance (**E**), and velocity (**F**) of control/co-cultured tumor cells. n=39 cells for control group, n=42 cells for co-cultured group. The unpaired t-test (**B, D, E, & F**) was adopted for statistical analysis.

4.4 Low membrane tension confers a survival advantage to breast cancer cells under NK cell cytotoxicity

Tumor cells are heterogeneous in mechanical properties like cell membrane tension and stiffness. It has been found that NK cells are mechano-sensitive to physical cues like substrate stiffness[176]. NK cells and T cells exert both pushing and pulling forces at the immunological synapse to sense the properties of target cells[260,261]. Based on these, we proposed that NK cells may selectively free tumor cells with low membrane tension. The differential killing of NK cells was detected by co-culture of mixed tumor cells with high and low membrane tension with NK cells at a 4:1 ratio (NK cells: tumor cells), followed by flow cytometry (Figure 4-4 **A**). First of all, NK cells selectively killed more TGL-BoM cells, which had higher membrane tension (Figure 4-3 **L-N**) compared with TGL-BrM cells. And this is a time-dependent killing (Figure 4-4 **B-E**). Low membrane tension renders TGL-BrM cells with higher immune evasion potential.

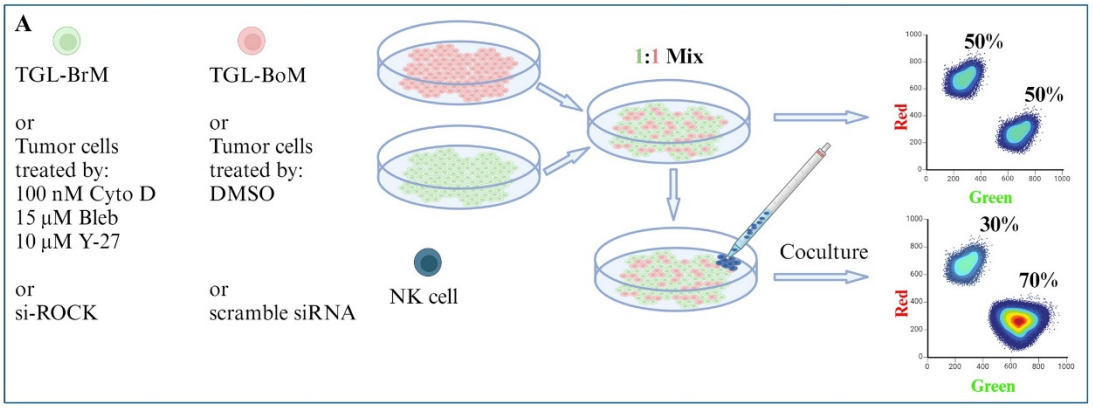
A
TGL-BrM
or
Tumor cells
treated by:
100 nM Cyto D
15 μM Bleb
10 μM Y-27
or
si-ROCK
TGL-BoM
or
Tumor cells
treated by:
DMSO
or
scramble siRNA
NK cell
1:1 Mix
Coculture
50%
50%
Red
Green
30%
70%
Red
Green

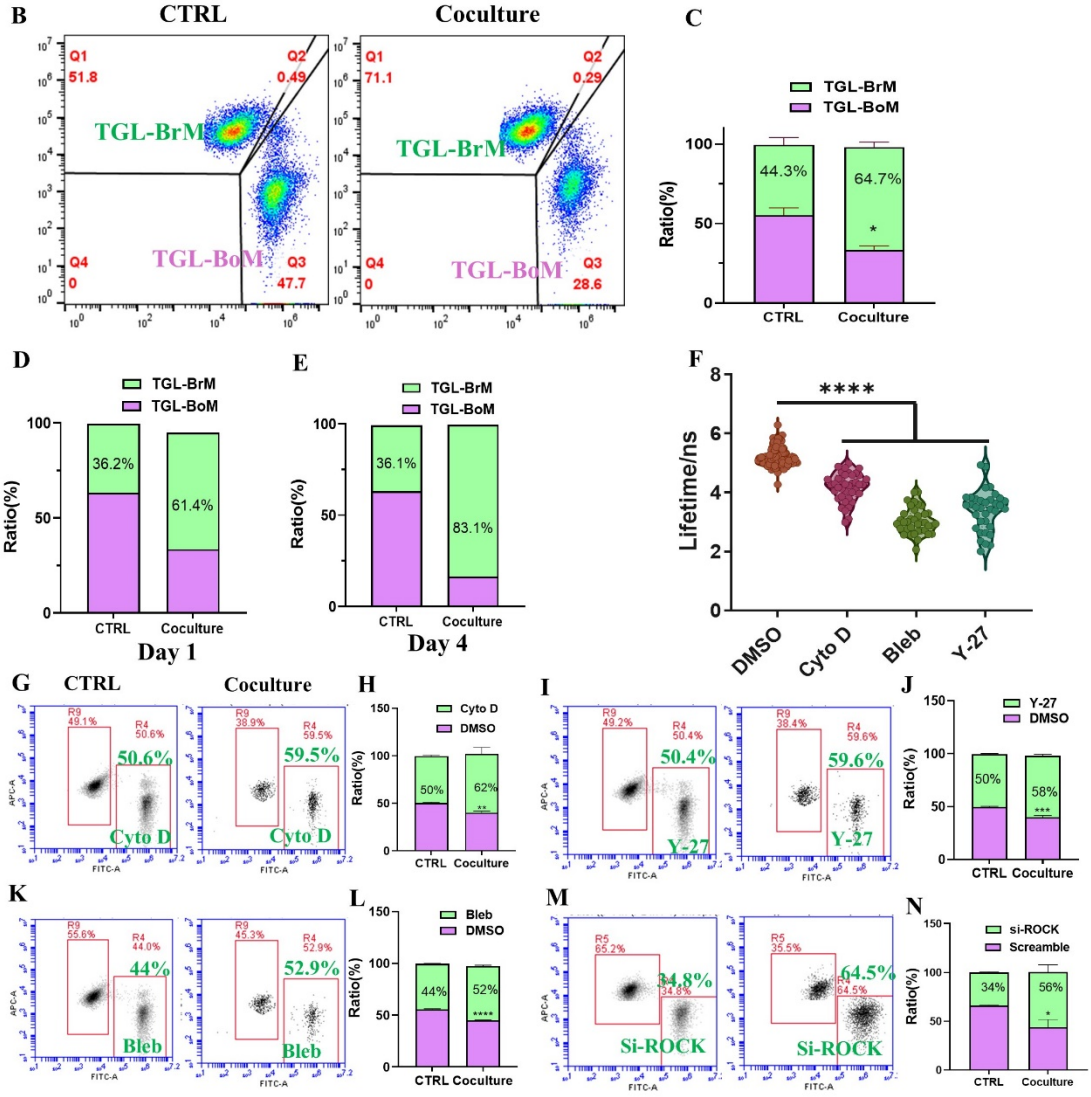
B
CTRL
Coculture
Q1
51.8
Q2
0.49
TGL-BrM
Q4
0
TGL-BoM
Q3
47.7
Q1
71.1
Q2
0.29
TGL-BrM
Q4
0
TGL-BoM
Q3
28.6
C
TGL-BrM
TGL-BoM
Ratio(%)
44.3%
64.7%
*
CTRL
Coculture
D
TGL-BrM
TGL-BoM
Ratio(%)
36.2%
61.4%
CTRL
Coculture
Day 1
E
TGL-BrM
TGL-BoM
Ratio(%)
36.1%
83.1%
CTRL
Coculture
Day 4
F
****
Lifetime/ns
DMSO
Cyto D
Bleb
Y-27
G
CTRL
Coculture
50.6%
Cyto D
59.5%
Cyto D
H
Cyto D
DMSO
Ratio(%)
50%
62%
**
CTRL
Coculture
I
50.4%
Y-27
59.6%
Y-27
J
Y-27
DMSO
Ratio(%)
50%
58%
***
CTRL
Coculture
K
44%
Bleb
52.9%
Bleb
L
Bleb
DMSO
Ratio(%)
44%
52%
****
CTRL
Coculture
M
34.8%
Si-ROCK
64.5%
Si-ROCK
N
si-ROCK
Screamble
Ratio(%)
34%
56%
*
CTRL
Coculture

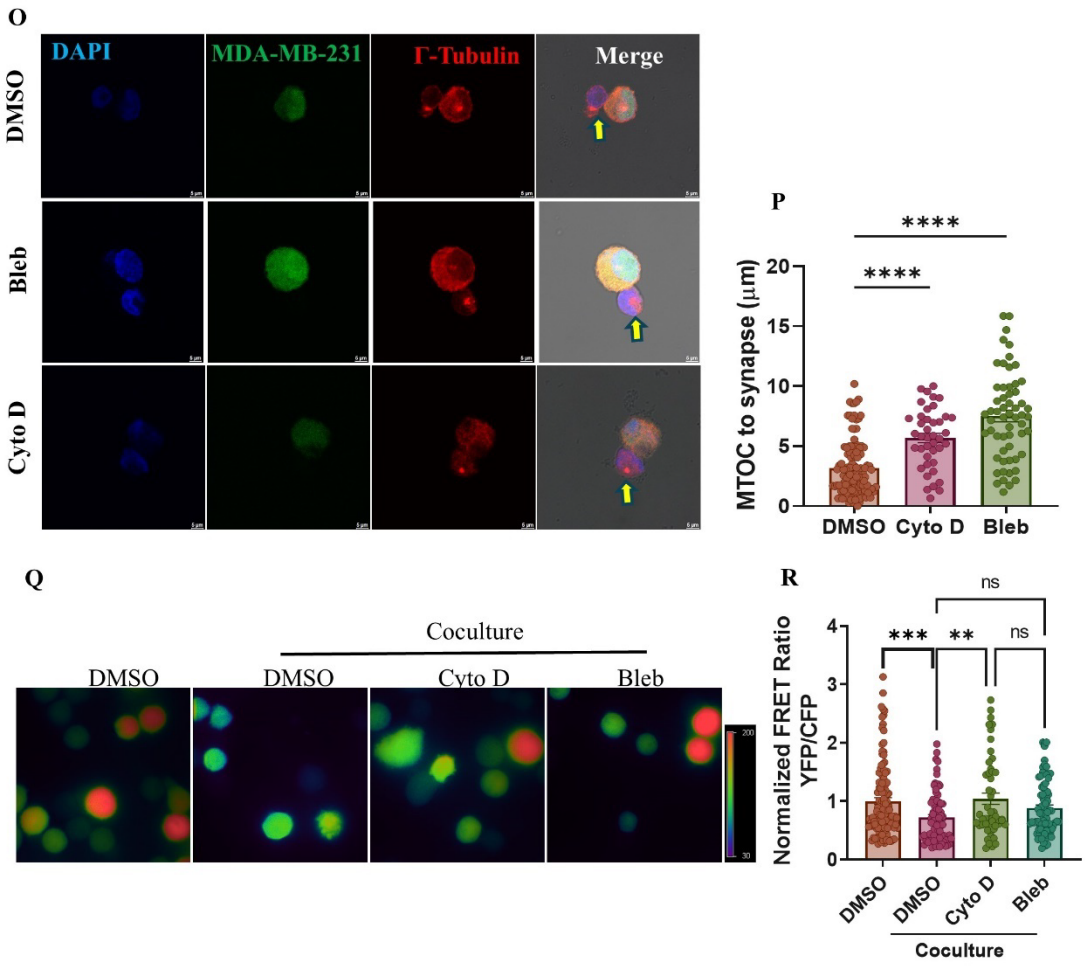

Figure 4-4 Tumor cells with low membrane tension are more resistant to NK cell killing

A Diagram of experimental design. **B** Flow cytometry of mixed TGL-BoM (green) and TGL-BrM (red) cells with and without co-culture with NK92 cells. **C** Statical analysis TGL-BoM VS TGL-BrM ratio in **B**. n=3 independent experiments. **D & E** TGL-BoM VS TGL-BrM ratio at day 1 (**D**) and day 4 (**E**). **F** Membrane tension indicated by probe fluorescence lifetime of control and drug-treated cells measured by FLIM. **G**, **I**, **K**, and **M** Flow cytometry of mixed drug-treated or si-MLCK tumor cells (green) and DMSO-treated or si-scramble tumor cells (red) with and without co-culture with NK92 cells. **H**, **J**, **L**, **& N** Statistical analysis of the ratio of two groups of cells in **G**, **I**, **K**, **& M**. n=3 independent experiments. **O** Immunostaining of MTOC (γ-tubulin) in the DMSO and drug-treated tumor cells. Yellow arrow: MTOC of NK cells. **P** Statistical analysis of MTOC polarization to synapse within NK cells after co-culture with the DMSO and drug-treated tumor cells. **Q** Representative images of granzyme B FRET ratio (YFP/CFP) in tumor cells with and without co-culture. **R** Statistical analysis granzyme B FRET ratio (YFP/CFP) in **Q**. The one-way ANOVA followed by Tukey's test (**F, P, & R**) and paired t-test (**C, H, J, & L**) were adopted for statistical analysis.

The cortical amount of actin filaments and the activity of the cortical actomyosin

determine the cortical tension and membrane tension. To investigate the effect of low membrane tension on killing resistance in WT tumor cells, tumor cells were first treated with typical drugs: Cyto D, Bleb, and Y-27 that inhibit actin polymerization, myosin activity, and ROCK activity, respectively. All these drugs decreased cell membrane tension (Figure 4-4 **F** & **G**). Indeed, within 4 h, tumor cells with low membrane tension were more resistant to NK cell cytotoxicity (Figure 4-4 **H** & **O**).

Stimulated by target cells will induce MTOC polarization towards the synapse. Immunostaining of γ-tubulin (indicating MTOC) in conjugated cells showed that the MTOC of NK cells was closer to Cyto D or Bleb-treated tumor cells, as shown in Figure 4-4 **P** & **Q**. MTOC carries many granules, which contain effector proteins like granzyme B and perforin. The survival of tumor cells with low membrane tension within a given time scale suggested a low killing efficiency relying on effector proteins like granzyme B. Indeed, NK cells delivered significantly less granzyme B into drug-treated tumor cells using a granzyme B FRET sensor (Figure 4-4 **R** & **S**).

These results suggested that tumor cells with lower membrane tension were more resistant to NK cell immune surveillance, mimicking the mechanical and immune evasion properties of TGL-BrM cells.

4.5 Increasing tumor cell membrane tension enhances NK cell cytotoxicity

Since tumor cells with low cell membrane tension are highly immune evasive, increasing the membrane tension may enhance the NK cell tumor surveillance. To verify this possibility, we overexpress ezrin in MDA-MB-231 cells, which is one of the main mediators for membrane-to-cortex attachment and is downregulated in co-cultured tumor cells (Figure 4-2 **C**, **F**, **G,** and Figure 4-5-1 **B**). Tumor cell Membrane tension significantly increased after overexpression of ezrin (Figure 4-5-1 **C**). Negative control (NC) MDA-MB-231 cells (dyed green) and ezrin-overexpressed (Ezrin) MDA-

MB-231 cells (dyed red) were mixed at a ratio of 1:1, followed by co-culture with NK92 cells (4:1) for 24 h. The changed ratios of tumor cells were detected (Figure 4-5-1 **A**). The results indicated that the proportion of Ezrin-overexpressing cells declined from 53.4% to 37.7% following co-culture with NK cells (Figure 4-5-1 **D & E**). A relative increase of 31.4% more Ezrin-MDA-MB-231 cells were killed within 24 h. This indicated that NK cells sensed the different membrane tension of control cells and ezrin-overexpressed tumor cells and might induce differential activation. Immunostaining of γ-tubulin (indicates MTOC) in conjugated tumor cell-NK cells showed that the MTOC of NK cells was closer to ezrin-overexpressed tumor cells, as shown in Figure 4-5-1 **F** & **G**. More elimination of ezrin-overexpressed tumor cells within a given time scale (24 h) requires higher killing efficiency relying on effector proteins like granzyme B. Indeed, NK cells delivered more granzyme B into ezrin-overexpressed tumor cells in both immunostaining and flow cytometry assays (Figure 4-5-1 **H-J**).

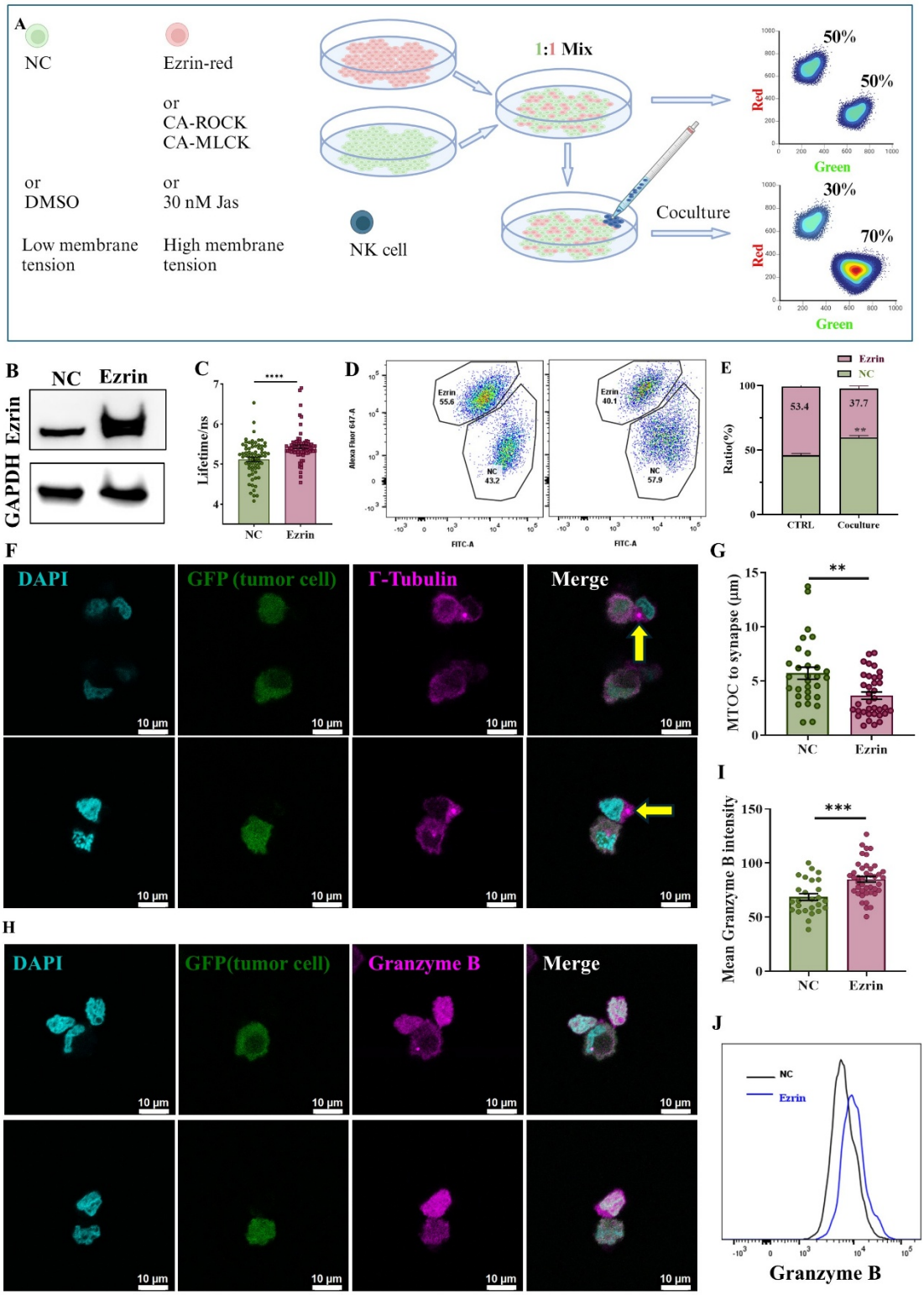

Figure 4-5-1 Increasing tumor cell membrane tension by overexpressing ezrin renders tumor cells more vulnerable to NK-mediated killing

A Diagram of experimental design. **B** Western blot of Ezrin in NC and ezrin-overexpressed MDA-MB-231 cells. **C** Statical analysis of the lifetime of the Flipper

probe in NC/ezrin-overexpressing tumor cells, positively correlated with cell membrane tension. n=73 for the NC group; n=74 for the Ezrin group. **D** Flow cytometry of mixed NC and ezrin-overexpressing tumor cells with or without co-culture for 24 h. **E** Statistical analysis of the ratio of NC VS ezrin-overexpressing tumor cells in **C**. n=3 independent experiments. **F** Immunostaining of MTOC (γ-tubulin) in NK cells when co-culturing with the NC/ezrin-overexpressing tumor cells. **G** Statistical analysis of the distance between the MTOC of NK cells and the synapses. Yellow arrow: MTOC of NK cells. n=30 for the NC group, n=36 for the Ezrin group. **H** Immunostaining of granzyme B in tumor cells. Cyan, nucleus; GFP, tumor cell; Purple, γ-tubulin. **I** Statistical analysis of the injected granzyme B into tumor cells in **H**. n=26 for the NC group, n=42 for the Ezrin group. **J** Flow cytometry of granzyme B in NC and ezrin-overexpressing tumor cells after co-culture with NK cells for 4 h. The paired t-test (**E**) and paired t-test (**C, G, and I**) were adopted for statistical analysis.

To further validate this, tumor cells were treated with Jasplakinolide (Jas), which promotes actin polarization, or transfected with inducible constitutively active ROCK (CA-ROCK), which promotes both actin polarization and myosin activity[262,263]. Jas treatment and CA-ROCK increased tumor membrane tension (Figure 4-5-2 **A & D**). Similarly, the cytotoxicity assay indicated that increasing tumor cell membrane tension by Jas or CA-ROCK could significantly promote NK cell killing (Figure 4-5-2 **B, C, E & F**). The MTOC of NK cells was closer to Jas-treated or CA-ROCK tumor cells (Figure 4-5-2 **G** & **H**). Moreover, more granzyme B was delivered into Jas-treated tumor cells (Figure 4-5-2 **I & J**). Importantly, after co-culture with NK cells those that survived immune evasive tumor cells could be shifted to immune sensitive phenotype by increasing membrane tension using Jas, as indicated by increased granzyme B delivery in tumor cells that were pre-co-cultured, followed by Jas treatment and then second co-culture with NK cells (Figure 4-5-2 **K & L**).

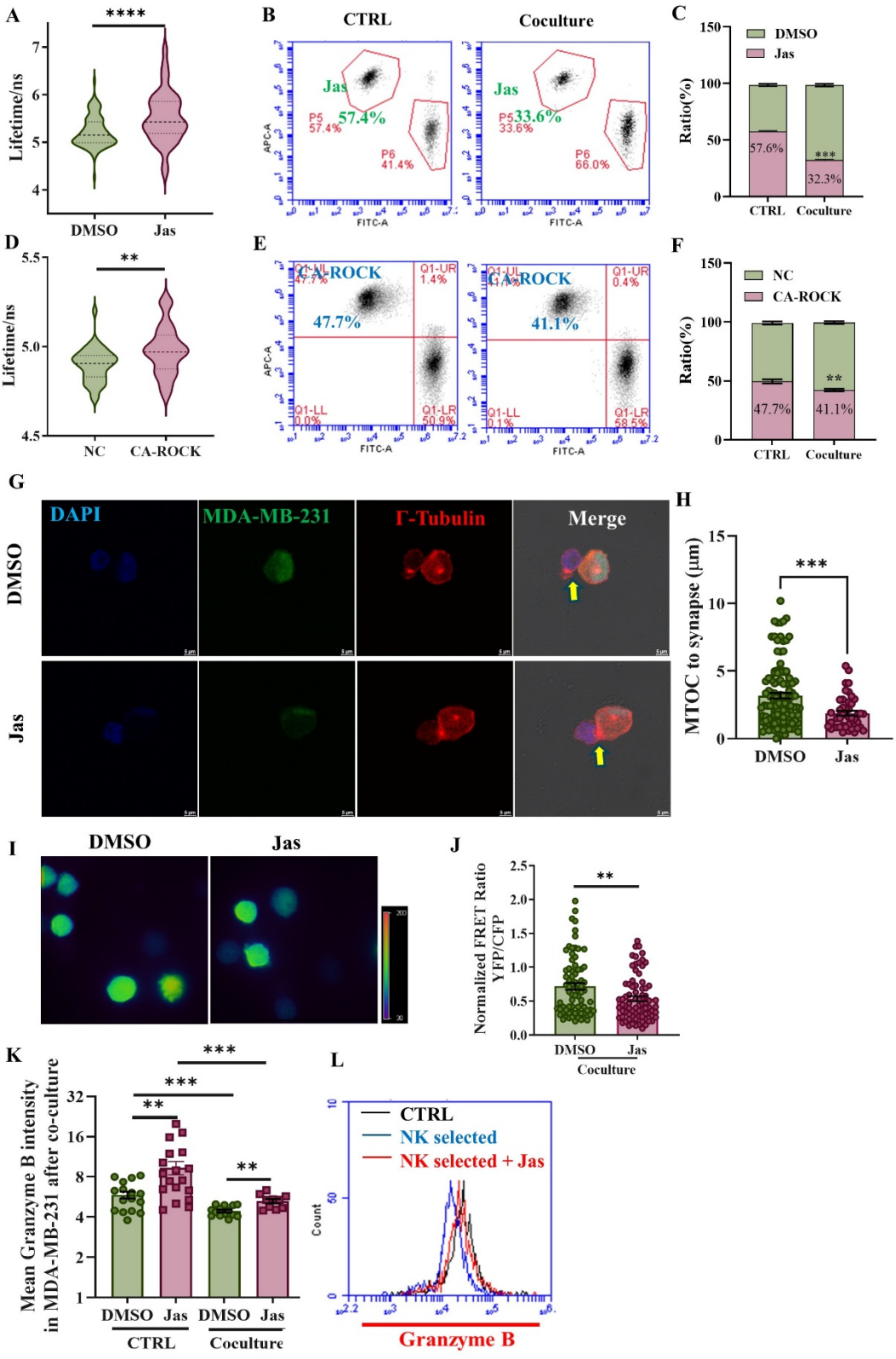

Figure 4-5-2 Increasing tumor cell membrane tension with Jas and CA-ROCK renders tumor cells more vulnerable to NK cell cytotoxicity.

A Lifetime of the Flipper probe in DMSO and Jas-treated tumor cells, positively correlated with cell membrane tension. n=102 for the DMSO group; n=41 for the Jas

group. **B** Flow cytometry of DMSO and Jas treated tumor cells with or without co-culture for 24 h. **C** Statistical analysis of the ratio of DMSO VS Jas Jas-treated tumor cells in **B**. n=3 independent experiments. **D** Lifetime of the Flipper probe in NC and CA-ROCK-expressing tumor cells, positively correlated with cell membrane tension. n=40 for the NC group; n=41 for the CA-ROCK group. **E** Flow cytometry of NC and CA-ROCK-expressing tumor cells with or without co-culture for 24 h. **F** Statistical analysis of the ratio of NC and CA-ROCK-expressing tumor cells in **E**. n=3 independent experiments. **G** Immunostaining of MTOC (γ-tubulin) in NK cells when co-culturing with the DMSO and Jas treated tumor cells. **H** Statical analysis of the distance between the MTOC of NK cells and the synapses in **G**. Yellow arrow: MTOC of NK cells. n=119 for the DMSO group, n=45 for the Jas group. **I** Representative images of FRET ratio (YFP/CFP) heatmap of granzyme B reporter expressing NK cells when co-culturing with the DMSO and Jas treated tumor cells. **J** Statical analysis of the FRET ratio in granzyme B reporter expressing NK cells in **I**. K Granzyme B intensity in DMSO and Jas treated tumor cells with or without co-culture with NK cells. **L** Flow cytometry of granzyme B in DMSO, NK-selected, and NK-selected + Jas treated tumor cells after co-culture with NK cells for 4 h. The one-way ANOVA followed by Tukey's test (**K**), paired t-test (**C & F**), and unpaired t-test (**A, D, H, & J**) were adopted for statistical analysis.

The above results were all based on in vitro experiments, which might not happen in vivo due to much more complicated situations. We tried to do this in severely immunodeficient NOD/SCID mice, which contain functionally defective NK cells but no B cells and T cells. To delete the endogenous mouse NK cells, Asialo GM1 Polyclonal Antibody was used to empty mouse NK cells in NOD/SCID mice before the experiment. A total of 1 million MDA-MB-231 cells with relatively low membrane tension (NC-mCherry) and high membrane tension (CA-ROCK-GFP) were mixed 1:1 (confirmed by flow cytometry before injection) and subcutaneously injected, followed by tail vein injection of PBS or 10 million NK92 cells once a week (Figure 4-5-3 **A**). Subcutaneous injection can avoid metastasis-induced changes in cell ratio in mixed tumors. All mice were fed with doxycycline-containing food to induce CA-ROCK expression. Tumors were collected and digested for flow cytometry or fixed for immunostaining. After 4 weeks of growth, the ratio of CA-ROCK rose from 50% up to 77.9% in the PBS-injection groups, indicating a higher proliferation compared with NC cells (Figure 4-5-3 **B**, **left panel**). As expected, in the NK cell-injection groups, the ratio

of CA-ROCK was only 58.7%, a relative 41.7% decrease (Figure 4-5-3 **B**, **right panel and C**). Similar results were found by immunostaining (Figure 4-5 **D & E**).

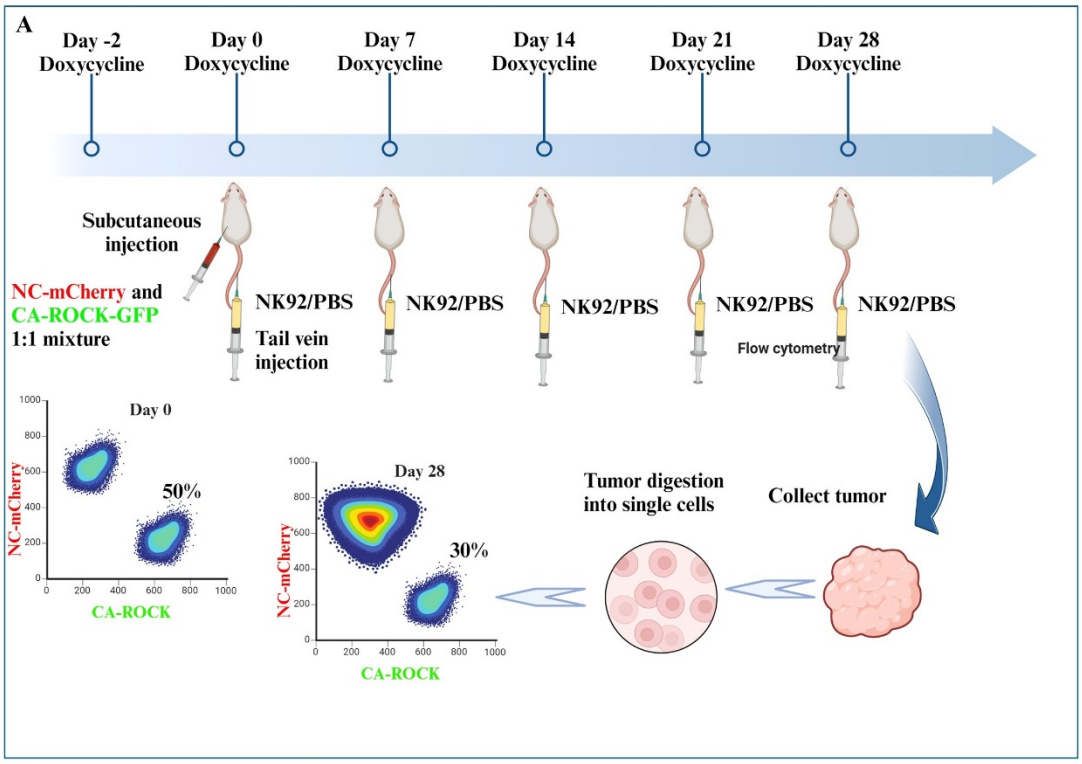

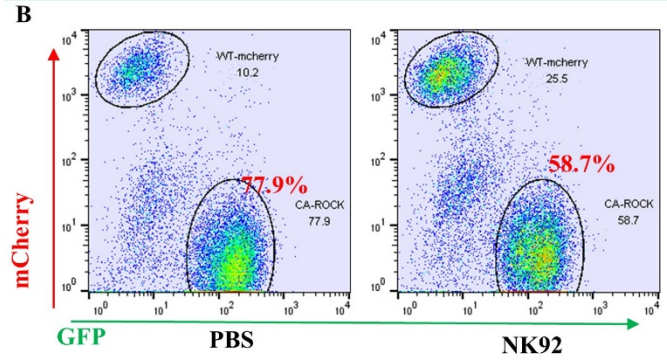

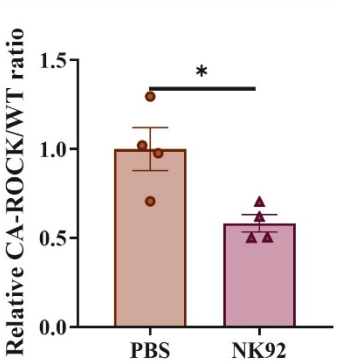

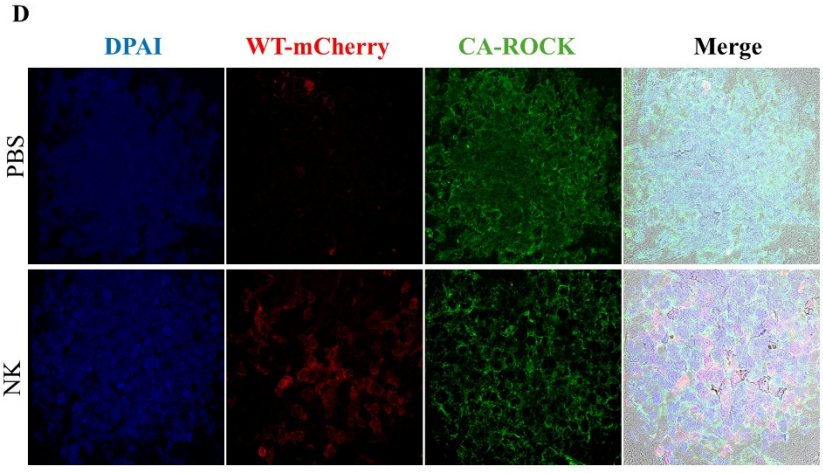

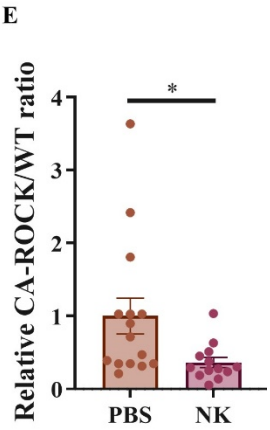

Figure 4-5-3 Increasing tumor cell membrane tension rendered tumor cells more vulnerable to NK cell cytotoxicity in vivo

A Diagram of experimental design. **B** Flow cytometry of NC-mCherry VS CA-ROCK-GFP expressing tumor cells in a primary tumor on day 28 with or without NK cells injection. **C** Statical analysis of the relative of NC-mCherry VS CA-ROCK-GFP expressing tumor cells in **B**. n=4 for both groups. **D** Immunostaining of primary tumor slides. **E** Statistical analysis of the relative of NC-mCherry VS CA-ROCK-GFP expressing tumor cells in **D.** n=15 for the NC group; n=13 for the CA-ROCK group. The unpaired t-test (**C & E**) was adopted for statistical analysis.

To summarize, through both in vitro and in vivo experiments, we provided evidence that increasing tumor cell membrane tension rendered tumor cells more vulnerable to NK cell cytotoxicity.

4.6 Targeting tumor cell membrane tension inhibits brain metastasis

The observed low tumor cell membrane tension after co-culture with NK cells (Figure 4-2) may be required for brain metastasis formation. To test this, we overexpress ezrin, which was downregulated after co-culture. Ezrin overexpression increased cell membrane tension (Figure 4-5-1 **C**) and decreased cell aspect ratio after co-culture with NK cells (Figure 4-6-1 **A** & **B**). Indeed, ezrin overexpression inhibited tumor cells' trans-BBB migration, especially after co-culture with NK cells. The number of trans-BBB migrated tumor cells after co-culture decreased to the control level (Figure 4-6-1 **C** & **D**).

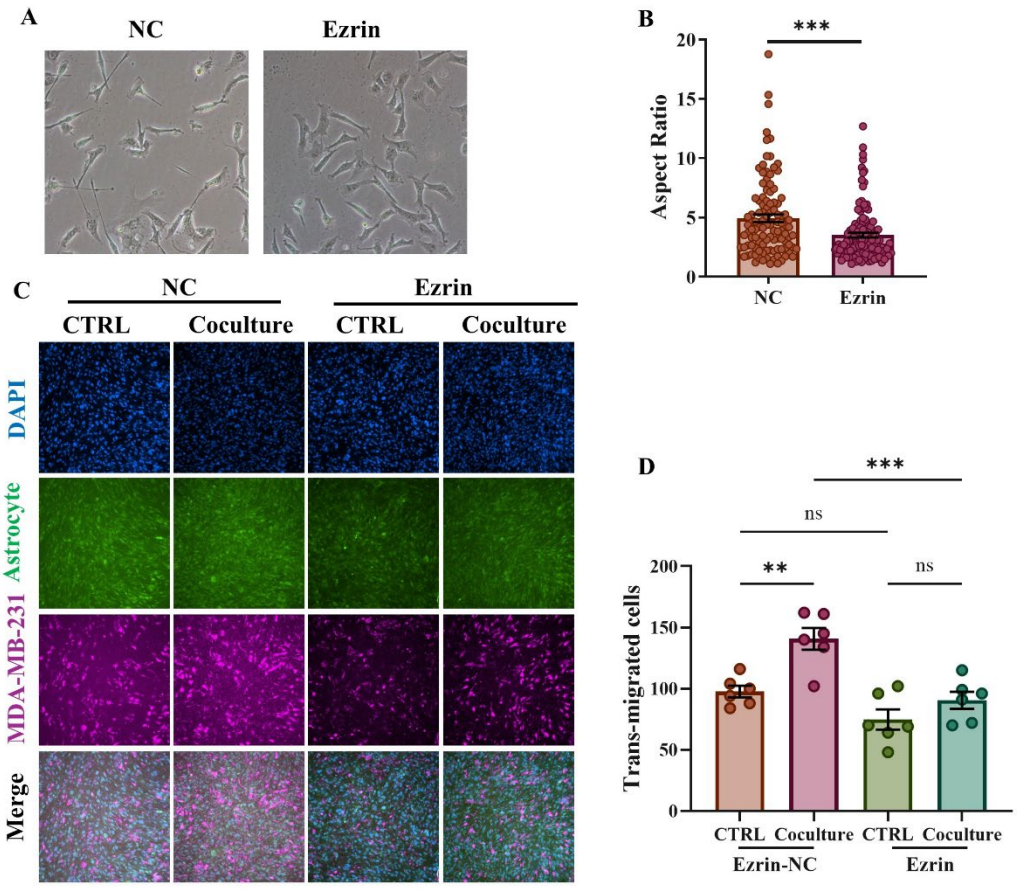

Figure 4-6-1 Targeting tumor cell membrane tension inhibits trans-BBB migration in vitro

A Morphology of NC and ezrin-overexpressing tumor cells after co-culture with NK cells. **B** Statistical analysis of cell aspect ratio in A. n=108 for the NC group, n=121 for the Ezrin group. **C** Representative images of trans-BBB migration of the NC/NC-Coculture/Ezrin/Ezrin-Coculture cells. Blue, DAPI; Green, astrocyte; Purple, tumor cell. **D** Statistical analysis of tumor cell trans-BBB migration in **C**. N=6 independent experiments. The one-way ANOVA followed by Tukey's test (**D**) and unpaired t-test (**B**) were adopted for statistical analysis.

More importantly, overexpressing ezrin significantly decreased brain metastasis occurrence and increased brain-metastasis-free survival (Figure 4-6-2 **A-F**). Meanwhile, metastasis occurrence to liver/ lung/bone was not affected (Figure 4-6-2 **G**). These data indicate that NK cell-promoted tumor cell brain metastasis could be specifically blocked by targeting tumor cell membrane tension.

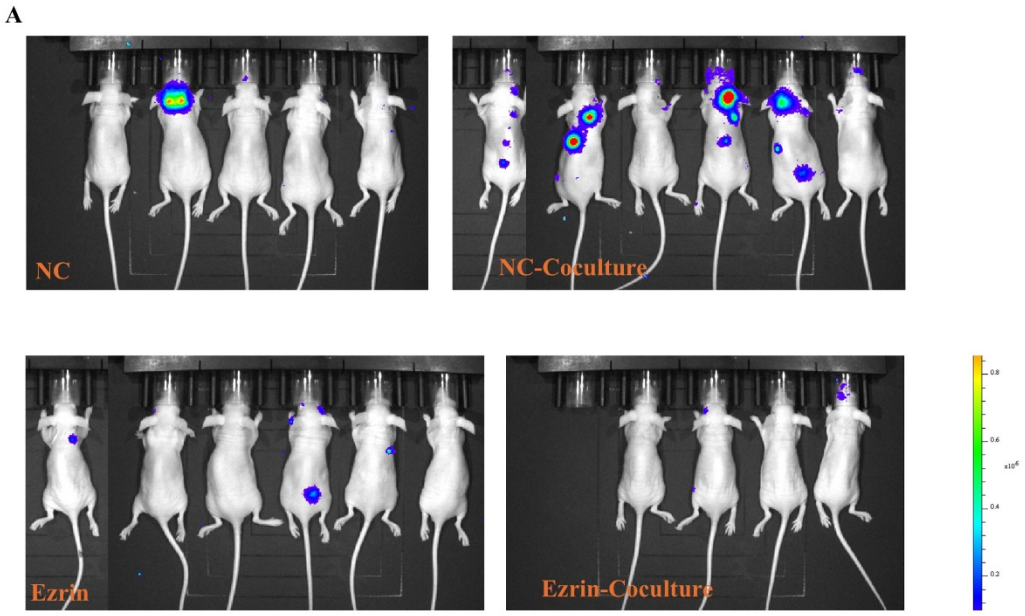
A
NC
NC-Coculture
Ezrin
Ezrin-Coculture

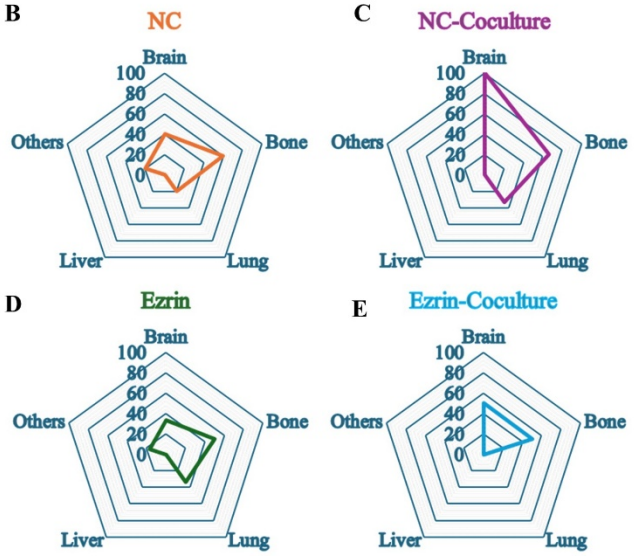
B
NC
C
NC-Coculture
D
Ezrin
E
Ezrin-Coculture
Brain
Bone
Lung
Liver
Others
100
80
60
40
20
0

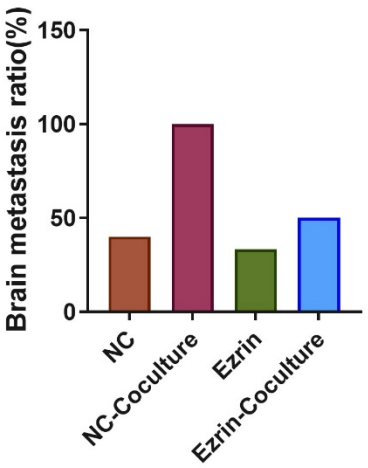
F
Brain metastasis ratio(%)
150
100
50
0
NC
NC-Coculture
Ezrin
Ezrin-Coculture

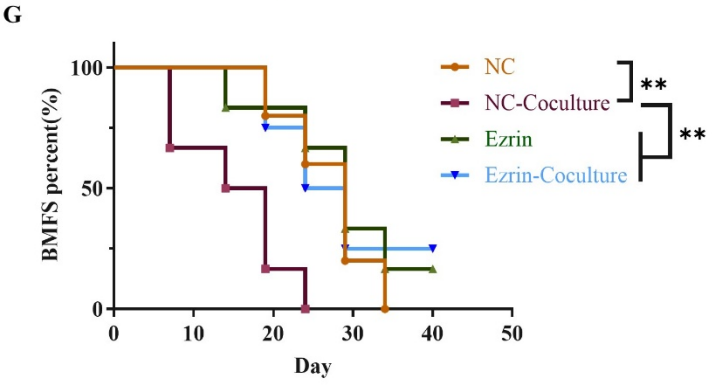
G
BMFS percent(%)
100
50
0
0
10
20
30
40
50
Day
NC
NC-Coculture
Ezrin
Ezrin-Coculture
**
**

Figure 4-6-2 Targeting tumor cell membrane tension inhibits brain metastasis in vivo

A IVIS images of nude mice intracardially injected with the NC/NC-Coculture/Ezrin/Ezrin-Coculture tumor cells. **B-E** Organ distribution of metastasis on day 24 after intracardiac injection of respective tumor cells. **C** Brain metastasis ratio of NC/NC-Coculture/Ezrin/Ezrin-Coculture cells on day 24 after intracardiac injection. **F** Kaplan-Meier plots of BMFS of nude mice intracardially injected with the NC/NC-Coculture/Ezrin/Ezrin-Coculture tumor cells. The one-way ANOVA followed by a log-rank test (**G**) was adopted for statistical analysis.

4.7 NK cell promoted brain metastasis through PI3K-Akt signaling

Low tumor cell membrane tension enhances tumor cell migration and metastasis, but how it specifically promotes brain metastasis is still unknown. To explore the mechanism, we analyzed our RNA-seq data and found that JAK-STAT1 (downstream of IFN-γ), TNF (downstream of TNF-α), and PI3K-Akt signaling were the top-enriched pathways in co-culture tumor cells (Figure 4-7-1 **A**). To test whether these cytokines could promote the brain metastatic potential of tumor cells, we used a conditional co-culture system (Figure 4-7-1 **B**). In this design, tumor cells were seeded both on the bottom of the well and the upside surface of a 0.4 μm insert. NK cells were added to the well but outside of the insert. Upon engagement with tumor cells on the bottom, NK cells would secrete multiple cytokines, which could freely diffuse into the insert with no entry of NK cells. Comparing the expression of a key brain metastasis-associated protein-Serpin B2, for control, co-cultured tumor cells, and tumor cells among the insert, it was found that no obvious increase in Serpin B2 expression of tumor cells among the insert (Figure 4-7-1 **C & D**) was detected. In consideration of the diffusion efficiency of cytokines into the insert, we also co-cultured tumor cells with NK92 cells for 24h first and collected the cell-free conditioned medium (CM). Then we treated MDA-MB-231 cells with the CM. However, no significant changes in brain metastasis-associated Cox2 expression (Figure 4-7-1 **E & F**), adhesion to the brain endothelial monolayer

(Figure 4-7-1 **G & H**), or morphology (Figure 4-7-1 **I**) were observed.

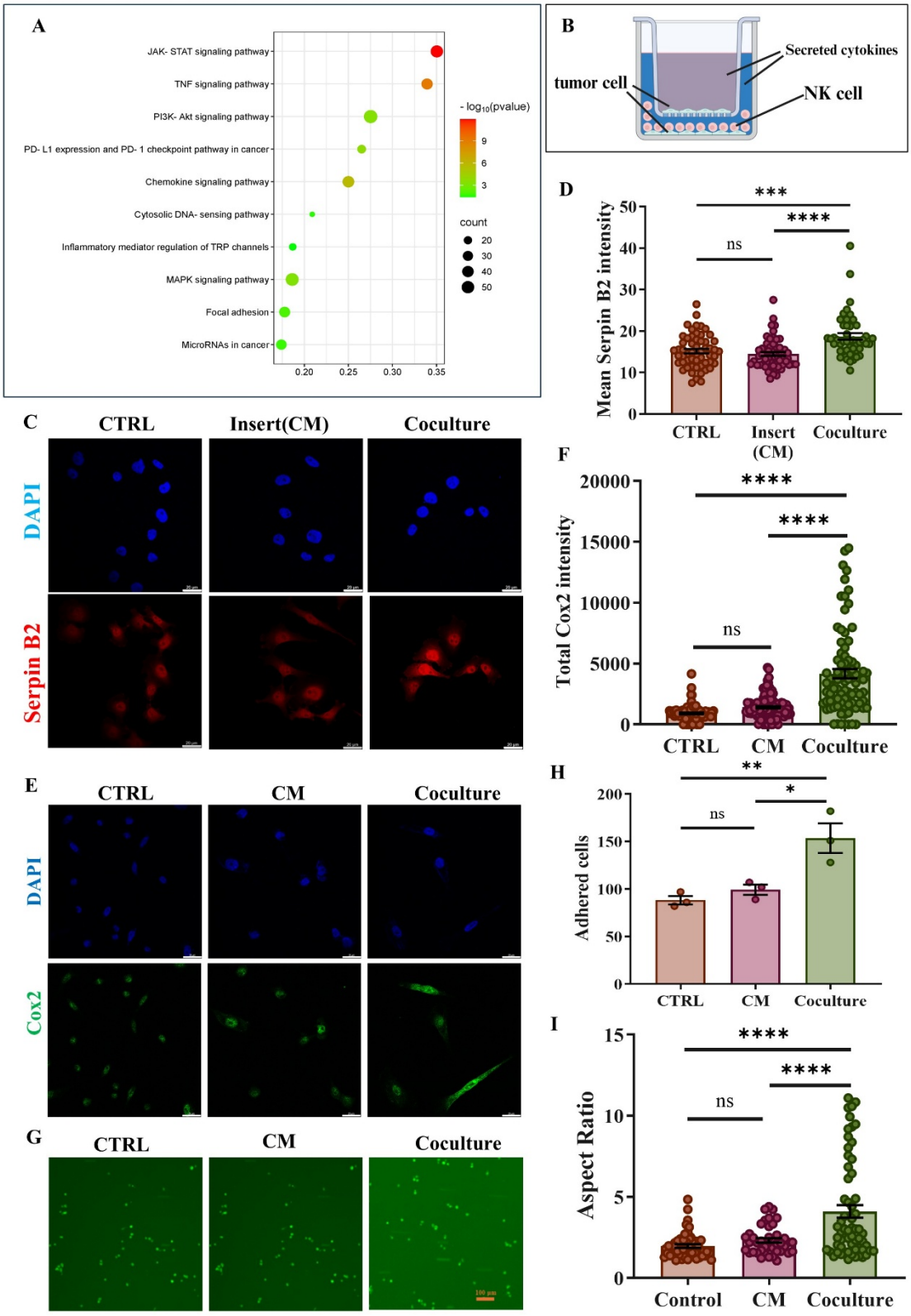

Figure 4-7-1 JAK-STAT and TNF signaling are not involved in NK-induced brain metastasis in vitro

A The top 10 enriched signaling in co-cultured MDA-MB-231 cells. **B** Experimental design of the co-culture system in a 0.4 μm trans-well to investigate the effect of NK cell-secreted cytokines. **C** Immunostaining of Serpin B2 of control/tumor cells in the insert/co-cultured tumor cells. **D** Statistical analysis of Serpin B2 expression in **C**. n=50 for the CTRL group; n=59 for the insert group; n=46 for the Coculture group. **E** Immunostaining of Cox2 of control/CM/co-cultured tumor cells. **F** Statistical analysis of Cox2 expression in **E**. n=88 for the CTRL group; n=114 for the CM group; n=84 for the Coculture group. **G** Representative images of control/CM/co-cultured tumor cells adhesion to the brain endothelial cell monolayer under 2 dyn/cm^2 FSS. **H** Statistical analysis of adhered tumor cell numbers in **G**. **I** Aspect ratio of control/CM/co-cultured tumor cells. n=51 for the CTRL group; n=41 for the CM group; n=61 for the Coculture group. The one-way ANOVA followed by Tukey's test (**D, F, H & I**) was adopted for statistical analysis.

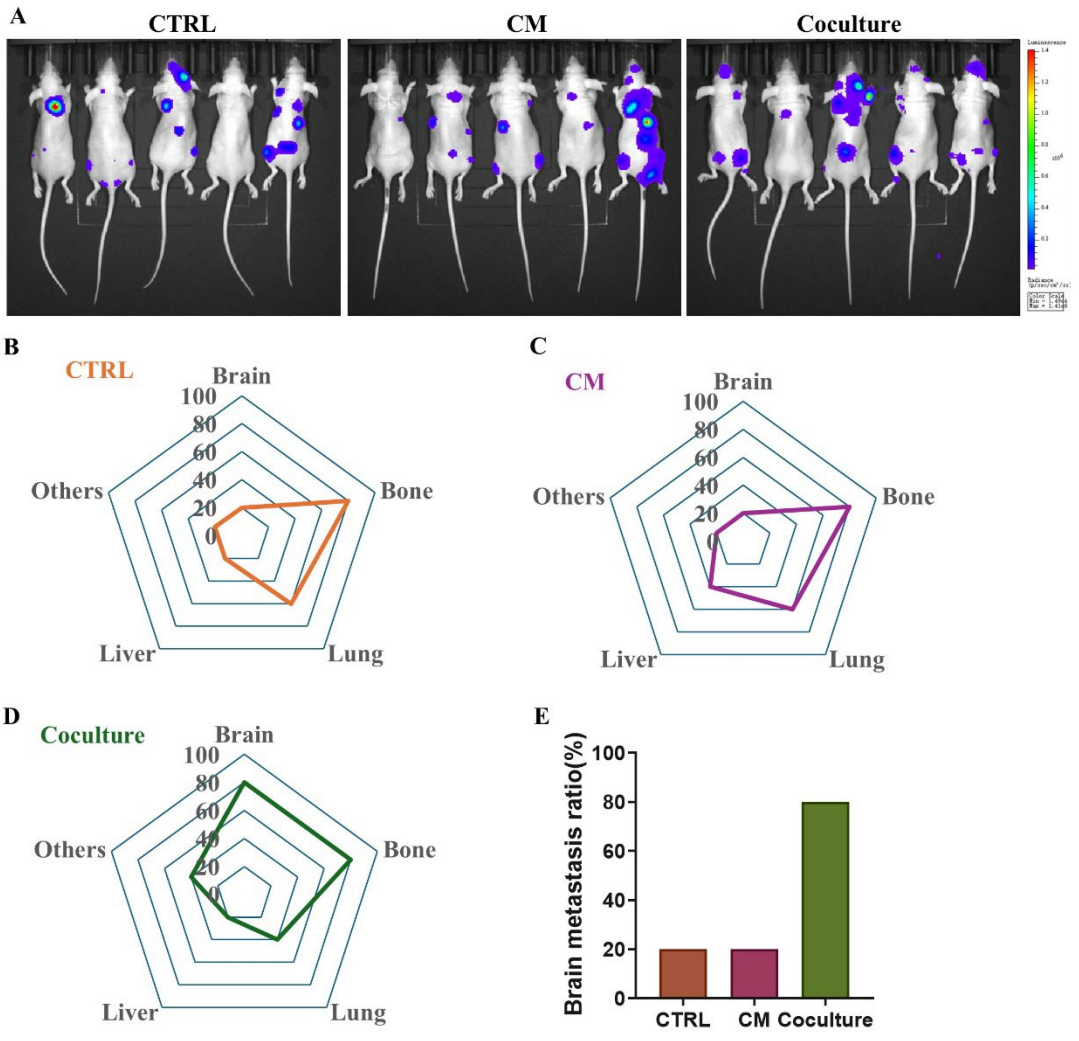

Figure 4-7-2 JAK-STAT and TNF signaling are not involved in NK-induced brain metastasis in vivo

A Luciferin imaging of nude mice with intracardiac injection of control/CM/co-cultured tumor cells on day 24. n=5 for all groups. **B** Organ distribution of metastasis based on Luciferin imaging of **A**. **C** Brain metastasis occurrence of control/CM/co-cultured tumor cells on day 24 based on Luciferin imaging of **A**.

More importantly, CM-treated tumor cells showed no increased brain metastasis occurrence or obvious organotropism change in vivo (Figure 4-7-2 **A**-**E**).

Next, we focused on the PI3K signaling. PI3K signaling has been proposed to promote breast cancer brain metastasis[110,111]. Indeed, PI3K signaling was enhanced in co-cultured tumor cells, represented by increased expression of PI3K-P85, Akt, and p-Akt (Figure 4-7-3 **A-D**). CM could not promote P85 expression (Figure 4-7-3 **A**), which further confirmed that NK cell-secreted cytokines did not promote brain metastasis. Interestingly, TGL-BrM cells also showed higher PI3K-P85 expression and downstream FOXO1 activation/nuclear export (Figure 4-7-3 **A right panel, E & F**), strongly implying the important role of the PI3K pathway in brain metastasis. To investigate whether membrane tension promoted brain metastasis through PI3K signaling, time-lapse imaging of live MDA-MB-231-FOXO1 reporter cells (GFP translocating from nucleus to cytoplasm once FOXO1 was activated by Akt) and tumor cell membrane tension was conducted at the same time. As shown in Figure 4-7-3 **G-I**, FOXO1 quickly translocated from the nucleus to the cytoplasm within 30 min after adding NK cells. At the same time, tumor cell membrane tension also sharply decreased.

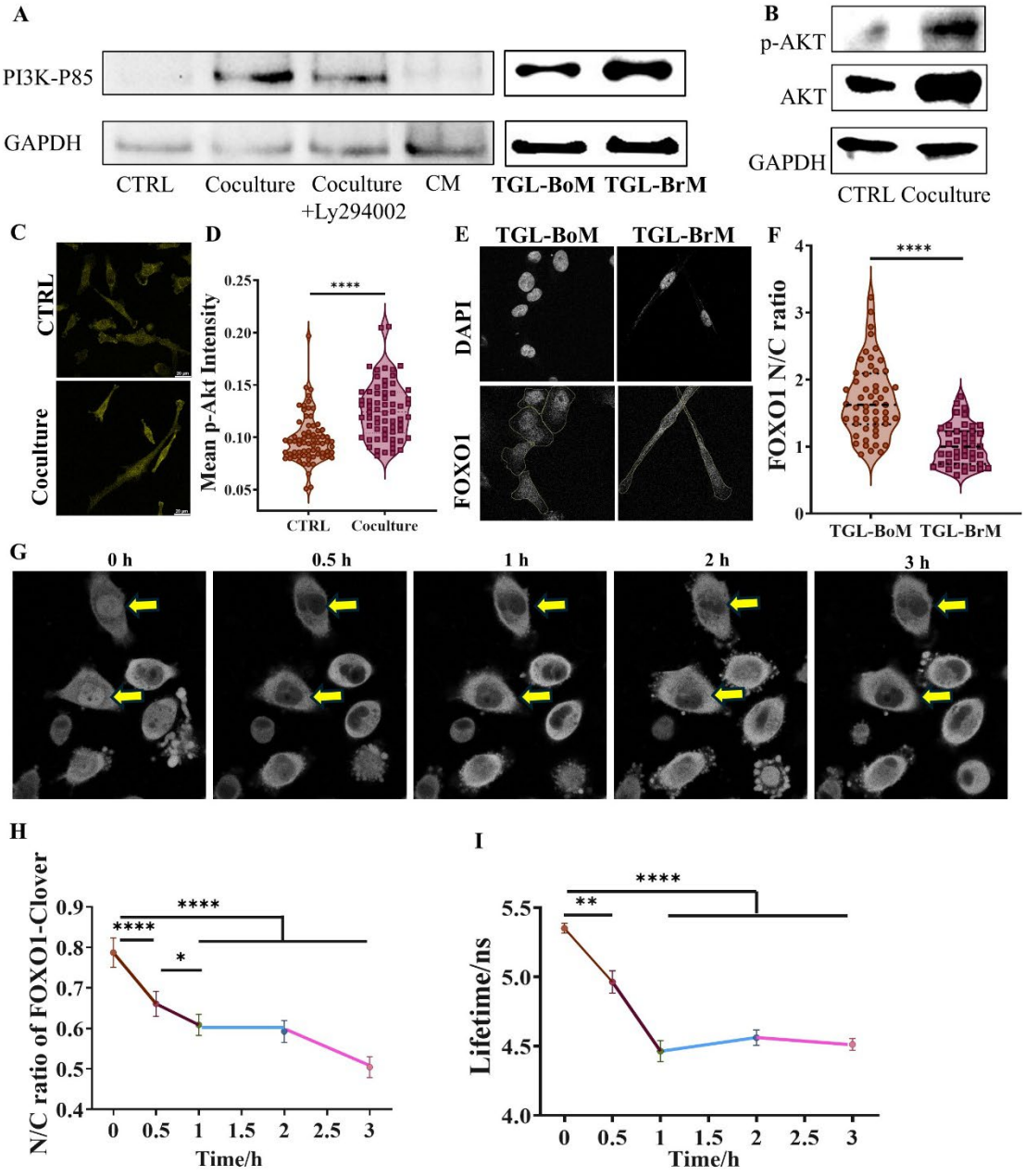

Figure 4-7-3 NK cells activate PI3K-Akt signaling in breast cancer cells

A Western blot of PI3K-P85 in CTRL, co-cultured, co-cultured+ly294002, CM, TGL-BoM, and TGL-BrM cells. **B** Western blot of Akt and p-Akt in CTRL/co-cultured tumor cells. **C** Immunostaining of p-Akt in CTRL/co-cultured tumor cells. **D** Statistical analysis of p-Akt intensity in CTRL/co-cultured tumor cells. n=71 for the CTRL group; n=65 for the co-culture group. **E** Representative images of FOXO1 nucleus/cytoplasm localization. **F** Statistical analysis of nucleus/cytoplasm (N/C) ratio of mean FOXO1 intensity. n=53 for the CTRL group; n=43 for the co-culture group. **G** Real-time imaging of FOXO1 reporter in live MDA-MB-231 cells using a confocal microscope under 37°C & 5% CO_2. NK cells were added at the time of 0 h. Arrows directed two obvious FOXO1 nuclei to cytoplasm translocation after NK cells addition. **H & I** Time-

lapse analysis of FOXO1 nucleus/cytoplasm translocation and membrane tension of the same tumor cells captured at the same time in **G**. n=70 cells. The RM one-way ANOVA followed by Tukey's test (**H & I**) and unpaired t-test (**D & F**) were adopted for statistical analysis.

Since ezrin anchors to the plasma membrane mainly through PIP2 and PI3K only phosphorylates PIP2 to generate PIP3 and to initiate downstream signaling, decreased ezrin expression and activity could release PIP2 for PI3K to target. Figure 4-3-2 **C & D** shows an increased plasma membrane PIP3 in tumor cells after co-culture, which might explain how membrane tension promotes brain metastasis through PI3K signaling. Initiation of PI3K signaling (Akt-specific activator sc79 treatment) would further decrease ERM expression and activity, as indicated by (Figure 4-7-4 **A**) and, as a result, decrease membrane tension (Figure 4-7-4 **B**) to form a positive feedback loop to promote brain metastasis-associated gene expression (Figure 4-7-4 **D**). Inhibiting PI3K activity of tumor cells with the specific drug Ly294002 after co-culture could partially rescue ERM expression and phosphorylation (Figure 4-7-4 **A**), which led to increased membrane tension (Figure 4-7-4 **C**) and, as a result, significantly inhibited brain metastasis-associated gene expression (Figure 4-7-4 **D**). These results were further confirmed by in vitro assays. Inhibiting tumor cells' PI3K activity after co-culture could decrease tumor cell adhesion to the brain endothelial monolayer but not HUVEC (Figure 4-7-4 **E-G**) and impaired Trans-BBB migration but not trans-HUVEC migration (Figure 4-7-5 **A, C, D & E**). Inhibiting Akt had a similar effect (Figure 4-7-5 **B**).

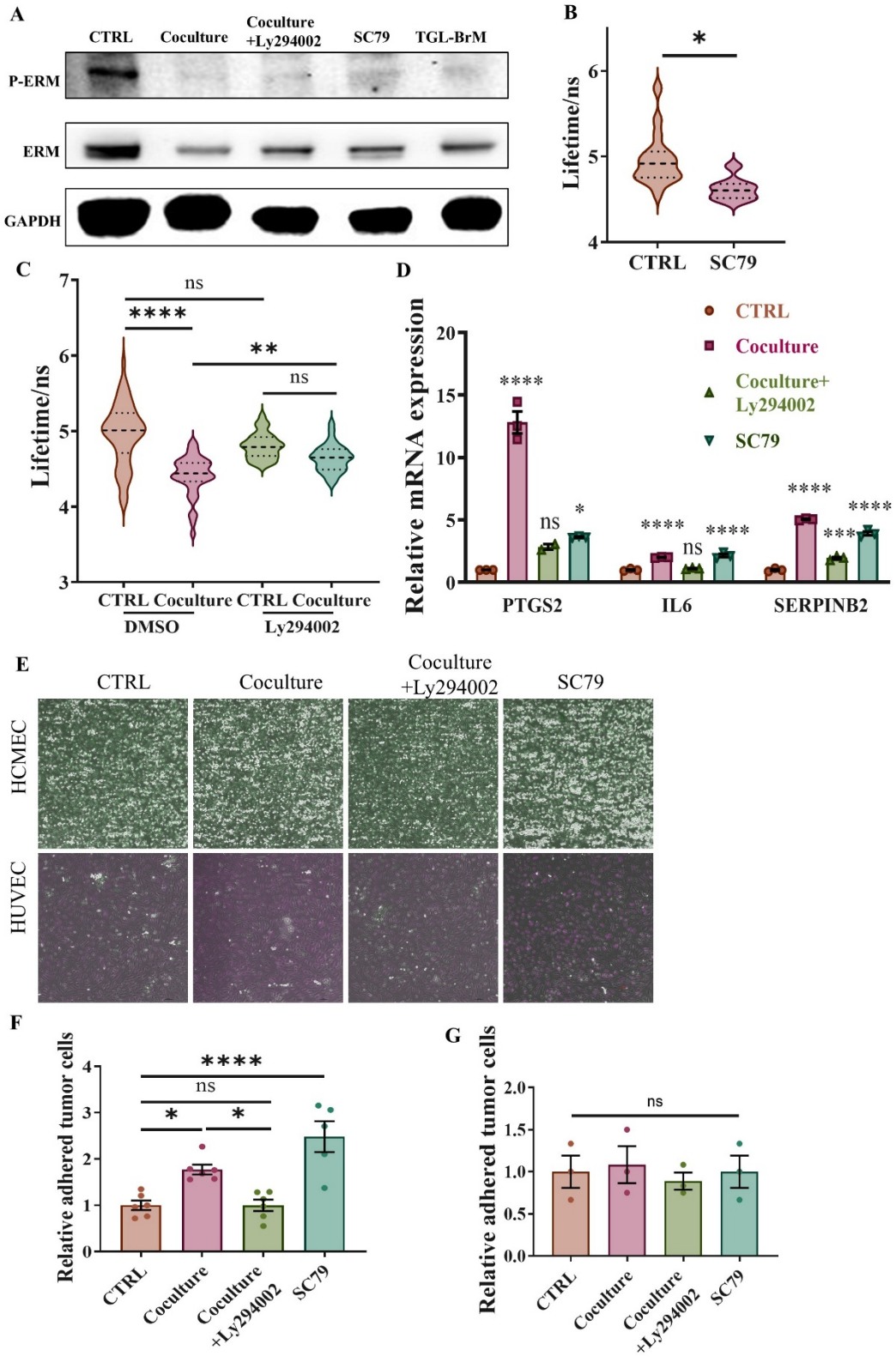

Figure 4-7-4 NK cells reduce tumor cell membrane tension and upregulate brain metastasis genes and adhesion to brain endothelium

A Western blot of ERM and p-ERM in CTRL, co-culture, co-culture+ly294002, SC79-treated, and TGL-BrM tumor cells. **B** Statistical analysis of tumor cell membrane

tension of tumor cells with or without activating Akt using SC79. **C** Statistical analysis of tumor cell membrane tension of CTRL and co-cultured MDA-MB-231 cells with or without inhibiting PI3K using Ly294002. **D** Brain metastasis-associated genes PTGS2, IL6, and SerpinB2 expression in CTRL, co-culture, co-culture+Ly294002, and SC79 treated tumor cells. **E** Representative images of CTRL, co-culture, co-culture+Ly294002, and SC79 treated tumor cells adhesion to brain endothelial HEVEC monolayer or HUVEC monolayer under 2 dyn/cm^2 FSS. HEVECs were stained with Cell Tracker Green; HUVECs were stained with Cell Tracker DeepRed. **F & G** Statistical analysis of tumor cells adhesion to brain endothelial HEVEC monolayer (**F**) or HUVEC monolayer (**G**) in **E**. n=6 independent experiments for **F**; n=3 independent experiments for **G**. The one-way ANOVA followed by Tukey's test (**F & G**), and unpaired t-test (**B, C, & D**) were adopted for statistical analysis.

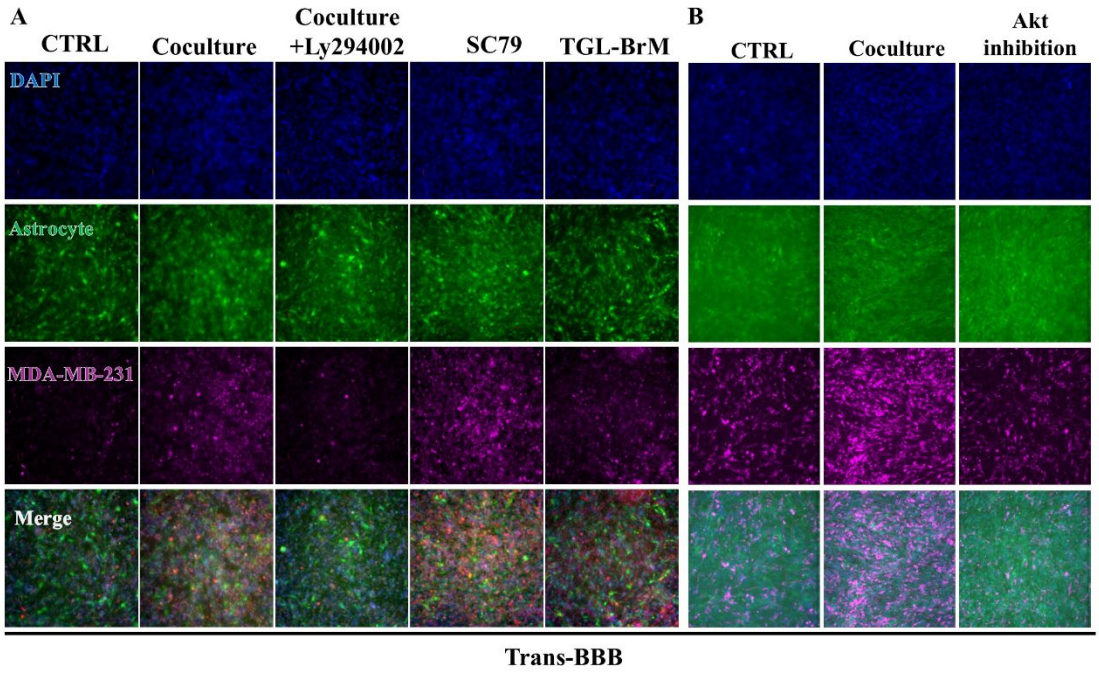

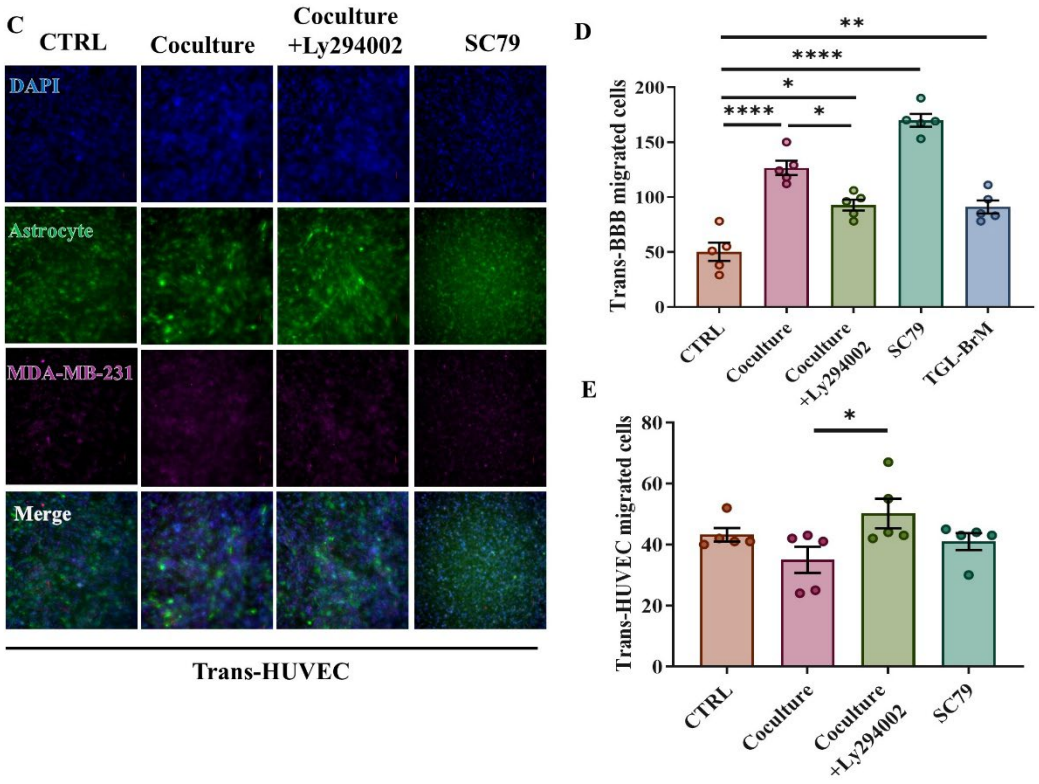

Figure 4-7-5 NK cells promote breast cancer trans-BBB migration through PI3K-Akt signaling

A Trans-BBB migration of CTRL, co-culture, co-culture+Ly294002, SC79-treated tumor cells, and TGL-BrM. **B** Trans-BBB migration of CTRL, co-culture, and Akt inhibited tumor cells after co-culture. **C** Trans-HUVEC migration of CTRL, co-culture, co-culture+Ly294002, SC79 treated tumor cells. **D & E** Statistical analysis of tumor cells Trans-BBB (**A**) or Trans-HUVEC (**C**). n=5 independent experiments for **A**; n=5 independent experiments for **C**. The one-way ANOVA followed by Tukey's test (**D & E**) was adopted for statistical analysis.

4.8 Membrane tension-PI3K signaling promotes NK-induced breast cancer brain metastasis through GLUT3-mediated glucose uptake

The above results prove that the ezrin/membrane tension-PI3K-Akt signaling is responsible for the enhanced tumor cell brain metastasis potential after co-culturing with NK cells. However, the key downstream effector protein of this signaling is still unknown. To figure out this question, we focused on the metabolic specificity of the brain tissue since metabolic adaptation is crucial for any secondary tumor formation.

Brain tissue is the biggest energy-consuming tissue. Under fasting conditions, more than half of the blood sugar is supplied to the brain[264]. Despite this, the interstitial glucose level is the lowest(1±0.1 mM) among all tissues[265]. Blood has the highest glucose level, typically ranging from 3.9 mM to 5.6 mM (World Health Organization) for a healthy human. The glucose levels of other organs are higher than the brain tissue but lower than the blood[266]. Thus, we proposed that the relatively low glucose level could be the limiting condition for brain metastasis formation.

Glucose transporters are responsible for glucose uptake from extracellular spaces. Among all types of glucose transporters, GLUT1 and GLUT3 show the highest expression in brain tissue, especially in neurons. Meanwhile, GLUT3 has the highest affinity to bind to glucose[267]. Malignant brain tumor cells have been found to overexpress GLUT3 to compete for glucose with resident cells[268]. Bulk RNA-seq analysis showed a significant increase of SLC2A3 (GLUT3 gene) but not SLC2A1 (GLUT1 gene) after co-culture (Figure 4-8-1 **A & B**), which is further confirmed by RT-qPCR and western blot (Figure 4-8-1 **C & D**). Interestingly, GLUT3 is also overexpressed in TGL-BrM cells and is under the control of ezri (Figure 4-8-1 **D**), as knocking out ezrin increased GLUT3 expression, but overexpression of ezrin had the opposite effect.

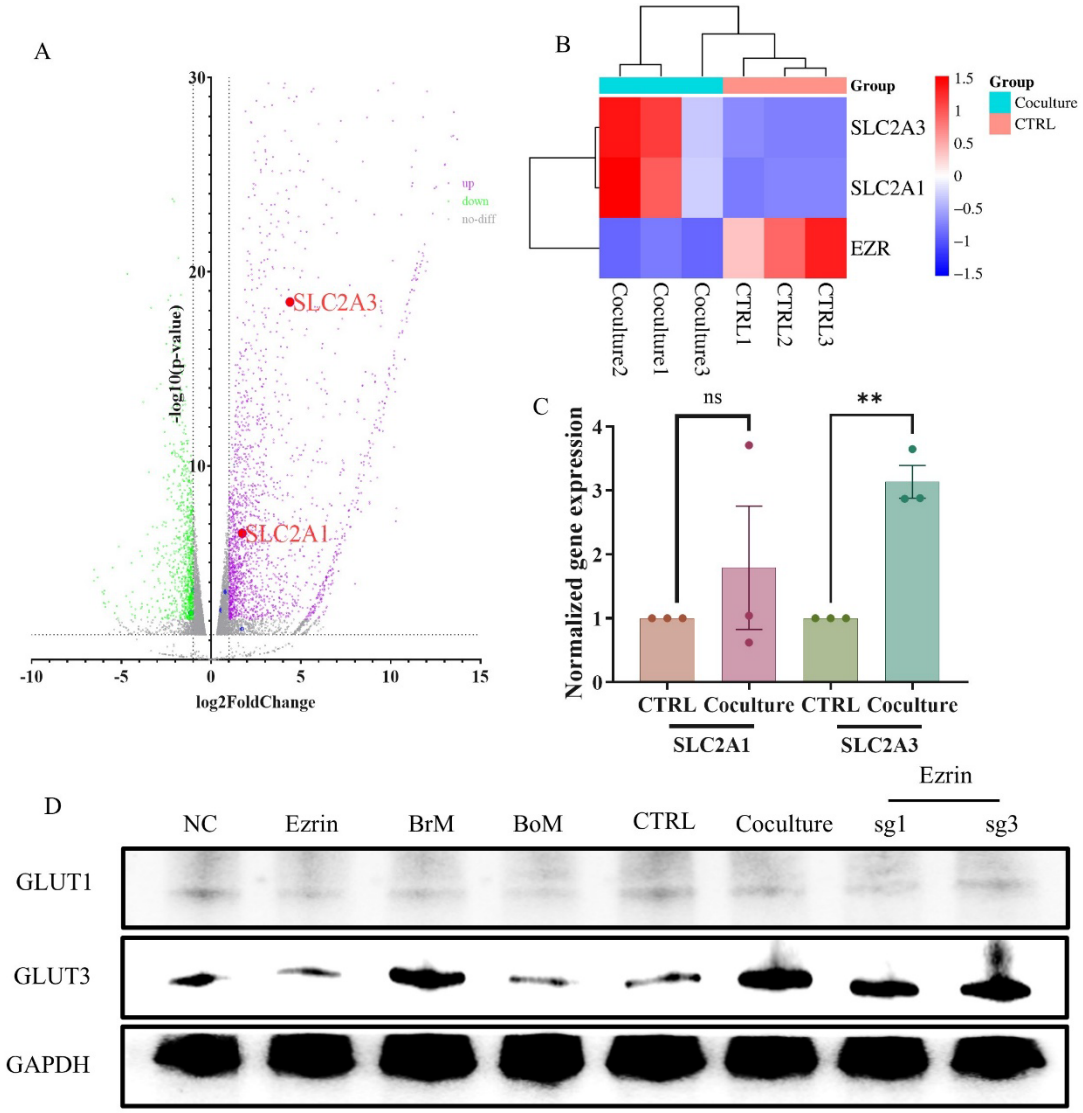

Figure 4-8-1 Co-culture with NK cells up-regulates GLUT3 in breast tumor cells
A volcano plot of up- and down-regulated genes of control VS co-cultured MDA-MB-231 cells. **B** Cluster heatmap of differentially expressed genes of SLC2A1, SLC2A3, and EZR. **C** Normalized SLC2A1 and SLC2A3 gene expression of control VS co-cultured MDA-MB-231 cells detected by RT-qPCR. **D** Protein expression of GLUT1 and GLUT3 among different cells and treatments detected by western blot. The unpaired t-test (**C**) was adopted for statistical analysis.

Expression of SLC2A3 has been proven to be under the transcriptional control of CREB, downstream of PI3K-Akt signaling[269]. Indeed, more phosphorylated CREB was enriched in the nucleus of tumor cells after co-culture (Figure 4-8-2 **A & B**). Inhibiting CREB activity with a specific drug (666-15) decreased SLC2A3 expression after co-

culture (Figure 4-8-1 **C**). Interestingly, most brain-metastasis-associated genes were also down-regulated after CREB inhibition, indicating that these genes may be under the transcriptional control of CREB (Figure 4-8-1 **C**). Treatment of co-cultured tumor cells with Ly294002 (PI3K antagonist) decreased SLC2A3 expression. In contrast, stimulating tumor cells with SC79 (Akt agonist) increased SLC2A3 expression (Figure 4-8-1 **D**).

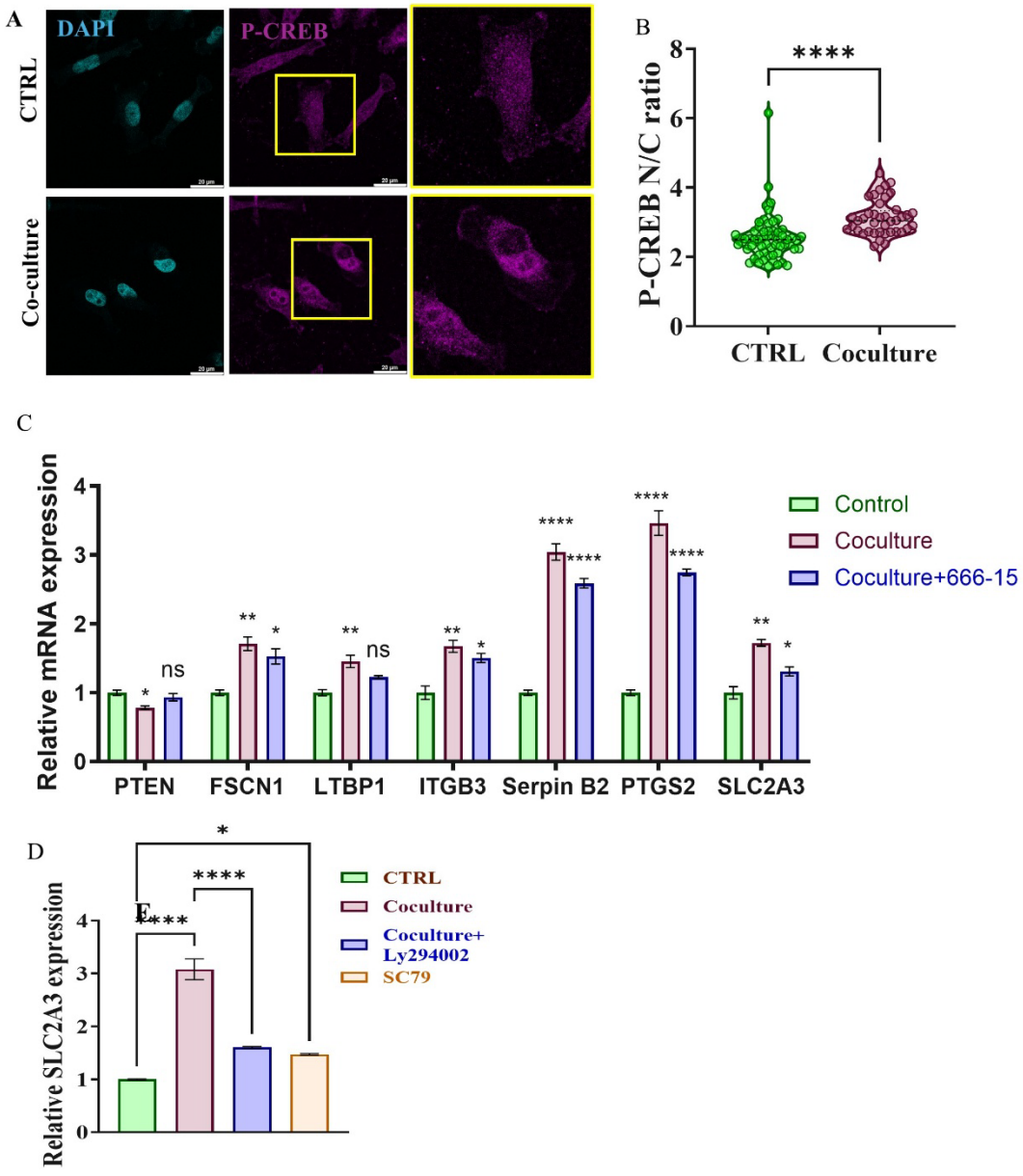

Figure 4-8-2 NK cells upregulate brain metastasis genes and GLUT3 in breast cancer cells via CREB

A Representative image of phosphor-CREB among control/co-cultured tumor cells. **B**

Statistical analysis of the N/C ratio of phosphor-CREB among control/co-cultured tumor cells in **A**. **C** Relative mRNA expression of SLC2A3 and brain-metastasis-associated genes of control/co-culture/co-culture+666-15 treated tumor cells. **D** Relative mRNA expression of SLC2A3 of control/co-culture/co-culture+Ly294002/SC79 treated tumor cells. The unpaired t-test (**B**) and one-way ANOVA followed by Tukey's test (**C & D**) were adopted for statistical analysis.

To transfer glucose from the extracellular spaces into cells, GLUT3 needs to translocate from intracellular vesicles to the cell membrane (Figure 4-8-3 **A**). Through western blot and immunofluorescence, we found that under normal conditions, GLUT3 was mainly located in the cytoplasm. However, after co-culturing with NK cells, GLUT3 was enriched in the cell membrane both under the 25 mM glucose level and the brain glucose level (1 mM) (Figure 4-8-3 **B-D**). Accordingly, this cell membrane-enriched GLUT3 uptake more glucose as indicated by a fluorescent-labeled glucose analog, 2-NBDG (Figure 4-8-3 **E & F**). The TGL-BrM cells also showed enhanced glucose uptake, which further confirmed the importance of this protein in brain metastasis (Figure 4-8-3 **G & H**).

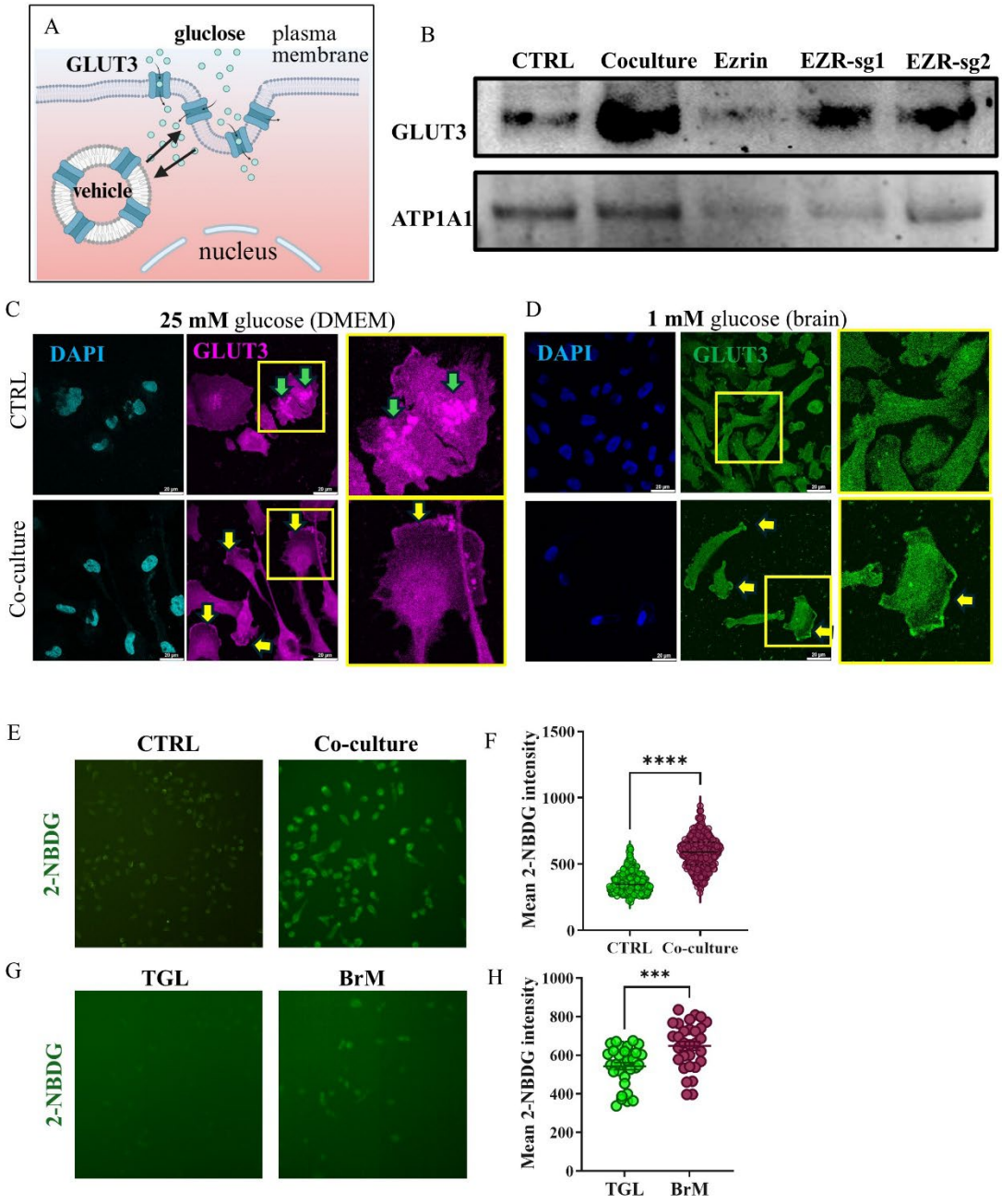

Figure 4-8-3 NK-selected breast cancer cells exhibit enhanced glucose uptake ability

A Diagram of GLUT3 cytoplasm-to-cell membrane translocation. **B** Membrane GLUT3 expression of control/co-culture/ezrin-overexpressed/ezrin-knockout tumor cells detected by western blot. **ATP1A1**, an internal reference of cell membrane proteins. **C** Representative images of GLUT3 location in control/co-cultured tumor cells under 25 mM glucose culture medium. **D** Representative images of GLUT3 location in control/co-cultured tumor cells under 1 mM glucose culture medium. **E** Representative images of glucose uptake in control/co-cultured tumor cells detected by a fluorescent-labeled 2-NBDG. **F** Statistical analysis of 2-NBDG uptake in **E**. **G** Representative images of glucose uptake in TGL/TGL-BrM cells. **H** Statistical analysis

of 2-NBDG uptake in **G**. The unpaired t-test (**F & H**) was adopted for statistical analysis.

The limitation of BBB permeability and the huge consumption by neurons lead to the low interstitial glucose level. Upregulation of GLUT3 in co-cultured tumor cells might enhance glucose metabolism and provide more energy in the brain microenvironment. To confirm this, we detected the glycolysis and mitochondrial respiration of tumor cells under 1 and 3 mM glucose that mimic the brain and other organs' interstitial glucose levels. Indeed, co-cultured tumor cells showed enhanced glycolysis, indicated by extracellular acid ratio (ECAR), and mitochondrial respiration, indicated by oxygen consumption ratio (OCR) (Figure 4-8-4 **A**) under 1 mM glucose. Meanwhile, this enhanced glucose metabolism was abolished by knocking down GLUT3, indicating the dominant role of GLUT3 in mediating glucose uptake and metabolism. Interestingly, under 3 mM glucose, all these cells showed similar glycolysis and mitochondrial respiration (Figure 4-8-4 **B**). This might be caused by the uptake of glucose through other GLUTs. Glucose injections will finally influence cell proliferation. Indeed, under 1 mM glucose, co-cultured tumor cells and TGL-BrM cells showed significantly higher proliferation, which was reversed by knocking down the GLUT3 gene (Figure 4-8-4 **C** and Figure 4-8-5 **A**). Knocking down the ezrin gene, which could increase GLUT3 expression, also promoted tumor cell proliferation under 1 mM glucose (Figure 4-8-5 **E & F**). On the contrary, under 3 mM or higher glucose conditions, there was no difference (Figure 4-8-4 **D-F** and Figure 4-8-5 **B-D**). The cell proliferation was further confirmed by Edu assay (Figure 4-8-4 **G & H**). These results indicated that low membrane tension-induced GLUT3 overexpression promoted tumor cell glucose uptake and finally enhanced tumor cell proliferation under low glucose levels in the brain.

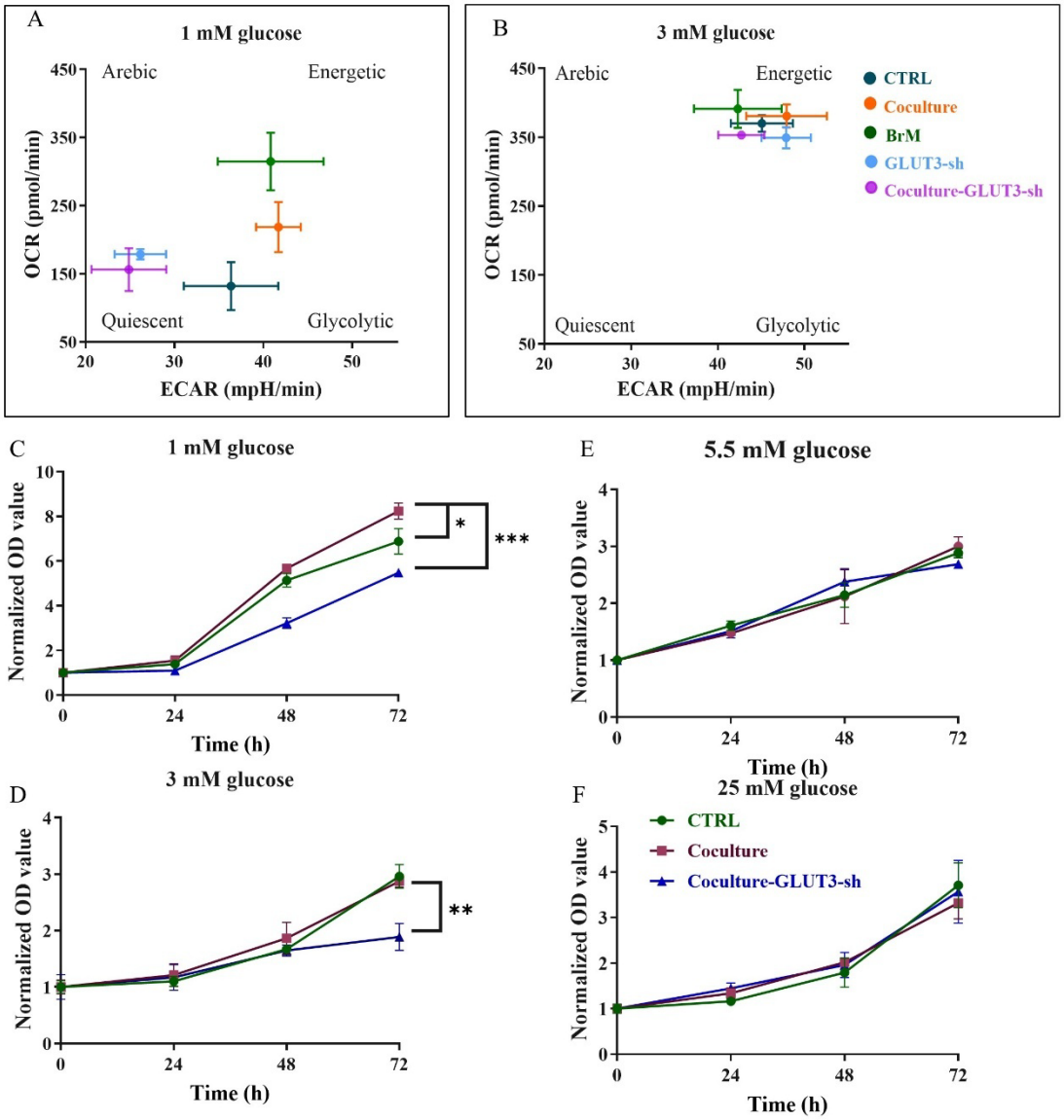
A
1 mM glucose
Arebic
Energetic
Quiescent
Glycolytic
OCR (pmol/min)
ECAR (mpH/min)
B
3 mM glucose
CTRL
Coculture
BrM
GLUT3-sh
Coculture-GLUT3-sh
C
1 mM glucose
Normalized OD value
Time (h)
*
***
D
3 mM glucose
**
E
5.5 mM glucose
F
25 mM glucose

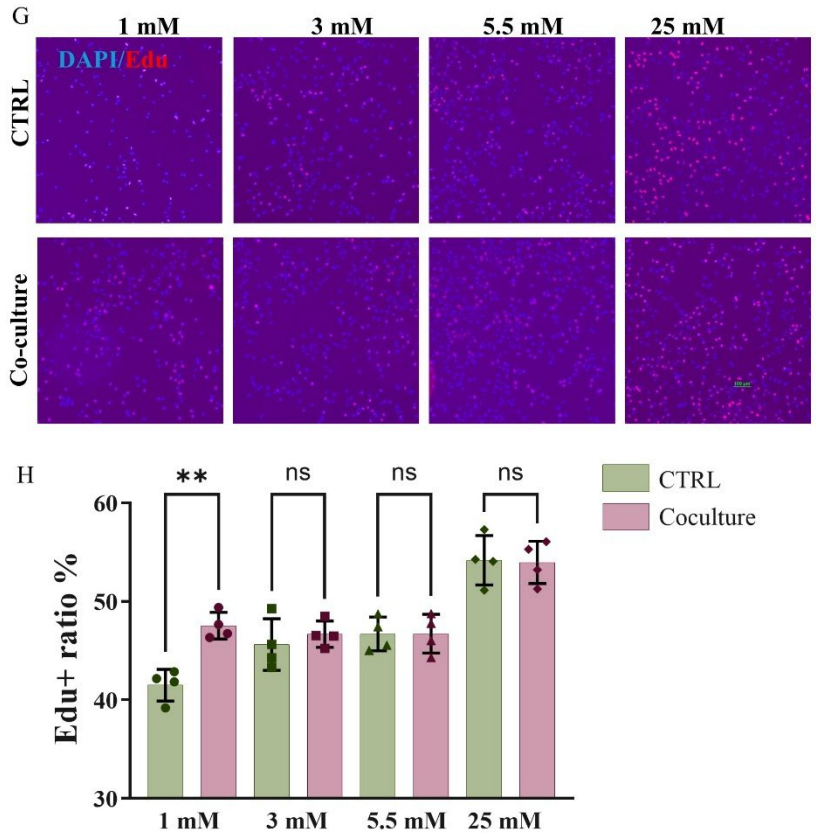

Figure 4-8-4 GLUT3 promotes the proliferation of NK-selected cells under the condition with low glucose level that mimics brain tissue

A & B Glucose metabolism pattern of CTRL/co-cultured/BrM/GLUT3-sh/co-cultured+GLUT3-sh cells indicated by the ECRA and OCR levels. **C-F** Proliferation of CTRL/co-cultured/co-cultured+GLUT3-sh cells indicated by CCK8 assay under 1mM (**C**), 3 mM (**D**), 5.5 mM (**E**), and 25 mM (**F**) glucose. **G** Proliferation of CTRL and co-cultured cells indicated by Edu assay under 1-25 mM glucose. **H** Statistical analysis of cell proliferation in **G**. The unpaired t-test (**H**) and one-way ANOVA followed by Tukey's test (**C-F** and **H**) were adopted for statistical analysis.

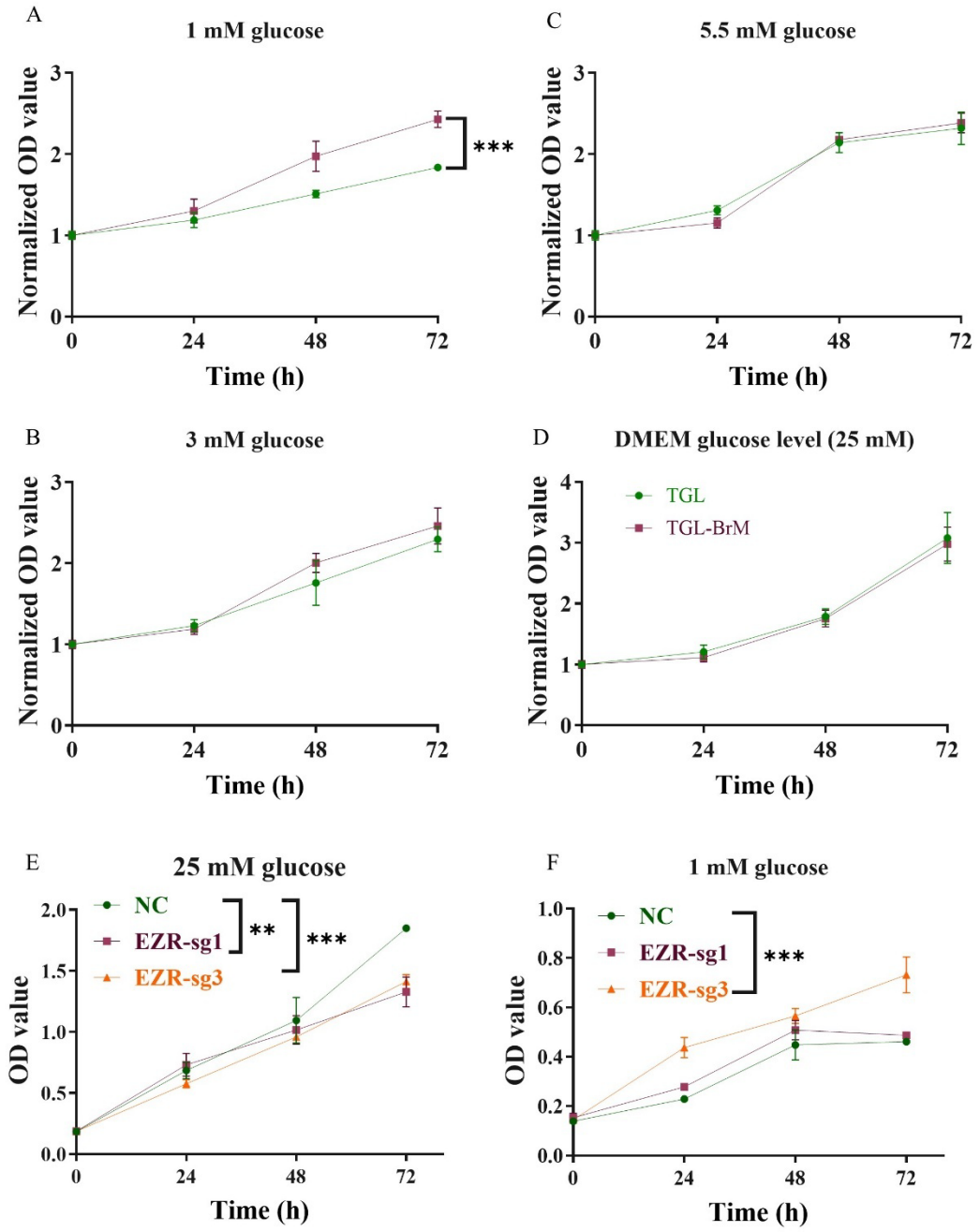

Figure 4-8-5 Brain metastatic cells and ezrin deficient tumor cells exhibit enhanced cell proliferation

A-D Proliferation of TGL/TGL-BrM cells indicated by CCK8 assay under 1mM (**A**), 3 mM (**B**), 5.5 mM (**C**), and 25 mM (**D**) glucose. **E & F** Proliferation of NC/ezrin-knocked out cells indicated by CCK8 assay under 1 mM (**E**) and 25 mM (**F**) glucose. The unpaired t-test (**A-D**) and one-way ANOVA followed by Tukey's test (**E & F**) were adopted for statistical analysis.

4.9 Expression of ezrin is negatively associated with NK cell infiltration and brain metastasis gene signature in breast cancer patients

NK cells can infiltrate into solid tumors of patients to eliminate tumor cells. Based on our in vitro and in vivo mouse model, NK cells in cancer patients may also specifically target tumor cells with high membrane tension and free, and induce tumor cells with low membrane tension. To test this possibility, we analyzed bulk and single-cell RNA-seq data of breast cancer patients. First, we found that NK cell infiltration levels were negatively correlated with ezrin but not with radixin or moesin gene expression of tumor cells (Figure 4-9-1 **A-C**), and, at the same time, positively correlated with the ezrin phosphatase PPP1R12A (Figure 4-9-1 **K**), which might indicate lower tumor cell membrane tension in NK cell-enriched solid tumors. This high NK cell infiltration was also positively associated with some key brain metastasis-associated genes, including CTSL, PTGS2, FSCN1, IL6, HBEGF, ITGB3, and NDRG1 (Figure 4-9-1 **D-J**), and PIK3CA (Figure 4-9-1 **L**).

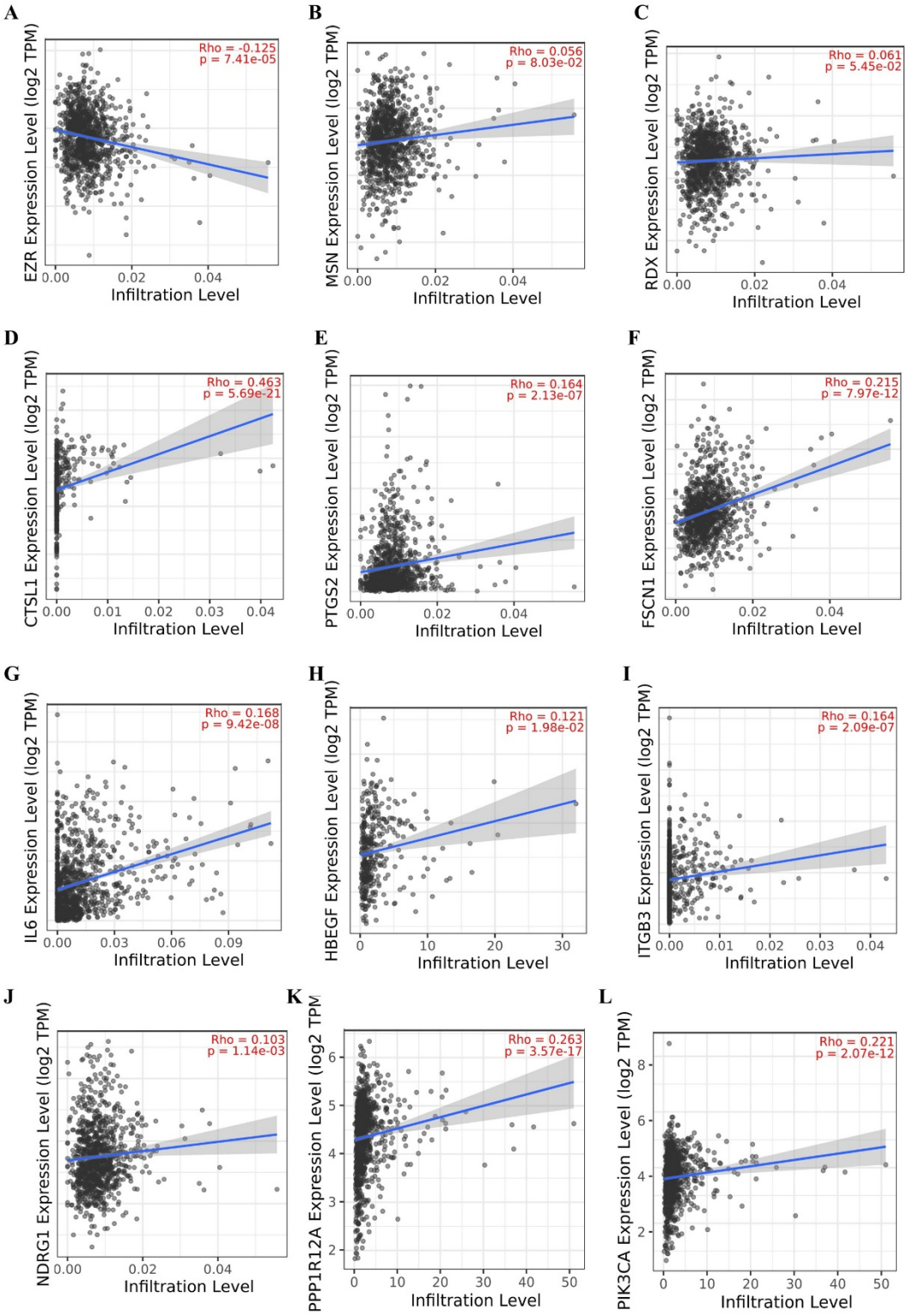

Figure 4-9-1 NK cell infiltration correlates positively with brain metastasis gene expression but negatively with ezrin expression in patients

A-L Correlation between respective tumor gene expression and NK cell infiltration in solid tumors of patients predicted results based on bulk RNA-seq data.

Moreover, single-cell analysis of the primary tumor indicated that ezrin expression was negatively correlated with breast cancer malignancy, with the lowest expression in TNBC cancer patients, who had the highest brain metastasis occurrence, followed by $Her2^+$ and ER^+ patients (Figure 4-8-2 **A**). Tumor cells with low ezrin expression were clearly enriched with brain metastasis-associated genes (Figure 4-8-2 **B**). Some enzymes that decrease ezrin activity were positively correlated with brain metastasis-associated genes (Figure 4-8-2 **C**). On the contrary, the ezrin kinase, which increases ezrin activity, was negatively correlated with brain metastasis-associated genes (Figure 4-8-2 **D**). However, there was no obvious correlation between ezrin and bone/lung/liver-metastasis-associated genes (Figure 4-8-2 **E-G**).

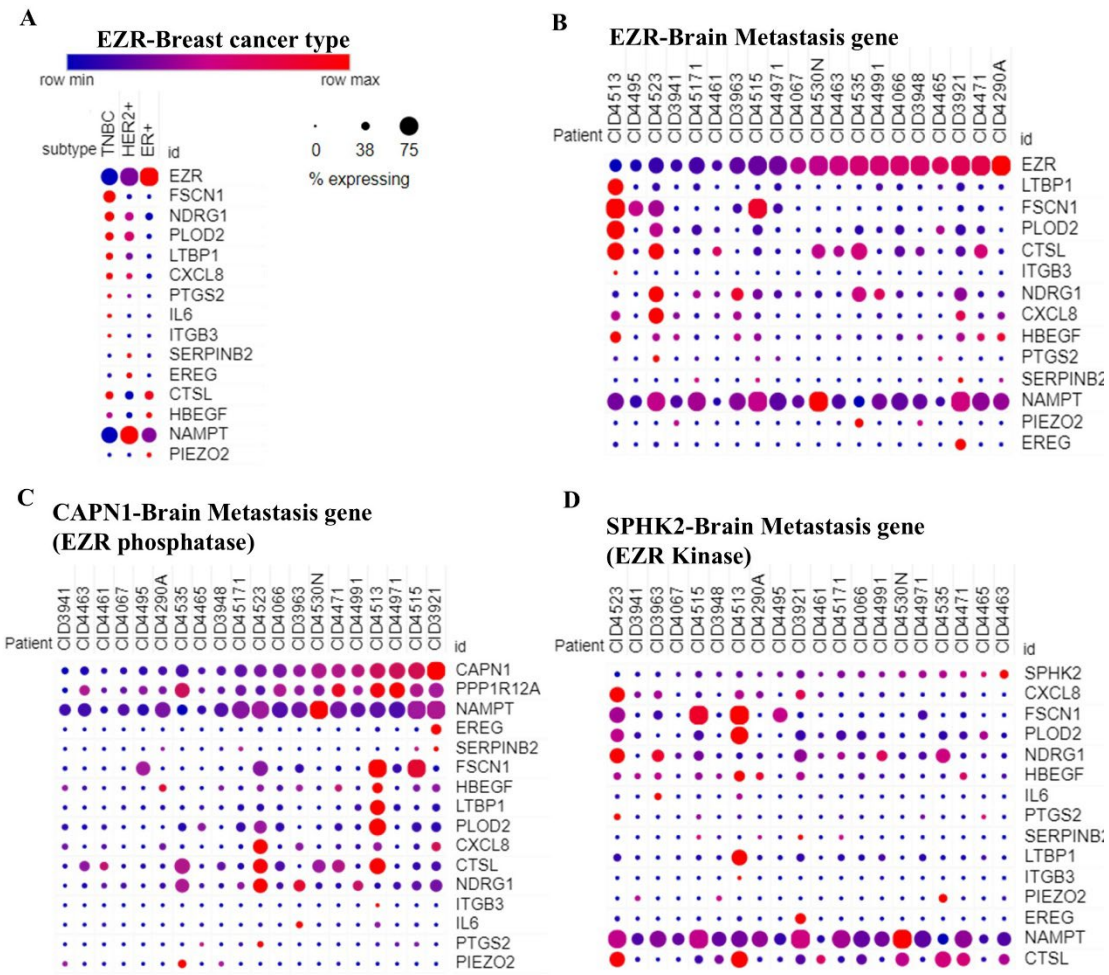

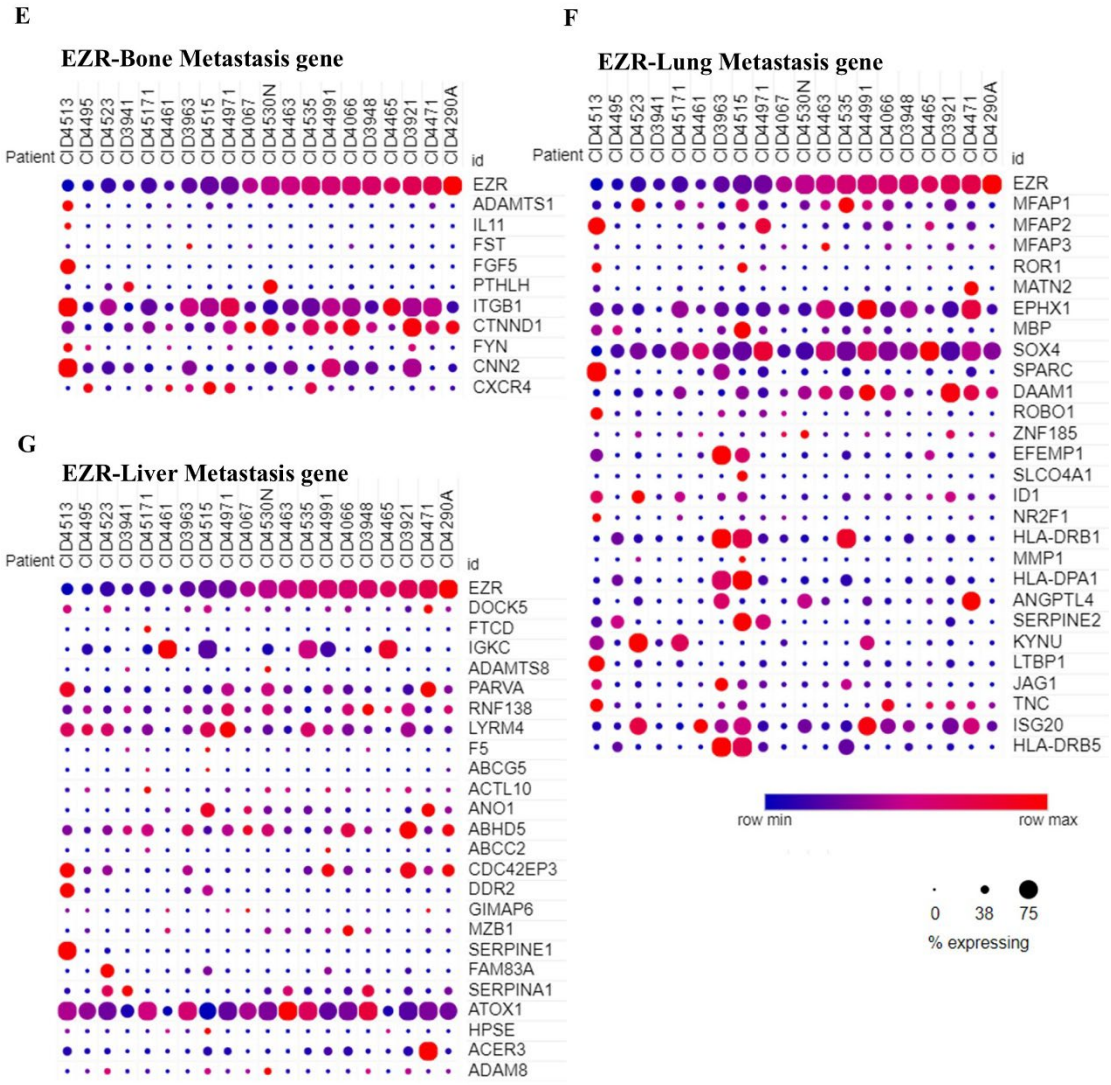

Figure 4-9-2 Negative correlation between ezrin and brain metastasis gene expression in patients

A Bubble map of ezrin and brain metastasis-associated gene expression in TNBC, Her2$^+$, and ER$^+$ breast cancer patients based on single-cell RNA-seq analysis. **B** Bubble map of ezrin and brain metastasis-associated gene expression in 20 breast cancer patients based on single-cell RNA-seq analysis. **C** Bubble map of ezrin phosphatases gene CAPN1 and PPP1R12A and brain metastasis-associated gene expression in 20 breast cancer patients based on single-cell RNA-seq analysis. **D** Bubble map of ezrin kinase gene SPHK2 and brain metastasis-associated gene expression in 20 breast cancer patients based on single-cell RNA-seq analysis. **E-G** Bubble map of ezrin and Bone/Lung/Liver-associated gene expression in 20 breast cancer patients based on single-cell RNA-seq analysis.

Furthermore, patients with low ezrin expression had relatively low BMFS (Figure 4-8-

3 **A**). Patients with high ezrin phosphatases gene PPP1R12A and PTP4A, encoding proteins that can decrease ezrin activity and, as a result, decrease membrane tension, also had relatively low BMFS (Figure 4-8 **B & C**).

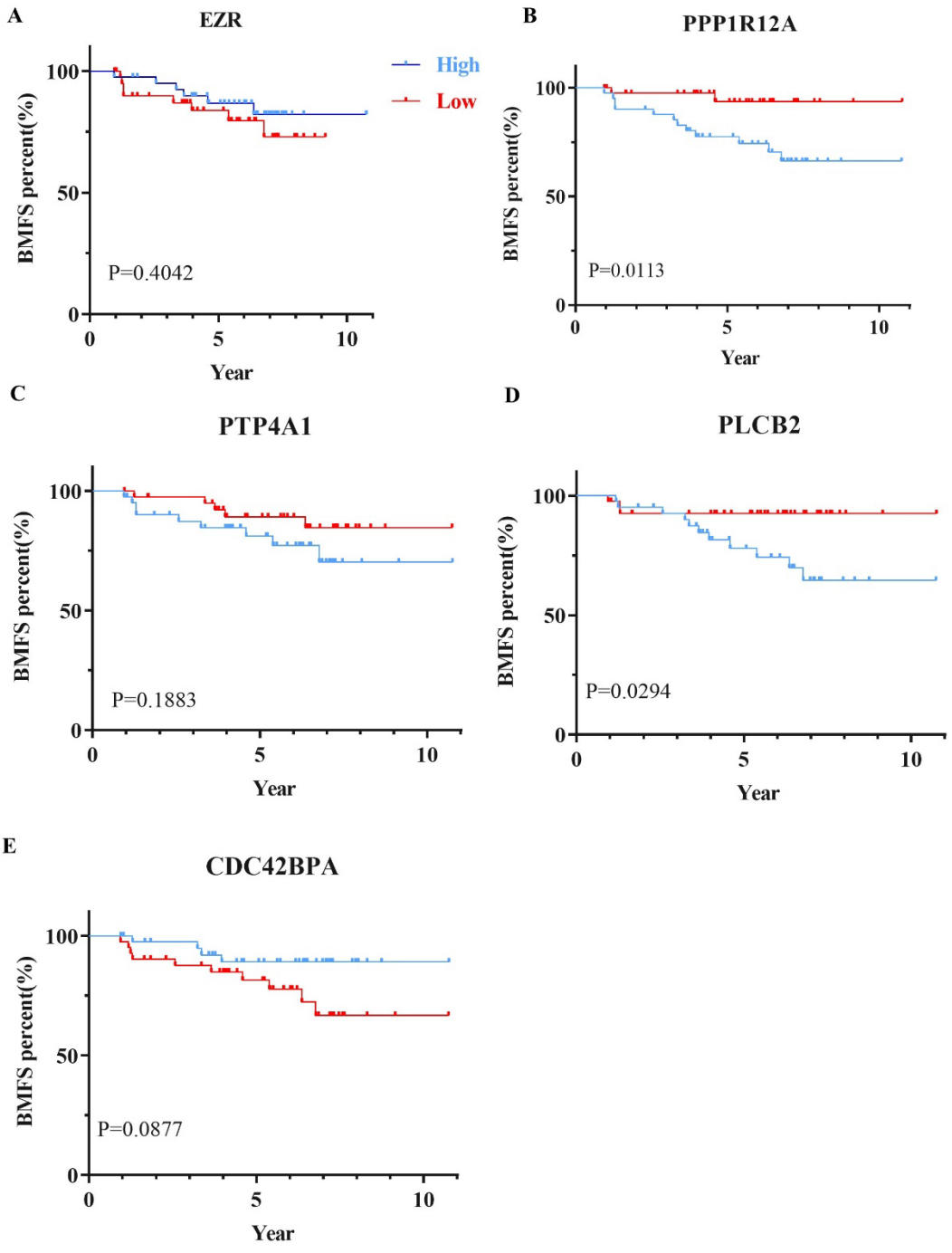

Figure 4-9-3 Ezrin expression and activity were negatively correlated with cancer patients' BMFS

A-E The correlation between ezrin (**A**), PPP1R12A (**B**), PTP4A1 (**C**), PLCB2 (**D**), and

CDC42BPA (**E**) expression and breast cancer patients' brain-metastasis-free survival (BMFS).

Similarly, patients with high PLC, encoding proteins that degrade PIP2 and limit ERM membrane binding to decrease membrane tension, had relatively low BMFS (Figure 4-8 **D**). On the contrary, patients with high ezrin kinase gene CDC42BPA expression, which increases ezrin activity and membrane tension, had relatively high BMFS (Figure 4-8 **E**).

These data suggested that high NK cell infiltration decreased ezrin gene expression and activity, which decreased tumor cell membrane tension and specifically enhanced brain metastatic potential.

Chapter 5: Fluid shear stress enhances NK cell's cytotoxicity towards circulating tumor cells through NKG2D-mediated mechano-sensing

Abstract

Metastasis constitutes a sequential process, wherein failure at any step may compromise the successful metastatic tumor formation. Various rate-limiting factors pose challenges to the fate of disseminated tumor cells and the efficiency of the metastasis process (e.g., <0.02%) [8,9]. Upon their entry into the vasculature, CTCs are subjected to multiple environmental stresses, such as anoikis, FSS, oxidative stress, and immune surveillance[10,11]. Only a limited subpopulation of CTCs is capable of surviving under these stresses to facilitate metastatic seeding. The frequency of CTCs in the vasculature correlates with the prognosis and survival of cancer patients[12,13]. Consequently, elucidating the synergistic effects of these critical factors on the survival of CTCs during hematogenous dissemination holds significant importance for the advancement of novel therapeutic strategies aimed at eradicating CTCs and preventing metastasis.

The immune system is crucial for removing tumor cells throughout the stages of metastasis [14]. Because CTCs have a short lifespan in the bloodstream, lasting about 30 minutes on average [11,15-17], effective immune responses must involve rapid recognition and destruction of these cells. NK cells are a key component of the human innate immune system, serving as significant destroyers of CTCs due to their ability to swiftly identify and eliminate malignant cells using germline-encoded activating receptors [18,19]. The count and activation levels of NK cells correlate strongly with the survival rates of cancer patients [20-23]. In the bloodstream, most NK cells are of the $CD56^{dim}$ subtype, which exhibits strong cytotoxic properties but has lower cytokine secretion capabilities compared to the $CD56^{bright}$ subtype[24-26]. Following the formation of conjugates via integrins such as LFA-1 [270,271], NK cells can be activated

through interactions with activating ligands, including MICA/B and ULBP1-6. These interactions directly induce target cell death by secreting perforin, which forms pores in the target cell membrane, and by transporting granzymes [272-281]. Furthermore, NK cells are capable of inducing death in target cells through the death receptor ligand Trail [282,283] and various cytokines, such as TNF-α[284,285] and IFN-γ[286-288].

Upon entering the bloodstream, CTCs encounter FSS, a condition absent in primary sites. This distinct mechanical stimulation significantly impacts CTCs, influencing their reprogramming in various ways. Notably, FSS has been shown to cause direct damage to CTCs in a magnitude-dependent fashion [62,63]. However, some subgroups of CTCs manage to survive and subsequently become targets for immune cells in the blood, primarily NK cells. Despite these challenges, small clusters of CTCs successfully evade circulation and establish metastatic colonies. Therefore, gaining a comprehensive understanding of the systematic effects of FSS and NK cells on CTCs is essential to elucidate how CTCs withstand such a hostile environment.

5.1 FSS promotes NK cell anti-CTCs killing

To investigate the influence of FSS on NK cell cytotoxicity, suspended breast tumor cells were used to mimic CTCs and co-cultured with NK92 cells at a 1:4 ratio under various levels of FSS (0, 1, 5, 10, and 20 dyn/cm^2) in a microfluidic system [29] (Figure 5-1-1 A). All shear stress refers to the wall shear stress. The distribution of shear stress within the tube varies according to the radial position, complicating the determination of the precise FSS experienced by individual tumor cells. We found that FSS above 5 dyn/cm^2 caused substantial death of NK cells (Figure 5-1-1 B). Consequently, only 0, 1, and 5 dyn/cm^2 were used in the remainder of this work. Tumor cells showed a shear magnitude-dependent apoptosis with and without co-culture (Figure 5-1-1 C). Notably, the death of tumor cells under the combined treatment of NK cells and FSS was significantly higher than the death induced by the single treatment of NK cells plus the

single treatment of FSS, represented by the death increment (Figure 5-1-1 D, red bar). At five dyn/cm^2 FSS, the tumor cell death increment was more than twofold that induced by NK cells (Figure 5-1-1 E), while this effect was negligible at one dyn/cm^2. This indicates a mutual effect between FSS and NK cells. Similarly, we noted shear magnitude-dependent caspase three activation and an increase in caspase activity (Figure 5-1-1 F & G) in tumor cells.

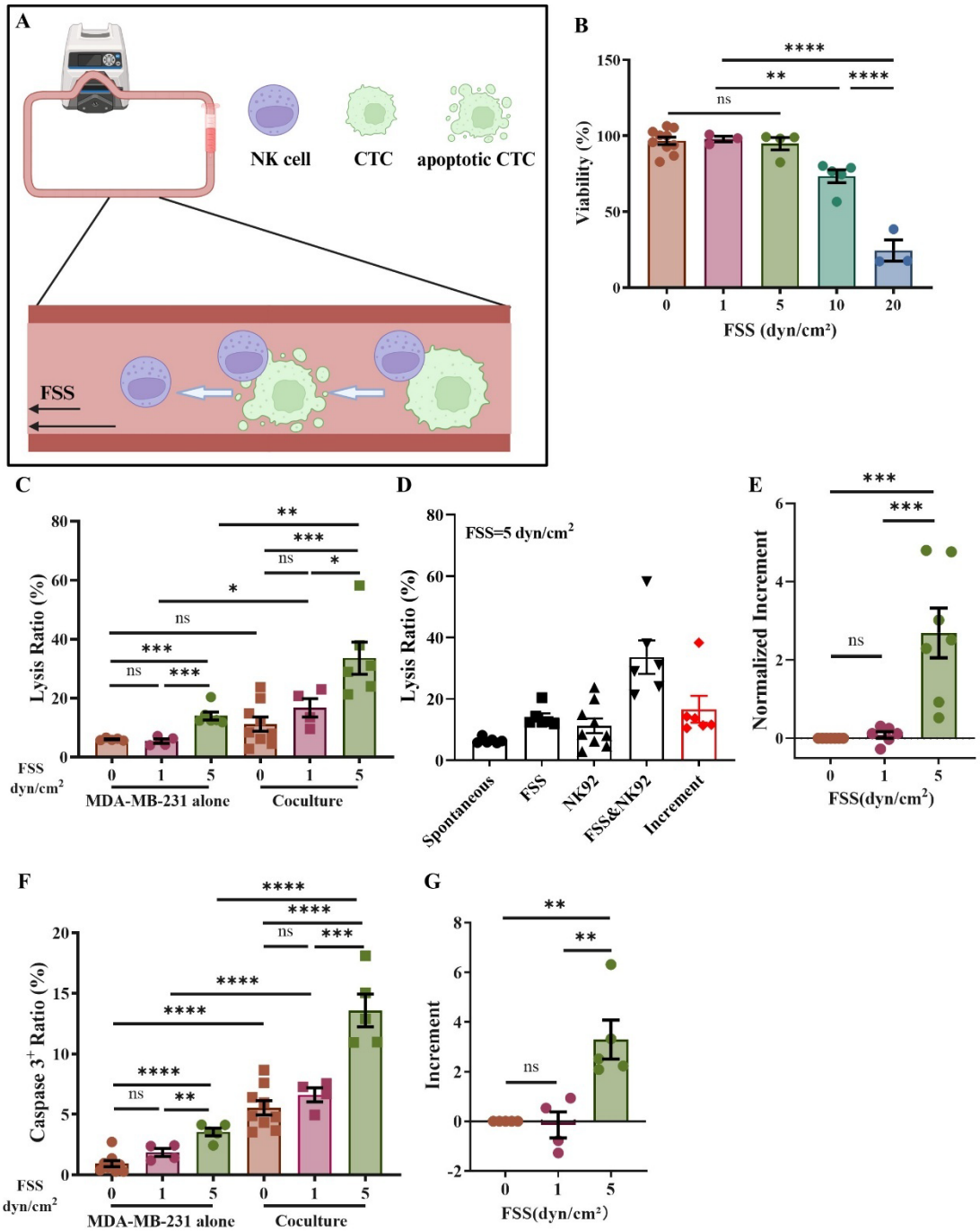

Figure 5-1 FSS promotes NK cell anti-CTCs killing

A Diagram of the circulation system. **B** Viability of NK92 cells under different FSS treatment for 4 h. **C** Death ratio of tumor cells under a series of FSS treatment alone and/or with co-culture. **D** Death ratio of spontaneous tumor cell death, FSS (5 dyn/cm^2) alone induced tumor cell death, co-culture alone induced tumor cell death, combined FSS (5 dyn/cm^2), and co-culture induced tumor cell death. **E** Incremental tumor cell death with normalization under different FSS. **F** Caspase 3 positive ratio of MDA-MB-231 cells. **G** Incremental tumor cell caspase 3$^+$ ratio under different FSS. The one-way ANOVA followed by Tukey's test (**B, C, E, F, & G**) was adopted for statistical analysis.

The above FSS (1 or 5 dyn/cm2) does not accurately represent the true FSS experienced by CTCs. To verify the observed phenomena under WSS, we first coated a fluid chip with poly-D-lysine (PDL), which can mediate cell adhesion independent of integrins, mimicking suspension within a limited time. After tumor cell adhesion, NK cells were allowed to spontaneously adhere and interact with these tumor cells for killing under 0, 0.1, and 0.2 dyn/cm2 WSS. Using fluorescent-labeled paxillin and lifeact-expressing tumor cell lines, we found that tumor cells adhered to PDL displayed similar morphology, F-actin, and focal adhesion as suspended cells (Figure 5-1-2 A-F).

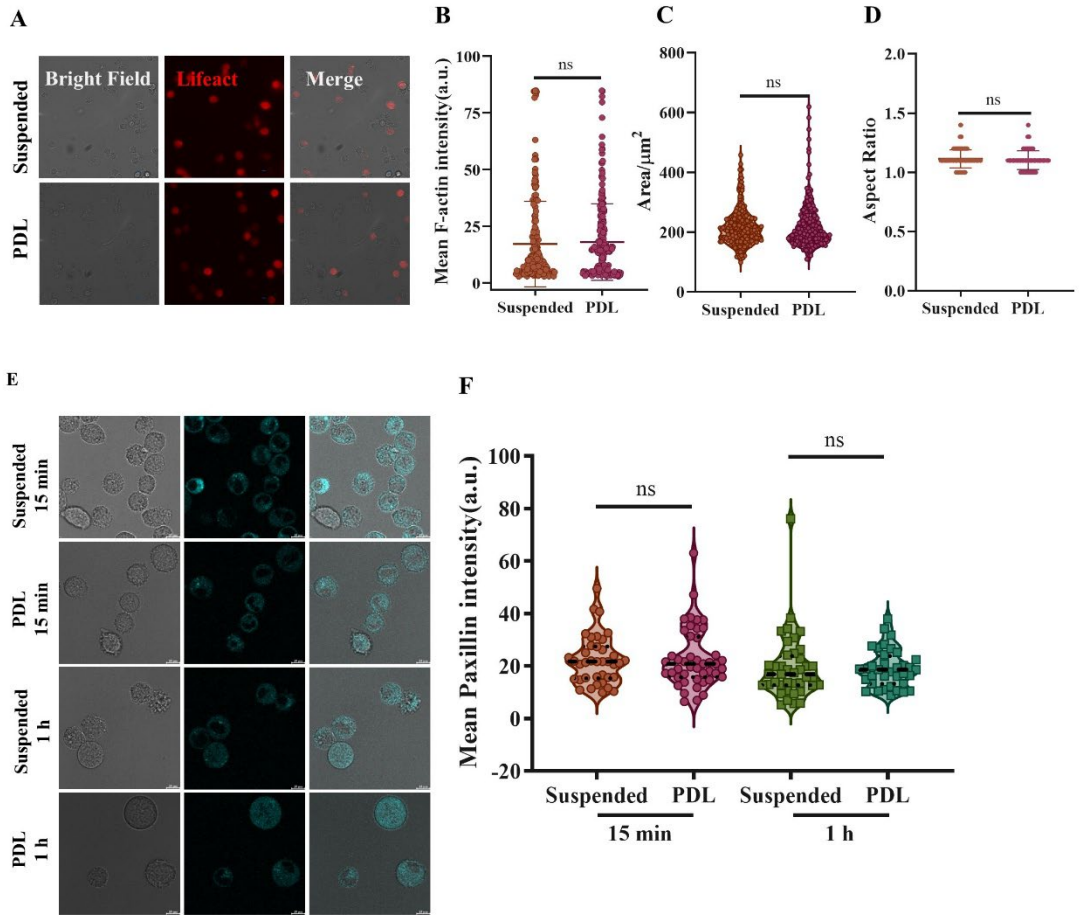

Figure 5-2 PDL-adhered tumor cells show similar properties to CTCs

A-D Mean F-actin intensity, area, and aspect ratio of suspended or PDL-adhered MDA-MB-231 cells. **E** & **F** Mean paxillin intensity of suspended or PDL-adhered MDA-MB-231 cells (**F**) and representative confocal images (**E**). The one-way ANOVA followed by Tukey's test (**F**) and unpaired t-test (**B-D**) were adopted for statistical analysis. ns, not significant.

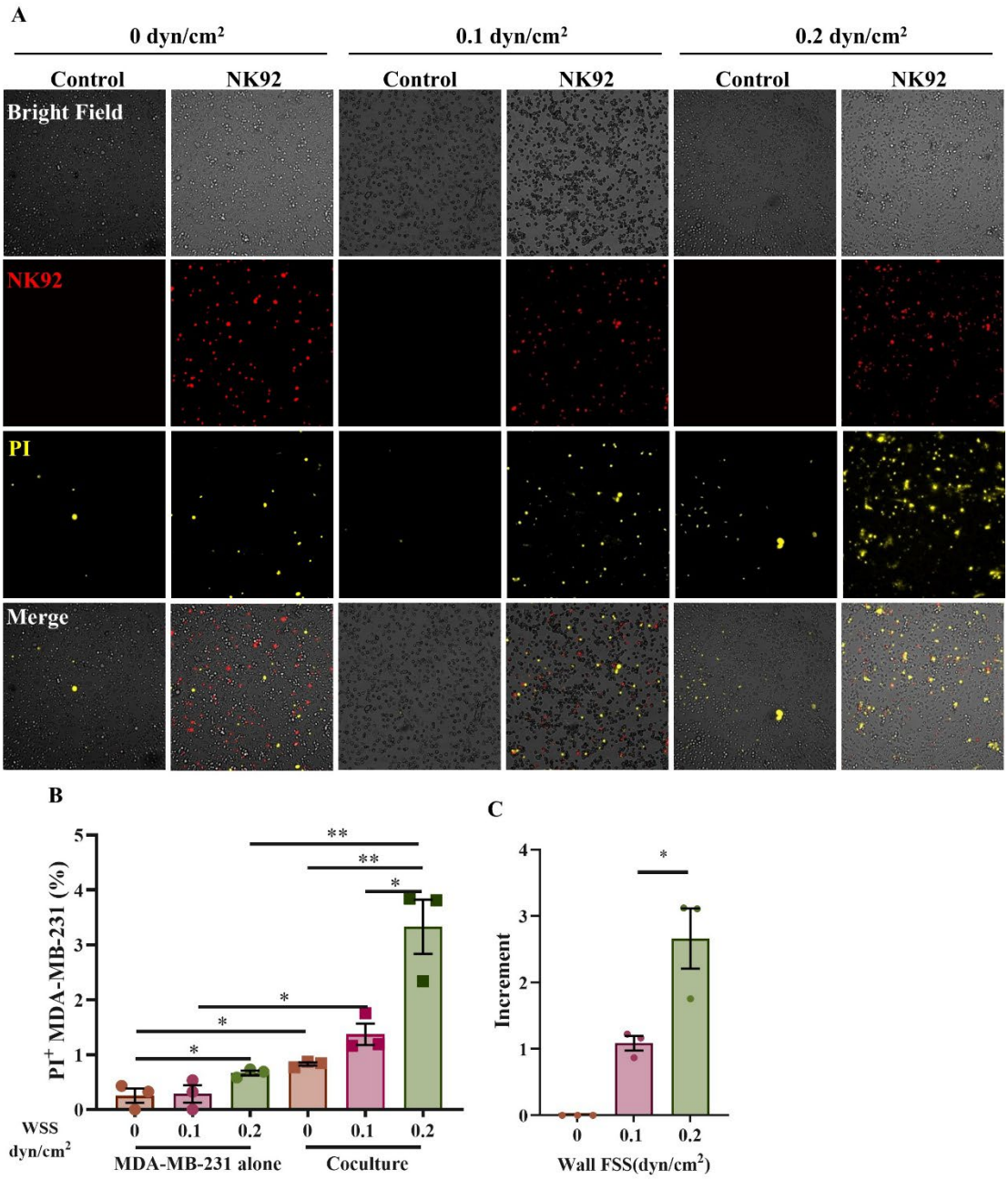

Figure 5-3 WSS promotes NK cell anti-CTCs killing

A Representative images of MDA-MB-231 cell apoptosis under 0, 0.1, 0.2 dyn/cm^2 WSS. **B** Tumor cells apoptotic ratio under different WSS with or without NK92 co-culture, indicated by propidium iodide. **C** Incremental death of tumor cells under different WSS. The one-way ANOVA followed by Tukey's test (**B & C**) was adopted for statistical analysis.

Both the overall and incremental cell death were shear-dependent (Figure 5-1-3 **A-C**), which were similar to the responses of lysis ratio in the microfluidic tubing (Figure 5-

1-3 **B-E**). Taken together, these findings suggest that FSS within the vasculature can promote NK cell cytotoxicity against CTCs.

5.2 FSS promotes NK cell anti-CTCs killing via the elevated secretion of Granzyme B

The major way NK cells kill CTCs is to form conjugates with them, secrete perforin through the immune synapse to form pores on the membranes of target cells, and deliver granzyme B, the primary effector enzyme, into target cells [278-281,289]. To clarify how FSS improved NK cells' killing ability, we initially examined the effect of FSS on NK-tumor cell-conjugates formation. The results indicated that conjugate formation between tumor cells and NK cells diminished as FSS increased. (Figure 5-2-1 **A**), while more tumor cells were apoptotic among the conjugates when exposed to high FSS (Figure 5-2-1 **B**). Additionally, CD107a, a recognized marker of NK cell activity, was significantly elevated in the NK cell membrane at 5 dyn/cm^2 FSS (Figure 5-2-1 C), indicating shear magnitude-dependent activation of NK cells. MTOC polarization, which carries perforin and granzyme B and moves towards the immune synapse, is responsible for the secretion of effector proteins to target tumor cells [168,280,290]. Interestingly, NK cell MTOC was gradually closer to the immune synapse with FSS increase (Figure 5-2-1 **D**), indicating that MTOC polarization is shear magnitude-dependent. Under 5 dyn/cm^2 FSS, the MTOCs were positioned nearest to the synapses (Figure 5-2-1 E), suggesting the highest activation of the conjugated NK cells. Importantly, NK cells injected more granzyme B into tumor cells under 5 dyn/cm^2 FSS (Figure 5-2-1 **F-I**), which could explain the increased CTCs death.

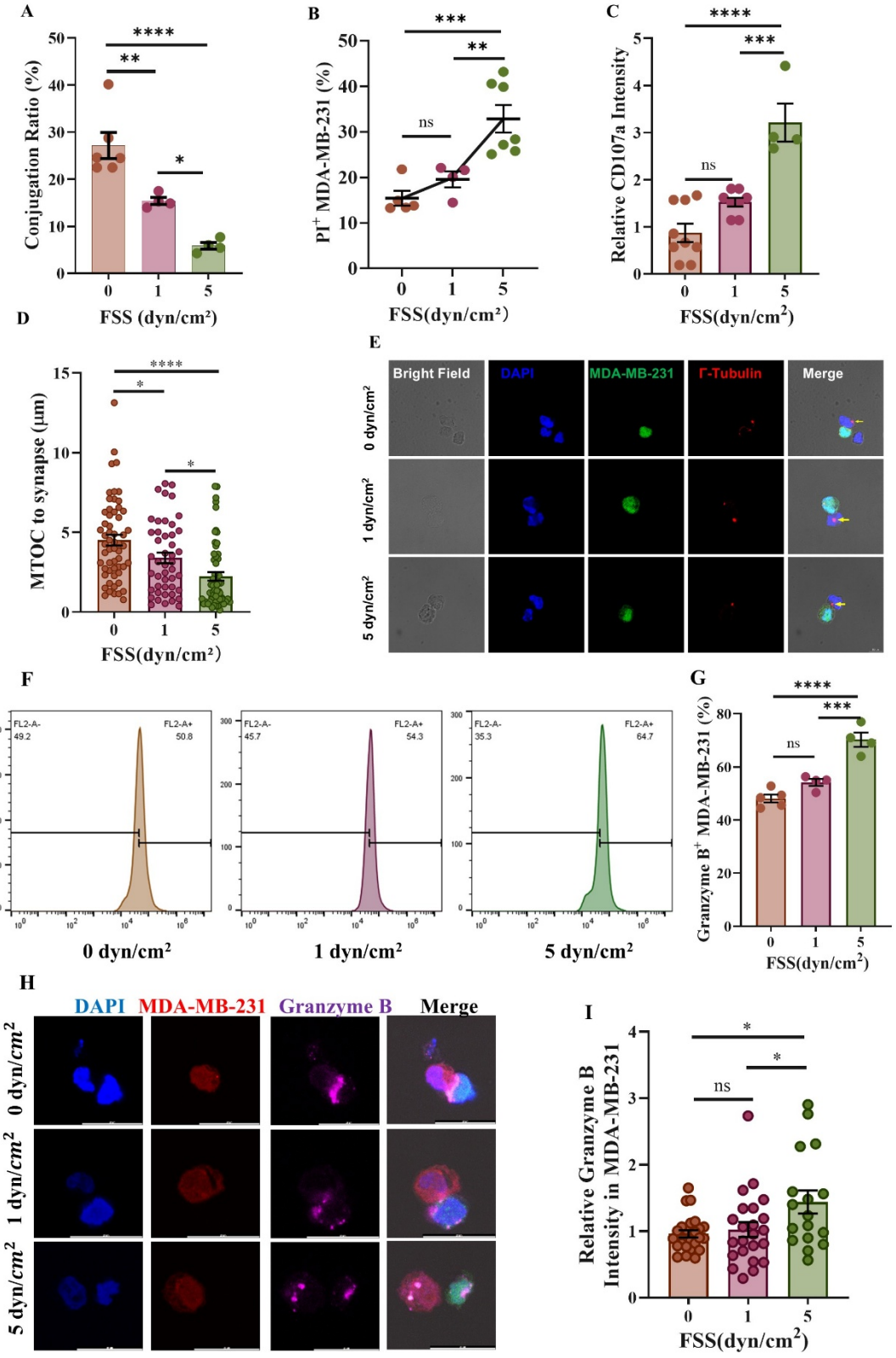

Figure 5-2-1 FSS promotes NK cell anti-CTCs killing via the elevated secretion of Granzyme B

A The NK-tumor cells conjugation ratio under FSS. **B** PI positive MDA-MB-231 cells percentage among conjugated MDA-MB-231. **C** Relative CD107a intensity of co-

cultured NK92 under different FSS. **D & E** MTOC polarization under different FSS. Yellow arrow, site of the MTOC. **F & G** Granzyme B positive tumor cells, detected by flow cytometry. **H & I** Granzyme B intensity in conjugated tumor cells, detected by IF. The one-way ANOVA followed by Tukey's test (**A**, **B, C, D, F, H, & I**) was adopted for statistical analysis.

Alternatively, NK cells can induce tumor cell death by secreting cytokines, including TNF-α [284,285] and IFN-γ [286-288], and tumor necrosis factor-related apoptosis-inducing ligand (Trail) [201,280,291,292]. To investigate the roles of these mechanisms, the influence of FSS and tumor cells on the secretion of TNF-α and IFN-γ in NK cells was examined. There was no significant difference in TNF-α secretion when different levels of FSS were exerted with and without tumor cells (Figure 5-2-2 A). Interestingly, the secreted IFN-γ decreased at 1 and 5 dyn/cm^2 FSS compared to 0 dyn/cm^2 (Figure 5-2-2 B). These findings suggest that FSS does not promote the secretion of TNF-α and IFN-γ. This might be because cytokine secretion is different from cytotoxic granule secretion in NK cells [293]. We further tested the cytotoxic effect of these cytokines under FSS. 30 pg/mL TNF-α or 70 pg/mL IFN-γ were used to treat MDA-MB-231 cells with or without FSS. The results showed that there was no difference in cell apoptosis when suspended tumor cells were circulated under FSS with or without TNF-α and IFN-γ (Figure 5-2-2 C & D). Further, the blocking antibody was adopted to inhibit the functions of Trail. However, no significant difference was observed in tumor cell death under FSS compared with control IgG (Figure 5-2-2 E). In addition, the conditioned medium was collected from the co-culture of suspended tumor cells and NK cells under FSS. There was no net increment of cell lysis under 1 and 5 dyn/cm^2 FSS (Figure 5-2-2 F), indicating that the cytokines secreted by NK cells may not contribute to the shear-induced increase in NK cell cytotoxicity.

Taken together, FSS impairs conjugate formation between NK and tumor cells while promoting NK cell activation and the delivery of granzyme B into target cells within the conjugates, which may enhance NK cells' cytotoxicity.

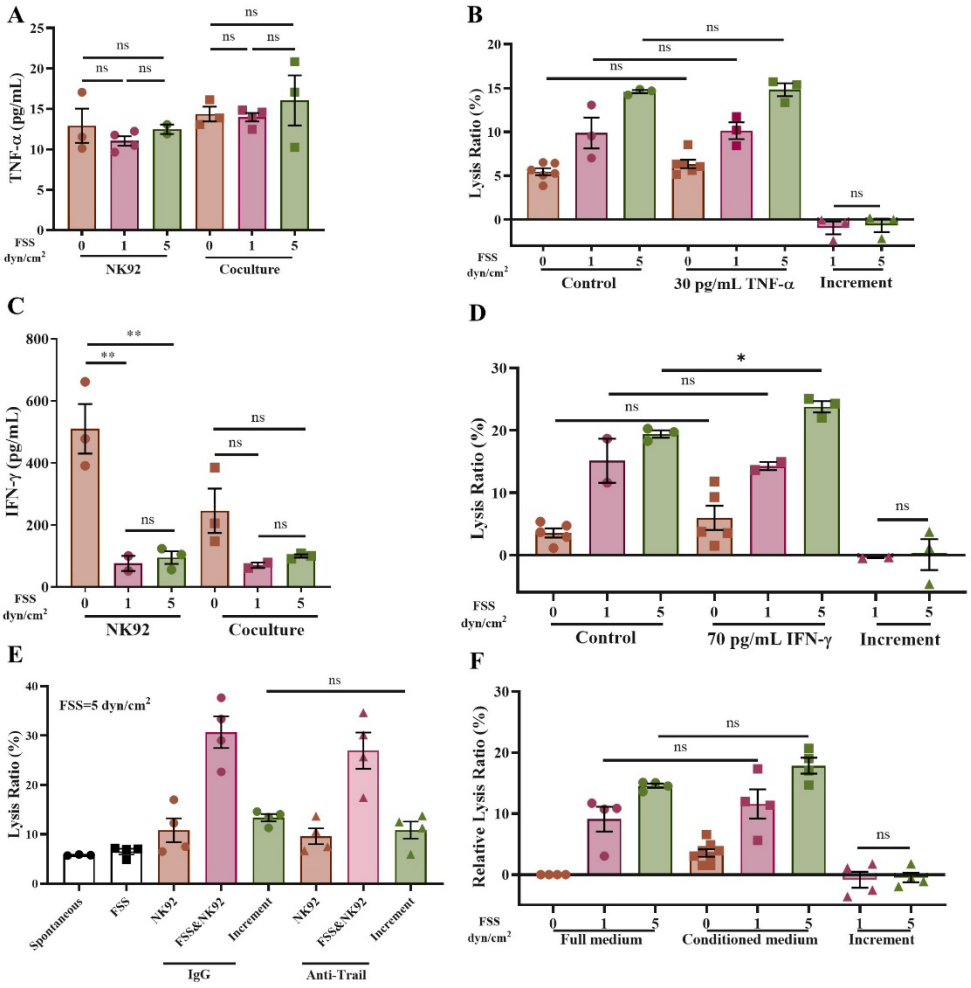

Figure 5-2-2 Cytokines are not involved in FSS-enhanced NK cell cytotoxicity

A TNF-α secretion of NK92 cells alone or when coculturing with MDA-MB-231 cells under 0, 1, 5 dyn/cm^2 FSS. **B** TNF-α induced MDA-MB-231 cell apoptosis under 0, 1, 5 dyn/cm^2 FSS. **C** IFN-γ secretion of NK92 cells alone or when coculturing with MDA-MB-231 cells under 0, 1, 5 dyn/cm^2 FSS. **D** IFN-γ induced MDA-MB-231 cell apoptosis under 0, 1, 5 dyn/cm^2 FSS. **E** Lysis ratio of MDA-MB-231 cells under 5 dyn/cm^2 FSS after blocking Trail with a specific antibody or not. **F** Conditioned medium originated from supernatant of NK92 and MDA-MB-231 co-culture mixture, induced MDA-MB-231 cell apoptosis under 0, 1, 5 dyn/cm^2 FSS. The one-way ANOVA followed by Tukey's test (**A-F**) was adopted for statistical analysis.

5.3 NK cells deliver more granzyme B into tumor cells under FSS triggered by NKG2D

After engaging with target cells, the activity of NK cells is determined by a balance of

activating and inhibitory signals [142,294,295]. NK cells express germline-encoded receptors that recognize the corresponding ligands on the membranes of transformed cells [294]. NKG2D, an important activating receptor expressed in NK cells, binds to several ligands that are structurally related to MHC class I and interacts with MICA, MICB, and some ULBPs in humans [296-300]. To test the role of NKG2D in shear-induced NK cell cytotoxicity, we first explored the influence of FSS on NKG2D and the expression of its ligand. Interestingly, shear treatment did not have a significant impact on the mRNA and protein levels of NKG2D in NK cells (Figure 5-3 **A & B**) and ligands on MDA-MB-231 cells (Figure 5-3 **C**). We next knocked down NKG2D in NK cells by electroporation (Figure 5-3 D) and found that silencing NKG2D significantly decreased the cytotoxicity increment under 5 dyn/cm^2 FSS (Figure 5-3 E). The amount of granzyme B in total tumor cells and conjugated ones was remarkably elevated under FSS, which was blunted by the inhibition of NKG2D (Figure 5-3 F & G). After ligation with MICA on target cells, PI3K and VAV1-Grb2 will be recruited to the intracellular domain of NKG2D with the We next knocked down NKG2D in NK cells by electroporation (Figure 5-3 **D**) and found that silencing NKG2D significantly decreased the cytotoxicity increment under 5 dyn/cm^2 FSS (Figure 5-3 **E**). The amount of granzyme B in total tumor cells and conjugated ones was remarkably elevated under FSS, which was blunted by the inhibition of NKG2D (Figure 5-3 **F & G**). After ligation with MICA on target cells, PI3K and VAV1-Grb2 will be recruited to the intracellular domain of NKG2D with the help of the adaptor protein DAP10[301-304] and Gab2[305] to transduce activating signals, which then facilitate the delivery of granzyme B into target cells. We then examined the activation of PI3K and Gab2 signaling under FSS. The shear treatment promoted the phosphorylation levels of both PI3K and Gab2 within the synapse region under 5 dyn/cm^2 FSS compared with the static condition (Figure 5-3 H-K). Together, these results suggest that FSS may promote NK cell cytotoxicity through NKG2D-mediated granzyme B injection.

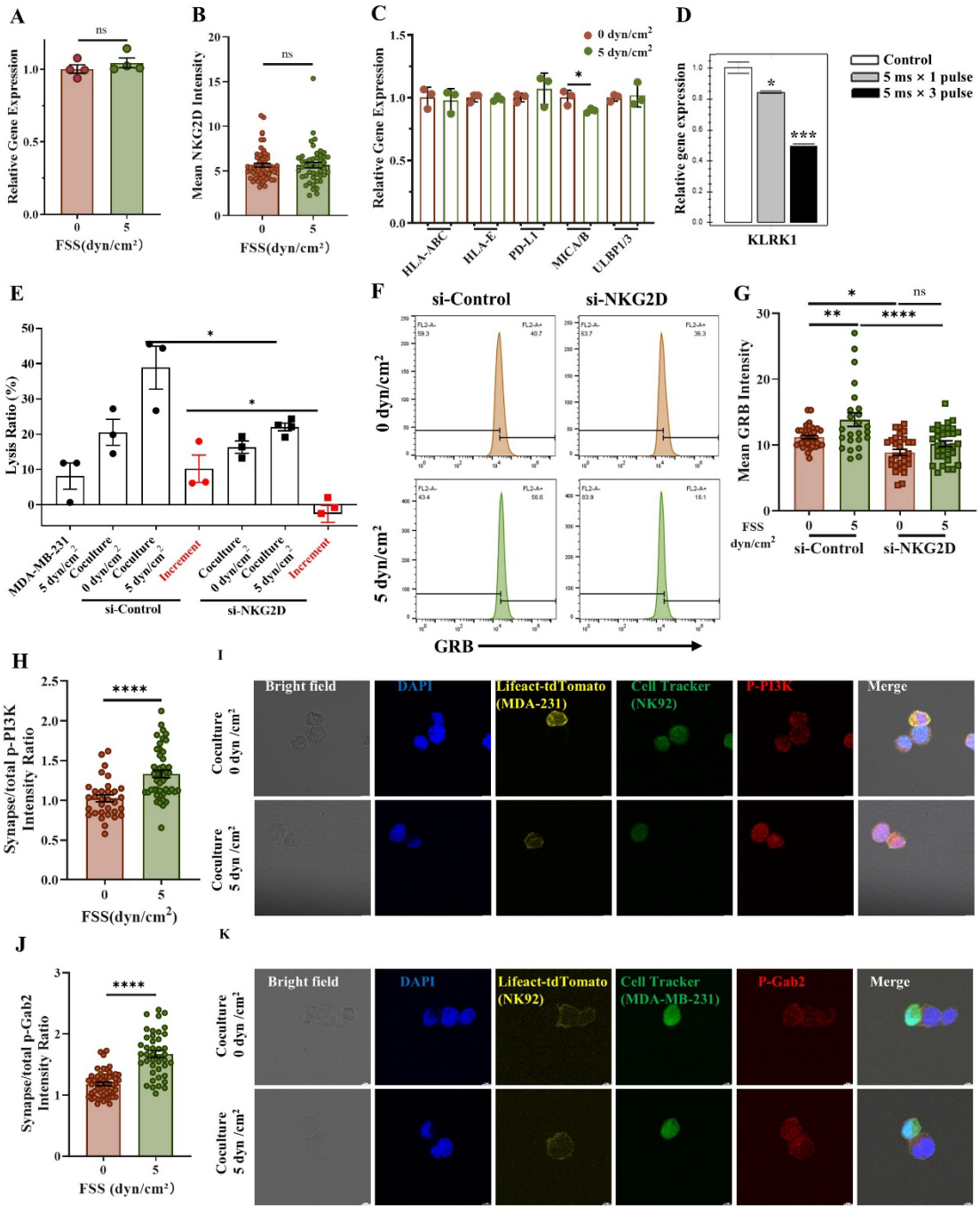

Figure 5-3 NK cells inject more granzyme B into tumor cells trigered by NKG2D

A&B Expression of NKG2D mRNA/protein in NK92 cells under 0 or 5 dyn/cm^2 FSS treatment for 4 h. **C** mRNA expression of activating/inhibitory ligands in MDA-MB-231 cells under 0 or 5 dyn/cm^2 FSS treatment for 4 h. **D** Knocking down efficiency of KLRK1 using electroporation transfection assay. **E** Lysis ratio of NK92 against MDA-MB-231 under 0 or 5 dyn/cm^2 FSS after knocking down NKG2D in NK92 cells. **F&G** Granzyme B entry into MDA-MB-231 after co-culturing with NK92 under 0 or 5 dyn/cm^2 FSS with or without knocking down of NKG2D in NK92 cells using flow cytometry (**F**) and an immune fluorescent assay (**G**). **H&I** Synapse/ total ratio of

phosph-PI3K fluorescent intensity of NK92 cells after co-culturing with MDA-MB-231 cells under 0 and 5 dyn/cm^2 FSS. **J&K** Synapse/ total ratio of phosph-Gab2 fluorescent intensity of NK92 cells after co-culturing with MDA-MB-231 cells under 0 and 5 dyn/cm^2 FSS. The one-way ANOVA followed by Tukey's test (**D, E, and G**) and unpaired t-test (**A, B, C, H, and J**) were adopted for statistical analysis.

5.4 NKG2D is mechano-sensitive to FSS

Our results indicate that NKG2D plays a role in the shear force-induced activation of NK cells. We next investigated whether NKG2D can directly detect and react to FSS. To examine this, we coated the surface of the microfluidic chip with MICA, a ligand known to bind NKG2D. NK cells were allowed to adhere to this surface and then treated under FSS. (Figure 5-4 **A**). As FSS increased, adhered NK cells exhibited higher CD107a expression on their membranes, indicating enhanced NK cell cytotoxicity. (Figure 5-4 **B**). However, the LFA-1 ligand, ICAM-1, could not promote CD107a expression under FSS. These findings suggest that shear forces might activate NK cells through direct NKG2D-MICA force sensing. When NKG2D interacts with MICA, DAP10, which connects to the intracellular domain of NKG2D, recruits Grb2-VAV1 and PI3K. This recruitment facilitates the formation of the immune synapse and activates NK cells activation [304,306]. Lck is proposed to phosphorylate both VAV1[307,308] and PI3K[309,310] to initiate the downstream signaling pathway. Using an Lck activity FRET sensor, we observed that FSS can enhance Lck activity after NK cells form conjugates with target cells. The high FRET ratio indicates low Lck activity. Silencing NKG2D reduced the decrease in the FRET ratio and restored Lck activity to control levels (Figure 5-4 **C & D**). FSS also facilitated the accumulation of phosphorylated VAV1 within the immune synapse, an effect that was entirely negated by silencing NKG2D. (Figure 5-4 **E**). PI3K is another kinase activated by Lck. We observed that Akt phosphorylation, which occurs downstream of PI3K, was notably increased under FSS, and this boost was reversed when NKG2D was knocked down. (Figure 5-4 **F & H**). Moreover, FSS enhanced the polarization of NK cell MTOC following conjugation with target cells (Figure 5-2 **D**). However, knocking down

NKG2D reduced this shear force-induced MTOC polarization. (Figure 4 **G & I**). Overall, these findings show that the activating receptor NKG2D can directly detect and react to FSS by triggering the Lck/Grb2/VAV1/PI3K signaling pathway following binding with MICA, which may enhance NK cell cytotoxicity.

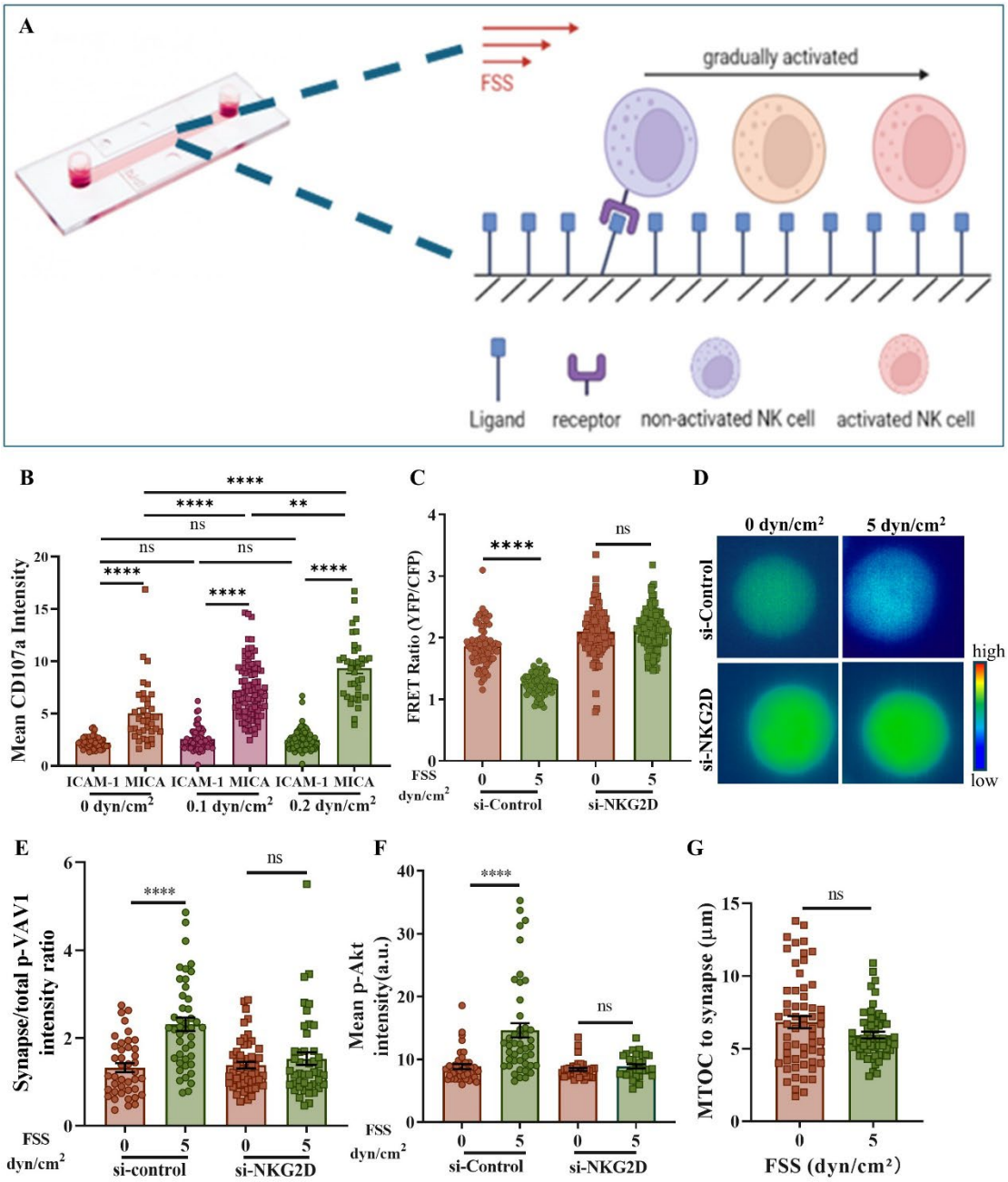

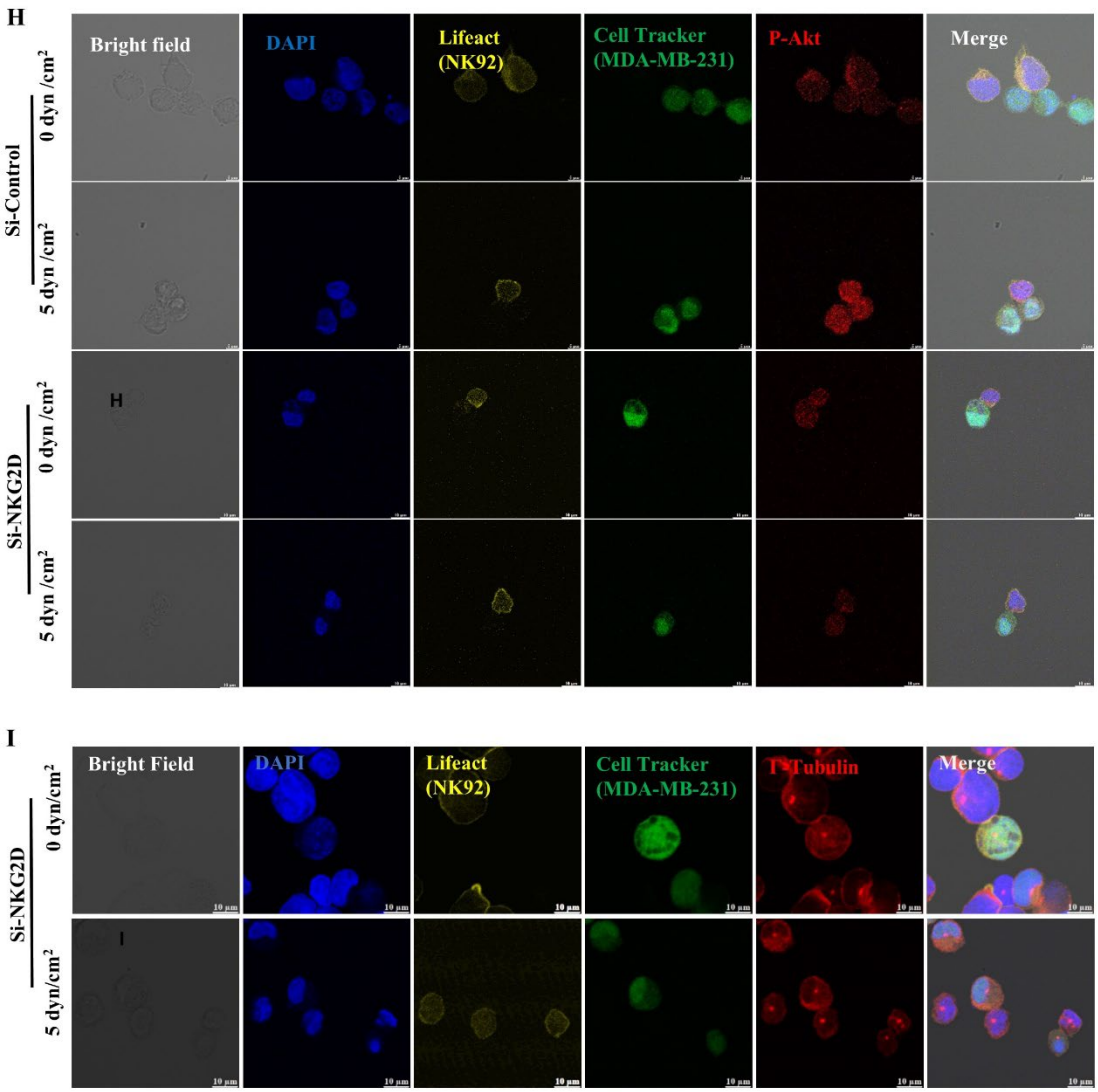

Figure 5-4 NKG2D is an FSS sensor

A Diagram of the NK cell activation assay among fluid chips. **B** CD107a expression level of NK92 cells under different WSS when adhering to MICA-coated chips. **C & D** FRET ratio (YFP/CFP) of NK92 cells when co-culturing with MDA-MB-231 cells under different FSS. A higher FRET ratio represents lower Lck activity. **E** Distribution of Phosphorylated VAV1 among NK92 cells when co-culturing with MDA-MB-231 cells under different FSS. **F & H** Phosphorylated Akt level of NK92 cells when co-culturing with MDA-MB-231 cells under different FSS. **G&I** MOTC polarization of NK92 cells when co-culturing with MDA-MB-231 cells under different FSS with or without knocking down of NKG2D. The one-way ANOVA followed by Tukey's test (**B, C, E & F**) and unpaired t-test (**G**) was adopted for statistical analysis.

Chapter 6: Conclusion and future perspectives

6.1 Discussion and conclusion

Tumor cells are continuously under surveillance of the immune system from the cancer initiation, progression, and metastasis, from the primary sites, through the blood/lymph circulation, and to the secondary organs. However, in most cancer patients, killer cells cannot eliminate tumor cells, nor can the current immunotherapies, represented by the CAR-T therapy. These surviving tumor cells gained both immune evasive biological characteristics, represented by downregulated MHC-1 molecules at the cell membrane[311], upregulated the immune checkpoint PD-L1 and other inhibitory ligands and cytokines[312-314], and recruitment of suppressive immune cells[52,315]. Meanwhile, the mechanics of invasive/malignant tumor cells, which are usually resistant to killer cells, are also different. Tumor cell mechanics have been proposed to correlate with cancer metastasis and organotropism. Whether the cancer killers may influence organotropism through targeting tumor cell mechanics remains largely unknown.

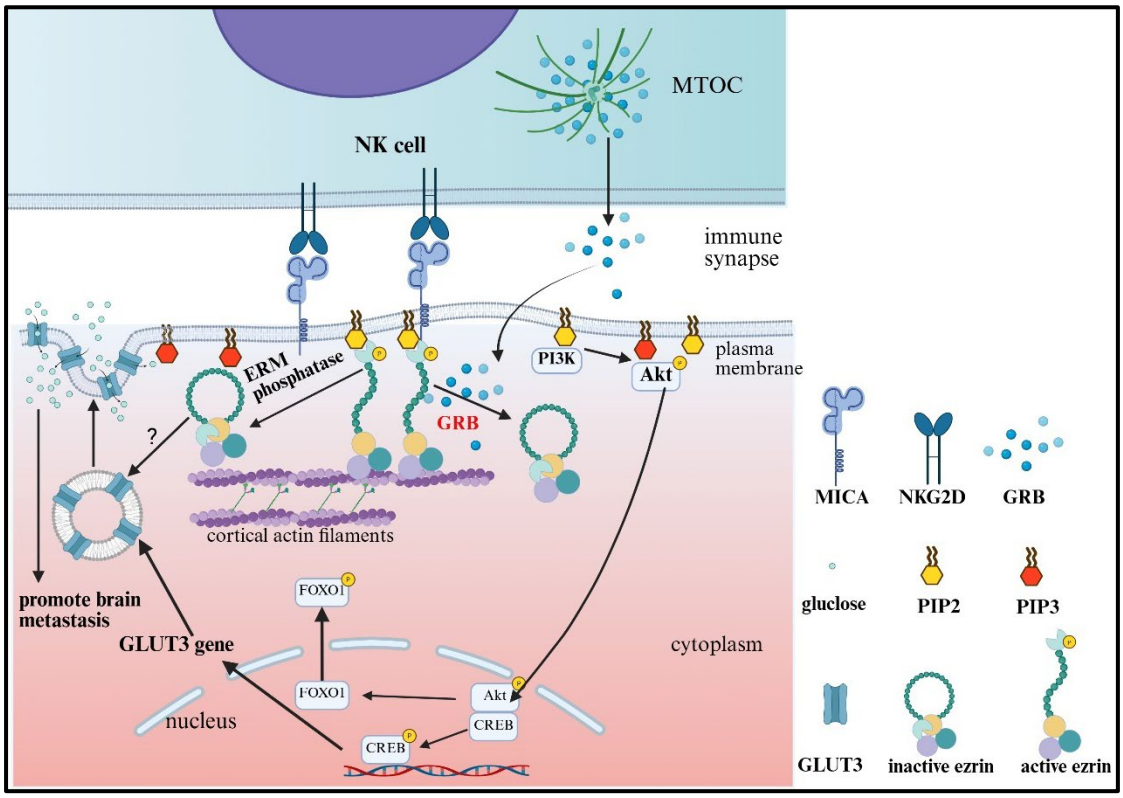

Figure 6-1 NK cells promote cancer brain metastasis through decreasing tumor cell membrane tension-PI3K-Akt-CREB-GLUT3 signaling

Our results demonstrate that NK cells, rather than other immune cells, are highly enriched in the primary tumor tissue of brain metastasis patients. In the NK cell niches, tumor cells specifically upregulate their brain metastasis-associated genes but not bone/lung/liver metastasis-associated genes. These underscore the essential function of NK cells in brain metastasis. W confirm this using a series of in vivo and in vitro assays. Characterization of tumor cells following co-culture with NK cells reveals that the surviving tumor cells exhibit significantly lower membrane tension. This is caused by the downregulated ezrin expression, decreased activity, and the low abundance of PIP2 in the plasma membrane after co-culture. Low membrane tension makes tumor cells resistant to NK cell cytotoxicity and prefers to metastasize to the brain, which can be reversed by increasing ezrin expression or actomyosin activity. PI3K-Akt signaling is found to be the downstream to promote brain metastasis, which provides another target for clinical applications.

On the other hand, among blood circulation, only a tiny subset of CTCs can survive the challenges of FSS and the immune system to seed metastasis[9,316]. Given enough time (>12 h), FSS alone (>20 dyn/cm^2) can effectively eliminate CTCs[28,63,200,317,318]. Unfortunately, in vivo measurements indicate that the half-life of CTCs in the vasculature may only be around 30 min[11,15-17]. Long-term and high-magnitude FSS challenges may barely be encountered by CTCs in vivo. There should be an alternative strategy for effective CTC killing. NK cells are crucial for attacking CTCs in the bloodstream. FSS is one of the mechanical cues that does not exist in primary tumor sites. Whether FSS can influence NK cell function is still unknown.

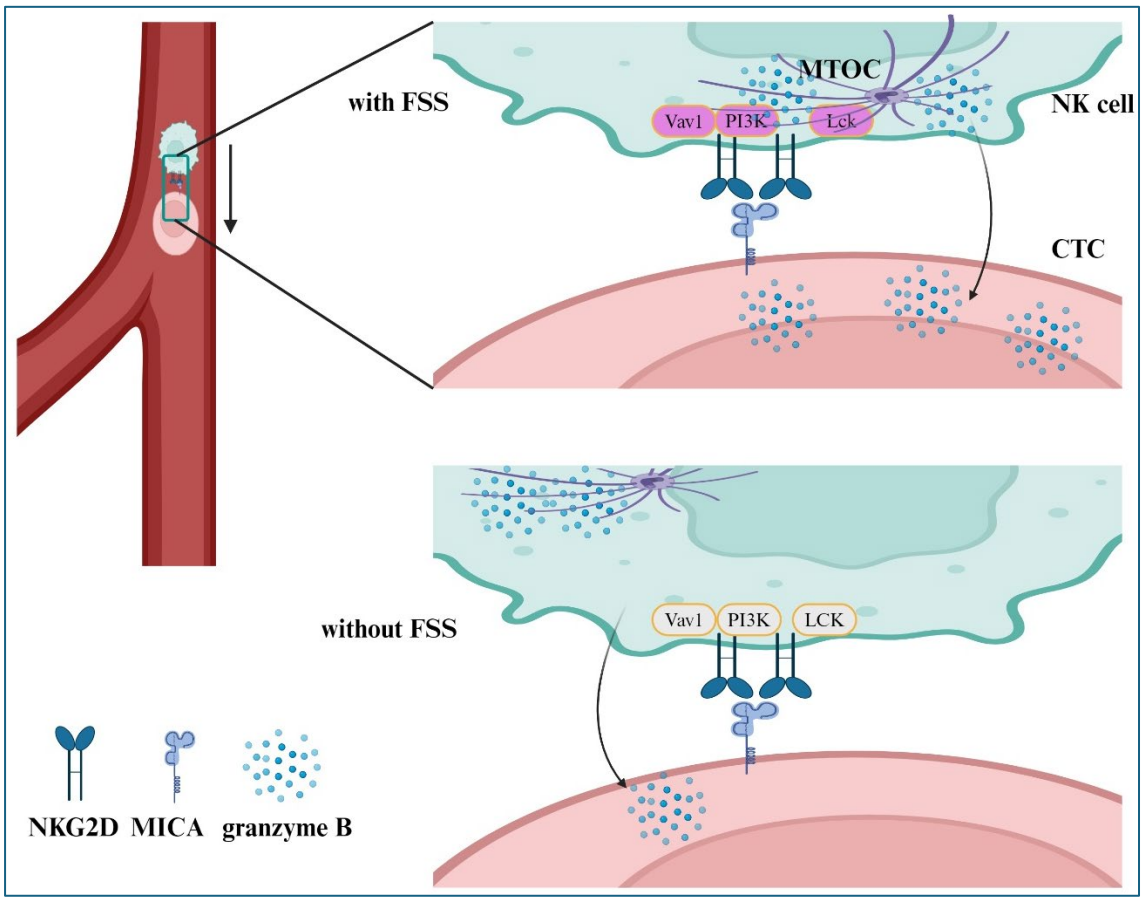

Figure 6-2 FSS promotes NK cell cytotoxicity against CTCs through NKG2D-mediated mechano-sensing

We report that FSS can promote NK cell cytotoxicity against CTCs within a physiological magnitude and duration. Death receptor ligand Trail and other cytokines

were not responsible for the increased CTCs under FSS. This may be caused by the insufficient trail and cytokine secretion within a short duration. On the contrary, more granzyme B is injected in CTCs under 5 dyn/cm^2 FSS, which explains the increased death. NKG2D is an important activating receptor to recognize transformed cells, and it is a potential mechanical sensor[169,176,177,185]. Our results reveal that NKG2D directly senses FSS through its binding to MICA on CTCs. Force transmission through NKG2D induces higher NK cell activation, effector protein-granzyme B injection, and finally, CTC death.

Although we found NK cells can efficiently eliminate CTCs with the help of FSS, very few CTCs can still evade NK cell killing and successfully seed metastasis. This may result from the protective effect of blood cells like platelets and neutrophils or cell softness. Further studies are needed on whether CTCs utilize other mechanisms to survive changes in circulation.

In summary, this study reports that FSS enhances NK cell cytotoxicity to CTCs in a shear-dependent manner. The increment is attributed to higher activation of NK cells under FSS mediated by the ligation between NKG2D and its ligands on CTCs. As a result, more granzyme B enters CTCs to induce apoptosis. Secreted cytokines or death receptor ligands are dispensable. Importantly, NKG2D can directly sense FSS when binding its ligands MICA and promote NK cell activation and cytotoxicity. Knocking down NKG2D erases FSS-enhanced NK cell activation signaling, granzyme B entry, and CTC death. These findings unveil a mechanically regulated CTCs killing ability of NK cells, which may provide a new strategy for NK cell-based immunotherapy.

6.2 Limitations and Future Perspectives

This study primarily focuses on the mechanical regulation of tumor cell brain metastasis and survival under FSS. First, we identified that after co-culture with NK cells, the decreased cell membrane tension-PI3K-Akt-CREB-GLUT3 signaling was responsible for enhanced brain metastasis. However, this work does not provide evidence that NK

cells promote brain metastasis in the primary tumor in vivo. Second, this work does not elucidate whether Ezrin-PI3K-CREB-GLUT3 signaling regulates tumor cell adhesion to brain endothelial and trans-BBB migration. Third, this work only focuses on breast cancer, and the major experiments of this study are based on the MDA-MB-231, a TNBC cell line. We do not investigate whether NK cells promote brain metastasis in other cancer types. Finally, we only use the NK92 cell line for all the experiments, which would be more convincing if we confirmed some key findings with primary NK cells from healthy adults.

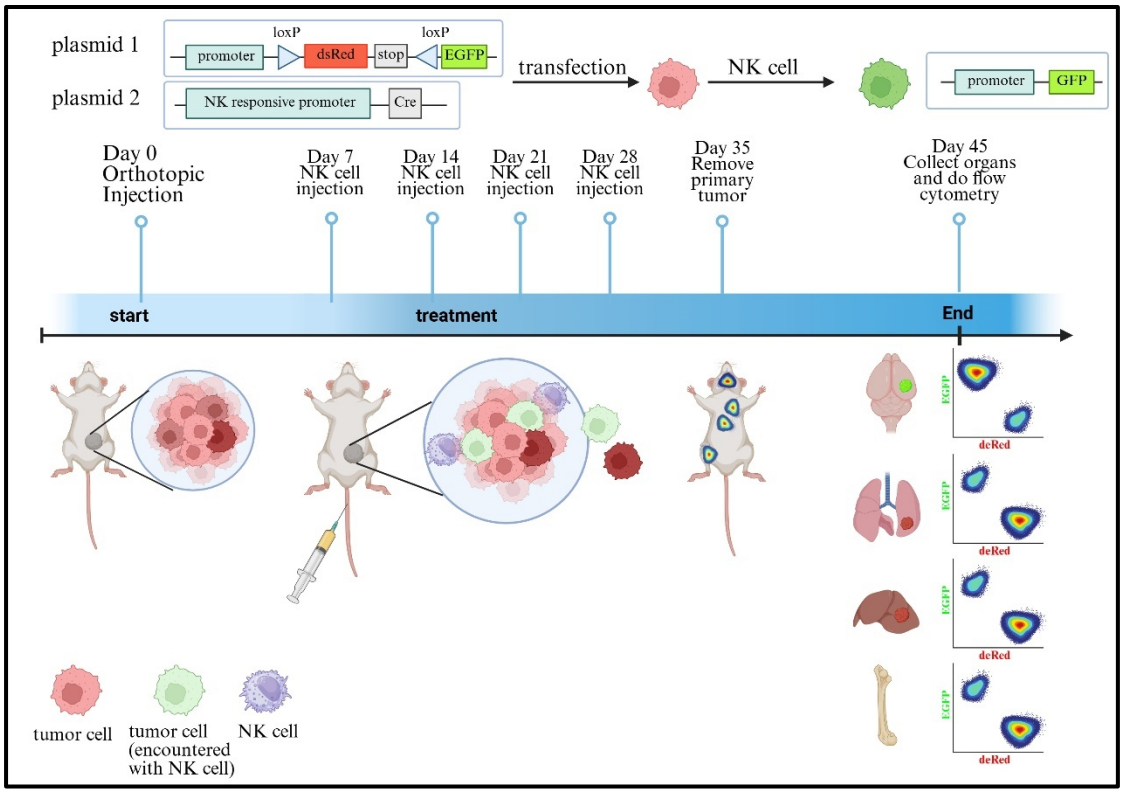

Figure 6-3 Diagram of future experimental design for in vivo detection of NK cells that promote brain metastasis.

Based on the above limitations, we will first generate a reporter system based on NK cell-induced fluorescence shifting in tumor cells (Figure 6-3). Once tumor cells encounter NK cells, they will permanently shift from red to green. We will detect the green vs. red ratio of tumor cells among the primary tumor and brain metastasis sites to consolidate our findings in live mice. Moreover, more cancer cell lines will be used to

investigate the effects of NK cells on their brain metastatic potential. Primary NK cells will be collected from healthy adult volunteers to confirm key experiments.

Reference

1. Gauthier, N.C.; Masters, T.A.; Sheetz, M.P. Mechanical feedback between membrane tension and dynamics. *Trends in cell biology* **2012**, *22*, 527-535.
2. Itoh, T.; Tsujita, K. Exploring membrane mechanics: The role of membrane-cortex attachment in cell dynamics. *Current Opinion in Cell Biology* **2023**, *81*, 102173, doi:https://doi.org/10.1016/j.ceb.2023.102173.
3. Gudipaty, S.A.; Lindblom, J.; Loftus, P.D.; Redd, M.J.; Edes, K.; Davey, C.; Krishnegowda, V.; Rosenblatt, J. Mechanical stretch triggers rapid epithelial cell division through Piezo1. *Nature* **2017**, *543*, 118-121.
4. Chalut, K.J.; Paluch, E.K. The actin cortex: a bridge between cell shape and function. *Developmental Cell* **2016**, *38*, 571-573.
5. Mao, F.; Yang, Y.; Jiang, H. Endocytosis and exocytosis protect cells against severe membrane tension variations. *Biophys J* **2021**, *120*, 5521-5529, doi:10.1016/j.bpj.2021.11.019.
6. Tsujita, K.; Satow, R.; Asada, S.; Nakamura, Y.; Arnes, L.; Sako, K.; Fujita, Y.; Fukami, K.; Itoh, T. Homeostatic membrane tension constrains cancer cell dissemination by counteracting BAR protein assembly. *Nature Communications* **2021**, *12*, 5930, doi:10.1038/s41467-021-26156-4.
7. Zhang, J.; Li, J.; Hou, Y.; Lin, Y.; Zhao, H.; Shi, Y.; Chen, K.; Nian, C.; Tang, J.; Pan, L.; et al. Osr2 functions as a biomechanical checkpoint to aggravate CD8(+) T cell exhaustion in tumor. *Cell* **2024**, *187*, 3409-3426.e3424, doi:10.1016/j.cell.2024.04.023.
8. Gonzalez, H.; Robles, I.; Werb, Z. Innate and acquired immune surveillance in the postdissemination phase of metastasis. *The FEBS Journal* **2018**, *285*, 654-664, doi:https://doi.org/10.1111/febs.14325.
9. Micalizzi, D.S.; Maheswaran, S.; Haber, D.A. A conduit to metastasis: circulating tumor cell biology. *Genes Dev* **2017**, *31*, 1827-1840, doi:10.1101/gad.305805.117.
10. Chaffer, C.L.; Weinberg, R.A. A Perspective on Cancer Cell Metastasis. *Science* **2011**, *331*, 1559-1564, doi:doi:10.1126/science.1203543.
11. Wirtz, D.; Konstantopoulos, K.; Searson, P.C. The physics of cancer: the role of physical interactions and mechanical forces in metastasis. *Nature Reviews Cancer* **2011**, *11*, 512-522, doi:10.1038/nrc3080.
12. Nagrath, S.; Sequist, L.V.; Maheswaran, S.; Bell, D.W.; Irimia, D.; Ulkus, L.; Smith, M.R.; Kwak, E.L.; Digumarthy, S.; Muzikansky, A.; et al. Isolation of rare circulating tumour cells in cancer patients by microchip technology. *Nature* **2007**, *450*, 1235-1239, doi:10.1038/nature06385.
13. Massagué, J.; Obenauf, A.C. Metastatic colonization by circulating tumour cells. *Nature* **2016**, *529*, 298-306, doi:10.1038/nature17038.
14. Kitamura, T.; Qian, B.Z.; Pollard, J.W. Immune cell promotion of metastasis. *Nat Rev Immunol* **2015**, *15*, 73-86, doi:10.1038/nri3789.
15. Meng, S.; Tripathy, D.; Frenkel, E.P.; Shete, S.; Naftalis, E.Z.; Huth, J.F.; Beitsch, P.D.; Leitch, M.; Hoover, S.; Euhus, D.; et al. Circulating tumor cells in patients with breast

cancer dormancy. *Clin Cancer Res* **2004**, *10*, 8152-8162, doi:10.1158/1078-0432.Ccr-04-1110.

16. Aceto, N.; Bardia, A.; Miyamoto, D.T.; Donaldson, M.C.; Wittner, B.S.; Spencer, J.A.; Yu, M.; Pely, A.; Engstrom, A.; Zhu, H. Circulating tumor cell clusters are oligoclonal precursors of breast cancer metastasis. *Cell* **2014**, *158*, 1110-1122.
17. Hamza, B.; Miller, A.B.; Meier, L.; Stockslager, M.; Ng, S.R.; King, E.M.; Lin, L.; DeGouveia, K.L.; Mulugeta, N.; Calistri, N.L.; et al. Measuring kinetics and metastatic propensity of CTCs by blood exchange between mice. *Nature Communications* **2021**, *12*, 5680, doi:10.1038/s41467-021-25917-5.
18. Vivier, E.; Nunès, J.A.; Vély, F. Natural killer cell signaling pathways. *Science* **2004**, *306*, 1517-1519, doi:10.1126/science.1103478.
19. Hashemi, E.; Malarkannan, S. Tissue-Resident NK Cells: Development, Maturation, and Clinical Relevance. *Cancers (Basel)* **2020**, *12*, doi:10.3390/cancers12061553.
20. Wu, M.; Mei, F.; Liu, W.; Jiang, J. Comprehensive characterization of tumor infiltrating natural killer cells and clinical significance in hepatocellular carcinoma based on gene expression profiles. *Biomed Pharmacother* **2020**, *121*, 109637, doi:10.1016/j.biopha.2019.109637.
21. Cursons, J.; Souza-Fonseca-Guimaraes, F.; Foroutan, M.; Anderson, A.; Hollande, F.; Hediyeh-Zadeh, S.; Behren, A.; Huntington, N.D.; Davis, M.J. A Gene Signature Predicting Natural Killer Cell Infiltration and Improved Survival in Melanoma Patients. *Cancer Immunol Res* **2019**, *7*, 1162-1174, doi:10.1158/2326-6066.Cir-18-0500.
22. Barry, K.C.; Hsu, J.; Broz, M.L.; Cueto, F.J.; Binnewies, M.; Combes, A.J.; Nelson, A.E.; Loo, K.; Kumar, R.; Rosenblum, M.D.; et al. A natural killer-dendritic cell axis defines checkpoint therapy-responsive tumor microenvironments. *Nat Med* **2018**, *24*, 1178-1191, doi:10.1038/s41591-018-0085-8.
23. Muntasell, A.; Rojo, F.; Servitja, S.; Rubio-Perez, C.; Cabo, M.; Tamborero, D.; Costa-García, M.; Martínez-Garcia, M.; Menéndez, S.; Vazquez, I.; et al. NK Cell Infiltrates and HLA Class I Expression in Primary HER2(+) Breast Cancer Predict and Uncouple Pathological Response and Disease-free Survival. *Clin Cancer Res* **2019**, *25*, 1535-1545, doi:10.1158/1078-0432.Ccr-18-2365.
24. Di Vito, C.; Mikulak, J.; Mavilio, D. On the Way to Become a Natural Killer Cell. *Frontiers in Immunology* **2019**, *10*, doi:10.3389/fimmu.2019.01812.
25. Quatrini, L.; Della Chiesa, M.; Sivori, S.; Mingari, M.C.; Pende, D.; Moretta, L. Human NK cells, their receptors and function. *Eur J Immunol* **2021**, *51*, 1566-1579, doi:10.1002/eji.202049028.
26. Myers, J.A.; Miller, J.S. Exploring the NK cell platform for cancer immunotherapy. *Nature Reviews Clinical Oncology* **2021**, *18*, 85-100, doi:10.1038/s41571-020-0426-7.
27. Fuhs, T.; Wetzel, F.; Fritsch, A.W.; Li, X.; Stange, R.; Pawlizak, S.; Kießling, T.R.; Morawetz, E.; Grosser, S.; Sauer, F.; et al. Rigid tumours contain soft cancer cells. *Nature Physics* **2022**, *18*, 1510-1519, doi:10.1038/s41567-022-01755-0.
28. Xin, Y.; Chen, X.; Tang, X.; Li, K.; Yang, M.; Tai, W.C.-S.; Liu, Y.; Tan, Y. Mechanics and Actomyosin-Dependent Survival/Chemoresistance of Suspended Tumor Cells in Shear Flow. *Biophysical Journal* **2019**, *116*, 1803-1814,

doi:https://doi.org/10.1016/j.bpj.2019.04.011.
29. Tang, K.; Xin, Y.; Li, K.; Chen, X.; Tan, Y. Cell Cytoskeleton and Stiffness Are Mechanical Indicators of Organotropism in Breast Cancer. *Biology* **2021**, *10*, 259.
30. Kamangar, F.; Dores, G.M.; Anderson, W.F. Patterns of cancer incidence, mortality, and prevalence across five continents: defining priorities to reduce cancer disparities in different geographic regions of the world. *Journal of clinical oncology* **2006**, *24*, 2137-2150.
31. Registry, H.K.C. Overview of Hong Kong Cancer Statistics of 2021. **2023**.
32. Siegel, R.L.; Miller, K.D.; Wagle, N.S.; Jemal, A. Cancer statistics, 2023. *CA Cancer J Clin* **2023**, *73*, 17-48, doi:10.3322/caac.21763.
33. Shaath, H.; Elango, R.; Alajez, N.M. Molecular Classification of Breast Cancer Utilizing Long Non-Coding RNA (lncRNA) Transcriptomes Identifies Novel Diagnostic lncRNA Panel for Triple-Negative Breast Cancer. *Cancers* **2021**, *13*, 5350.
34. Miah, S.; Bagu, E.; Goel, R.; Ogunbolude, Y.; Dai, C.; Ward, A.; Vizeacoumar, F.S.; Davies, G.; Vizeacoumar, F.J.; Anderson, D.; et al. Estrogen receptor signaling regulates the expression of the breast tumor kinase in breast cancer cells. *BMC Cancer* **2019**, *19*, 78, doi:10.1186/s12885-018-5186-8.
35. Nicolini, A.; Ferrari, P.; Duffy, M.J. Prognostic and predictive biomarkers in breast cancer: Past, present and future. *Seminars in Cancer Biology* **2018**, *52*, 56-73, doi:https://doi.org/10.1016/j.semcancer.2017.08.010.
36. Vaz-Luis, I.; Winer, E.P.; Lin, N.U. Human epidermal growth factor receptor-2-positive breast cancer: does estrogen receptor status define two distinct subtypes? *Annals of Oncology* **2013**, *24*, 283-291, doi:10.1093/annonc/mds286.
37. Slamon, D.J.; Clark, G.M.; Wong, S.G.; Levin, W.J.; Ullrich, A.; McGuire, W.L. Human breast cancer: correlation of relapse and survival with amplification of the HER-2/neu oncogene. *science* **1987**, *235*, 177-182.
38. Harris, M.A.; Savas, P.; Virassamy, B.; O'Malley, M.M.R.; Kay, J.; Mueller, S.N.; Mackay, L.K.; Salgado, R.; Loi, S. Towards targeting the breast cancer immune microenvironment. *Nature Reviews Cancer* **2024**, *24*, 554-577, doi:10.1038/s41568-024-00714-6.
39. Siegel, R.L.; Miller, K.D.; Jemal, A. Cancer statistics, 2016. *CA Cancer J Clin* **2016**, *66*, 7-30, doi:10.3322/caac.21332.
40. Dillekås, H.; Rogers, M.S.; Straume, O. Are 90% of deaths from cancer caused by metastases? *Cancer Med* **2019**, *8*, 5574-5576, doi:10.1002/cam4.2474.
41. Wang, R.; Zhu, Y.; Liu, X.; Liao, X.; He, J.; Niu, L. The Clinicopathological features and survival outcomes of patients with different metastatic sites in stage IV breast cancer. *BMC Cancer* **2019**, *19*, 1091, doi:10.1186/s12885-019-6311-z.
42. Welch, D.R.; Hurst, D.R. Defining the Hallmarks of Metastasis. *Cancer Research* **2019**, *79*, 3011-3027, doi:10.1158/0008-5472.Can-19-0458.
43. Fares, J.; Fares, M.Y.; Khachfe, H.H.; Salhab, H.A.; Fares, Y. Molecular principles of metastasis: a hallmark of cancer revisited. *Signal Transduction and Targeted Therapy* **2020**, *5*, 28, doi:10.1038/s41392-020-0134-x.
44. Luzzi, K.J.; MacDonald, I.C.; Schmidt, E.E.; Kerkvliet, N.; Morris, V.L.; Chambers,

A.F.; Groom, A.C. Multistep Nature of Metastatic Inefficiency: Dormancy of Solitary Cells after Successful Extravasation and Limited Survival of Early Micrometastases. *The American Journal of Pathology* **1998**, *153*, 865-873, doi:10.1016/S0002-9440(10)65628-3.

45. Strilic, B.; Offermanns, S. Intravascular Survival and Extravasation of Tumor Cells. *Cancer Cell* **2017**, *32*, 282-293, doi:10.1016/j.ccell.2017.07.001.
46. Wong, C.W.; Lee, A.; Shientag, L.; Yu, J.; Dong, Y.; Kao, G.; Al-Mehdi, A.B.; Bernhard, E.J.; Muschel, R.J. Apoptosis: an early event in metastatic inefficiency. *Cancer research* **2001**, *61*, 333-338.
47. Morrow, M.; Burstein, H.J.; Harris, J.R. Malignant tumors of the breast. In *DeVita, Hellman, and Rosenberg's Cancer: Principles & Practice of Oncology: Tenth Edition*; 2015.
48. Lemke, S.B.; Nelson, C.M. Dynamic changes in epithelial cell packing during tissue morphogenesis. *Current Biology* **2021**, *31*, R1098-R1110, doi:10.1016/j.cub.2021.07.078.
49. COMŞA, Ş.; CÎMPEAN, A.M.; RAICA, M. The Story of MCF-7 Breast Cancer Cell Line: 40 years of Experience in Research. *Anticancer Research* **2015**, *35*, 3147-3154.
50. Guzman, A.; Ziperstein, M.J.; Kaufman, L.J. The effect of fibrillar matrix architecture on tumor cell invasion of physically challenging environments. *Biomaterials* **2014**, *35*, 6954-6963, doi:https://doi.org/10.1016/j.biomaterials.2014.04.086.
51. Tormoen, G.W.; Crittenden, M.R.; Gough, M.J. Role of the immunosuppressive microenvironment in immunotherapy. *Adv Radiat Oncol* **2018**, *3*, 520-526, doi:10.1016/j.adro.2018.08.018.
52. Munn, D.H.; Bronte, V. Immune suppressive mechanisms in the tumor microenvironment. *Current Opinion in Immunology* **2016**, *39*, 1-6, doi:https://doi.org/10.1016/j.coi.2015.10.009.
53. Tang, T.; Huang, X.; Zhang, G.; Hong, Z.; Bai, X.; Liang, T. Advantages of targeting the tumor immune microenvironment over blocking immune checkpoint in cancer immunotherapy. *Signal Transduction and Targeted Therapy* **2021**, *6*, 72, doi:10.1038/s41392-020-00449-4.
54. Arner, E.N.; Rathmell, J.C. Metabolic programming and immune suppression in the tumor microenvironment. *Cancer Cell* **2023**, *41*, 421-433, doi:https://doi.org/10.1016/j.ccell.2023.01.009.
55. Reinfeld, B.I.; Madden, M.Z.; Wolf, M.M.; Chytil, A.; Bader, J.E.; Patterson, A.R.; Sugiura, A.; Cohen, A.S.; Ali, A.; Do, B.T.; et al. Cell-programmed nutrient partitioning in the tumour microenvironment. *Nature* **2021**, *593*, 282-288, doi:10.1038/s41586-021-03442-1.
56. Raines, L.N.; Huang, S.C.-C. Is glucose the scapegoat for tumor evasion? *Cancer Cell* **2021**, *39*, 907-909, doi:10.1016/j.ccell.2021.06.006.
57. Mortezaee, K. Immune escape: A critical hallmark in solid tumors. *Life Sciences* **2020**, *258*, 118110, doi:https://doi.org/10.1016/j.lfs.2020.118110.
58. Abizanda-Campo, S.; Virumbrales-Muñoz, M.; Humayun, M.; Marmol, I.; Beebe, D.J.; Ochoa, I.; Oliván, S.; Ayuso, J.M. Microphysiological systems for solid tumor

immunotherapy: opportunities and challenges. *Microsystems & Nanoengineering* **2023**, *9*, 154, doi:10.1038/s41378-023-00616-x.

59. López-Soto, A.; Gonzalez, S.; Smyth, M.J.; Galluzzi, L. Control of Metastasis by NK Cells. *Cancer Cell* **2017**, *32*, 135-154, doi:10.1016/j.ccell.2017.06.009.
60. Lo, H.C.; Xu, Z.; Kim, I.S.; Pingel, B.; Aguirre, S.; Kodali, S.; Liu, J.; Zhang, W.; Muscarella, A.M.; Hein, S.M.; et al. Resistance to natural killer cell immunosurveillance confers a selective advantage to polyclonal metastasis. *Nature Cancer* **2020**, *1*, 709-722, doi:10.1038/s43018-020-0068-9.
61. Xu, Z.; Li, K.; Xin, Y.; Tang, K.; Yang, M.; Wang, G.; Tan, Y. Fluid shear stress regulates the survival of circulating tumor cells via nuclear expansion. *J Cell Sci* **2022**, *135*, doi:10.1242/jcs.259586.
62. Xin, Y.; Chen, X.; Tang, X.; Li, K.; Yang, M.; Tai, W.C.; Liu, Y.; Tan, Y. Mechanics and Actomyosin-Dependent Survival/Chemoresistance of Suspended Tumor Cells in Shear Flow. *Biophys J* **2019**, *116*, 1803-1814, doi:10.1016/j.bpj.2019.04.011.
63. Xin, Y.; Li, K.; Yang, M.; Tan, Y. Fluid Shear Stress Induces EMT of Circulating Tumor Cells via JNK Signaling in Favor of Their Survival during Hematogenous Dissemination. *Int J Mol Sci* **2020**, *21*, doi:10.3390/ijms21218115.
64. Guo, W.; Giancotti, F.G. Integrin signalling during tumour progression. *Nature reviews Molecular cell biology* **2004**, *5*, 816-826.
65. Weiss, L. Biomechanical interactions of cancer cells with the microvasculature during hematogenous metastasis. *Cancer and Metastasis Reviews* **1992**, *11*, 227-235.
66. Stegner, D.; Dütting, S.; Nieswandt, B. Mechanistic explanation for platelet contribution to cancer metastasis. *Thrombosis research* **2014**, *133*, S149-S157.
67. Ghajar, C.M.; Peinado, H.; Mori, H.; Matei, I.R.; Evason, K.J.; Brazier, H.; Almeida, D.; Koller, A.; Hajjar, K.A.; Stainier, D.Y. The perivascular niche regulates breast tumour dormancy. *Nature cell biology* **2013**, *15*, 807-817.
68. Kienast, Y.; Von Baumgarten, L.; Fuhrmann, M.; Klinkert, W.E.; Goldbrunner, R.; Herms, J.; Winkler, F. Real-time imaging reveals the single steps of brain metastasis formation. *Nature medicine* **2010**, *16*, 116-122.
69. Coleman, R.E. Metastatic bone disease: clinical features, pathophysiology and treatment strategies. *Cancer Treatment Reviews* **2001**, *27*, 165-176, doi:https://doi.org/10.1053/ctrv.2000.0210.
70. Gennari, A.; Conte, P.; Rosso, R.; Orlandini, C.; Bruzzi, P. Survival of metastatic breast carcinoma patients over a 20-year period: A retrospective analysis based on individual patient data from six consecutive studies. *Cancer* **2005**, *104*, 1742-1750.
71. Hess, K.R.; Varadhachary, G.R.; Taylor, S.H.; Wei, W.; Raber, M.N.; Lenzi, R.; Abbruzzese, J.L. Metastatic patterns in adenocarcinoma. *Cancer* **2006**, *106*, 1624-1633.
72. Bachmann, C.; Schmidt, S.; Staebler, A.; Fehm, T.; Fend, F.; Schittenhelm, J.; Wallwiener, D.; Grischke, E. CNS metastases in breast cancer patients: prognostic implications of tumor subtype. *Medical Oncology* **2015**, *32*, 1-6.
73. Schön, C.A.; Görg, C.; Ramaswamy, A.; Barth, P.J. Splenic metastases in a large unselected autopsy series. *Pathology-Research and Practice* **2006**, *202*, 351-356.
74. Fidler, I.J. The pathogenesis of cancer metastasis: the 'seed and soil' hypothesis

revisited. *Nat Rev Cancer* **2003**, *3*, 453-458, doi:10.1038/nrc1098.

75. Pang, L.; Xiang, F.; Yang, H.; Shen, X.; Fang, M.; Li, R.; Long, Y.; Li, J.; Yu, Y.; Pang, B. Single-cell integrative analysis reveals consensus cancer cell states and clinical relevance in breast cancer. *Scientific Data* **2024**, *11*, 289, doi:10.1038/s41597-024-03127-0.
76. Steeg, P.S. Targeting metastasis. *Nature reviews cancer* **2016**, *16*, 201-218.
77. Hoshino, A.; Costa-Silva, B.; Shen, T.-L.; Rodrigues, G.; Hashimoto, A.; Tesic Mark, M.; Molina, H.; Kohsaka, S.; Di Giannatale, A.; Ceder, S. Tumour exosome integrins determine organotropic metastasis. *Nature* **2015**, *527*, 329-335.
78. Cambria, E.; Coughlin, M.F.; Floryan, M.A.; Offeddu, G.S.; Shelton, S.E.; Kamm, R.D. Linking cell mechanical memory and cancer metastasis. *Nature Reviews Cancer* **2024**, *24*, 216-228, doi:10.1038/s41568-023-00656-5.
79. Guimarães, C.F.; Gasperini, L.; Marques, A.P.; Reis, R.L. The stiffness of living tissues and its implications for tissue engineering. *Nature Reviews Materials* **2020**, *5*, 351-370, doi:10.1038/s41578-019-0169-1.
80. Hawley, J.R.; Kalra, P.; Mo, X.; Raterman, B.; Yee, L.D.; Kolipaka, A. Quantification of breast stiffness using MR elastography at 3 Tesla with a soft sternal driver: A reproducibility study. *Journal of magnetic resonance imaging* **2017**, *45*, 1379-1384.
81. Budday, S.; Ovaert, T.C.; Holzapfel, G.A.; Steinmann, P.; Kuhl, E. Fifty Shades of Brain: A Review on the Mechanical Testing and Modeling of Brain Tissue. *Archives of Computational Methods in Engineering* **2020**, *27*, 1187-1230, doi:10.1007/s11831-019-09352-w.
82. Kamar, F.G.; Posner, J.B. Brain metastases. *Semin Neurol* **2010**, *30*, 217-235, doi:10.1055/s-0030-1255225.
83. Darlix, A.; Louvel, G.; Fraisse, J.; Jacot, W.; Brain, E.; Debled, M.; Mouret-Reynier, M.A.; Goncalves, A.; Dalenc, F.; Delaloge, S.; et al. Impact of breast cancer molecular subtypes on the incidence, kinetics and prognosis of central nervous system metastases in a large multicentre real-life cohort. *Br J Cancer* **2019**, *121*, 991-1000, doi:10.1038/s41416-019-0619-y.
84. Witzel, I.; Oliveira-Ferrer, L.; Pantel, K.; Müller, V.; Wikman, H. Breast cancer brain metastases: biology and new clinical perspectives. *Breast Cancer Res* **2016**, *18*, 8, doi:10.1186/s13058-015-0665-1.
85. Goldberg, S.B.; Gettinger, S.N.; Mahajan, A.; Chiang, A.C.; Herbst, R.S.; Sznol, M.; Tsiouris, A.J.; Cohen, J.; Vortmeyer, A.; Jilaveanu, L. Pembrolizumab for patients with melanoma or non-small-cell lung cancer and untreated brain metastases: early analysis of a non-randomised, open-label, phase 2 trial. *The lancet oncology* **2016**, *17*, 976-983.
86. Parakh, S.; Park, J.J.; Mendis, S.; Rai, R.; Xu, W.; Lo, S.; Drummond, M.; Rowe, C.; Wong, A.; McArthur, G. Efficacy of anti-PD-1 therapy in patients with melanoma brain metastases. *British journal of cancer* **2017**, *116*, 1558-1563.
87. Tawbi, H.A.; Forsyth, P.A.; Algazi, A.; Hamid, O.; Hodi, F.S.; Moschos, S.J.; Khushalani, N.I.; Lewis, K.; Lao, C.D.; Postow, M.A. Combined nivolumab and ipilimumab in melanoma metastatic to the brain. *New England Journal of Medicine* **2018**, *379*, 722-730.

88. Furtado, D.; Björnmalm, M.; Ayton, S.; Bush, A.I.; Kempe, K.; Caruso, F. Overcoming the blood–brain barrier: the role of nanomaterials in treating neurological diseases. *Advanced materials* **2018**, *30*, 1801362.
89. Zhang, T.-T.; Li, W.; Meng, G.; Wang, P.; Liao, W. Strategies for transporting nanoparticles across the blood–brain barrier. *Biomaterials science* **2016**, *4*, 219-229.
90. Sweeney, M.D.; Zhao, Z.; Montagne, A.; Nelson, A.R.; Zlokovic, B.V. Blood-brain barrier: from physiology to disease and back. *Physiological reviews* **2018**.
91. Knowland, D.; Arac, A.; Sekiguchi, K.J.; Hsu, M.; Lutz, S.E.; Perrino, J.; Steinberg, G.K.; Barres, B.A.; Nimmerjahn, A.; Agalliu, D. Stepwise recruitment of transcellular and paracellular pathways underlies blood-brain barrier breakdown in stroke. *Neuron* **2014**, *82*, 603-617.
92. Han, L.; Jiang, C. Evolution of blood–brain barrier in brain diseases and related systemic nanoscale brain-targeting drug delivery strategies. *Acta Pharmaceutica Sinica B* **2021**, *11*, 2306-2325, doi:https://doi.org/10.1016/j.apsb.2020.11.023.
93. Wells, R.G. Tissue mechanics and fibrosis. *Biochim Biophys Acta* **2013**, *1832*, 884-890, doi:10.1016/j.bbadis.2013.02.007.
94. Jensen, G.; Holloway, J.L.; Stabenfeldt, S.E. Hyaluronic Acid Biomaterials for Central Nervous System Regenerative Medicine. *Cells* **2020**, *9*, doi:10.3390/cells9092113.
95. Lau, L.W.; Cua, R.; Keough, M.B.; Haylock-Jacobs, S.; Yong, V.W. Pathophysiology of the brain extracellular matrix: a new target for remyelination. *Nature Reviews Neuroscience* **2013**, *14*, 722-729.
96. Nevalainen, T.; Autio, A.; Hurme, M. Composition of the infiltrating immune cells in the brain of healthy individuals: effect of aging. *Immunity & Ageing* **2022**, *19*, 45, doi:10.1186/s12979-022-00302-y.
97. Wu, S.Y.; Watabe, K. The roles of microglia/macrophages in tumor progression of brain cancer and metastatic disease. *Front Biosci (Landmark Ed)* **2017**, *22*, 1805-1829, doi:10.2741/4573.
98. Zhang, B.; Li, X.; Tang, K.; Xin, Y.; Hu, G.; Zheng, Y.; Li, K.; Zhang, C.; Tan, Y. Adhesion to the Brain Endothelium Selects Breast Cancer Cells with Brain Metastasis Potential. *International Journal of Molecular Sciences* **2023**, *24*, 7087.
99. Wu, K.; Fukuda, K.; Xing, F.; Zhang, Y.; Sharma, S.; Liu, Y.; Chan, M.D.; Zhou, X.; Qasem, S.A.; Pochampally, R.; et al. Roles of the Cyclooxygenase 2 Matrix Metalloproteinase 1 Pathway in Brain Metastasis of Breast Cancer *. *Journal of Biological Chemistry* **2015**, *290*, 9842-9854, doi:10.1074/jbc.M114.602185.
100. Bos, P.D.; Zhang, X.H.F.; Nadal, C.; Shu, W.; Gomis, R.R.; Nguyen, D.X.; Minn, A.J.; van de Vijver, M.J.; Gerald, W.L.; Foekens, J.A.; et al. Genes that mediate breast cancer metastasis to the brain. *Nature* **2009**, *459*, 1005-1009, doi:10.1038/nature08021.
101. Fares, J.; Kanojia, D.; Rashidi, A.; Ulasov, I.; Lesniak, M.S. Genes that Mediate Metastasis across the Blood–Brain Barrier. *Trends in Cancer* **2020**, *6*, 660-676, doi:10.1016/j.trecan.2020.04.007.
102. Brastianos, P.K.; Carter, S.L.; Santagata, S.; Cahill, D.P.; Taylor-Weiner, A.; Jones, R.T.; Van Allen, E.M.; Lawrence, M.S.; Horowitz, P.M.; Cibulskis, K. Genomic characterization of brain metastases reveals branched evolution and potential

therapeutic targets. *Cancer discovery* **2015**, *5*, 1164-1177.
103. Blazquez, R.; Wlochowitz, D.; Wolff, A.; Seitz, S.; Wachter, A.; Perera-Bel, J.; Bleckmann, A.; Beißbarth, T.; Salinas, G.; Riemenschneider, M.J.; et al. PI3K: A master regulator of brain metastasis-promoting macrophages/microglia. *Glia* **2018**, *66*, 2438-2455, doi:https://doi.org/10.1002/glia.23485.
104. Levina, A.; Fleming, K.D.; Burke, J.E.; Leonard, T.A. Activation of the essential kinase PDK1 by phosphoinositide-driven trans-autophosphorylation. *Nature Communications* **2022**, *13*, 1874, doi:10.1038/s41467-022-29368-4.
105. Hoxhaj, G.; Manning, B.D. The PI3K–AKT network at the interface of oncogenic signalling and cancer metabolism. *Nature Reviews Cancer* **2020**, *20*, 74-88, doi:10.1038/s41568-019-0216-7.
106. Engelman, J.A.; Luo, J.; Cantley, L.C. The evolution of phosphatidylinositol 3-kinases as regulators of growth and metabolism. *Nat Rev Genet* **2006**, *7*, 606-619, doi:10.1038/nrg1879.
107. Mao, Y.; Xi, L.; Li, Q.; Cai, Z.; Lai, Y.; Zhang, X.; Yu, C. Regulation of cell apoptosis and proliferation in pancreatic cancer through PI3K/Akt pathway via Polo-like kinase 1. *Oncol Rep* **2016**, *36*, 49-56, doi:10.3892/or.2016.4820.
108. Xia, C.; Meng, Q.; Cao, Z.; Shi, X.; Jiang, B.H. Regulation of angiogenesis and tumor growth by p110 alpha and AKT1 via VEGF expression. *J Cell Physiol* **2006**, *209*, 56-66, doi:10.1002/jcp.20707.
109. Xue, G.; Restuccia, D.F.; Lan, Q.; Hynx, D.; Dirnhofer, S.; Hess, D.; Rüegg, C.; Hemmings, B.A. Akt/PKB-mediated phosphorylation of Twist1 promotes tumor metastasis via mediating cross-talk between PI3K/Akt and TGF-β signaling axes. *Cancer Discov* **2012**, *2*, 248-259, doi:10.1158/2159-8290.Cd-11-0270.
110. Tehranian, C.; Fankhauser, L.; Harter, P.N.; Ratcliffe, C.D.H.; Zeiner, P.S.; Messmer, J.M.; Hoffmann, D.C.; Frey, K.; Westphal, D.; Ronellenfitsch, M.W.; et al. The PI3K/Akt/mTOR pathway as a preventive target in melanoma brain metastasis. *Neuro Oncol* **2022**, *24*, 213-225, doi:10.1093/neuonc/noab159.
111. Ji, M.; Wang, D.; Lin, S.; Wang, C.; Li, L.; Zhang, Z.; Jin, J.; Wu, D.; Dong, Y.; Xu, H.; et al. A novel PI3K inhibitor XH30 suppresses orthotopic glioblastoma and brain metastasis in mice models. *Acta Pharmaceutica Sinica B* **2022**, *12*, 774-786, doi:https://doi.org/10.1016/j.apsb.2021.05.019.
112. Shiovitz, S.; Korde, L.A. Genetics of breast cancer: a topic in evolution. *Ann Oncol* **2015**, *26*, 1291-1299, doi:10.1093/annonc/mdv022.
113. Zhang, S.; Xiao, X.; Yi, Y.; Wang, X.; Zhu, L.; Shen, Y.; Lin, D.; Wu, C. Tumor initiation and early tumorigenesis: molecular mechanisms and interventional targets. *Signal Transduction and Targeted Therapy* **2024**, *9*, 149, doi:10.1038/s41392-024-01848-7.
114. Gamble, L.A.; McClelland, P.H.; Teke, M.E.; Samaranayake, S.G.; Juneau, P.; Famiglietti, A.L.; Blakely, A.M.; Redd, B.; Davis, J.L. Defining features of hereditary lobular breast cancer due to CDH1 with magnetic resonance imaging and tumor characteristics. *npj Breast Cancer* **2023**, *9*, 77, doi:10.1038/s41523-023-00585-4.
115. Narod, S.A. BRCA mutations in the management of breast cancer: the state of the art.

Nature Reviews Clinical Oncology **2010**, *7*, 702-707, doi:10.1038/nrclinonc.2010.166.
116. Kurose, K.; Gilley, K.; Matsumoto, S.; Watson, P.H.; Zhou, X.-P.; Eng, C. Frequent somatic mutations in PTEN and TP53 are mutually exclusive in the stroma of breast carcinomas. *Nature Genetics* **2002**, *32*, 355-357, doi:10.1038/ng1013.
117. Lynch, E.D.; Ostermeyer, E.A.; Lee, M.K.; Arena, J.F.; Ji, H.; Dann, J.; Swisshelm, K.; Suchard, D.; MacLeod, P.M.; Kvinnsland, S.; et al. Inherited Mutations in PTEN That Are Associated with Breast Cancer, Cowden Disease, and Juvenile Polyposis. *The American Journal of Human Genetics* **1997**, *61*, 1254-1260, doi:10.1086/301639.
118. Lim, W.; Olschwang, S.; Keller, J.J.; Westerman, A.M.; Menko, F.H.; Boardman, L.A.; Scott, R.J.; Trimbath, J.; Giardiello, F.M.; Gruber, S.B.; et al. Relative frequency and morphology of cancers in STK11 mutation carriers1 1The authors are grateful to the patients and clinicians who participated in this study. *Gastroenterology* **2004**, *126*, 1788-1794, doi:https://doi.org/10.1053/j.gastro.2004.03.014.
119. Mosele, F.; Stefanovska, B.; Lusque, A.; Tran Dien, A.; Garberis, I.; Droin, N.; Le Tourneau, C.; Sablin, M.P.; Lacroix, L.; Enrico, D.; et al. Outcome and molecular landscape of patients with PIK3CA-mutated metastatic breast cancer. *Annals of Oncology* **2020**, *31*, 377-386, doi:https://doi.org/10.1016/j.annonc.2019.11.006.
120. Novikov, N.M.; Zolotaryova, S.Y.; Gautreau, A.M.; Denisov, E.V. Mutational drivers of cancer cell migration and invasion. *Br J Cancer* **2021**, *124*, 102-114, doi:10.1038/s41416-020-01149-0.
121. Samuels, Y.; Diaz, L.A.; Schmidt-Kittler, O.; Cummins, J.M.; DeLong, L.; Cheong, I.; Rago, C.; Huso, D.L.; Lengauer, C.; Kinzler, K.W.; et al. Mutant PIK3CA promotes cell growth and invasion of human cancer cells. *Cancer Cell* **2005**, *7*, 561-573, doi:https://doi.org/10.1016/j.ccr.2005.05.014.
122. Davis, N.M.; Sokolosky, M.; Stadelman, K.; Abrams, S.L.; Libra, M.; Candido, S.; Nicoletti, F.; Polesel, J.; Maestro, R.; D'Assoro, A.; et al. Deregulation of the EGFR/PI3K/PTEN/Akt/mTORC1 pathway in breast cancer: possibilities for therapeutic intervention. *Oncotarget* **2014**, *5*, 4603-4650, doi:10.18632/oncotarget.2209.
123. Koboldt, D.C.; Fulton, R.S.; McLellan, M.D.; Schmidt, H.; Kalicki-Veizer, J.; McMichael, J.F.; Fulton, L.L.; Dooling, D.J.; Ding, L.; Mardis, E.R. TCGA-Network, Comprehensive molecular portraits of human breast tumours. *Nature* **2012**, *490*, 61-70.
124. Li, J.; Yen, C.; Liaw, D.; Podsypanina, K.; Bose, S.; Wang, S.I.; Puc, J.; Miliaresis, C.; Rodgers, L.; McCombie, R. PTEN, a putative protein tyrosine phosphatase gene mutated in human brain, breast, and prostate cancer. *science* **1997**, *275*, 1943-1947.
125. Ungerleider, N.A.; Rao, S.G.; Shahbandi, A.; Yee, D.; Niu, T.; Frey, W.D.; Jackson, J.G. Breast cancer survival predicted by TP53 mutation status differs markedly depending on treatment. *Breast Cancer Research* **2018**, *20*, 1-8.
126. Fond, A.M.; Ravichandran, K.S. Clearance of Dying Cells by Phagocytes: Mechanisms and Implications for Disease Pathogenesis. In *Apoptosis in Cancer Pathogenesis and Anti-cancer Therapy: New Perspectives and Opportunities*, Gregory, C.D., Ed.; Springer International Publishing: Cham, 2016; pp. 25-49.
127. Slattum, G.; McGee, K.M.; Rosenblatt, J. P115 RhoGEF and microtubules decide the

direction apoptotic cells extrude from an epithelium. *Journal of Cell Biology* **2009**, *186*, 693-702, doi:10.1083/jcb.200903079.

128. Chan, C.W.; Housseau, F. The 'kiss of death' by dendritic cells to cancer cells. *Cell Death & Differentiation* **2008**, *15*, 58-69, doi:10.1038/sj.cdd.4402235.
129. Dunn, G.P.; Bruce, A.T.; Ikeda, H.; Old, L.J.; Schreiber, R.D. Cancer immunoediting: from immunosurveillance to tumor escape. *Nature Immunology* **2002**, *3*, 991-998, doi:10.1038/ni1102-991.
130. Mantovani, A.; Marchesi, F.; Malesci, A.; Laghi, L.; Allavena, P. Tumour-associated macrophages as treatment targets in oncology. *Nature Reviews Clinical Oncology* **2017**, *14*, 399-416, doi:10.1038/nrclinonc.2016.217.
131. Matsumura, Y. Barriers to antibody therapy in solid tumors, and their solutions. *Cancer Sci* **2021**, *112*, 2939-2947, doi:10.1111/cas.14983.
132. Yeap, W.H.; Wong, K.L.; Shimasaki, N.; Teo, E.C.Y.; Quek, J.K.S.; Yong, H.X.; Diong, C.P.; Bertoletti, A.; Linn, Y.C.; Wong, S.C. CD16 is indispensable for antibody-dependent cellular cytotoxicity by human monocytes. *Scientific Reports* **2016**, *6*, 34310, doi:10.1038/srep34310.
133. Cornel, A.M.; Mimpen, I.L.; Nierkens, S. MHC Class I Downregulation in Cancer: Underlying Mechanisms and Potential Targets for Cancer Immunotherapy. *Cancers (Basel)* **2020**, *12*, doi:10.3390/cancers12071760.
134. Sari, G.; Rock, K.L. Tumor immune evasion through loss of MHC class-I antigen presentation. *Current Opinion in Immunology* **2023**, *83*, 102329, doi:https://doi.org/10.1016/j.coi.2023.102329.
135. Zaretsky, J.M.; Garcia-Diaz, A.; Shin, D.S.; Escuin-Ordinas, H.; Hugo, W.; Hu-Lieskovan, S.; Torrejon, D.Y.; Abril-Rodriguez, G.; Sandoval, S.; Barthly, L. Mutations associated with acquired resistance to PD-1 blockade in melanoma. *New England Journal of Medicine* **2016**, *375*, 819-829.
136. Wang, J.; Lu, Q.; Chen, X.; Aifantis, I. Targeting MHC-I inhibitory pathways for cancer immunotherapy. *Trends in Immunology* **2024**, *45*, 177-187, doi:10.1016/j.it.2024.01.009.
137. Romee, R.; Foley, B.; Lenvik, T.; Wang, Y.; Zhang, B.; Ankarlo, D.; Luo, X.; Cooley, S.; Verneris, M.; Walcheck, B.; et al. NK cell CD16 surface expression and function is regulated by a disintegrin and metalloprotease-17 (ADAM17). *Blood* **2013**, *121*, 3599-3608, doi:10.1182/blood-2012-04-425397.
138. Wu, S.-Y.; Fu, T.; Jiang, Y.-Z.; Shao, Z.-M. Natural killer cells in cancer biology and therapy. *Molecular Cancer* **2020**, *19*, 120, doi:10.1186/s12943-020-01238-x.
139. Zhang, Y.; Wallace, D.L.; De Lara, C.M.; Ghattas, H.; Asquith, B.; Worth, A.; Griffin, G.E.; Taylor, G.P.; Tough, D.F.; Beverley, P.C. In vivo kinetics of human natural killer cells: the effects of ageing and acute and chronic viral infection. *Immunology* **2007**, *121*, 258-265.
140. Chiossone, L.; Dumas, P.-Y.; Vienne, M.; Vivier, E. Natural killer cells and other innate lymphoid cells in cancer. *Nature Reviews Immunology* **2018**, *18*, 671-688, doi:10.1038/s41577-018-0061-z.
141. Vivier, E.; Artis, D.; Colonna, M.; Diefenbach, A.; Di Santo, J.P.; Eberl, G.; Koyasu,

S.; Locksley, R.M.; McKenzie, A.N.J.; Mebius, R.E.; et al. Innate Lymphoid Cells: 10 Years On. *Cell* **2018**, *174*, 1054-1066, doi:10.1016/j.cell.2018.07.017.

142. Huntington, N.D.; Cursons, J.; Rautela, J. The cancer–natural killer cell immunity cycle. *Nature Reviews Cancer* **2020**, *20*, 437-454, doi:10.1038/s41568-020-0272-z.
143. Wu, S.Y.; Fu, T.; Jiang, Y.Z.; Shao, Z.M. Natural killer cells in cancer biology and therapy. *Mol Cancer* **2020**, *19*, 120, doi:10.1186/s12943-020-01238-x.
144. Caligiuri, M.A. Human natural killer cells. *Blood, The Journal of the American Society of Hematology* **2008**, *112*, 461-469.
145. Moretta, L. Dissecting CD56dim human NK cells. *Blood* **2010**, *116*, 3689-3691, doi:10.1182/blood-2010-09-303057.
146. Freud, A.G.; Caligiuri, M.A. Human natural killer cell development. *Immunological reviews* **2006**, *214*, 56-72.
147. Romagnani, C.; Juelke, K.; Falco, M.; Morandi, B.; D'Agostino, A.; Costa, R.; Ratto, G.; Forte, G.; Carrega, P.; Lui, G. CD56brightCD16− killer Ig-like receptor− NK cells display longer telomeres and acquire features of CD56dim NK cells upon activation. *The Journal of Immunology* **2007**, *178*, 4947-4955.
148. Nersesian, S.; Schwartz, S.L.; Grantham, S.R.; MacLean, L.K.; Lee, S.N.; Pugh-Toole, M.; Boudreau, J.E. NK cell infiltration is associated with improved overall survival in solid cancers: A systematic review and meta-analysis. *Translational Oncology* **2021**, *14*, 100930, doi:https://doi.org/10.1016/j.tranon.2020.100930.
149. Wang, W.; Liu, Y.; He, Z.; Li, L.; Liu, S.; Jiang, M.; Zhao, B.; Deng, M.; Wang, W.; Mi, X.; et al. Breakthrough of solid tumor treatment: CAR-NK immunotherapy. *Cell Death Discovery* **2024**, *10*, 40, doi:10.1038/s41420-024-01815-9.
150. Page, A.; Chuvin, N.; Valladeau-Guilemond, J.; Depil, S. Development of NK cell-based cancer immunotherapies through receptor engineering. *Cellular & Molecular Immunology* **2024**, *21*, 315-331, doi:10.1038/s41423-024-01145-x.
151. Carrillo-Bustamante, P.; Keşmir, C.; de Boer, R.J. The evolution of natural killer cell receptors. *Immunogenetics* **2016**, *68*, 3-18, doi:10.1007/s00251-015-0869-7.
152. Kumar, S. Natural killer cell cytotoxicity and its regulation by inhibitory receptors. *Immunology* **2018**, *154*, 383-393, doi:10.1111/imm.12921.
153. Long, E.O.; Kim, H.S.; Liu, D.; Peterson, M.E.; Rajagopalan, S. Controlling natural killer cell responses: integration of signals for activation and inhibition. *Annu Rev Immunol* **2013**, *31*, 227-258, doi:10.1146/annurev-immunol-020711-075005.
154. Bauer, S.; Groh, V.; Wu, J.; Steinle, A.; Phillips, J.H.; Lanier, L.L.; Spies, T. Activation of NK cells and T cells by NKG2D, a receptor for stress-inducible MICA. *Science* **1999**, *285*, 727-729, doi:10.1126/science.285.5428.727.
155. Jiang, P.; Jing, S.; Sheng, G.; Jia, F. The basic biology of NK cells and its application in tumor immunotherapy. *Front Immunol* **2024**, *15*, 1420205, doi:10.3389/fimmu.2024.1420205.
156. Oyer, J.L.; Gitto, S.B.; Altomare, D.A.; Copik, A.J. PD-L1 blockade enhances anti-tumor efficacy of NK cells. *Oncoimmunology* **2018**, *7*, e1509819, doi:10.1080/2162402x.2018.1509819.
157. Mortara, L.; Balza, E.; Sassi, F.; Castellani, P.; Carnemolla, B.; De Lerma Barbaro, A.;

Fossati, S.; Tosi, G.; Accolla, R.S.; Borsi, L. Therapy-induced antitumor vaccination by targeting tumor necrosis factor-α to tumor vessels in combination with melphalan. *European journal of immunology* **2007**, *37*, 3381-3392.

158. Schneider, W.M.; Chevillotte, M.D.; Rice, C.M. Interferon-stimulated genes: a complex web of host defenses. *Annu Rev Immunol* **2014**, *32*, 513-545, doi:10.1146/annurev-immunol-032713-120231.
159. Gocher, A.M.; Workman, C.J.; Vignali, D.A.A. Interferon-γ: teammate or opponent in the tumour microenvironment? *Nature Reviews Immunology* **2022**, *22*, 158-172, doi:10.1038/s41577-021-00566-3.
160. Park, S.-M.; Schickel, R.; Peter, M.E. Nonapoptotic functions of FADD-binding death receptors and their signaling molecules. *Current Opinion in Cell Biology* **2005**, *17*, 610-616, doi:https://doi.org/10.1016/j.ceb.2005.09.010.
161. Sheard, M.A.; Asgharzadeh, S.; Liu, Y.; Lin, T.Y.; Wu, H.W.; Ji, L.; Groshen, S.; Lee, D.A.; Seeger, R.C. Membrane-bound TRAIL supplements natural killer cell cytotoxicity against neuroblastoma cells. *J Immunother* **2013**, *36*, 319-329, doi:10.1097/CJI.0b013e31829b4493.
162. Coënon, L.; Geindreau, M.; Ghiringhelli, F.; Villalba, M.; Bruchard, M. Natural Killer cells at the frontline in the fight against cancer. *Cell Death & Disease* **2024**, *15*, 614, doi:10.1038/s41419-024-06976-0.
163. Shi, F.-D.; Ljunggren, H.-G.; La Cava, A.; Van Kaer, L. Organ-specific features of natural killer cells. *Nature Reviews Immunology* **2011**, *11*, 658-671, doi:10.1038/nri3065.
164. Huse, M. Mechanical forces in the immune system. *Nat Rev Immunol* **2017**, *17*, 679-690, doi:10.1038/nri.2017.74.
165. Sohrabi, A.; Lefebvre, A.; Harrison, M.J.; Condro, M.C.; Sanazzaro, T.M.; Safarians, G.; Solomon, I.; Bastola, S.; Kordbacheh, S.; Toh, N.; et al. Microenvironmental stiffness induces metabolic reprogramming in glioblastoma. *Cell Rep* **2023**, *42*, 113175, doi:10.1016/j.celrep.2023.113175.
166. Wong, D.C.P.; Ding, J.L. The mechanobiology of NK cells- 'Forcing NK to Sense' target cells. *Biochimica et Biophysica Acta (BBA) - Reviews on Cancer* **2023**, *1878*, 188860, doi:https://doi.org/10.1016/j.bbcan.2023.188860.
167. Billadeau, D.D.; Brumbaugh, K.M.; Dick, C.J.; Schoon, R.A.; Bustelo, X.R.; Leibson, P.J. The Vav-Rac1 pathway in cytotoxic lymphocytes regulates the generation of cell-mediated killing. *J Exp Med* **1998**, *188*, 549-559, doi:10.1084/jem.188.3.549.
168. Mentlik, A.N.; Sanborn, K.B.; Holzbaur, E.L.; Orange, J.S. Rapid lytic granule convergence to the MTOC in natural killer cells is dependent on dynein but not cytolytic commitment. *Mol Biol Cell* **2010**, *21*, 2241-2256, doi:10.1091/mbc.e09-11-0930.
169. Le Saux, G.; Bar-Hanin, N.; Edri, A.; Hadad, U.; Porgador, A.; Schvartzman, M. Nanoscale Mechanosensing of Natural Killer Cells is Revealed by Antigen-Functionalized Nanowires. *Advanced Materials* **2019**, *31*, 1805954, doi:10.1002/adma.201805954.
170. Matalon, O.; Ben-Shmuel, A.; Kivelevitz, J.; Sabag, B.; Fried, S.; Joseph, N.; Noy, E.;

Biber, G.; Barda-Saad, M. Actin retrograde flow controls natural killer cell response by regulating the conformation state of SHP-1. *Embo j* **2018**, *37*, doi:10.15252/embj.201696264.

171. Sanchez, E.E.; Tello-Lafoz, M.; Guo, A.J.; de Jesus, M.; Elbanna, Y.A.; Winer, B.Y.; Budhu, S.; Chan, E.; Rosiek, E.; Kondo, T.; et al. Apoptotic contraction drives target cell release by cytotoxic T cells. *Nat Immunol* **2023**, *24*, 1434-1442, doi:10.1038/s41590-023-01572-4.
172. Wong, D.C.P.; Xia, Z.; Shao, N.; Yow, I.; Thivakar, T.; Yeo, J.Y.; Salazar, A.M.; Liou, Y.C.; Low, B.C.; Ding, J.L. Hiltonol, a dsRNA Mimic, Promotes NK Cell Anticancer Cytotoxicity Through TAZ Cytoplasmic Sequestration. *Advanced Therapeutics* **2023**, *6*, doi:10.1002/adtp.202300016.
173. Wong, D.C.P.; Lee, E.H.C.; Er, J.; Yow, I.; Koean, R.A.G.; Ang, O.; Xiao, J.; Low, B.C.; Ding, J.L. Lung Cancer Induces NK Cell Contractility and Cytotoxicity Through Transcription Factor Nuclear Localization. *Frontiers in Cell and Developmental Biology* **2022**, *10*, doi:10.3389/fcell.2022.871326.
174. Melder, R.J.; Kristensen, C.A.; Munn, L.L.; Jain, R.K. Modulation of A-NK cell rigidity: In vitro characterization and in vivo implications for cell delivery. *Biorheology* **2001**, *38*, 151-159.
175. Melder, R.J.; Jain, R.K. Kinetics of interleukin-2 induced changes in rigidity of human natural killer cells. *Cell biophysics* **1992**, *20*, 161-176.
176. Mordechay, L.; Le Saux, G.; Edri, A.; Hadad, U.; Porgador, A.; Schvartzman, M. Mechanical Regulation of the Cytotoxic Activity of Natural Killer Cells. *ACS Biomaterials Science & Engineering* **2021**, *7*, 122-132, doi:10.1021/acsbiomaterials.0c01121.
177. Friedman, D.; Simmonds, P.; Hale, A.; Bere, L.; Hodson, N.W.; White, M.R.H.; Davis, D.M. Natural killer cell immune synapse formation and cytotoxicity are controlled by tension of the target interface. *Journal of Cell Science* **2021**, *134*, jcs.258570, doi:10.1242/jcs.258570.
178. Xu, W.; Mezencev, R.; Kim, B.; Wang, L.; McDonald, J.; Sulchek, T. Cell stiffness is a biomarker of the metastatic potential of ovarian cancer cells. **2012**.
179. Hayashi, K.; Iwata, M. Stiffness of cancer cells measured with an AFM indentation method. *Journal of the mechanical behavior of biomedical materials* **2015**, *49*, 105-111.
180. Rianna, C.; Radmacher, M.; Kumar, S. Direct evidence that tumor cells soften when navigating confined spaces. *Molecular biology of the cell* **2020**, *31*, 1726-1734.
181. Zhou, Y.; Wang, D.; Zhou, L.; Zhou, N.; Wang, Z.; Chen, J.; Pang, R.; Fu, H.; Huang, Q.; Dong, F.; et al. Cell softness renders cytotoxic T lymphocytes and T leukemic cells resistant to perforin-mediated killing. *Nature Communications* **2024**, *15*, 1405, doi:10.1038/s41467-024-45750-w.
182. Liu, Y.; Zhang, T.; Zhang, H.; Li, J.; Zhou, N.; Fiskesund, R.; Chen, J.; Lv, J.; Ma, J.; Zhang, H.; et al. Cell Softness Prevents Cytolytic T-cell Killing of Tumor-Repopulating Cells. *Cancer Research* **2021**, *81*, 476-488, doi:10.1158/0008-5472.Can-20-2569.
183. Lei, K.; Kurum, A.; Kaynak, M.; Bonati, L.; Han, Y.; Cencen, V.; Gao, M.; Xie, Y.-Q.;

Guo, Y.; Hannebelle, M.T.M.; et al. Cancer-cell stiffening via cholesterol depletion enhances adoptive T-cell immunotherapy. *Nature Biomedical Engineering* **2021**, *5*, 1411-1425, doi:10.1038/s41551-021-00826-6.

184. Di, X.; Gao, X.; Peng, L.; Ai, J.; Jin, X.; Qi, S.; Li, H.; Wang, K.; Luo, D. Cellular mechanotransduction in health and diseases: from molecular mechanism to therapeutic targets. *Signal Transduction and Targeted Therapy* **2023**, *8*, 282, doi:10.1038/s41392-023-01501-9.
185. Fan, J.; Shi, J.; Zhang, Y.; Liu, J.; An, C.; Zhu, H.; Wu, P.; Hu, W.; Qin, R.; Yao, D.; et al. NKG2D discriminates diverse ligands through selectively mechano-regulated ligand conformational changes. *The EMBO Journal* **2022**, *41*, e107739, doi:https://doi.org/10.15252/embj.2021107739.
186. Huang, R.; Rofstad, E.K. Integrins as therapeutic targets in the organ-specific metastasis of human malignant melanoma. *J Exp Clin Cancer Res* **2018**, *37*, 92, doi:10.1186/s13046-018-0763-x.
187. Warren, J.S.A.; Xiao, Y.; Lamar, J.M. YAP/TAZ Activation as a Target for Treating Metastatic Cancer. *Cancers (Basel)* **2018**, *10*, doi:10.3390/cancers10040115.
188. Mohammadi, H.; Sahai, E. Mechanisms and impact of altered tumour mechanics. *Nature Cell Biology* **2018**, *20*, 766-774, doi:10.1038/s41556-018-0131-2.
189. Lu, P.; Takai, K.; Weaver, V.M.; Werb, Z. Extracellular matrix degradation and remodeling in development and disease. *Cold Spring Harbor perspectives in biology* **2011**, *3*, a005058.
190. Xiao, Q.; Ge, G. Lysyl Oxidase, Extracellular Matrix Remodeling and Cancer Metastasis. *Cancer Microenvironment* **2012**, *5*, 261-273, doi:10.1007/s12307-012-0105-z.
191. Butcher, D.T.; Alliston, T.; Weaver, V.M. A tense situation: forcing tumour progression. *Nature Reviews Cancer* **2009**, *9*, 108-122.
192. Gaggioli, C.; Hooper, S.; Hidalgo-Carcedo, C.; Grosse, R.; Marshall, J.F.; Harrington, K.; Sahai, E. Fibroblast-led collective invasion of carcinoma cells with differing roles for RhoGTPases in leading and following cells. *Nature Cell Biology* **2007**, *9*, 1392-1400, doi:10.1038/ncb1658.
193. Rice, A.J.; Cortes, E.; Lachowski, D.; Cheung, B.C.H.; Karim, S.A.; Morton, J.P.; del Río Hernández, A. Matrix stiffness induces epithelial–mesenchymal transition and promotes chemoresistance in pancreatic cancer cells. *Oncogenesis* **2017**, *6*, e352-e352, doi:10.1038/oncsis.2017.54.
194. Horta, C.A.; Doan, K.; Yang, J. Mechanotransduction pathways in regulating epithelial-mesenchymal plasticity. *Current Opinion in Cell Biology* **2023**, *85*, 102245, doi:https://doi.org/10.1016/j.ceb.2023.102245.
195. Lomakin, A.J.; Cattin, C.J.; Cuvelier, D.; Alraies, Z.; Molina, M.; Nader, G.P.F.; Srivastava, N.; Sáez, P.J.; Garcia-Arcos, J.M.; Zhitnyak, I.Y.; et al. The nucleus acts as a ruler tailoring cell responses to spatial constraints. *Science* **2020**, *370*, doi:10.1126/science.aba2894.
196. Ju, R.J.; Falconer, A.D.; Schmidt, C.J.; Enriquez Martinez, M.A.; Dean, K.M.; Fiolka, R.P.; Sester, D.P.; Nobis, M.; Timpson, P.; Lomakin, A.J.; et al. Compression-dependent

microtubule reinforcement enables cells to navigate confined environments. *Nature Cell Biology* **2024**, *26*, 1520-1534, doi:10.1038/s41556-024-01476-x.

197. Thiam, H.-R.; Vargas, P.; Carpi, N.; Crespo, C.L.; Raab, M.; Terriac, E.; King, M.C.; Jacobelli, J.; Alberts, A.S.; Stradal, T.; et al. Perinuclear Arp2/3-driven actin polymerization enables nuclear deformation to facilitate cell migration through complex environments. *Nature Communications* **2016**, *7*, 10997, doi:10.1038/ncomms10997.
198. Papaioannou, T.G.; Stefanadis, C. Vascular wall shear stress: basic principles and methods. *Hellenic J Cardiol* **2005**, *46*, 9-15.
199. Moose, D.L.; Krog, B.L.; Kim, T.-H.; Zhao, L.; Williams-Perez, S.; Burke, G.; Rhodes, L.; Vanneste, M.; Breheny, P.; Milhem, M.; et al. Cancer Cells Resist Mechanical Destruction in Circulation via RhoA/Actomyosin-Dependent Mechano-Adaptation. *Cell Reports* **2020**, *30*, 3864-3874.e3866, doi:10.1016/j.celrep.2020.02.080.
200. Ma, S.; Fu, A.; Chiew, G.G.; Luo, K.Q. Hemodynamic shear stress stimulates migration and extravasation of tumor cells by elevating cellular oxidative level. *Cancer Lett* **2017**, *388*, 239-248, doi:10.1016/j.canlet.2016.12.001.
201. Mitchell, M.J.; King, M.R. Fluid shear stress sensitizes cancer cells to receptor-mediated apoptosis via trimeric death receptors. *New journal of physics* **2013**, *15*, 015008.
202. Xu, Z.; Li, K.; Xin, Y.; Tang, K.; Yang, M.; Wang, G.; Tan, Y. Fluid shear stress regulates the survival of circulating tumor cells via nuclear expansion. *Journal of Cell Science* **2022**, *135*, doi:10.1242/jcs.259586.
203. Choi, H.Y.; Yang, G.M.; Dayem, A.A.; Saha, S.K.; Kim, K.; Yoo, Y.; Hong, K.; Kim, J.H.; Yee, C.; Lee, K.M.; et al. Hydrodynamic shear stress promotes epithelial-mesenchymal transition by downregulating ERK and GSK3β activities. *Breast Cancer Res* **2019**, *21*, 6, doi:10.1186/s13058-018-1071-2.
204. Triantafillu, U.L.; Park, S.; Klaassen, N.L.; Raddatz, A.D.; Kim, Y. Fluid shear stress induces cancer stem cell-like phenotype in MCF7 breast cancer cell line without inducing epithelial to mesenchymal transition. *International journal of oncology* **2017**, *50*, 993-1001.
205. Triantafillu, U.L.; Park, S.; Kim, Y. Fluid Shear Stress Induces Drug Resistance to Doxorubicin and Paclitaxel in the Breast Cancer Cell Line MCF7. *Advanced Therapeutics* **2019**, *2*, 1800112, doi:https://doi.org/10.1002/adtp.201800112.
206. Katira, P.; Bonnecaze, R.T.; Zaman, M.H. Modeling the mechanics of cancer: effect of changes in cellular and extra-cellular mechanical properties. *Front Oncol* **2013**, *3*, 145, doi:10.3389/fonc.2013.00145.
207. Fletcher, D.A.; Mullins, R.D. Cell mechanics and the cytoskeleton. *Nature* **2010**, *463*, 485-492, doi:10.1038/nature08908.
208. Janmey, P.A.; McCulloch, C.A. Cell mechanics: integrating cell responses to mechanical stimuli. *Annu. Rev. Biomed. Eng.* **2007**, *9*, 1-34.
209. Lewis, A.H.; Grandl, J. Mechanical sensitivity of Piezo1 ion channels can be tuned by cellular membrane tension. *Elife* **2015**, *4*, e12088.
210. O 'Neil, R.G.; Heller, S. The mechanosensitive nature of TRPV channels. *Pflügers*

Archiv **2005**, *451*, 193-203.
211. Carlson, A.E. Mechanical stimulation activates Drosophila eggs via Trpm channels. *Proceedings of the National Academy of Sciences* **2019**, *116*, 18757-18758, doi:doi:10.1073/pnas.1913150116.
212. Glyakina, A.V.; Galzitskaya, O.V. Bioinformatics Analysis of Actin Molecules: Why Quantity Does Not Translate Into Quality? *Front Genet* **2020**, *11*, 617763, doi:10.3389/fgene.2020.617763.
213. Lodish, H.F. *Molecular cell biology*; Macmillan: 2008.
214. Wegner, A.; Isenberg, G. 12-fold difference between the critical monomer concentrations of the two ends of actin filaments in physiological salt conditions. *Proc Natl Acad Sci U S A* **1983**, *80*, 4922-4925, doi:10.1073/pnas.80.16.4922.
215. Yang, C.; Svitkina, T. Filopodia initiation: focus on the Arp2/3 complex and formins. *Cell Adh Migr* **2011**, *5*, 402-408, doi:10.4161/cam.5.5.16971.
216. Korobova, F.; Svitkina, T. Arp2/3 complex is important for filopodia formation, growth cone motility, and neuritogenesis in neuronal cells. *Mol Biol Cell* **2008**, *19*, 1561-1574, doi:10.1091/mbc.e07-09-0964.
217. Funk, J.; Merino, F.; Venkova, L.; Heydenreich, L.; Kierfeld, J.; Vargas, P.; Raunser, S.; Piel, M.; Bieling, P. Profilin and formin constitute a pacemaker system for robust actin filament growth. *eLife* **2019**, *8*, e50963, doi:10.7554/eLife.50963.
218. Courtemanche, N. Mechanisms of formin-mediated actin assembly and dynamics. *Biophys Rev* **2018**, *10*, 1553-1569, doi:10.1007/s12551-018-0468-6.
219. Gavara, N.; Chadwick, R.S. Relationship between cell stiffness and stress fiber amount, assessed by simultaneous atomic force microscopy and live-cell fluorescence imaging. *Biomechanics and modeling in mechanobiology* **2016**, *15*, 511-523.
220. Kwon, S.; Yang, W.; Moon, D.; Kim, K.S. Comparison of Cancer Cell Elasticity by Cell Type. *J Cancer* **2020**, *11*, 5403-5412, doi:10.7150/jca.45897.
221. Nieto, M.A.; Huang, R.Y.; Jackson, R.A.; Thiery, J.P. EMT: 2016. *Cell* **2016**, *166*, 21-45, doi:10.1016/j.cell.2016.06.028.
222. Lv, J.; Liu, Y.; Cheng, F.; Li, J.; Zhou, Y.; Zhang, T.; Zhou, N.; Li, C.; Wang, Z.; Ma, L.; et al. Cell softness regulates tumorigenicity and stemness of cancer cells. *Embo j* **2021**, *40*, e106123, doi:10.15252/embj.2020106123.
223. Ayscough, K.R.; Stryker, J.; Pokala, N.; Sanders, M.; Crews, P.; Drubin, D.G. High rates of actin filament turnover in budding yeast and roles for actin in establishment and maintenance of cell polarity revealed using the actin inhibitor latrunculin-A. *The Journal of cell biology* **1997**, *137*, 399-416.
224. Fujiwara, I.; Zweifel, M.E.; Courtemanche, N.; Pollard, T.D. Latrunculin A Accelerates Actin Filament Depolymerization in Addition to Sequestering Actin Monomers. *Current Biology* **2018**, *28*, 3183-3192.e3182, doi:10.1016/j.cub.2018.07.082.
225. Bubb, M.R.; Senderowicz, A.M.; Sausville, E.A.; Duncan, K.L.; Korn, E.D. Jasplakinolide, a cytotoxic natural product, induces actin polymerization and competitively inhibits the binding of phalloidin to F-actin. *J Biol Chem* **1994**, *269*, 14869-14871.
226. Bubb, M.R.; Spector, I.; Beyer, B.B.; Fosen, K.M. Effects of jasplakinolide on the

kinetics of actin polymerization. An explanation for certain in vivo observations. *J Biol Chem* **2000**, *275*, 5163-5170, doi:10.1074/jbc.275.7.5163.

227. Bruce Alberts, A.J., Julian Lewis, David Morgan, Martin Raff, Keith Roberts, Peter Walter ; with problems by John Wilson, Tim Hunt. Molecular biology of the cell. **2015**.
228. McLaughlin, S.; Wang, J.; Gambhir, A.; Murray, D. PIP2 and Proteins: Interactions, Organization, and Information Flow. *Annual Review of Biophysics* **2002**, *31*, 151-175, doi:https://doi.org/10.1146/annurev.biophys.31.082901.134259.
229. Hao, J.J.; Liu, Y.; Kruhlak, M.; Debell, K.E.; Rellahan, B.L.; Shaw, S. Phospholipase C-mediated hydrolysis of PIP2 releases ERM proteins from lymphocyte membrane. *J Cell Biol* **2009**, *184*, 451-462, doi:10.1083/jcb.200807047.
230. Fehon, R.G.; McClatchey, A.I.; Bretscher, A. Organizing the cell cortex: the role of ERM proteins. *Nature Reviews Molecular Cell Biology* **2010**, *11*, 276-287, doi:10.1038/nrm2866.
231. Gary, R.; Bretscher, A. Ezrin self-association involves binding of an N-terminal domain to a normally masked C-terminal domain that includes the F-actin binding site. *Mol Biol Cell* **1995**, *6*, 1061-1075, doi:10.1091/mbc.6.8.1061.
232. Fievet, B.T.; Gautreau, A.; Roy, C.; Del Maestro, L.; Mangeat, P.; Louvard, D.; Arpin, M. Phosphoinositide binding and phosphorylation act sequentially in the activation mechanism of ezrin. *J Cell Biol* **2004**, *164*, 653-659, doi:10.1083/jcb.200307032.
233. Yonemura, S.; Matsui, T.; Tsukita, S.; Tsukita, S. Rho-dependent and -independent activation mechanisms of ezrin/radixin/moesin proteins: an essential role for polyphosphoinositides in vivo. *J Cell Sci* **2002**, *115*, 2569-2580, doi:10.1242/jcs.115.12.2569.
234. Belkina, N.V.; Liu, Y.; Hao, J.J.; Karasuyama, H.; Shaw, S. LOK is a major ERM kinase in resting lymphocytes and regulates cytoskeletal rearrangement through ERM phosphorylation. *Proc Natl Acad Sci U S A* **2009**, *106*, 4707-4712, doi:10.1073/pnas.0805963106.
235. Matsui, T.; Maeda, M.; Doi, Y.; Yonemura, S.; Amano, M.; Kaibuchi, K.; Tsukita, S.; Tsukita, S. Rho-kinase phosphorylates COOH-terminal threonines of ezrin/radixin/moesin (ERM) proteins and regulates their head-to-tail association. *J Cell Biol* **1998**, *140*, 647-657, doi:10.1083/jcb.140.3.647.
236. Ng, T.; Parsons, M.; Hughes, W.E.; Monypenny, J.; Zicha, D.; Gautreau, A.; Arpin, M.; Gschmeissner, S.; Verveer, P.J.; Bastiaens, P.I.; et al. Ezrin is a downstream effector of trafficking PKC-integrin complexes involved in the control of cell motility. *Embo j* **2001**, *20*, 2723-2741, doi:10.1093/emboj/20.11.2723.
237. Yang, H.S.; Hinds, P.W. Increased ezrin expression and activation by CDK5 coincident with acquisition of the senescent phenotype. *Mol Cell* **2003**, *11*, 1163-1176, doi:10.1016/s1097-2765(03)00135-7.
238. Ren, L.; Hong, S.H.; Cassavaugh, J.; Osborne, T.; Chou, A.J.; Kim, S.Y.; Gorlick, R.; Hewitt, S.M.; Khanna, C. The actin-cytoskeleton linker protein ezrin is regulated during osteosarcoma metastasis by PKC. *Oncogene* **2009**, *28*, 792-802, doi:10.1038/onc.2008.437.
239. Orian-Rousseau, V.; Morrison, H.; Matzke, A.; Kastilan, T.; Pace, G.; Herrlich, P.;

Ponta, H. Hepatocyte growth factor-induced Ras activation requires ERM proteins linked to both CD44v6 and F-actin. *Molecular biology of the cell* **2007**, *18*, 76-83.

240. Naba, A.; Reverdy, C.; Louvard, D.; Arpin, M. Spatial recruitment and activation of the Fes kinase by ezrin promotes HGF-induced cell scattering. *The EMBO journal* **2008**, *27*, 38-50.
241. Arpin, M.; Chirivino, D.; Naba, A.; Zwaenepoel, I. Emerging role for ERM proteins in cell adhesion and migration. *Cell adhesion & migration* **2011**, *5*, 199-206.
242. Clucas, J.; Valderrama, F. ERM proteins in cancer progression. *Journal of Cell Science* **2014**, *127*, 267-275, doi:10.1242/jcs.133108.
243. Forte, E.; Orsatti, L.; Talamo, F.; Barbato, G.; De Francesco, R.; Tomei, L. Ezrin is a specific and direct target of protein tyrosine phosphatase PRL-3. *Biochimica et Biophysica Acta (BBA)-Molecular Cell Research* **2008**, *1783*, 334-344.
244. Kiss, A.; Erdődi, F.; Lontay, B. Myosin phosphatase: Unexpected functions of a long-known enzyme. *Biochimica et Biophysica Acta (BBA) - Molecular Cell Research* **2019**, *1866*, 2-15, doi:https://doi.org/10.1016/j.bbamcr.2018.07.023.
245. Roberts, R.E.; Martin, M.; Marion, S.; Elumalai, G.L.; Lewis, K.; Hallett, M.B. Ca2+-activated cleavage of ezrin visualised dynamically in living myeloid cells during cell surface area expansion. *Journal of Cell Science* **2020**, *133*, doi:10.1242/jcs.236968.
246. Linde, N.; Casanova-Acebes, M.; Sosa, M.S.; Mortha, A.; Rahman, A.; Farias, E.; Harper, K.; Tardio, E.; Reyes Torres, I.; Jones, J.; et al. Macrophages orchestrate breast cancer early dissemination and metastasis. *Nature Communications* **2018**, *9*, 21, doi:10.1038/s41467-017-02481-5.
247. Wculek, S.K.; Malanchi, I. Neutrophils support lung colonization of metastasis-initiating breast cancer cells. *Nature* **2015**, *528*, 413-417, doi:10.1038/nature16140.
248. DeNardo, D.G.; Barreto, J.B.; Andreu, P.; Vasquez, L.; Tawfik, D.; Kolhatkar, N.; Coussens, L.M. CD4(+) T cells regulate pulmonary metastasis of mammary carcinomas by enhancing protumor properties of macrophages. *Cancer Cell* **2009**, *16*, 91-102, doi:10.1016/j.ccr.2009.06.018.
249. Wu, K.; Fukuda, K.; Xing, F.; Zhang, Y.; Sharma, S.; Liu, Y.; Chan, M.D.; Zhou, X.; Qasem, S.A.; Pochampally, R.; et al. Roles of the cyclooxygenase 2 matrix metalloproteinase 1 pathway in brain metastasis of breast cancer. *J Biol Chem* **2015**, *290*, 9842-9854, doi:10.1074/jbc.M114.602185.
250. Valiente, M.; Obenauf, Anna C.; Jin, X.; Chen, Q.; Zhang, Xiang H.F.; Lee, Derek J.; Chaft, Jamie E.; Kris, Mark G.; Huse, Jason T.; Brogi, E.; et al. Serpins Promote Cancer Cell Survival and Vascular Co-Option in Brain Metastasis. *Cell* **2014**, *156*, 1002-1016, doi:https://doi.org/10.1016/j.cell.2014.01.040.
251. Gril, B.; Paranjape, A.N.; Woditschka, S.; Hua, E.; Dolan, E.L.; Hanson, J.; Wu, X.; Kloc, W.; Izycka-Swieszewska, E.; Duchnowska, R. Reactive astrocytic S1P3 signaling modulates the blood–tumor barrier in brain metastases. *Nature communications* **2018**, *9*, 2705.
252. Kang, Y.; Siegel, P.M.; Shu, W.; Drobnjak, M.; Kakonen, S.M.; Cordón-Cardo, C.; Guise, T.A.; Massagué, J. A multigenic program mediating breast cancer metastasis to bone. *Cancer cell* **2003**, *3*, 537-549.

253. Kwok, T.; Yeguvapalli, S.; Chitrala, K.N. Identification of Genes Crucial for Biological Processes in Breast Cancer Liver Metastasis Relapse. *Int J Mol Sci* **2024**, *25*, doi:10.3390/ijms25105439.
254. Liu, J.; Wang, D.; Zhang, C.; Zhang, Z.; Chen, X.; Lian, J.; Liu, J.; Wang, G.; Yuan, W.; Sun, Z.; et al. Identification of liver metastasis-associated genes in human colon carcinoma by mRNA profiling. *Chin J Cancer Res* **2018**, *30*, 633-646, doi:10.21147/j.issn.1000-9604.2018.06.08.
255. Ma, R.; Feng, Y.; Lin, S.; Chen, J.; Lin, H.; Liang, X.; Zheng, H.; Cai, X. Mechanisms involved in breast cancer liver metastasis. *Journal of Translational Medicine* **2015**, *13*, 64, doi:10.1186/s12967-015-0425-0.
256. Minn, A.J.; Gupta, G.P.; Siegel, P.M.; Bos, P.D.; Shu, W.; Giri, D.D.; Viale, A.; Olshen, A.B.; Gerald, W.L.; Massagué, J. Genes that mediate breast cancer metastasis to lung. *Nature* **2005**, *436*, 518-524.
257. Houk, Andrew R.; Jilkine, A.; Mejean, Cecile O.; Boltyanskiy, R.; Dufresne, Eric R.; Angenent, Sigurd B.; Altschuler, Steven J.; Wu, Lani F.; Weiner, Orion D. Membrane Tension Maintains Cell Polarity by Confining Signals to the Leading Edge during Neutrophil Migration. *Cell* **2012**, *148*, 175-188, doi:https://doi.org/10.1016/j.cell.2011.10.050.
258. Rouven Brückner, B.; Pietuch, A.; Nehls, S.; Rother, J.; Janshoff, A. Ezrin is a Major Regulator of Membrane Tension in Epithelial Cells. *Scientific Reports* **2015**, *5*, 14700, doi:10.1038/srep14700.
259. Colom, A.; Derivery, E.; Soleimanpour, S.; Tomba, C.; Molin, M.D.; Sakai, N.; González-Gaitán, M.; Matile, S.; Roux, A. A fluorescent membrane tension probe. *Nature Chemistry* **2018**, *10*, 1118-1125, doi:10.1038/s41557-018-0127-3.
260. de Jesus, M.; Settle, A.H.; Vorselen, D.; Gaetjens, T.K.; Galiano, M.; Romin, Y.; Lee, E.; Wong, Y.Y.; Fu, T.-M.; Santosa, E. Single-cell topographical profiling of the immune synapse reveals a biomechanical signature of cytotoxicity. *Science immunology* **2024**, *9*, eadj2898.
261. Le Saux, G.; Bar-Hanin, N.; Edri, A.; Hadad, U.; Porgador, A.; Schvartzman, M. Nanoscale Mechanosensing of Natural Killer Cells is Revealed by Antigen-Functionalized Nanowires. *Adv Mater* **2019**, *31*, e1805954, doi:10.1002/adma.201805954.
262. Amano, M.; Ito, M.; Kimura, K.; Fukata, Y.; Chihara, K.; Nakano, T.; Matsuura, Y.; Kaibuchi, K. Phosphorylation and activation of myosin by Rho-associated kinase (Rho-kinase). *Journal of Biological Chemistry* **1996**, *271*, 20246-20249.
263. Maekawa, M.; Ishizaki, T.; Boku, S.; Watanabe, N.; Fujita, A.; Iwamatsu, A.; Obinata, T.; Ohashi, K.; Mizuno, K.; Narumiya, S. Signaling from Rho to the actin cytoskeleton through protein kinases ROCK and LIM-kinase. *Science* **1999**, *285*, 895-898.
264. Warner, S.O.; Yao, M.V.; Cason, R.L.; Winnick, J.J. Exercise-Induced Improvements to Whole Body Glucose Metabolism in Type 2 Diabetes: The Essential Role of the Liver. *Frontiers in Endocrinology* **2020**, *Volume 11 - 2020*, doi:10.3389/fendo.2020.00567.
265. Gruetter, R.; Novotny, E.J.; Boulware, S.D.; Rothman, D.L.; Mason, G.F.; Shulman,

G.I.; Shulman, R.G.; Tamborlane, W.V. Direct measurement of brain glucose concentrations in humans by 13C NMR spectroscopy. *Proc Natl Acad Sci U S A* **1992**, *89*, 1109-1112, doi:10.1073/pnas.89.3.1109.

266. Appelboom, J.W.; Brodsky, W.A.; Rehm, W.S. The concentration of glucose in mammalian liver. *J Gen Physiol* **1959**, *43*, 467-479, doi:10.1085/jgp.43.2.467.
267. Simpson, I.A.; Carruthers, A.; Vannucci, S.J. Supply and demand in cerebral energy metabolism: the role of nutrient transporters. *Journal of Cerebral Blood Flow & Metabolism* **2007**, *27*, 1766-1791.
268. Flavahan, W.A.; Wu, Q.; Hitomi, M.; Rahim, N.; Kim, Y.; Sloan, A.E.; Weil, R.J.; Nakano, I.; Sarkaria, J.N.; Stringer, B.W.; et al. Brain tumor initiating cells adapt to restricted nutrition through preferential glucose uptake. *Nat Neurosci* **2013**, *16*, 1373-1382, doi:10.1038/nn.3510.
269. Dai, W.; Xu, Y.; Mo, S.; Li, Q.; Yu, J.; Wang, R.; Ma, Y.; Ni, Y.; Xiang, W.; Han, L.; et al. GLUT3 induced by AMPK/CREB1 axis is key for withstanding energy stress and augments the efficacy of current colorectal cancer therapies. *Signal Transduction and Targeted Therapy* **2020**, *5*, 177, doi:10.1038/s41392-020-00220-9.
270. Matsumoto, G.; Omi, Y.; Lee, U.; Nishimura, T.; Shindo, J.; Penninger, J.M. Adhesion mediated by LFA-1 is required for efficient IL-12-induced NK and NKT cell cytotoxicity. *Eur J Immunol* **2000**, *30*, 3723-3731, doi:10.1002/1521-4141(200012)30:12<3723::Aid-immu3723>3.0.Co;2-9.
271. Mace, E.M.; Monkley, S.J.; Critchley, D.R.; Takei, F. A dual role for talin in NK cell cytotoxicity: activation of LFA-1-mediated cell adhesion and polarization of NK cells. *J Immunol* **2009**, *182*, 948-956, doi:10.4049/jimmunol.182.2.948.
272. Wu, Z.; Zhang, H.; Wu, M.; Peng, G.; He, Y.; Wan, N.; Zeng, Y. Targeting the NKG2D/NKG2D-L axis in acute myeloid leukemia. *Biomedicine & Pharmacotherapy* **2021**, *137*, 111299, doi:10.1016/j.biopha.2021.111299.
273. Lanier, L.L. NKG2D Receptor and Its Ligands in Host Defense. *Cancer Immunol Res* **2015**, *3*, 575-582, doi:10.1158/2326-6066.Cir-15-0098.
274. Chiusolo, V.; Jacquemin, G.; Yonca Bassoy, E.; Vinet, L.; Liguori, L.; Walch, M.; Kozjak-Pavlovic, V.; Martinvalet, D. Granzyme B enters the mitochondria in a Sam50-, Tim22- and mtHsp70-dependent manner to induce apoptosis. *Cell Death & Differentiation* **2017**, *24*, 747-758, doi:10.1038/cdd.2017.3.
275. Chowdhury, D.; Lieberman, J. Death by a Thousand Cuts: Granzyme Pathways of Programmed Cell Death. *Annual Review of Immunology* **2008**, *26*, 389-420, doi:10.1146/annurev.immunol.26.021607.090404.
276. Thiery, J.; Keefe, D.; Saffarian, S.; Martinvalet, D.; Walch, M.; Boucrot, E.; Kirchhausen, T.; Lieberman, J. Perforin activates clathrin- and dynamin-dependent endocytosis, which is required for plasma membrane repair and delivery of granzyme B for granzyme-mediated apoptosis. *Blood* **2010**, *115*, 1582-1593, doi:10.1182/blood-2009-10-246116.
277. Brodbeck, T.; Nehmann, N.; Bethge, A.; Wedemann, G.; Schumacher, U. Perforin-dependent direct cytotoxicity in natural killer cells induces considerable knockdown of spontaneous lung metastases and computer modelling-proven tumor cell dormancy in

a HT29 human colon cancer xenograft mouse model. *Molecular Cancer* **2014**, *13*, 244, doi:10.1186/1476-4598-13-244.

278. Rousalova, I.; Krepela, E. Granzyme B-induced apoptosis in cancer cells and its regulation (Review). *Int J Oncol* **2010**, *37*, 1361-1378, doi:10.3892/ijo_00000788.
279. Pinkoski, M.J.; Heibein, J.A.; Barry, M.; Bleackley, R.C. Nuclear translocation of granzyme B in target cell apoptosis. *Cell Death & Differentiation* **2000**, *7*, 17-24, doi:10.1038/sj.cdd.4400604.
280. Prager, I.; Watzl, C. Mechanisms of natural killer cell-mediated cellular cytotoxicity. *Journal of leukocyte biology* **2019**, *105*, 1319-1329.
281. Sordo-Bahamonde, C.; Lorenzo-Herrero, S.; Payer Á, R.; Gonzalez, S.; López-Soto, A. Mechanisms of Apoptosis Resistance to NK Cell-Mediated Cytotoxicity in Cancer. *Int J Mol Sci* **2020**, *21*, doi:10.3390/ijms21103726.
282. Takeda, K.; Cretney, E.; Hayakawa, Y.; Ota, T.; Akiba, H.; Ogasawara, K.; Yagita, H.; Kinoshita, K.; Okumura, K.; Smyth, M.J. TRAIL identifies immature natural killer cells in newborn mice and adult mouse liver. *Blood* **2005**, *105*, 2082-2089, doi:10.1182/blood-2004-08-3262.
283. Takeda, K.; Hayakawa, Y.; Smyth, M.J.; Kayagaki, N.; Yamaguchi, N.; Kakuta, S.; Iwakura, Y.; Yagita, H.; Okumura, K. Involvement of tumor necrosis factor-related apoptosis-inducing ligand in surveillance of tumor metastasis by liver natural killer cells. *Nat Med* **2001**, *7*, 94-100, doi:10.1038/83416.
284. Donato, N.J.; Klostergaard, J. Distinct stress and cell destruction pathways are engaged by TNF and ceramide during apoptosis of MCF-7 cells. *Experimental Cell Research* **2004**, *294*, 523-533, doi:https://doi.org/10.1016/j.yexcr.2003.11.021.
285. Liu, Z.-g.; Hsu, H.; Goeddel, D.V.; Karin, M. Dissection of TNF receptor 1 effector functions: JNK activation is not linked to apoptosis while NF-κB activation prevents cell death. *Cell* **1996**, *87*, 565-576.
286. Song, M.; Ping, Y.; Zhang, K.; Yang, L.; Li, F.; Zhang, C.; Cheng, S.; Yue, D.; Maimela, N.R.; Qu, J.; et al. Low-Dose IFNγ Induces Tumor Cell Stemness in Tumor Microenvironment of Non–Small Cell Lung Cancer. *Cancer Research* **2019**, *79*, 3737-3748, doi:10.1158/0008-5472.Can-19-0596.
287. Li, P.; Du, Q.; Cao, Z.; Guo, Z.; Evankovich, J.; Yan, W.; Chang, Y.; Shao, L.; Stolz, D.B.; Tsung, A.; et al. Interferon-gamma induces autophagy with growth inhibition and cell death in human hepatocellular carcinoma (HCC) cells through interferon-regulatory factor-1 (IRF-1). *Cancer Letters* **2012**, *314*, 213-222, doi:https://doi.org/10.1016/j.canlet.2011.09.031.
288. Kim, E.J.; Lee, J.M.; Namkoong, S.E.; Um, S.J.; Park, J.S. Interferon regulatory factor-1 mediates interferon-γ-induced apoptosis in ovarian carcinoma cells. *Journal of cellular biochemistry* **2002**, *85*, 369-380.
289. Basu, R.; Whitlock, B.M.; Husson, J.; Le Floc'h, A.; Jin, W.; Oyler-Yaniv, A.; Dotiwala, F.; Giannone, G.; Hivroz, C.; Biais, N.; et al. Cytotoxic T Cells Use Mechanical Force to Potentiate Target Cell Killing. *Cell* **2016**, *165*, 100-110, doi:10.1016/j.cell.2016.01.021.
290. Orange, J.S. Formation and function of the lytic NK-cell immunological synapse.

Nature Reviews Immunology **2008**, *8*, 713-725.

291. Yuan, X.; Gajan, A.; Chu, Q.; Xiong, H.; Wu, K.; Wu, G.S. Developing TRAIL/TRAIL death receptor-based cancer therapies. *Cancer and Metastasis Reviews* **2018**, *37*, 733-748, doi:10.1007/s10555-018-9728-y.
292. Carneiro, B.A.; El-Deiry, W.S. Targeting apoptosis in cancer therapy. *Nature Reviews Clinical Oncology* **2020**, *17*, 395-417, doi:10.1038/s41571-020-0341-y.
293. Reefman, E.; Kay, J.G.; Wood, S.M.; Offenhäuser, C.; Brown, D.L.; Roy, S.; Stanley, A.C.; Low, P.C.; Manderson, A.P.; Stow, J.L. Cytokine Secretion Is Distinct from Secretion of Cytotoxic Granules in NK Cells. *The Journal of Immunology* **2010**, *184*, 4852-4862, doi:10.4049/jimmunol.0803954.
294. Lanier, L.L. NK cell recognition. *Annu Rev Immunol* **2005**, *23*, 225-274, doi:10.1146/annurev.immunol.23.021704.115526.
295. Bryceson, Y.T.; March, M.E.; Ljunggren, H.G.; Long, E.O. Activation, coactivation, and costimulation of resting human natural killer cells. *Immunol Rev* **2006**, *214*, 73-91, doi:10.1111/j.1600-065X.2006.00457.x.
296. Bauer, S.; Groh, V.; Wu, J.; Steinle, A.; Phillips, J.H.; Lanier, L.L.; Spies, T. Activation of NK Cells and T Cells by NKG2D, a Receptor for Stress-Inducible MICA. *Science* **1999**, *285*, 727-729, doi:doi:10.1126/science.285.5428.727.
297. Raulet, D.H.; Gasser, S.; Gowen, B.G.; Deng, W.; Jung, H. Regulation of Ligands for the NKG2D Activating Receptor. *Annual Review of Immunology* **2013**, *31*, 413-441, doi:10.1146/annurev-immunol-032712-095951.
298. Lanier, L.L. NKG2D Receptor and Its Ligands in Host Defense. *Cancer Immunology Research* **2015**, *3*, 575-582, doi:10.1158/2326-6066.Cir-15-0098.
299. Fernández-Messina, L.; Reyburn, H.; Vales-Gomez, M. Human NKG2D-ligands: cell biology strategies to ensure immune recognition. *Frontiers in Immunology* **2012**, *3*, doi:10.3389/fimmu.2012.00299.
300. Duan, S.; Guo, W.; Xu, Z.; He, Y.; Liang, C.; Mo, Y.; Wang, Y.; Xiong, F.; Guo, C.; Li, Y.; et al. Natural killer group 2D receptor and its ligands in cancer immune escape. *Molecular Cancer* **2019**, *18*, doi:10.1186/s12943-019-0956-8.
301. Wu, J.; Song, Y.; Bakker, A.B.; Bauer, S.; Spies, T.; Lanier, L.L.; Phillips, J.H. An activating immunoreceptor complex formed by NKG2D and DAP10. *Science* **1999**, *285*, 730-732, doi:10.1126/science.285.5428.730.
302. Karimi, M.; Cao, T.M.; Baker, J.A.; Verneris, M.R.; Soares, L.; Negrin, R.S. Silencing Human NKG2D, DAP10, and DAP12 Reduces Cytotoxicity of Activated CD8⁺ T Cells and NK Cells. *The Journal of Immunology* **2005**, *175*, 7819-7828, doi:10.4049/jimmunol.175.12.7819.
303. Marusina, A.I.; Burgess, S.J.; Pathmanathan, I.; Borrego, F.; Coligan, J.E. Regulation of Human DAP10 Gene Expression in NK and T Cells by Ap-1 Transcription Factors. *The Journal of Immunology* **2008**, *180*, 409-417, doi:10.4049/jimmunol.180.1.409.
304. Upshaw, J.L.; Arneson, L.N.; Schoon, R.A.; Dick, C.J.; Billadeau, D.D.; Leibson, P.J. NKG2D-mediated signaling requires a DAP10-bound Grb2-Vav1 intermediate and phosphatidylinositol-3-kinase in human natural killer cells. *Nat Immunol* **2006**, *7*, 524-

532, doi:10.1038/ni1325.
305. Niu, C.; Li, M.; Chen, Y.; Zhang, X.; Zhu, S.; Zhou, X.; Zhou, L.; Li, Z.; Xu, J.; Hu, J.F.; et al. LncRNA NCAL1 potentiates natural killer cell cytotoxicity through the Gab2-PI3K-AKT pathway. *Front Immunol* **2022**, *13*, 970195, doi:10.3389/fimmu.2022.970195.
306. Wilton, K.M.; Overlee, B.L.; Billadeau, D.D. NKG2D–DAP10 signaling recruits EVL to the cytotoxic synapse to generate F-actin and promote NK cell cytotoxicity. *Journal of Cell Science* **2019**, *133*, doi:10.1242/jcs.230508.
307. Han, J.; Das, B.; Wei, W.; Van Aelst, L.; Mosteller, R.D.; Khosravi-Far, R.; Westwick, J.K.; Der, C.J.; Broek, D. Lck regulates Vav activation of members of the Rho family of GTPases. *Mol Cell Biol* **1997**, *17*, 1346-1353, doi:10.1128/mcb.17.3.1346.
308. Barreira, M.; Rodríguez-Fdez, S.; Bustelo, X.R. New insights into the Vav1 activation cycle in lymphocytes. *Cell Signal* **2018**, *45*, 132-144, doi:10.1016/j.cellsig.2018.01.026.
309. Cuevas, B.; Lu, Y.; Watt, S.; Kumar, R.; Zhang, J.; Siminovitch, K.A.; Mills, G.B. SHP-1 regulates Lck-induced phosphatidylinositol 3-kinase phosphorylation and activity. *J Biol Chem* **1999**, *274*, 27583-27589, doi:10.1074/jbc.274.39.27583.
310. Wan, Z.; Shao, X.; Ji, X.; Dong, L.; Wei, J.; Xiong, Z.; Liu, W.; Qi, H. Transmembrane domain-mediated Lck association underlies bystander and costimulatory ICOS signaling. *Cellular & Molecular Immunology* **2020**, *17*, 143-152.
311. Taylor, B.C.; Balko, J.M. Mechanisms of MHC-I Downregulation and Role in Immunotherapy Response. *Frontiers in Immunology* **2022**, *13*, doi:10.3389/fimmu.2022.844866.
312. Cha, J.-H.; Chan, L.-C.; Li, C.-W.; Hsu, J.L.; Hung, M.-C. Mechanisms Controlling PD-L1 Expression in Cancer. *Molecular Cell* **2019**, *76*, 359-370, doi:https://doi.org/10.1016/j.molcel.2019.09.030.
313. Yi, M.; Li, T.; Niu, M.; Zhang, H.; Wu, Y.; Wu, K.; Dai, Z. Targeting cytokine and chemokine signaling pathways for cancer therapy. *Signal Transduction and Targeted Therapy* **2024**, *9*, 176, doi:10.1038/s41392-024-01868-3.
314. Duan, S.; Guo, W.; Xu, Z.; He, Y.; Liang, C.; Mo, Y.; Wang, Y.; Xiong, F.; Guo, C.; Li, Y.; et al. Natural killer group 2D receptor and its ligands in cancer immune escape. *Molecular Cancer* **2019**, *18*, 29, doi:10.1186/s12943-019-0956-8.
315. Tie, Y.; Tang, F.; Wei, Y.-q.; Wei, X.-w. Immunosuppressive cells in cancer: mechanisms and potential therapeutic targets. *Journal of Hematology & Oncology* **2022**, *15*, 61, doi:10.1186/s13045-022-01282-8.
316. Klein, C.A. Framework models of tumor dormancy from patient-derived observations. *Current Opinion in Genetics & Development* **2011**, *21*, 42-49, doi:https://doi.org/10.1016/j.gde.2010.10.011.
317. Fan, R.; Emery, T.; Zhang, Y.; Xia, Y.; Sun, J.; Wan, J. Circulatory shear flow alters the viability and proliferation of circulating colon cancer cells. *Scientific Reports* **2016**, *6*, 27073, doi:10.1038/srep27073.
318. Regmi, S.; Fu, A.; Luo, K.Q. High Shear Stresses under Exercise Condition Destroy Circulating Tumor Cells in a Microfluidic System. *Scientific Reports* **2017**, *7*, 39975,

doi:10.1038/srep39975.